An investigation into the effect of particle and formulation properties on the performance of pharmaceutical powders using novel experimental and modelling techniques

Maen Alshafiee

Department of Pharmacy, School of Applied sciences. University of Huddersfield

A thesis submitted in partial fulfilment of the requirements for a Doctor of Philosophy in Pharmaceutical sciences

Copyright statement

i. *The author of this thesis (including any appendices and/ or schedules to this thesis) owns any copyright in it (the "Copyright") and s/he has given The University of Huddersfield the right to use such Copyright for any administrative, promotional, educational and/or teaching purposes.*

ii. *Copies of this thesis, either in full or in extracts, may be made only in accordance with the regulations of the University Library. Details of these regulations may be obtained from the Librarian. Details of these regulations may be obtained from the Librarian. This page must form part of any such copies made.*

iii. *The ownership of any patents, designs, trademarks and any and all other intellectual property rights except for the Copyright (the "Intellectual Property Rights") and any reproductions of copyright works, for example graphs and tables ("Reproductions"), which may be described in this thesis, may not be owned by the author and may be owned by third parties. Such Intellectual Property Rights and Reproductions cannot and must not be made available for use without permission of the owner(s) of the relevant Intellectual Property Rights and/or Reproductions.*

Declaration

Some of the chapters of this thesis have been published in peer-reviewed journals. Where this is the case, a note to the reader section is included in the relevant chapter to explain where aspects of the chapter have been published.

Maen Alshafiee is the first author in both publications, with Dr Kofi Asare-Addo as the corresponding author due to his supervisory role.

Acknowledgements

All praise to Allah, the most merciful and most gracious, who gave me the ability, strength and power to be able to complete this thesis.

This thesis is dedicated to the martyrs of my home country and those who have and were injured during the war. Those courageous people who died or are still suffering- I would say that justice will win someday.

Foremost, I would like to thank my parents, who helped me during my journey to reach this point. To my mom, who struggled a lot during my upbringing. I will never forget your tears and your hard work to ensure that my brother, sisters and I had all that we needed. To my dad also, who gave us everything he could to ensure we had the best life. I also would like to thank my brother Abdulmalek and my beloved sisters, from whom I learned a lot.

I would like to thank my supervisor Dr Kofi Asare-Addo, who gave me the freedom to explore new ideas. His unlimited support and encouragement were the main drive for me to finish this thesis. I want to say that I was lucky to have you as a supervisor during my thesis. From you, I learned how to be patient and how to able to publish and write high-quality research. I would also thank my second supervisor Dr Karl Walton for all his support during my PhD journey.

I would like to thank my partner, Ola, who helped me during this road and who was very patient during my PhD. Your endless sacrifices were one of the main reasons for me to reach this point. To my lovely kids also, Omar and Ayla, who gave me the motivation to complete this thesis.

Finally- I would thanks all my PhD teammates: Adam, Ana, Nihad and Benedict. I wish you all the success in your own PhD, studies or current work.

Contents

List of Figures

List of Tables

List of Equations

List of Abbreviations

Abbreviation	Description
API	Active Pharmaceutical Ingredient
AR	Aspect Ratio
ASD	Amorphous Solid Dispersions
AUC	Area Under the Curve
BET	Brunauer–Emmett–Teller surface area
BSC	Biopharmaceutical Classification System
DE	Dissolution Efficiency
DEM	Discrete Element Modelling
DOE	Design Of Experiment
DPI	Dry Powder Inhaler
DSC	Differential Scanning Calorimetry
EQPC	Diameter of a circle of equal projection area
FASSIF	Fasted state simulated intestinal fluid
FBRM	Focus beam reflective measurement
FDPM	Frequency-Domain Photon Migration
FEM	Finite Element Modelling
FFC	Flow Function Coefficient
FPF	Fine Particle Fraction
FVM	Focus variation microscopy
HPLC	High Performance Liquid Chromatography
HME	Hot Melt Extrusion
HSC	High Sensitivity Circuilty
ICH	International Conference of Harmonisation
LVDT	Linear Variable Differential Transformer
MDT	Mean Dissolution Time
MPM	Material Point Method (MPM)
MRI	Magnetic Resonance Imaging
MST	Material Science Tetrahedron

MVA	Multivariate analysis
ODTs	Oral Disintegrating Tablets
PAT	Process Analytical Tool
PCA	Principal Component Analysis
PECVD	Plasma-Enhanced Chemical Vapour Deposition
PBPK	Physiological Based Pharmacokinetic Models
PLS	Partial Least Square
RBF	Radial Basis Function
RMS	Root-Mean-Square
RST	Ring Shear Tester
SAXS	Solution Atomisation and Crystallisation by sonication
SDI	Surface Dissolution imaging
SEM	Scanning Electron Microscopy
SMD	Surface Weighted (or Sauter) Mean Diameter
TEM	Transmission electron microscopy
ToF-SIMS	Time-of-Flight Secondary Ion Mass Spectrometry
TPI	Terahertz Pulsed imaging
TSG	Twin-Screw Granulator
VAS	Visual Analogue Scale
XPS	X-ray photoelectron spectroscopy
XRPD	X-Ray Powder Diffraction
XμT	X-ray microtomography

List of publications

- Maen Alshafiee, Mohammad K. Aljammal, Daniel Markl, Adam Ward, Karl Walton, Liam Blunt, Sachin Korde, Sudhir K. Pagire, Adrian L. Kelly, Anant Paradkar, Barbara R. Conway, Kofi Asare-Addo, Hot-melt extrusion process impact on polymer choice of glyburide solid dispersions: The effect of wettability and dissolution, International Journal of Pharmaceutics,2019, https://doi.org/10.1016/j.ijpharm.2019.01.038.

- Maen Alshafiee, Wafa' H. AlAlaween, Daniel Markl, Mithushan Soundaranathan, Ammar Almajaan, Karl Walton, Liam Blunt, Kofi Asare-Addo, A predictive integrated framework based on the radial basis function for the modelling of the flow of pharmaceutical powders, International Journal of Pharmaceutics,2019, https://doi.org/10.1016/j.ijpharm.2019.118542

Abstract

This thesis provides a piece of comprehensive information on the interrelationship between particle properties, formulation properties, and the performance of pharmaceutical powders. Three main performance categories were investigated; these include flow, disintegration, and dissolution. The effect of formulation properties on the dissolution performance of a pharmaceutical formulation containing a low soluble active pharmaceutical ingredient was explored. A novel, dynamic contact angle measurement technique was used to understand wetting behaviour and provide correlations with dissolution testing using biorelevant dissolution media. In addition, this thesis explored the link between the microstructure obtained by X-ray microtomography and the dissolution performance. The thesis also investigates how formulation properties such as disintegrant type and the amount of lubricant affects the disintegration behaviour of pharmaceutical tablets by coupling a novel surface imaging instrument with an in-line particle size analyser.

This thesis also presents novel data analysis techniques with the aim to build a modelling framework that can be used to relate particle properties of pharmaceutical powders such as particle size and shape to their flow performance. Radial basis function (RBF) and neural network techniques were used to achieve this goal. Traditional data analysis techniques such as multivariate data analysis were used to build correlations between particle properties and powder performance. This is of great importance in the early stages of drug discovery activities. The information from this thesis therefore demonstrates how novel experimental and modelling techniques can be used to related particle properties and formulation properties to the performance of pharmaceutical powders.

Chapter 1 - Literature review

1.1 Material science tetrahedron concept

The concept of material science tetrahedron (MST) was first introduced in the field of material sciences to help guide the industry to link between the chemical crystals and their performance (National Council Research, 2000). This was later introduced in pharmaceutical research and development by Sun (Sun, 2009). The MST concept is illustrated in Figure 1.1. This concept consists of four main blocks. These blocks include structure, properties, processing parameters and performance. The term performance can be referred to the safety, efficacy, manufacturability, bioavailability and stability of the corresponding material or dosage form. Using this concept, a change in one of the elements of the tetrahedron will subsequently affect all the remaining elements. A change in the crystal structure, for example, or crystal habit, will influence how to process a specific material. The relationship between the performance and each other blocks of the MST is discussed in sections 1.1.1, 1.1.2 and 1.1.3. In addition, the use of emerging modelling techniques to help explore the relationship between theses blocks is further discussed.

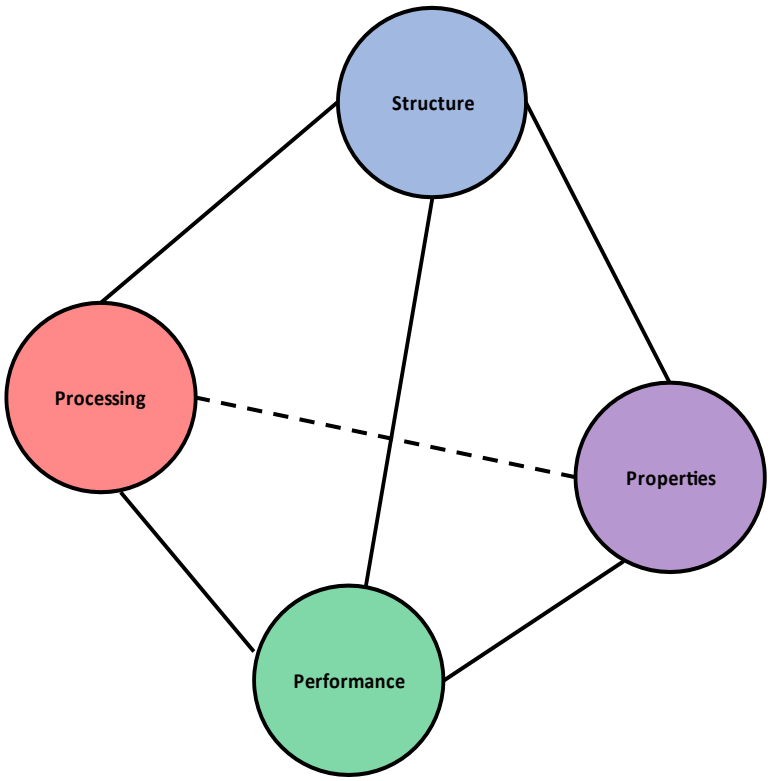

Figure 1.1 Material science tetrahedron concept (Sun, 2009)

1.1.1 The relationship between structure and performance

A significant body of research has explored the relationship between the structure and the performance of active pharmaceutical dosage forms (APIs). Some of the interesting examples include sulfamerazine, glyburide and ketoprofen. Sulfamerazine, for instance, has two polymorphs; form I and form II. While form I is packed in flat-layers, form II is packed in zigzag layers. When compressed, these polymorphic forms show different mechanical properties (performance), with a form I having superior tabletability over form II. This was attributed to the creation of slip planes in form I, which gives this form better plasticity and ultimately better

tabletability and compressibility (Sun & Grant, 2001). The presence of water can also have a significant change in the same crystal with an identical configuration. For example, hydrates and monohydrates of para-aminobenzoic acid have the same zigzag crystal structure. However, they showed different compaction properties, with the tabletability of monohydrates being 4.5 folds better than the tabletability of the anhydrous form (Sun & Grant, 2004). Ketoprofen has also been studied to determine how different faces, mainly (100) and (110), interact with 17 excipients. This study showed that four excipients had poorer binding energy on the (100) face, and five excipients had poorer binding energy on the (110) face. Lactose and glucose interacted differently to these faces. Binding energy comparison between lactose or glucose to ketoprofen showed that lactose had a stronger binding energy to ketoprofen than glucose(Roberts et al., 2016).

1.1.2 The relationship between properties and performance

Particle and powder properties have also been studied. Particle size has always played an essential role in the dissolution rate of different pharmaceutical powders and ultimately in the bioavailability of corresponding dosage forms. As particle size decreased, the surface area of pharmaceutical powders increased, which in turn results in increases in the dissolution rate of the corresponding pharmaceutical dosage forms. Five grades of glyburide were studied by Wei et al. (2008a).These grades showed no differences in solid-state properties where similar crystallinity was observed. However, these grades showed significant differences in vivo, mainly due to particle

size changes. Handling and processing of pharmaceutical powders are greatly affected by particle size. A considerable body of research has been devoted to the understanding of particle and granular flow properties and the factors affecting these properties using various pharmaceutical powders (Adebisi et al., 2016; Asare-Addo et al., 2015; Gaisford & Saunders, 2013; Navaneethan, Missaghi, & Fassihi, 2005; Šupuk et al., 2013; Visser, 1989). For instance, it has been found that particle flow properties are significantly affected by particle size and shape for both brittle and elastic pharmaceutical powders (Garg et al., 2018). Garg et al. (2018) studied two commonly used brittle pharmaceutical powders, namely, calcium phosphate and dicalcium phosphate. It was shown that calcium phosphate with a relatively larger particle size displayed good flow properties and less cohesiveness when compared to the dicalcium phosphate (smaller particle size) . Fu et al. (2012) investigated three grades of lactose powders, and the obtained results indicated that the powder flow properties of the three grades were significantly affected by both the particle size and shape. The flow of elastic powders such as microcrystalline cellulose (MCC) was also sensitive to the changes in the particle size and shape (Hou & Sun, 2008). Hou and Sun (2008) also examined the flow of eleven grades of MCC. The results demonstrated a decrease in the powder flow rate with a decrease in the particle size even though the chemical nature and particle morphology were similar. In addition, it was found that a change in the particle morphology towards a more spherical morphology led to better flow and less cohesiveness. Furthermore, surface modifications (e.g. using silicified MCC) also led to better flow properties (Hou & Sun, 2008). These findings highlight the

importance of particle and bulk properties of pharmaceutical powder on their performance. With the implementation of continuous mixing technology, there is an urgent need to study how different critical quality attributes of pharmaceutical materials are changing during processing. For example, a change of particle size and shape could be a major challenge during pharmaceutical manufacturing and changes in particle size will result in affecting the performance of pharmaceutical materials especially in bioavailability and handling.

Formulation techniques have always been utilised in the world of pharmaceutical manufacturing in order to enhance the performance of pharmaceutical dosage forms. These methods gained high attention after utilising innovative combinatorial chemistry and high-throughput screening tools in drug discovery, which led to more APIs with poorly soluble properties reaching the clinical stages of drug development processes (Fahr & Liu, 2007). Poorly soluble drugs are very challenging during pharmaceutical development. Solubility and dissolution tend to be the rate-limiting step for these compounds entering the systemic circulations and giving the desired therapeutic response (Adebisi et al., 2016; Conway and Asare-Addo 2016).

Moreover, the mechanical properties of oral tablets are essential to ensure sufficient hardness, dimensions, content, and weight uniformity (Hamad, 2010).

1.1.3 The relationship between processing parameters and performance

Gamble et al. (2017) studied how process variables affect particle attritions in a multi-compartment blend during continuous manufacturing. The authors demonstrated that the particle attrition of theophylline occurred in two parts of the system; at the bottom of the hopper and within the screw feed itself. They also demonstrated that a change in the screw feed rate had a final effect on the particle size of theophylline and, ultimately, the performance of pharmaceutical dosage form. A change in the processing parameters such as temperature, speed and twin screw configuration resulted in a change in the dissolution (performance) of the hot melt extrusion (HME) product (Van den Mooter, 2012).

1.1.4 Emerging modelling techniques

Modelling techniques have emerged with advances in computational tools employed in MST. This can be applied to any blocks of the material science tetrahedron concept. One of the interesting examples that will be explored in this thesis is to understand the relationship between the bulk properties and flow (performance). In fact, several attempts have been focusing on modelling and predicting the powder flow properties of materials that are essential in many pharmaceuticals, chemical and agricultural industry applications. Therefore, some research papers have focused on modelling and predicting the powder flow behaviour and its properties. In general, modelling paradigms can be classified as either physical (or semi-physical) or data-based models.Besides, the discrete element method (DEM), as a numerical method that is

usually utilised to model/simulate the motion of a relatively large number of small particles, has been utilised to simulate the flow behaviour of various powders (Fraige et al., 2008; Luding, 2005). Such a method allows one to model and considers the effect of equipment dynamics on the flow behaviour. Due to the importance of DEM and data driven model in powder flow, the following subsections will discuss DEM and data driven modelling in more details.

1.1.4.1 Discrete element modelling (DEM)

As powder flow is mainly influenced by the interaction between particles, it will be evident for any modelling work to address these interactions. DEM, therefore, was evolved as an alternative modelling technique that taking into account particle properties of powder. In DEM, each particle has a specific property such as particle size, particle shape and density. The movement of each particle is calculated using Newton second law of motion (Baxter et al., 2000) (equation 1.1)

$$m\frac{dv}{dt} = fg + fc + Fnc \qquad \textbf{Eq. 1.1}$$

Where m: mass of the particle, v: transitional velocity, fg: gravational constant, fc: contatct constant and fnc: non-contact constant

The motion of a specific particle is determined ny determining both the driving forces and dragging forces for each particle and then by using equation 1.1 the movement of each particle can be calculated. This method awas utilized to simulate the flow behaviour of various powders (Fraige et al.,2008; Luding, 2005). DEM methods,

however, are considered to be computationally taxing, particularly when more than billions of particles need to be considered, which is the actual case in powder flow (AlAlaween et al., 2017). For these main limitations of mechnaitic modelling, alternative modelling techniques were explored in this thesis such as data-driven modelling. On the one hand, mechanistic (or semi-mechanistic) based models can be implicitly built on some assumptions (e.g. monodisperse particle size distribution) that are not usually valid and may lead, as a result, to inaccurate results (AlAlaween et al., 2017). In addition, some of these models (e.g. DEM) are considered to be computationally taxing, particularly when more than billions of particles need to be considered, which is the actual case in powder flow (AlAlaween et al., 2017).

1.1.4.2 Data driven modelling

Data-driven models, as the name indicates, rely significantly on the available data and its quality, which may include not only the number of the data points but also their distribution in the space under investigation (AlAlaween et al., 2018). As such, sparse and limited amount of data can decrease the performance of a data-driven models (AlAlaween et al., 2018). Modelling and predicting the powder flow behaviour is indeed a challenging task, this being due to (i) large number of parameters (e.g. several particle size and shape factors) that affect the powder flow; (ii) a huge variety of excipients and APIs as well as mixtures of various excipients and APIs that may possess different flow characteristics to their parent materials. Huge efforts are being made towards the understanding of powders and as such their predictions. Authors such as Wang *et al.* (2016) have successfully established mathematical correlations

between cohesion and the flow function coefficient. Their analysis of 41 powders using a ring shear tester enabled the proposed method that augmented shear cell data analysis and significantly reduced the complexity of the shear cell data also (Wang et al., 2016). Leung et al. (2017) further studied 1130 powders to test this correlation. The authors identified a near-perfect inverse correlation between the flow function coefficient and cohesion. It was concluded that improving the flowability of pharmaceutical powder required an alteration in the interparticlute properties rather than altering the friction properties of pharmaceutical powders. A big data approached was also used by Megarry et al. (2019) where the authors examined 3909 historical experimental data from a shear cell. Their characterisation aided in establishing an operating space that can be used as a process flow map to guide formulators in future development.

1.1.4.2.1 Partial least square (PLS) regression

PLS is one of the useful techniques that has evolved in the recent years as a powerful data-driven statistical technique in the field of pharmaceutical sciences. The technique itself developed in the late sixties by Wold (Wold, 1966). PLS is similar to any other type of regression where a relationship between Xs and Ys is investigated. However, in the case of PLS, Xs are set of different variables grouped together in a specific matrix while y can be either one single response or many responses. The first step of any PLS starts by normalisation of the data. Then principal component analysis (PCA) is performed to determine the loading of each variable and scores associated with each loading. By doing this, the number of predictors is reduced and a set of components

which has a maximum correlation between the predictors and responses will be identified. PLS is then performed by identifying the common plane that connect PCA of Xs matrix to the PCA to ys matrix (Wold, 1966). One of the main limitations of PLS is the poor extrapolation capability of the model. The prediction capability can therefore be limited to the set of data PLS used to build the model.

PLS was used in modelling of powder flow and was developed to linearly relate the particle size and shape distributions represented by multiple descriptors to the bulk powder flowability of various pharmaceutical materials. Particle size and shape data were firstly restructured and arranged into two different subgroups: one for the single component within the study and the rest for binary mixtures. FFC values were also arranged into two response matrices: one for the single component and the other for the binary components. PLS was then performed to construct a statistical model that can predict the FFC values (Yu et al., 2011). This model, however, has some limitations. These limitations include the sample size used in the previous PLS which limits the prediction capabilities of this model. Another main drawback to such this model is the inability to perform an extrapolation outside the range of the data studied. Furthermore, the previous study (Yu et al., 2011) found FFC values data are nonlinear which could also limit the prediction capabilities of PLS in flow prediction (Qin & McAvoy, 1992)

1.1.4.2.2 Radial basis function (RBF)

The RBF network usually maps an N -dimensional input space (**x**) to a one-dimensional output space (y_T). Such a network typically consists of an input layer, basis functions acting as a hidden layer and an output layer (AlAlaween et al., 2017; Bishop & M., 1995). Basis functions ($\phi_i(\mathbf{x})$) are functions of the radial Euclidian distance from a defined centre. A Gaussian function is a common selection for the basis function, which can be written as expressed in equation 1.2 (Bishop & M., 1995):

$$\emptyset_i = e^{-(\frac{x-\mu_i}{2\sigma_i^2})} \qquad \textbf{Eq. 1.2}$$

where $\boldsymbol{\mu}_i$ and $\boldsymbol{\sigma}_i$ are the centre and the standard deviation of the i^{th} function, respectively. The output of the mapping can then be expressed as a linear combination of these basis functions as expressed in equation 1.3 (Bishop & M., 1995) :

$$y(x) = \sum_{i=1}^{I} w_i \emptyset_i\,(x) + w_0 \qquad \textbf{Eq. 1.3}$$

where w_0 and w_i are the bias and the coefficient connecting the i^{th} basis function to the output layer, respectively. The general structure of the RBF network is presented in Figure 1.2.

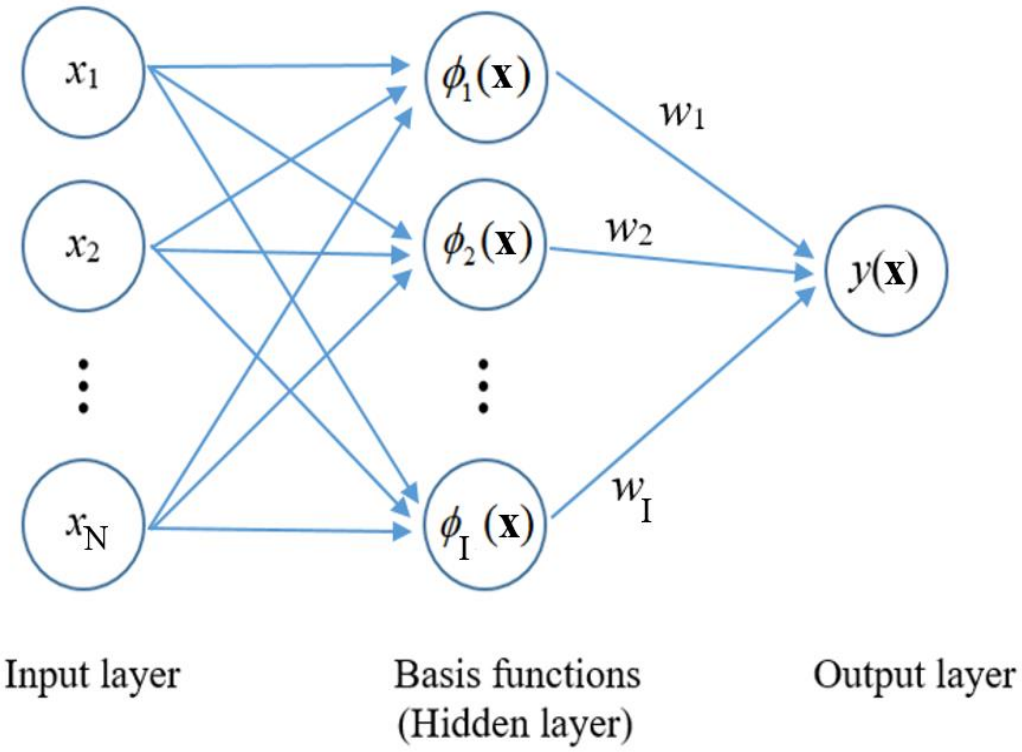

Figure 1.2 The Radial Basis Function (RBF) network structure adapted from (Bishop & M., 1995)

The number of neurons in the input and output layers are determined by the process under investigation (i.e., the numbers of the inputs and outputs). In order to minimize the error of predicting each output, multi-input single output (MISO) model is commonly utilized. The optimal number of the basis functions is the one that achieves a trade-off between good training and good generalization capabilities. Thus, it corresponds to the minimum error usually measured via the root mean square error (RMSE).

The RBF parameters (e.g., connecting coefficients and bias) are usually optimized via the use of the back-propagation network. In general, back-propagation is a supervised learning algorithm that aims to minimize the mean squared error between the target output and the predicted output (AlAlaween et al., 2017; Bishop & M., 1995; Duda, Hart, & Stork, 2001). Such an algorithm typically involves two phases, namely, forward and backward phases. The forward phase calculates the network predicted output according to the inputs, whereas the backward phase adapts the network parameters (e.g., the connecting coefficients) based on the error performance via the use of an elicited optimization algorithm. Various optimization algorithms including, but not limited to, gradient descent, quasi-Newton optimisation, conjugate gradient, Levenberg-Marquardt and nature inspired optimization algorithms (e.g., Genetic algorithm), have been presented in the related literature (Duda et al., 2001; Leung et al., 2017).

1.1.4.2.3 Integrated neural networks

The integrated network, as a data-based model, relies on predicting the output via two phases. The structure of such a network for MISO is depicted in Figure 1.3.

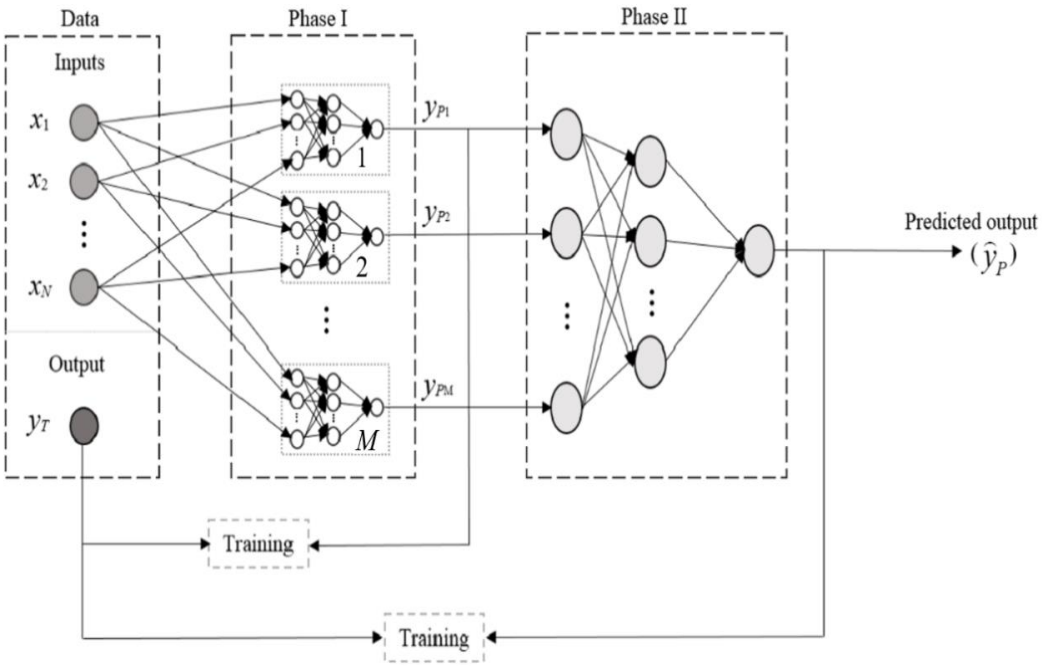

Figure 1.3 The architecture of the integrated network adapted from (Duda et al., 2001)

In the first phase, the *N*-dimensional input space (**x**) and the one-dimensional target space (y_T) are utilized to develop and train *M* models having different structures (e.g. number of basis functions). Then, the predicted outputs (i.e. the predicted flow properties from each model) from these models (y_{P1}, y_{P2}… y_{PM}) and the target output are used, in the second phase, to develop and train a single model leading to the final predicted output ($\hat{y}_P$) (Duda et al., 2001). The idea of this integrated network is that the different model structures in the first phase can play a complementary role in representing the underlying patterns between the input parameters investigated and the flowability parameters (i.e. FCC and RHOB). Furthermore, training the model in two phases helps in extracting the associated knowledge from the available limited data (Duda et al., 2001).

The predicted output of the integrated network can analytically be expressed as a combination of composition and superposition of the basis functions as expressed in equation 1.4 (Duda et al., 2001):

$$y(p) = \sum_{m=1}^{M} w_m^2 \emptyset_m \left(\sum_{k=1\S}^{K} w_k \, \emptyset_k(x) + w_0 \right) + w_0^2 \qquad \textbf{Eq. 1.4}$$

where K is the number of the basis functions in each model in the first phase and M represents the number of the RBF models defined in the first phase

Furthermore, a kinematic flow model, as a semi-physical based paradigm, was also established to characterise the particles flow in a two-dimensional moving bed using three materials, namely, Polyethylene (PE), Polyvinylchloride (PVC) and Phenylformaldheyde (PF) resin (Wu et al., 2008). The presented modelling paradigms (i.e., physical- and data-driven models) have, in general, their limitations and strengths.

On the one hand, physical (or semi-physical) based models, for instance, can be implicitly built on some assumptions (e.g. the size distribution is monomodal) that are not usually valid and may lead, as a result, to inaccurate results (AlAlaween et al., 2017). In addition, some of these models (e.g. DEM) are considered to be computationally taxing, particularly when more than billions of particles need to be considered, which is the actual case in powder flow (AlAlaween et al., 2017). As the name indicates, data-driven models rely significantly on the available data, which may include the number of the data points and their distribution in the space under

investigation (AlAlaween et al., 2018). As such, a sparse and limited amount of data can decrease the performance of data driven models (AlAlaween et al., 2018). Modelling and predicting the powder flow behaviour is indeed a challenging task, this being due to (i) a large number of parameters (e.g., particle shape and different types of pharmaceutical powders) that affect the flow properties (such high dimensionality poses serious challenges that affect a model performance); and (ii) the different tools and equipment that can be used to fed powders.

In this literature review, the effect of particle properties and formulation properties on the performance of pharmaceutical dosage forms is explored. Processing parameters have not been studied in this thesis and have not been included in this literature review as it is out of scope for the thesis.

1.2 Particle properties and the performance of solid dosage forms

1.2.1 The effect of particle size on the performance

Before exploring the effect of particle size on the performance of solid dosage forms, it would be important to discuss the scientific basis around particle sizing measurements.

1.2.1.1 Introduction to particle sizing techniques

Quality of the pharmaceutical products requires a comprehensive understanding of physicochemical properties of materials used, in-process components and finished

product itself through effective innovation and development (FDA, 2004). Particle size and shape control are essential critical quality attributes that need to be controlled.

International conference of harmonisation (ICH 6A) issued a decision tree on when to set an acceptance criterion for particle size distribution. According to this decision tree, acceptance criteria should be set up with solid dosage forms and dosage forms containing undissolved particles if particles size is critical to dissolution, solubility, bioavailability, processability, stability, content uniformity or product appearance. Particle size analysis, like any process analytical tool (PAT) can be off-line or in-line. Off-line particle sizing involves removing the sample, separating it from the production line and then performing analysis. In-line particle sizing, on the other hand, involves the sizing of the sample whilst in the production process, and thus the sample is not removed from the production stream (FDA, 2004). Examples of off-line methods include light and electronic microscopy, sieving and laser diffraction methods. Focus beam reflective measurement (FBRM) is an example of an in-line method that has attracted much attention in recent years due to the ability of real-time tracking particle growth and particle size changes as the process evolves. This tool is of great importance in crystallisation as it offers precise control of crystals size (Chew et al., 2007).

Each particle technique has its own advantages and limitations. For example, the amount used in scanning electron microscopy is very limited and does not represent the whole population of particles that exists in the powder bed. Laser diffraction also

has its cons, including the assumption of considering particles as spheres which is not always the case with powders. In fact, powders can consist of both spherical and irregular-shape particles (Eshel et al., 2004). In addressing these limitations, a variety of particle sizing techniques are used in this thesis.

Particle size and shape descriptors are used to compare pharmaceutical powders. As these descriptors are used extensively in this thesis, it will be discussed in more details.

D [v,0.90], D[v,86], D [v,0.5], D[v,0.16] and D[v,0.10] have been used throughout the thesis which represent percentile points of the 90%, 86%, 50%, 16% and 10% of the undersize particle size distribution, respectively. Figure 1.4 describes D [v,0.90], D [v,0.5] and D[v,0.10], which are the three commonly used descriptors in the pharmaceutical industry. D [4,3] has also been used throughout our thesis, which links particle quantity and weighing. D [4,3] is defined as a volume-weighted mean diameter and can be calculated using equation 1.5 (Merkus, 2009):

$$D[4,3] = \frac{\sum n_i D_i^3}{\sum n_i D_i^4} \qquad \textbf{Eq. 1.5}$$

Where n_i is the number based frequency of a specific particle in a specific class i, which have a mean diameter Di.

Another descriptor that is usually used is the SMD which is the surface weighted (or Sauter) mean diameter and calculated using equation 1.5 (Merkus, 2009)

$$SMD = \frac{\sum n_i D_i^3}{\sum n_i D_i^2}$$ **Eq. 1.6**

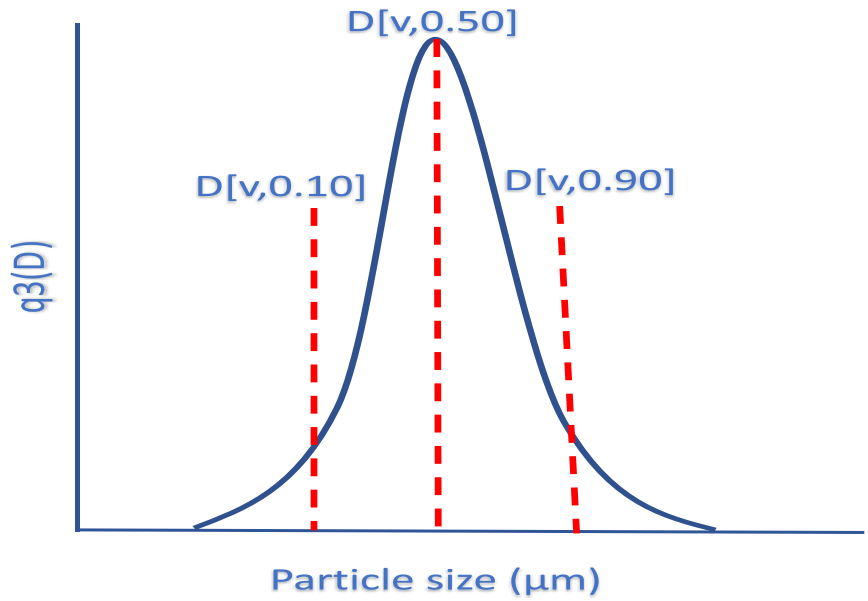

Figure 1.4 Illustrative description of D [v, 0.10], D [v, 0.50] and D [v, 0.90]. q3 (D) is the Fractional volume density distribution

In terms of particle shape descriptors, these descriptors can be classified into two main categories; those that can be derived from those the diameter of a circle equivalent to projected area (EQPC) or Feret diameter. EQPC diameter is the diameter of the equivalent sphere . Sphericity (s) is the main particle shape descriptor that used in describing particle shape based on EQPC. This calculation mode is preferable when dealing with a spherical particle. Feret's diameter, on the other hand, is more appropriate when dealing with non-spherical diameters and Aspect ratio (AR) is a

characteristic shape descriptor to describe these particles. This diameter is illustrated in **Figure 1.5**(Yu & Hancock, 2008).

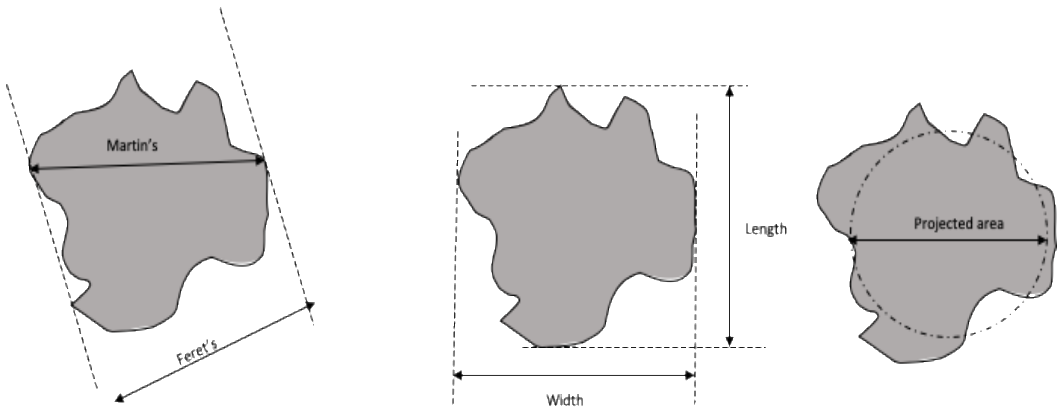

Figure 1.5 The differences between feret's diameter, martin's diameter, length, width and projected area adapted from (Yu & Hancock, 2008)

Sphericity values are usually between 0-1 where particles of 1 is a typical sphere. Particles with a smaller value of sphericity are considered to have an irregular shape. Aspect ratio (AR) values, on the other hand, give us an indication of how particles are elongated and have a range between ($0<AR \leq 1$) (Sympatec, 2018).

In this thesis, both sphericity and aspect ratio descriptors are used. (S10,3), (S16,3), (S50,3), (S84,3), (S90,3) and (S99,3) are percentile points of the 10%, 16%, 50%, 84% ,90% and 99% of the particle shape distribution. S refers to shape factor and has been used with both sphericity and aspect ratio descriptions (Sympatec, 2018).

1.2.1.1.1 Effect of particle size on the dissolution behaviour

In the case of oral solid dosage forms and in order for the drug to exert its biological activity, tablets should disintegrate, then the disintegrating tablets should deaggregated to allow drug dissolution before it is being absorbed the systemic circulation (**Figure 1.6**)

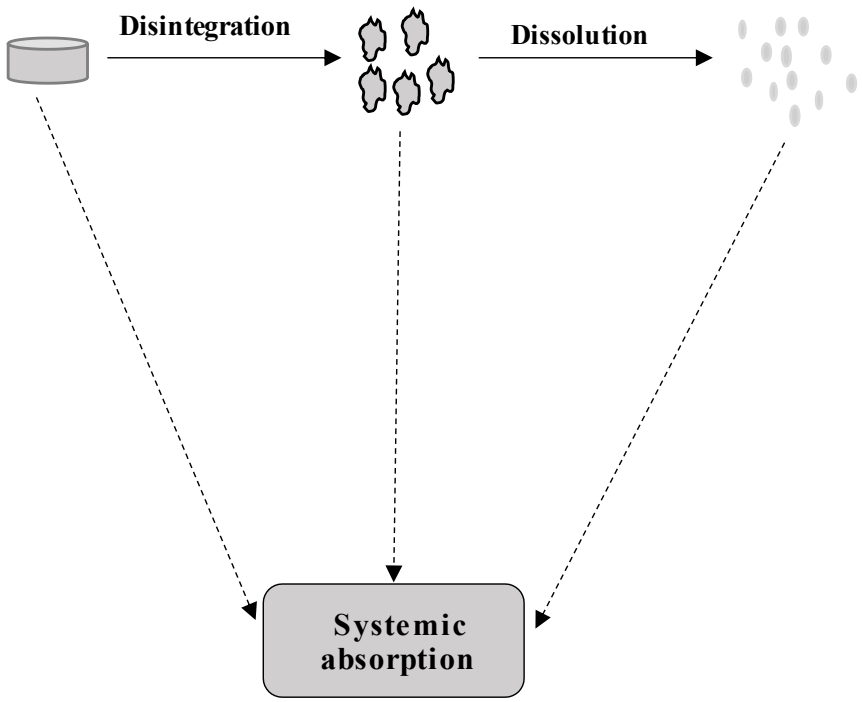

Figure 1.6 Schematic diagram of systemic absorption of APIs

Factors affecting drug dissolution phenomena have been described by the Noyes-Whitney equation (equation 1.7). Noyes–Whitney proposed an equation for predicting drug dissolution based on the physicochemical properties of the drug studied. According to this equation, drug dissolution is affected by surface area changes. An

increase in the surface area leads to an increase in the water saturation on the surface of drug particles. This, in turn, enhances the dissolution rate, which therefore results in an improvement in bioavailability.

$$\frac{dc}{dt} = \frac{DA}{h}(Cs - C) \qquad \textbf{Eq. 1.6}$$

Where dc/dt = rate of drug dissolution at the time (t), D=Diffusion rate constant, A = surface area of particles, Cs = drug's saturated solubility, and C is the concentration of drug in bulk, and h is the thickness of the stagnant layer

To increase surface area; several strategies could be used, such as:

1- Decreasing particle size by milling: reducing particle size will increase surface area and consequently enhance the dissolution rate.
2- Manipulating particle shape.

Decreasing particle size is important to enhance the dissolution rate of active pharmaceutical ingredients, especially when a drug belongs to Class II biopharmaceutical classification system wheresolubility is the rate-limiting step for dissolution.

A considerable body of literature has reported the effect of particle size changes on the dissolution and consequently the bioavailability of pharmaceutical materials. Jinno et al. (2006) investigated the effect of particle size reduction on the dissolution and bioavailability of cilostazol, a BCSII drug. Particle size reduction was achieved using hammer milling, jet milling or spray drying. The dissolution behaviour of these three formulations (hammer milled, jet milled and spray dried) was investigated using both water and biorelevant media (simulated intestinal fluid). Using water as a medium, dissolution profiles showed that as particle size decreased (comparing hammer milled and jet milled formulations which had a median particle size of 13 µm and 2.4 µm, respectively) , the amount of drug dissolved increased. A similar trend was observed using biorelevant dissolution media. Bioavailability studies showed a significantly enhanced bioavailability of cilostazol, using spray-dried formulations. However, jet-milled and hammer-milled formulations did not differ significantly in bioavailability. Chu et al. (2012) examined the dissolution kinetics of four size fractions of various poorly soluble drugs. The four size groups studied were <45 µm, 45-150 µm, 150-250 µm, and 250-600 µm. As expected, the amount of drug dissolved increased as particle size decreased. A linear correlation was obtained between the mean dissolution time (MDT) and the mean particle size of the APIs studied. MDT increased as particle size increased, indicating the importance of controlling particle size in the performance of oral pharmaceutical dosage forms However, reducing particle size does not always guarantee an enhanced dissolution and sometimes can have a negative effect on the dissolution rate. Mosgarraf and Nystrom investigated the effect of particle size and

shape on the dissolution rate of various active pharmaceutical ingredients and suggested that micronisation is not always sufficient to increase the dissolution rate. A study found that decreasing particle size did not always increase the dissolution rate mainly because of differences in particle shape for powders with a similar particle size. Glibenclamide and barium sulphate, for example, showed significant differences in dissolution profiles despite having similar particle size distribution profiles. Gibeniclamide and barium sulphate had a mean particle size of 1.84 µm and 1.77 µm, respectively. The surface specific dissolution rate corrected for solubility for these two drugs were 2.53 and 1.63, respectively (Mosharraf & Nyström, 1995). Finholt et al. (1974) reported that decreasing particle size has led to a decrease in the dissolution rate of some active pharmaceutical ingredients. This was attributed to poor wetting properties of some APIs, smaller effective surface area, which will, in turn, lead to a lower dissolution rate Effect of particle size on the drug release of sustained and controlled release formulations

Modified release dosage forms are defined as dosage forms where the time and/or rate of release is drug substance in the formulation is altered. These modified release dosage forms can be classified as; extended-release dosage forms (two-fold decrease in dose frequency), delayed-release dosage forms (time-dependent releases), targeted release dosage forms (physiological site dependant release) and orally disintegrated tablets (disintegration occurs in the mouth cavity). Extended-release dosage forms can be controlled release, sustained release and long-acting drug product (Leon Shargel, 2012).

The effect of particle size of both drug and excipients on the drug release behaviour of modified pharmaceutical systems have been studied extensively. Heng et al. examined the effects of particle size and concentration on the release behaviour of swellable hydrophilic matrix tablets using aspirin as a model drug. Matrix tablets were prepared using different size fractions of HPMC. The mean particle size of aspirin was also controlled and remained at around 58 μm in all formulations to minimise its effect on the dissolution rate. These formulations were further compressed into 350 mg tablets, and the release behaviour was studied using the USP II dissolution apparatus. Both particle size and the concentration of HPMC used in the study were critical factors in affecting these the drug release behaviour of tablets. In general, an inverse correlation was observed between particle size of HPMC and the release behaviour of aspirin from matrix tablets. However, the degree of this change was also dependent on the concentration of HPMC. The mean particle size of 113 μm of HPMC was a critical point where, below this point, the particle size effect had less impact on the release behaviour of aspirin tablets. This is mainly because below 113 μm, the mechanism of drug release involved was fit with a first order kinetic with a combination of erosion and diffusion as controlling factors of drug release from the matrix.

On the other hand, formulations containing a mean particle size of HPMC of more than 113 μm showed that aspirin release behaviour decreased as the particle size of HPMC increased. Results also showed that particle size changes have no effect on the release mechanism of aspirin tablets, with other factors such as viscosity, porosity, and tortuosity affecting the release mechanism (Heng et al., 2001). These observations

were in agreement with previous researches on HPMC matrix tablets (Mitchell et al., 1993; Velasco et al., 1999)

Similar research was conducted using alginate sodium instead of HPMC. Liew et al. (2006) examined the effect of sodium alginate particle size on the drug release behaviour of alginate-based matrix system. Seventeen grades of sodium alginate were obtained by both sieving and cryogenic milling were used in this study. A laser diffractometer was used to particle size these grades. Results of particle size analysis showed that particle size ranged between 41µm and 241 µm. The study showed a good correlation between the particle size and the dissolution parameters at a 10 % concentration of alginate sodium. In general, as particle size decreased, the time taken to achieve 25 % of drug release increased until particle size reached 80µm . A similar trend was observed with the time taken to achieve 75 % of drug release. As particle size decreased, the surface area increased and ultimately, the number of particles hydrated upon water contact. This increased alginate hydration and ultimately resulted in decreasing dissolution parameters. Furthermore, drug release sensitivity to particle size changes increased as alginate concentration increased between 10% and 30%. For example, the dissolution parameters of >200 µm fraction were doubled when the alginate concentration increased from 10% to 30 %. However, as sodium alginate concentration moved between 30-50 %, the effect of particle size was less evident.

Sadeghi et al. (2004) investigated the effect the particle size of eudragit-propranolol solid dispersions had on the drug release of propranolol. The study showed that

reducing the mean particle size of solid dispersions used to ~125 µm resulted in a significant reduction of the amount of drug released. However, below 125 µm, the effect of particle size reduction was insignificant. These findings were also consistent with previous studies conducted on propranolol (Dabbagh et al.,1996) and pseudoephedrine (Katikaneni et al., 1995) modified release systems.

The particle size effect of xanthan gum on the release behaviour of ibuprofen was dependent on the concentration of xanthan gum used. At 10 % and 20 % concentration, the effect of particle size on the release behaviour was insignificant. However, on using 30% of xanthan gum in the formulation, the release behaviour was significantly dependant on the particle size of xanthan gum. As the particle size of xanthan gum increased, the ibuprofen release increased. On the other hand, as particle size decreased, the drug release decrease and more sustainable released was achieved. This can be attributed to the ability of fine particles to hydrate more quickly than the coarse particle (Verhoeven et al., 2006)

Not only the particle size of the matrix-forming material is an essential factor affecting the release of the drug, but also channelling agent, which is sometimes incorporated in modified release systems. Three channelled agents (NaCl, mannitol, and Emdex) with different particle size fractions were used to assess the effect of particle size of these agentson the release behaviour of methylene blue-containing core. A core consisting of a drug and a coating layer of Eudragit RS100 and one of the channel agents were formulated and compressed using a two-step compression method. This

study illustrated the importance of the particle size of the outer layer on the release behaviour of the drug. The study showed that steady release and better zero-order release could be achieved using smaller particle size fractions of channelling agents. The study also suggested that as the particle size of each channelling agent increases, the time required to release the drug studied decreased, suggesting that using a small particle size of the channelling agent will extend the release of the drug studied. This example illustrates how vital to control particle size, especially when formulating targeting oral dosage forms (González-Rodríguez et al., 2001).

The effect of particle size on drug percolation in modified release systems has been studied by Caraballo et al. (1996).Leuenberger (1982) previously defined percolation with two thresholds; lower percolation threshold, which is defined as critical porosity of matrix tablets below which the drug is encapsulated within the matrix and will result in an incomplete release of the drug, and upper percolation threshold, which can be obtained matrices followed Higuchi release and is defined as the volume fraction of the matrix substance which is required to keep the system intact. Caraballo et al. (1996) found that increasing particle size mean diameter of a model drug in a non-swellable acrylic polymer system used as a matrix former has increased the drug percolation thresholds. A linear regression relationship was observed between drug particle size and percolation thresholds.

1.2.1.1.2 Effect of particle size on the mouthfeel

Controlling particle size is of great importance when designing oral disintegrating tablets (ODTs). Particle size less than 200µm is considered the size that does not cause any mouthfeel (Mizumoto et al., 2008). Furthermore, Kimura et al. (2015) did a systematic study on the effect of particle size changes on mouthfeel using healthy volunteers. A visual analogue scale (VAS) was used to conduct the study where granules were placed in the mouth for 60 s before spitting it out, and the feeling response was recorded depending on the roughness. Results of this study show that as particle size increased, VAS scores increased. This indicates the importance of controlling the size of initial particles , especially when designing oral disintegrating tablets .

1.2.1.1.3 Effect of particle size on the bioperformance of dry powder inhalers

Dry powder inhalers usually consist of a drug in the micronised form (1-5 µm) and a carrier which usually lactose. Depending on the disease being treated and the pathology of the disease itself, the particle size of the drug should be optimised to be either in the lower range of (1-5 µm) or the higher range of (1-5 µm). For example, in asthmatic patients where the proximal airway is more critical than distal alveolar deposition, the particle size of bronchodilators (3-5 µm) are more efficient than smaller particles of the range of (1-5µm) and therefore, it is vital to control the particle size of APIs used as bronchodilators to improve inhaled drug therapy (Usmani et al. , 2005). On the contrary, in some pulmonary diseases where distal inflammation occurs,

it would be essential to target distal alveolar disposition and therefore, the particle size of anti-inflammatory APIs such as corticosteroids should be in the lower range of (1-5 µm) (Martin, 2002).

As seen from previous examples, controlling the particle size of the API is very important, especially when targeting either the proximal or distal part of the lungs. In addition to API particle size, carrier particle size is very crucial to a successful dry powder inhaler (DPI) formulation. A study by Islam et al. (2004) showed that as lactose particle size decreased, the fine particle fraction (FPF%) of Salmeterol Xinafoate increased It is also essential to control the amount of lactose fines within a dry powder inhaler formulation. Incorporation of a small amount of fines has shown to enhance de-aggregation (Shah & Misra, 2004), decrease electrostatic chargers (Bennett et al. 1999), decrease cohesiveness between drug particles and consequently improve performance of dry powder inhalers (Ibrahim et al., 2000).

1.2.1.2 The effect of particle size on manufacturability and processing of pharmaceutical dosage forms

1.2.1.2.1 Effect of particle size on the flow of pharmaceutical powders

Two main forces affect powder flow: driving forces which consists of gravitation, powder mass and the angle of inclination of the powder to any bed and dragging forces which are cohesion forces between similar surfaces, adhesion between unlike surfaces, water bridges and mechanical interlocking, and electrostatic forces. Powder will be

free flowing if driving forces were much more than dragging forces (Figure 1.7). Poor powder flow therefore occurs when dragging forces are the primary forces in the powder bed (Gaisford & Saunders, 2013). Powders thus ranked as “poorly flowable” may have problems with die- filling before compression (Chattoraj & Sun, 2018). On the other hand, with “good powder flow”, formulators can ensure uniform packaging and constant die-filling. Also, sufficient powder flow is vital to prevent tablet capping and lamination as poor powder flow can cause air trapping and consequently capping and lamination of produced tablets. Inconsistent powder flow may increase the number of fine particles which may in turn result in an increase in die-wall friction which will cause lubrication problems (Aulton & Taylor, 2013).

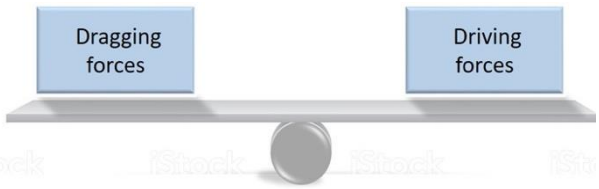

Figure 1.7 Forces affecting powder flow

Factors affecting powder flow can include particle properties such as particle size (Hou & Sun, 2008; Liu et al., 2008), particle size distribution (Liu et al., 2008), particle shape (Fu et al., 2012; Liu et al., 2008), surface properties (Jallo et al., 2012; Spillmann et al., 2008; Yang et al., 2005; Zhou et al., 2011) and moisture content (Lumay et al., 2016)..

As particle size increases, the effect of gravitational force will increase. This will lead to a favourable balance toward driving forces. As a general rule, powders with more

than 250 μm will not have any flow problems (Aulton & Taylor, 2013). On the other hand, decreasing particle size will result in increasing cohesion forces between particles as interfacial interaction between particles increase. This will, in turn, shift towards an increase in dragging forces which in turn leads to poor powder flow (Gaisford & Saunders, 2013). Hou and Sun (2008) quantified the effect of particle size on flow using a ring shear tester. Eleven grades of microcrystalline cellulose (MCC) were characterised. Results showed that as the particle size of MCC decreased, the flow function coefficient (FFC) value decreased. A smaller value for FFC is an indication of poor powder flow. A similar trend was observed with elongated MCC grades, spherical MCC grades and silicified MCC grades. Particle size distribution is also a critical parameter for powder flow. In fact, flowability of powder with a narrow particle size distribution increases as particle size increases. Powders with a similar median particle size was shown to improve flowability as particle size distribution narrowed (Liu et al., 2008). It is also worth mentioning that different size fractions of the same powder may behave differently in terms of flow when comparing it to the bulk material. As mentioned above, particle size increase will generally improve flowability. However, there are some cases where finer particles have showed a better flowability than coarser particles especially when these powders have a different particle size distribution. Liu et al. (2008) found the finest size fraction (median particle size of 39.9 μm) had a better flowability than bulk ibuprofen (median particle size of 70 μm) used in their study. This was due to their narrow particle size distribution when compared with the bulk ibuprofen powder. This emphasis the fact

that powders with a narrow particle size distribution but smaller particles may flow better than larger particles but with a wider size distribution .

Particle shape is another important factor that affect flow and this was highlighted earlier in the section 1.2.3.17 of this thesis

Modification of surface forces by coating surface with different guest particles have been shown to alter flow properties of pharmaceutical materials. Cohesive corn starch particles were coated with a different particle size of nano-silica. The resulting powders were characterised using a Hosokawa powder tester to determine the angle of repose. Depending on the coating device used, the mean particle size of silica used, and the amount of silica and processing time, the flow was altered. Larger particles of nano silica (~500 nm) did not improve the flow. This was attributed to large particles being unable to reduce van der Waals forces between the corn starch particles. However, smaller particles of nano (average particle size of 20 nm) silica showed a decrease in the cohesive forces between corn starch which resulted in improving the flow of corn starch (Yang et al., 2005). Similar findings were observed when using magnetically assisted dry coating of some APIs. Similarly to previous studies, dry coated particles showed a positive improvement in flowability when compared with their non-coated counterpart (Jallo et al., 2012). The flowability and surface energy of lactose treated by plasma-enhanced chemical vapour deposition (PECVD) were investigated. This study showed that processing parameters such as monomer flow rate, radio frequency (RF) power and oxygen to monomer ratio plays an essential role in the flowability of lactose powder. Treated powders showed an improvement in flow

by a factor of 3.1 Though authors proved that this improvement of flow was primarily due to plasma-induced changes in surface topography, a changing of processing parameters showed a correlation between flow and surface free energy (Spillmann et al., 2008). Zhou et al. investigated the effect of mechanical lubricant coating on the flow of lactose particles. A reduction of powder cohesion properties was observed, and a particle shape change towards a more spherical shape was observed using scanning electron microscopy (SEM) and supported by Brunauer–Emmett–Teller (BET) surface area. A chemical surface modification was also been observed and confirmed by both Time-of-Flight Secondary Ion Mass Spectrometry (ToF-SIMS) and X-ray photoelectron spectroscopy (XPS). This modification of both physical and chemical surface properties of lactose particles thus altered the flowability of lactose powders (Zhou et al., 2011).

Moisture content also plays an essential role in the flow of pharmaceutical materials. When the moisture content is very low, particle-particle friction shows an emergence of electrical charges which may increase the cohesiveness of the powder. This may result in a drive toward poor powder flow. On the other hand, when the powder is placed in a high humidity environment, liquid bridges may be formed which can result in an increase in cohesive forces leading to a poor powder flow (Figure 1.8) (Lumay et al., 2016).

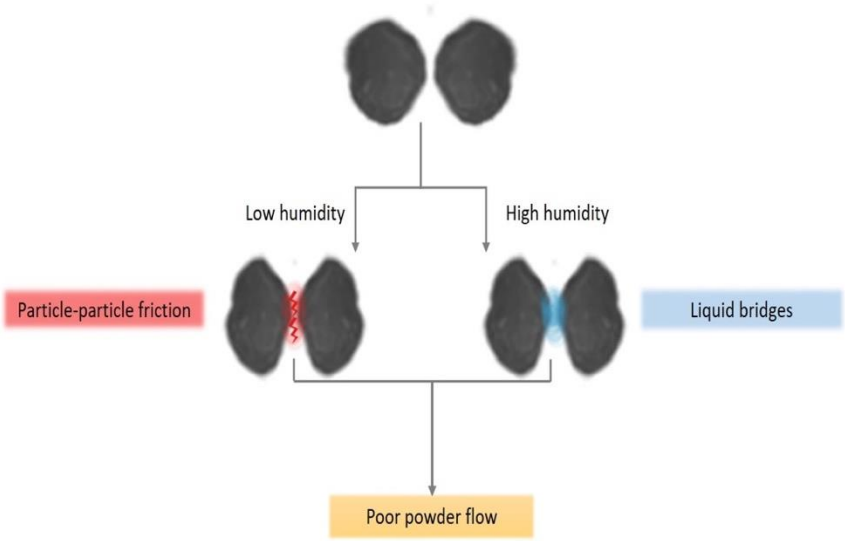

Figure 1.8 The effect of moisture on powder flow adapted from (Lumay et al., 2016)

Formulation factors also have an important effect on flow. In fact, one of the traditional approaches used to improve flow is the addition of glidant or flow activators. Powder flow activators work by reducing the cohesion and adhesion of powders. Among these flow activators are colloidal silicon dioxide, magnesium oxide, silicon coated talc and silicon coated sodium carbonate (Aulton & Taylor, 2013). With its small particle size and large surface area, colloidal silicon dioxide has an optimal flow characteristic and has been used to improve the powder flow of many pharmaceutical dosage forms (Sheskey et al., 2017). York investigated the effect of fine silica, magnesium stearate and purified talc on the flowability of lactose and calcium hydrogen phosphate. Fine silica showed a superior capability of improving powder flow in comparison to magnesium stearate and purified talc (York, 1975b). Similar findings were observed with Goh et al where an addition of lubricant tended to improve powder flow (Goh et al., 2018).

Wet or dry granulation also improves the flow behaviour of pharmaceutical powders. In both methods, agglomerated powders have a larger isodiametric particle size compared with the cohesive powders which has an irregular shape and smaller particle size. This causes particles to flow better (Aulton & Taylor, 2013)

1.2.1.2.2 Effect of particle size on mixing

As discussed in section (1.1.2), APIs with smaller particle sizes may have a higher surface area. This in turns results in more drug being absorbed through the gastrointestinal tract and hence a higher bioavailability. However, pure APIs are usually not administered alone, and they need to be mixed with other excipients to improve the manufacturability of these APIs. Therefore, ensuring mixture stability within a powder bed is critical and vital when designing a successful dosage form. Mixture uniformity is critical to achieving both content uniformity and weight uniformity, especially when dealing with a low dose of API. Swaminathan & Kildsig (2002) evaluated mixtures stability of aspirin using three grades of lactose. A mixture of lactose and aspirin was prepared using three size fractions of lactose: 103µm, 60µm and 36µm. Swaminathan and Kildsig found that as the particle size of lactose decreased, mixture stability decreased with agglomerates of drug and lactose particle were observed with a mixture contains 37µm size fraction of lactose. Decreasing the particle size of lactose resulted in an increase in both cohesiveness and coefficient of variation of lactose powder and ultimately induced segregation.

As mentioned before, as particle size decreases, the cohesiveness of powder increases, and that will affect the choice of an appropriate mixer. Chowhan & Linn (1979) studied the mixing of cohesive drug with different size fractions of citric acid anhydrous. Depending on the size fraction used, it was concluded that a v-shaped mixer was suitable for mixing the cohesive drug with 424µm and 104µm size fractions of citric acid. However, the v-shaped mixer failed to mix the cohesive drug with micronised excipient with a mean diameter of 3.7µm. Instead, the cylinder shear mixer proved to be more appropriate for mixing cohesive drugs with the micronised excipient

Particle size variations within the mixture can also cause segregation. Coarse particles tend to roll down the surface of bulk powder, leaving fine particle behind. That is why it is imperative to control particle size during the manufacturing of pharmaceutical dosage forms. Smaller particle size tends to fill the gaps between larger particles and ultimately fall until segregation become apparent. Particle size variations can also promote trajectory segregation, and larger particle size will travel a distance relative to their mean diameter. Therefore, a larger particle will travel to the walls of the mixer, whilst fine particles will be concentrated in the centre (Venables & Wells, 2001). The frequency-domain photon migration (FDPM) technique was used to evaluate the effect of excipient particle size on the stability of the dual mixture. FDPM is an emerging optical technique that can complement the near-infrared technique to evaluate mixture stability. Results of this study showed that the absorption coefficient of the specific blend was dependent on both the particle size of the excipient and the

concentration of the API (Torrance et al., 2004). Nakumara et al. (2004) examined the effect of particle size change during trituration by colouring lactose particle with erythrosine. This study showed that the mixing degree is primarily affected by the particle size of initial components and mixing speed and time. Using 60 rotations has resulted in inhomogeneous mixtures for particle size less than 42 μm. However, the mixing degree expressed by the coefficient of variation decreases as particle size increases and rotation speed decreases

Rohrs et al. (2006) proposed a model that can be used to define upper and lower limits for particle size to ensure uniformity of mixing and consequently content uniformity for tablets and capsule. Equation 1.8 predicts the volume median diameter D[v,0.50] based on the coefficient of variation and the dose of the drug to ensure content uniformity is achieved.

$$d'_g = \sqrt[3]{\left(\frac{6\pi}{\pi.p}\right) e^{-4.5.ln^2}\sigma_g.\left(\frac{Cv}{100}\right)^2.10^3} \qquad \textbf{Eq. 1.7}$$

Where: C*v* = Coefficient of variation (RSD) of the dose (%), D= Dose(mg)

ρ= density of the drug (g/cc) and σg is defined according to equation 1.9

$$\sigma g = (\frac{da}{db})^{\frac{1}{za-zb}}$$ **Eq. 1.8**

Where da and db are the particle size, and za and zb are the z-values of the standard normal distribution at ath and bth the percentiles.

1.2.1.2.3 Effect of particle size on granulation

Studying the effect of particle size changes on granulation behaviour has attracted many scientists in the pharmaceutical industry. Particle size changes of resulted granules depend greatly on both the particle size and the mechanical properties of starting materials. The decrease or increase in the granular particle size was also dependent on both the mechanical properties of the API and the diluent used. For example, Shiraishi et al. (1995) used theophylline as a model drug to investigate various size fractions on tablet properties produced. Shiraishi et al (1995) found that the mechanical properties of tablets were improved by using small size fractions of theophylline. Research conducted by MacKaplow et al. (2000) showed that increasing the particle size of lactose particles resulted in larger and less porous wet granules. However, upon drying, the resulted dry granule size distribution was less sensitive to the initial particle size of lactose and more dependent on the liquid to solid ratio. This can be attributed to the ability of lactose particles to increase recrystallising lactose bridges that hold granules together. Increasing particle size of primary lactose was shown to have large consequences on the granule growth rate, granule porosity and wet granule size distribution.

Herting & Kleinebudde (2007) further investigated the effect of both theophylline and the initial particle size of MCC during the dry granulation process. The study proved a considerable increase in mechanical strength expressed by the tensile strength of tablets as the particle size of the initial materials decreased. The use of a smaller particle size fraction of MCC resulted in larger granules and better flowability. The study has also found that inadequate tensile strength observed with the dry granulation process can be mitigated by decreasing the particle size of initial materials. These examples illustrate the importance of controlling the particle size of the initial materials during both wet and dry granulation processes.

1.2.1.2.4 Effect of particle size on compression and compaction

Compaction is defined as an increase in the mechanical strength as compression force increases, while compression is defined as a decrease in the bulk volume resulting from the displacement of air between particles. Therefore, it is directly related to bonding and consolidation between particles which will ultimately affect the hardness and tensile strength of resultant compacts. On the other hand, compression directly correlates to the porosity and the surface area of powders. This will, in turn, have an effect on the disintegration and, to more extent, on the dissolution behaviour of tablets (Qiu et al., 2016).

To characterise the compaction of pharmaceutical materials, formulation scientists usually rely on three main graphs:

1. Tensile strength vs applied compaction pressure, which is referred to as tabletability
2. Solid fraction vs applied compaction pressure, which is referred to as compressibility
3. Tensile strength vs applied compaction pressure, which is referred to as Compactibility

In order for materials to deform and consolidate, they undergo a deformation mechanism. The consolidation process can be plastic, elastic or brittle. Elastic materials return to their original shape once compression is removed. A typical example of elastic materials is rubber. Plastic materials, on the other hand, deforms permanently once the applied pressure is removed. Cellulose is a commonly used pharmaceutical excipient that is plastically deformed once compressed. Fragmented materials or brittle materials are materials that fragment once compression pressure is applied. Dicalcium phosphate is a classic example of brittle material. Some materials, however, can behave with more than one consolidation mechanism. Visco-elastic materials, for example, are pressure defendant and before a specific pressure point will deform elastically and after specific pressure point will behave plastically. Pressure point where materials consolidation mechanism change is called the yield point. A typical example of visco-elastic materials in the pharmaceutical industry is starch. In addition, some materials can behave in a brittle-plastic fashion where materials are fragmented before the yield pressure point then deforms plastically after that point. Lactose is a typical example of brittle-plastic materials. Understanding the mechanical

behaviour of tablet formulation is very important during the tablet manufacturing process, and understanding the underlying factors that affect that deformation is therefore of significant importance for successful tablet manufacturing (Qiu et al., 2016)

Factors affecting deformation behaviour may include crystal form, particle size, particle shape, surface roughness and processing parameters. The effect of crystal form modification has been studied extensively by many researchers. Sun et al. showed that different forms of sulfamerzine produced tablets with different compressibility and tabletting performance. Form I crystals of sulfamerzine with flat layers were easier to compact than form II with a zigzag structure (Sun & Grant, 2001) (Sun, 2009). Karki et al. produced a co-crystal layered solid form of paracetamol to improve mechanical properties of paracetamol tablets (Karki et al., 2009). Upadhyay et al. showed that form II of ranitidine hydrochloride had better deformability and compressibility than form I, while form I showed poor compressibility but better tabletability at a specific compaction pressure (Upadhyay et al., 2013).

Particle size is another critical factor that may affect the deformation and manufacturability of pharmaceutical materials. Sun and Grant used different size fractions of L-lysine monohydrochloride dihydrate powder to investigate the effect of particle size on the mechanical properties of manufactured tablets. Results showed that smaller particles showed a higher tensile strength at the same compression force (Sun & Grant, 2001).

The effect of initial particle size on the mechanical properties of pharmaceutical tablets during compression has been studied extensively. This effect is highly dependent on both material properties and processing parameters such as tabletting speed. In most cases, powders with smaller particle size tend to produce a stronger tablet due to the increase in surface bonding between particles. However, some powders such as dicalcium phosphate and sucrose fragment extensively during compression, and the resulted mechanical properties are independent of the initial particle size of starting materials. Sun and Grant (2001a) studied the effect of initial particle size on tabletting behaviour (porosity, tensile strength and yield strength) of L-lysine monohydrochloride dihydrate powders. In terms of porosities, the study showed that larger particles produced tablets with lower porosities than smaller particles.

Furthermore, larger particle produced less porous tablets at the same compression force. In terms of tensile strength, particles with more than 355 μm diameter showed increased tensile strength as compression increases. However, particles with less than 355 μm required less compression force to reach a plateau of tensile strength. This can be attributed to the higher surface area of smaller particles and consequently better compressibility. Furthermore, particle larger than 595 μm showed a comparable value of tensile strength upon compression, indicating these particles undergo extensive fragmentation and decrease the effect of initial particle size differences. In terms of yield strength, compacts produced from larger size fractions showed higher yield strength values upon compression (Changquan Sun & Grant, 2001a). Narayan & Hancock (2005) studied the effect of particle size changes on the roughness of

pharmaceutical tablets using different fractions of MCC and lactose monohydrate particles. Results showed that as particle size increased, the surface roughness expressed by Sq values increased as particle sizes of both MCC and lactose increased with Sq values for lactose increased more rapidly compared with MCC corresponding Sq values. Furthermore, a correlation found between TS and Sq values for both MCC and lactose particles. Smoother compacts with lower Sq values and smaller particle size produced higher values of tensile strengths.

Particle size changes can also affect the bonding mechanism between particles. Adolfsson et al. studied a range of pharmaceutical materials with different compaction properties to investigate the effect of material type and particle size on tensile strength. Adolfsson et al. (1997). classified materials depending on the intra-particulate structure of pharmaceutical material studied. The study investigated the effect of particle size changes on the tensile strength of compacts. When the inter-particulate structure was dominant by ionic bonds such as in sodium chloride, an increase in tensile strength was observed as particle size decreased. This can be attributed to an increase in the surface area upon particle size reduction and, consequently, increased bonding. However, compression of the larger size fractions of sodium chloride resulted in compression stress being localised, which induced movements and, hence, the formation of solid bridges. When the intra-particulate bonding structure was formed by ionic bond and weak distance forces such as those observed with dicalcium phosphate, a higher tendency of fragmentation did not localise pressure upon compression. Therefore, high local stresses were not created due to the absence of

inter-particulate contact points. Decreasing particle size of dicalcium phosphate resulted in an increase in the number of particles, and consequently, interlocking due to the surface nature of dicalcium phosphate was attributed to the possible intra-particulate bonding mechanism. If the intra-particulate structure was formed by covalent bonds and weak distance forces such as those observed with lactose and sucrose, neither particle size nor compression pressure seemed to affect the tensile strength. This could be attributed that bonding by solid bridges was unlikely to occur. Cabiscol et al.(2020) examined the effect of particle size on powder compaction and tensile strength using limestone as a powder model. The study investigated particle size changes on the mechanism of cohesion, interlocking and electrostatic force on tabletting behaviour. Cabiscol et al. (2020) found that as particle size decreased, the tensile strength increased until particle size reach less than 10 μm when tablet tensile strength become insensitive to size variations. Garekani et al.(2001) examined the effect of particle size changes on the compression behaviour of paracetamol tablets. The study compared two fractions of paracetamol in terms of yield strength, elastic energy and plastic energy. The study found that the primary mechanism involving in the compression is fragmentation with larger particle size fraction undergos more fragmentation than smaller particle size. Furthermore, smaller particle size fraction showed more elastic recovery and elastic energy in comparison with the larger particle size fraction. This can be attributed to larger fraction undergo extensive fragmentation and increase bonding due to the formation of new particles during fragmentation

Kushner et al. (2011) examined the effect of excipient material properties variation on drug product quality attributes of tablets produced using roller compactor. Different grades of MCC and spray dried lactose were used. MCC acted as ductile filler while lactose served as brittle one. The study found that as the mean particle size of starting material increased by 32 µm, the mean particle size diameter of blend and granules produced increased by ~30 µm. This increase has enhanced the flow of both blends, and granulated powder measured using ring shear tester and expressed in the term of flow function coefficient (FFC).Furthermore, Kushner et al. (2011) studied the effect of particle size of magnesium stearate on the ribbon tensile strength and tablet hardness. A decrease of magnesium stearate mean particle size by 19 µm resulted in an increase of tablet hardness and ribbon tensile strength by 18-28%. Shah & Augsburger (2002) examined the effect of particle size of sodium starch glycollate on the water uptake and settling volume. Their research concluded a strong correlation between the particle size of sodium starch glycollate and disintegration behaviour. As the particle size of sodium starch glycollate decreased, both liquid uptake and settling volume increased and consequently, the disintegration time decreased. A similar trend was observed with croscarmellose (CSS). Similarly, a noticeable change in CSS particle size has resulted in a change in the swelling behaviour of CSS and, ultimately, the disintegration time. An increase in particle size resulted in an increase in the swelling behaviour and decreased disintegration time (Zhao & Augsburger, 2006).

The lubrication efficacy of magnesium stearate is one of the critical parameters during tablet and capsule manufacturing. Haware et al. (2014) studied the effect of both

molecular and particle properties on the lubrication efficacy of bovine- and vegetable-derived magnesium stearate. The effect of particle size of magnesium stearate was dependent on the crystallinity of magnesium stearate itself. For an amorphous system, particle size does not affect the lubrication efficacy. However, particle size has a significant influence on the lubrication efficacy of crystalline form. A decrease in particle size will increase the surface area of magnesium stearate, and as a result, better lubrication is achieved. These findings were consistent with previous literature (Dansereau et al., 2005).

1.2.1.2.5 Effect of particle size on coating

Coating is one of the crucial steps in pharmaceutical manufacturing, especially when designing a controlled release dosage form. Physical properties such as particle size of additive materials is one of the essential factors that prevent membrane rupture of the coater. Yao et al. (1998) studied the effect of particle size of hydroxypropylcellulose (HPC) as a coating polymer on the dissolution rate of theophylline tablets. Decreasing the particle size of HPCs resulted in decreasing the dissolution rate of theophylline tablets indicating the importance of particle size on the integrity of film formed upon coating. Felton & McGinity (1999) investigated the effect of pigment particle size on the adhesion on Eudragit L polymer in coating formulations. The adhesion of the pigment was observed to increase as the particle size of yellow iron oxide and mica pigment decreases. This was explained as using smaller particles of the polymer may enhance the interfacial contact of the polymer

which may ultimately enhance the adhesion of the pigment. Dry coating is also sensitive to particle size variation effect. Yang et al. (2020) investigated the effect of using different size fraction of cellulose acetate on the film formation and its visual appearance. The study found that deposited particles were able to produce a uniform film with no boundaries when the size fraction of cellulose acetate was below 26.7µm. The efficacy of the film formed was further investigated by dissolution testing using a model drug. Dissolution testing confirmed the differences between different particle size fractions with below 26.7µm showed a zero-order drug release with no dose-dumping. This phenomenon can be explained by using Huang's equation (equation 1.6).

$$t = \frac{k\mu dp}{\gamma} \qquad \textbf{Eq. 1.9}$$

Where k and γ are constants, dp is the particle diameter, µ viscosity of coating powder, and t is the time for two particles to coalesce during coating.

According to equation 1.10, as particle size increases, the time required for particles to coalesce increases, leading to the formation of a rough non-uniform film. On the other hand, as particle size decreases, the time required to make smooth and uniform film decreased (Huang et al., 2015)

1.2.2 Effect of particle size on the stability of solid dosage forms

Particle size changes within formulations during storage can be a problem for stability, especially for nanosuspensions and microemulsions. De & Robinson (2004) studied particle size and temperature (4°C-50°C) on the physical stability of nanosphere and microsphere. The study found that aggregation increased as temperature increased from 4 °C - 50 °C with the highest aggregation observed with the smallest PLGA particles that had a mean particle size of 266nm. However, the extent of aggregation decreased as particle size increase between 300 and 2000 nm. These changes in size were not accompanied by any changes in the thermograms of particles indicating no chemical or thermal degradation occurred.

The effect of particle size on the physical and chemical stability of the amorphous simvastatin system was studied by Zhang et al. (2009). Amorphous simvastatin was prepared using both quench-cooled and cryo-milling methods. The quench cooled amorphous system was prepared using two fractions of simvastatin. One fraction of 150-180 µm and another was less than 10µm. The solubility study indicated that the particle size has a negligible effect on the solubility of the amorphous system prepared using the quench cooling method. However, the amorphous system prepared from the quench cooled method showed a higher solubility profile than the cryo-milled one. In terms of physical stability, the amorphous system prepared from the larger particle size fraction showed the highest stability with the slowest crystallisation rate. This indicates the importance of the particle size of the starting materials on affecting the

physical stability of amorphous systems which sometimes can be overlooked or neglected.

The influence of particle size on the stability of metered-dose inhaler was studied by Berry et al. (2004). Different APIs with a mean particle size range from 1.14-1.77 µm was used in this study. This study showed that as particle size increased from 1.14 µm to 1.77 µm , the dose recovered in cascade impactor decreased from 99 % to 94 %, respectively, and the corresponding aerodynamic particle size increased from 2.58 µm to 4.38 µm. The study showed a linear relationship between the percent of fines which had a particle size of less than 3 µm and the percent of fine particles. As this percentage of particle <3µm increased, the %FPF increased . The stability of API after two weeks of temperature cycles was also sensitive to API changes. Eliminating temperature cycles, no changes were observed in the percent of the dose recovered, %FPF and aerodynamic mean particle size. However, subjecting the formulation to temperature cycles, the batch with a larger particle size was more sensitive to changes in the %FPF and the mean aerodynamic diameter. An 18% decrease in %FPF and a 17% increase in aerodynamic diameter were observed for smaller particles. However, for coarse particles, the %FP decreased by 52% and the aerodynamic mean diameter was increased by 57%. This shift was attributed to being size-dependent particle growth and/or aggregation

As discussed, earlier, particle size is one of the key properties that may affect the performance, manufacturability and stability of pharmaceutical dosage forms. In

addition to particle size, particle shape is also considered as a key property that also has an effect on the performance, manufacturability and stability of pharmaceutical solid forms. The following sections will discuss that in more details.

1.2.3 Effect of particle shape on the performance of solid dosage forms

Particle shape has increasingly attracted the attention of the pharmaceutical community. Particle shape and crystal habit are two critical parameters that need to be controlled in all stages of drug discovery and development. This section will investigate the effect of particle shape on different aspects of drug discovery and development. This section will also give an insight into the importance of particle shape in some of these critical aspects. These include crystallisations, bulk powder properties, granulation and milling, compatibility and dissolution.

1.2.3.1 Effect of particle shape on the biopharmaceutical performance of oral and inhaled dosage forms

Studies on the effect of particle shape on dissolution have emerged recently due to advances in imaging techniques and quantifying particle shape descriptors more accurately. Literature data showed that particle shaped of APIs could have an effect of the surface area, dissolution diffusion layer, contact angle and dispersive free energy (**Figure 1.9**).

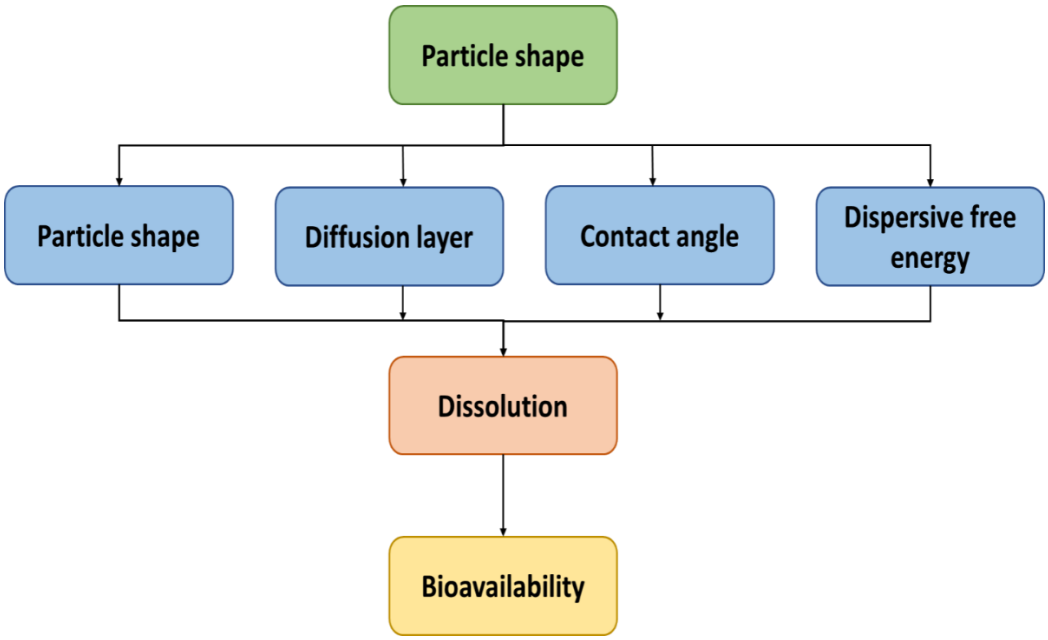

Figure 1.9 Illustration of how particle shape affects the dissolution behaviour of APIs adapted from Gou et al. (2015) and Modi et al. (2013)

Some literature examples include works conducted by Guo et al. (2015) and Modi et al. (2013). Guo et al. (2015) studied the effect of particle shape on the dissolution performance of lovastatin crystals. Rod-shaped lovastatin particles were prepared using nanoprecipitation, while spherical particle prepared using wet ball milling. These particles were further characterised in terms of particle size and crystallinity to eliminate their effect on dissolution. The particle sizing study has a similar hydrodynamic diameter. Differential scanning calorimetry (DSC) study confirmed that both needle and spherical shapes are in the same crystal state. However, the peak of DSC tends to be less intense than the unprocessed lovastatin. This can be attributed to decreasing particle size will increase Gibbs free energy and, as a result, will decrease the intensity of the corresponding peaks. Dissolution studies using phosphate

buffer of pH6.8 showed that the dissolution rate of rod-shaped particles is higher than the spherical ones. Guo et al. (2015) suggested that this can be attributed to two main factors; firstly, rod-shaped particle showed a higher surface area compared to the spherical one, and according to the Noyes-Whitney equation, increasing the surface area will result in enhancing the dissolution rate. Secondly, transmission electron microscopy (TEM) showed that the diffusion layer thickness around rod and spherical shapes are significantly different, with the former has a smaller diffusion layer. Decreasing the diffusion layer will achieve a faster diffusion and dissolution rate. Oral Bioavailability study using beagle dogs was aligned with the findings from the in-vitro dissolution study. Rod-shaped particles have higher oral bioavailability compared with spherical particles with Cmax for rod-shaped particles nearly doubled Cmax for spherical particles. This example indicates how important crystal shape is vital as that will affect both dissolution rate and bioavailability.

Celecoxib is another example that its crystal habit has altered in order to improve the dissolution rate. Celecoxib is a class II drug with low solubility and high permeability. Two crystal shapes of celecoxib were prepared by recrystallisation from toluene by changing the supersaturation and temperature. Acicular shape and plate shape particles were obtained and further characterised. The two shapes were further biopharmaceutical assessed. Crystallinity study using DSC showed that the two habits remain in the crystal form, with both have a sharp melting point of ~160 ºC. Particle size analysis showed that both shapes have a mean particle size of ~250 µm, indicating that particle size will not be a factor for these shapes to be different. Solubility study

showed that there are insignificant differences between the two shapes. However, contact angle measurement using sessile drop showed that the wettability profiles of those two crystals are significantly different. Using polar and semi-polar wetting solvents, plate particles showed a lower contact angle value when compared with the acicular particles. This clearly highlights that plate particles have higher wettability in both polar and semi-polar media. Further surface energy analysis showed that plate shape has higher polar surface energy than acicular shape.

In contrast, values of dispersive free energy were higher with acicular shape than plate shape. This was ascribed to the surface anisotropy and differences of hydrophilicity between crystal faces of each shape. As expected, dissolution profiles using water or phosphate buffer of these two shapes were significantly different. Plate shaped particles showed a higher dissolution rate compared with the acicular particles. Further bioavailability study was agreed with the dissolution study with plates habit showed higher values of area under the curve (AUC) and Cmax when compared with the corresponding values of the acicular-shaped particles (Modi et al., 2013)

1.2.3.1.1 Effect of particle shape in the crystallisation of APIs

Crystal shape control and optimisation are essential steps during the crystallisation and drying process. Insufficient control can lead to extended filtration and drying times or extra processing steps such as recrystallisation or milling. During filtration, cake filtration is one of the problems that could face crystallisation scientists because of the particle size and shape effect. Cake filtration is defined as a process that occurs

as a result of filtration of different shape and size of pharmaceutical materials and hugely affects the production cost of pharmaceutical powders. This phenomenon occurs when the slurry contains different particle size fractions of the material filtered. Larger particles tend to form a deposit at the top of the filter, and smaller particles held within the porous skeleton formed by larger particle. This formed cake will also experience a compression force resulting from the slurry above the cake formed. The influence of particle shape properties on cake resistance and compressibility during filtration was studied by Bourcier et al. (2016). Researchers precipitated both calcium carbonate and uranium oxalates particles into different shapes, including sphere, cubes, needle and plates. The effect of particle shape was further investigated quantitively by measuring compressibility, cake resistance and filtration time. Experimental studies found that particle shape was the second important factor after size affecting cake-specific resistance. Spherical particle, for example, showed a lower cake-resistance than plates. The study showed that as shape volume decreased, the cake-resistance increased (Bourcier et al.,2016). Furthermore, the impact of a shape-volume factor was less evident on compressibility. In terms of filtration time, the study showed that as pressure increased, filtration time decreased. Filtration time also increased as cake resistance increased. As filtration time increased, the production cost of pharmaceutical materials will be increased. This explains why particle shape on cake resistance has a significant impact on the cost of pharmaceutical powders produced by filtration. The higher the cake resistance, the longer it takes for the

powder to be filtered, which will ultimately increase the production cost of pharmaceutical powders (Bourcier et al., 2016).

Beck & Andreassen (2012) investigated how crystallisation conditions affect the crystal habit of calcium carbonate. Calcium carbonate was recrystallised in an aqueous solution at a temperature from 5 ºC to 90 ºC. Depending on the supersaturation and temperature applied, different morphologies were obtained. For example, at high temperature and low saturation, hexagonal, plate-like crystals were observed. However, as initial supersaturation increased, a flower-like crystal morphology was observed.

Different crystal morphologies tend to have different surface energy and cohesion values. A study conducted by Shah et al. (2014) investigated particle shape on both cohesion and surface energy. Mefenamic acid used in this study as a model drug. Mefenamic acid was recrystallised using solvents with different solubility and polarity. Recrystallisation study showed that crystals obtained from polar protic solvent have cubic crystal habit, while plate-like crystals were obtained using polar aprotic solvents. On the other hand, non-polar solvent produced needle-like crystals. The elongation factor of each shape was calculated using Morphologi G3. A wettability study using a sessile drop and conducted on a single crystal showed facets of mefenamic acid with different contact angles with faces (0 0 1) and (1 0 0) are the most hydrophilic. This has been attributed to the availability of hydroxyl groups on faces (1 0 0) and (0 0 1), which give these faces the highest values of hydrophilicity. ,

The surface energy study showed a correlation between elongation factor obtained from image analysis and surface energy values. Cohesiveness study showed that hexagonal cube-shaped particles showed to have eight times less cohesive than elongated needle-like particles. This observation was related to both surface energy and surface area. To eliminate the effect of surface area on cohesion, the surface area was normalised. The effect of surface energy on cohesion was also normalised by salination (Al-Chalabi et al., 1990). Removing the effect of energy surface area showed that needle-shaped crystals are ~2.5x more cohesive than hexagonal cubic shape crystals. This example indicates the importance of crystal habit on the cohesiveness of pharmaceutical powders.

1.2.3.1.2 Effect of particle shape in the drying of recrystallised API

Drying conditions tend to affect crystal habit and material properties of APIs. Kougoulos et al. (2011) studied the effect of of switching from tray drying to agitated drying on the particle shape of resulted particles . Particles produced using tray drying were soft, loose agglomerates. By using agitated drying, particles formed agglomerated particles. In addition, by changing the process parameters of agitated drying such drying temperature and agitated rate, materials bulk properties from both drying methods were significantly different. Agitated dried materials had more fine particles, higher bulk density, and higher specific surface area when compared with tray dried materials.. The effect of agitated drying on the crystal shape of KCl (Lekhal et al., 2003) and L-threonine (Lekhal et al., 2004) was studied in a water system .

Depending on the drying rates used, either attrition or agglomeration was observed. Attrition of crystals occurs when the drying rate is low, and/or shear rate is high. These conditions will guarantee that particle-particle collision will occur, and small crystal fragments will be produced. However, at higher drying rates, collision will decrease, and harder agglomerates will produce.

1.2.3.1.3 Effect of particle shape on the manufacturability and sticking propensity of pharmaceutical tablets

The effect of crystal shape on manufacturability and sticking of APIs was studied using ibuprofen as a model drug (Hooper et al., 2017). Ibuprofen was recrystallised using hexane, toluene, acetonitrile and ethanol. Crystal habits obtained were correlated with the polarity of the solvent used. Increasing polarity found to increase the shape regularity. For example, crystals obtained from hexane were needle/lath particles, where those obtained from ethanol were plate/prismatic shaped. Dynamic image analysis confirmed these findings. Increasing the polarity resulted in a shift in aspect ratios of crystals obtained with ethanol have the highest values of aspect ratios. X-ray powder diffraction (XRPD) and DSC studies confirmed that the crystallinity of the four crystal habits did not change. Surface energy results showed that there is a significant difference between crystal habits obtained from solvents used. Crystal habits obtained from polar solvents showed a higher particle surface energy when compared with particle recrystallised from non-polar solvents. A sticking study performed on four batches of ibuprofen showed that the sticking behaviour increased

as particle surface energy increased with particles obtained from polar solvent have a higher sticking propensity than particles obtained from non-polar solvents. A correlation between particles aspect ratio and sticking behaviour can be obtained. As the particles aspect ratio of particles increased, the sticking behaviour increased. Surface area results showed that the Brunauer-Emmett-Teller (BET) surface area surface area did not change significantly between the four recrystallised ibuprofen batches (Hooper et al., 2017). This study indicates that changes in sticking behaviour could be attributed to either surface energy or crystal habit. Nonetheless, it would be essential to investigate the degree to which particle shape or surface energy affects sticking. This could be achieved by using a salination method proposed by Al-Chalabi et al. (1990) and studied by Shah et al. (2014) to investigate the effect of particle shape and particle surface energy on the cohesiveness of pharmaceutical powders.

1.2.3.1.4 Crystal habit and tabletting behaviour

The tabletting behaviour of pharmaceutical powder is affected by crystal shape. Rasenack & Müller (2002) investigated the effect of both ibuprofen and paracetamol crystal habits on tabletting behaviour. Different crystal shapes of paracetamol and ibuprofen were prepared by a solvent change method. The resultant shapes were characterised and evaluated in term of mechanical properties. A T factor ($J.cm^4$) was defined and used according to equation 1.11 to evaluate differences between these shapes

$$T = Pd * Et * Fc * Fmax * Sfmax\ (\text{upper punch}) * e \qquad \textbf{Eq. 1.10}$$

Where Pd is the plastic deformation, Et is the total energy (Nm), Fc is the crushing strength (N), Fmax (KN) is upper punch force, Sfmax is the upper punch displacement (mm), and e is the volume of the tablet (cm^3). Rasenack and Muller supposed that tabletability would be better as the T factor increased. Plate-shaped particles of ibuprofen showed a higher T factor compared with needle-shaped habit. This was further confirmed by producing tablets with a minimum sticking using 90% ibuprofen content using the plate-shaped particles. For paracetamol, the values of different crystal habit were significantly different between different shapes. Small plates with the highest T factor value, followed by prismatic shaped crystals (Rasenack & Müller, 2002). Although this study gave a clear indication of the importance of how different crystal habits affect the performance of pharmaceutical powder, some flaws need to be highlighted in this research. Firstly, is the use of the T factor as a way to evaluate tabletability and the scientific rationale behind the equation presented in the study. Secondly, the researcher did not indicate if the observed difference in tabletability behaviour was attributed to particle size or particle shape or a combined effect.

The effect of crystal habit on the flow behaviour of both lubricated and unlubricated powders was evaluated by (Podczeck & Miah (1996). A ring shear tester was used to evaluate the flow of different pharmaceutical powders with different particle shape and size descriptors. In addition, the angle of internal friction, which represent the

friction between powder particles, was used to investigate the effect of particle size and shape. This study found that the flow factor depends on particle shape for unlubricated powder, while the angle of internal friction was dependent on both particle size and shape (Podczeck & Miah, 1996). Although this study compared different shapes, it would be more scientific to compare different particle shapes of the same powder rather than comparing different powders with different shapes. This because different powders have different mechanical properties and different values of plasticity, elasticity and surface energies which have previously found to affect the flow of pharmaceutical materials.

To address these issues, Hou & Sun (2008) used different MCC grades to investigate the effect of particle shape on the flow properties of MCC grades. Eleven grades of MCC was used in this study. Two of these grades were silicified in order to investigate the effect of surface modification on the flow. A clear correlation was obtained between particle size and flow function coefficient. Smaller particles tend to affect the powder flow adversely. Spherical shaped particles tend to flow better when compared with elongated ones indicating the particle shape significantly affect the flow behaviour.

Furthermore, the effect of surface modification on the flow was size-dependent. Smaller particle was shown to flow better when the surface is modified. However, larger particles did not improve the flow when the surface was modified (Hou & Sun, 2008). This study, however, did not quantitively evaluate the effect of particle shape

on the flow performance of pharmaceutical powder. The study used shape terms without using particle shape descriptors to relate particles shape to the performance of powder quantitively. It also did not identify the effect of particle size and shape from each other on flow. It would be more reasonable to do some kind of sieving and compare the same size fraction of particles with different shapes to eliminate the effect of particle size.

Kaerger and Price, (2004). studied the particle shape of paracetamol particles on both the flow and compressibility profiles. Paracetamol particles were prepared using both micronisation (milling) and novel engineered solution atomisation and crystallisation by sonication (SAXS). SAXS method is an electrospraying method that produces monodispersed particles collected in a vessel containing nonsolvent of drug used. The collection vessel is housed in an ultra-sonication bath . Paracetamol particles produced using the SAXS method were spherical and compared with the untreated particles and micronised particles with a needle shape morphology. The untreated particles showed to be larger than both the micronised and SAXS particles. Micronized and SAXS particles have a mean particle size between 2-6µm. The similarity in particle size profiles of those two grades is of great importance to eliminate the effect of particle size and investigate the effect of particle shape on both the flowability and compressibility of these two grades. This study also showed that SAXS particles have a higher bulk and tapped densities and better flow than the micronised particles. Compactibility profiles of both micronised and SAXS particles were similar, with a tensile strength of tablets produced were around ~60 MPa. However, untreated tablets

showed lower tensile strength values than both SAXS and micronised particles. This can be attributed to the effect of particle size rather than shape. Smaller particle enhances the surface area and improves compression (Kaerger et al., 2004)

1.2.3.1.5 Effect of particle shape on granulation

Another example of the effect of particle properties on the performance of granules prepared using high shear mixer was presented by Martino et al. (2007). Metronidazole was used in this study because of high drug loading and low tabletability profile. Metronidazole was recrystallised using a salting method with three solvents; water, ethyl acetate and butanol. The resultant particles were different in both crystal habit and mean particle size. Needle shaped particles were larger with a mean diameter of 379 µm. However, stick-shaped and isodimensional particles were similar in size with a mean particle size of around 250 µm. Metronidazole was blended with the same excipients and further granulated using a high shear mixer at the same conditions. The resulting granules were further characterised. Bulk density results showed that iso-dimensional particles were higher than stick-shaped ones. Tabletebility profiles were significantly different, with iso dimensional particles has a superior tabletability. However, tablets porosity of stick-shaped particles was higher than those of iso-dimensional particles. This is because those iso-dimensional particles have a higher density to decrease their volume comparing with stick-shaped particles (Martino et al., 2007)

The effect of processing parameters of granulated particles on the shape of these particles was further studied by Beer et al. (2014). Beer et al. (2014) compared the shape of granules produced from both high shear and continuous granulation methods. The continuous granulation method was conducted using a twin-screw granulator (TSG). A principal component analysis was conducted to compare particle shape descriptors. The analysis found that granules produced from TSG tend to be less spherical and convex with a high aspect ratio than those produced using batch processing. This was attributed to the geometry of the twin-screw granulated with being a more constrained environment. This can also justify that granules produced from TSG are denser than those from corresponding high shear processing.

1.2.3.1.6 Effect of particle shape on mixing

The effect of particle shape on the powder mixture stability was studied by Swaminathan and Kildsig (2002) using aspirin as a model drug and two grades of microcrystalline cellulose (MCC PH102 and MCC PH302) and spray-dried lactose. These three grades have a mean particle size of ~100µm. However, the particle shapes of the three grades were significantly different. Spray dried lactose particles were spherical with an aspect ratio of 1.36, while microcrystalline cellulose has a fibre shape with PH302 has a higher aspect ratio than PH102, 1.36 and 1.61, respectively. A mixture of 1 % of aspirin and the three grades were prepared using a tubular V blender. The coefficient of variation (CV%) was determined by sampling the mixture at a specific time interval and determine the amount of aspirin in the mixture. This

study found that as the aspect ratio of the carrier increased, the CV% for the initial mixture increased, indicating that the stability of the mixture decreased. However, as mixing time increased and the stable mixture is formed by a low CV%, no further changed to CV% is observed as mixing increased. This behaviour was attributed to differences in the flow of the three grades studied. Flow study using the angle of repose and flow through orifice showed that flow increased as the aspect ratio of particles decreased. Changing the aspect ratio of the drug was also found to have an effect on segregation behaviour, especially in the rate constant of segregation. The rate constants of segregation were more significant, with components with similar shape factors than particles with different shape factors (Swaminathan & Kildsig, 2002). This example illustrates the importance of particle shape control during the mixing of pharmaceutical powders. Mixture stability is essential, especially when designing oral dosage forms. Poor stability mixture can lead to low content and weight uniformity.

1.2.3.1.7 Particle shape and flow

Particle shape and size was historically demonstrated to affect the bulk properties and flow characteristics of pharmaceutical powders. Fu et al. (2012) studied the effect of particle shape of the flow behaviour using three different lactose grades. Two of these grades had a similar particle size distribution but different particle shape. Particle sensitivity circularity (HSC) which is an indication of how close a specific particle to a circle was used as a parameter to compare between these grades in terms of sphericity. The higher the HSC value, the more spherical the grade is. Flow of these

grades was characterised using both dynamic FT4 powder rheometer and static ring shear tester. Results from the FT4 showed that the specific energy (SE) necessary to achieve specific flow pattern in a particular volume was affected by particle shape. Particles with a higher particle sensitivity circularity (HSC) showed lower values of SE in comparison with SpheroLac® 100, and InhaLac® 230 which are almost identical regarding circularity (similar HSC values). HSC factor can range from 0-1. Particles with a value of HSC=1 are completely circular. As the HSC value decreases, the irregularity of particle shape increased. Flowlac 100 showed a mean HSC of 0.91, while Spherolac100 has a mean HSC of 0.83, indicating that Flowlac100 is more spherical than Spherolac100 Furthermore, compressibility values which are defined as the ability of the powder to become consolidated when subject to specific stress were changed by particle shape. Particles with a higher value of HSC showed lower compressibility values in comparison with the other two grades. As sphericity increases, the flow function coefficient obtained from static flow characterisation also increased indicating the importance of particle shape on the flow of pharmaceutical materials (Fu et al., 2012)

. This example shows the importance of controlling particle shape when the flow of pharmaceutical materials is a critical parameter. It also indicates how particle properties such as shape are essential, especially when designing a process and improve performance.

1.2.3.1.8 Crystal shape and milling

Ho et al. (2012) studied the effect of crystal shape on milling behaviour of organic crystal using D-mannitol as model crystals. D-mannitol was recrystallised to get a needle-shaped particle. Half of the recrystallised particles were milled using a ball mill. Both unmilled and milled powders were sieved to obtain different sieve fractions. The milled and unmilled materials were characterised in term of surface energy using inverse gas chromatography and particle shape using dynamic image analysis. Results showed that the fracture behaviour of needle-shaped particles depends on the crystal slip system, surface energy, and, more importantly, particle shape. Particle shape and impact mechanism were the main factors that affect the particle fracture during milling rather than crystal lattice interaction. For needle shaped particle, the fracture will occur in the shortest axe of the particle with the low energy of attachment despite being not the most active slip plane (Ho et al., 2012). This example highlights that by careful control of particle shape, scientists can predict milling behaviour of pharmaceutical crystals. This kind of prediction is of great importance as it will be possible to tailor particles to meet downstream processing and formulation requirements.

1.2.4 Particle reduction techniques

Micronisation is one of the preferred routes to enhance the dissolution rate of class II drugs (Vogt et al., 2008). Mechanical micronisation is one of the top-down solvent-free technique and one of the traditional methods that has been used for a long time. It involves transforming coarse particles into ultra-fine particles by utilising

mechanical energy (Leleux & Williams, 2014). Mechanical micronisation enhances the dissolution rate by decreasing particle size and consequently increasing the surface area, which will increase the dissolution rate. It is worth mentioning that particle reduction techniques have little effect on the solubility of particles as it does not alter the solid-state of these particles (Vogt et al., 2008). However, micronisation below 1µm has been shown to affect the solubility of pharmaceutical powders (Vogt et al., 2008). In this section, commonly used micronisation techniques will be discussed. These techniques include hammer-milling, ball milling, jet milling and pin milling.

1.2.4.1 Hammer-mill technique

This technique involves the use of a range of hammer-like shafts connected to a centre that rotates. Upon rotation, particles are hit with these rotating hammers. The mill is supplied with a screen with a preferred size range, so particles will not leave until the desired particle size range is achieved. Hammers can be replaced by using stainless steel balls that filled 80% of the mill, and the powder is fed and further reduced in size by impaction with these balls. As the whole mill vibrating, the required size reduction achieved.

1.2.4.2 Ball milling

With ball milling, particle size reduction is achieved by utilising both attrition and impaction. A cylinder filled with beads; usually, zirconium oxide is used. The size of these beads is a critical parameter for controlling the preferred particle size. During

ball milling, it is essential to control the amount of fed material as too much or too low amount can negatively affect the efficacy of milling. It is also vital to control operation procedures such as rotation speed. Danazol is one of the poorly soluble drugs that belong to Class II BCS. It has a poorly water solubility (10µg/ml) and poor bioavailability. Liversidge and Cundy (1995) used ball mill to improve dissolution performance and consequently bioavailability. Decreasing particle size resulted in a ten folds reduction of particle size and ten folds increase in specific surface area. This has also resulted in enhancing bioavailability tenfold .

During ball milling, it is essential to monitor the crystallinity of the drug. Some drugs can convert from their crystalline form to the least stable amorphous form. Examples of these drugs include indomethacin (Patterson et al., 2005) and sulfathiazole-PVP (Boldyrev et al., 1994). However, some drugs such as carbamazepine can be stable upon milling and do not convert from the crystalline to the amorphous form (Patterson et al., 2007)

1.2.4.3 Jet milling|

The jet mill is another example where both attrition and impaction are employed. In this method, the air is injected into the mill at a high-pressure velocity. This high pressure will allow particles to colloid to each other allowing particles to fracture. This mill is usually supplied with a particle size classifier which allows only particles with the desired size to pass. This will ensure that particles above the desired size are retained until further particle size reduction is achieved. Ibuprofen particle has been

reported to micronised using this method. A starting particle with a mean diameter of 102 µm was used. This material was subjected to a continuous fluid energy mill. The resulted particles were in a range of 10 and 5 µm. Feeding rate and air pressure were the two most important factors affecting the resulting ' mean diameter of particles. As the feeding rate increases, the grinding efficiency decreased with larger particle obtained. Increasing the feeding pressure resulted in obtaining more fines and improving the grinding efficacy (Han et al., 2011; Teng et al., 2009). This method has been used to micronise powders with different mechanical properties, including those that are considered as soft materials such as Pluronic F-68 (Saleem & Smyth, 2010). Mechanical properties of starting materials are also very important in affecting the breakage rate and, consequently, the grinding performance. Experimental studies showed that the particle rate of breakage increases as the hardness decreases (Vegt et al., 2009).

1.2.4.4 Pin mill

This mill consists of two main parts; an upper fixed plate and a lower rotating plate. Each of these plates is supplied with a set of pins. Particles are fed into an upper feed-in hole. Then, the powder is milled by both attrition and impaction mechanism. Bonakdar and Ghaderi (2018) evaluated the effect of rotation speed and the nature of the material on particle size changes of paracetamol, aspirin and lactose. For aspirin and paracetamol, increasing the rotation speed has resulted in an apparent shift of particle size toward the fine region. For lactose, the shift was not apparent until

reaching a high rotation speed of 30000 rpm. This indicates that lactose particle at low rotation speed go through chipping and surface abrasion, while at a high rotation speed, these particles will undergo fragmentation and disintegration (Bonakdar & Ghadiri, 2018)

1.3 Formulation properties and the performance of oral pharmaceutical dosage forms

As discussed earlier, a successful oral dosage form must be safe, effective and stable. Formulation properties are one of the critical parameters that formulation scientists need to consider in achieving these goals. The primary level of importance in achieving those goals is controlling solubility, dissolution and stability. Poorly soluble drugs are very challenging during pharmaceutical development. Solubility and dissolution tend to be the rate-limiting step for these compounds entering the systemic circulations and giving the desired therapeutic response (Adebisi et al., 2016; Conway and Asare-Addo 2016). The secondary level of importance controls the mechanical properties of oral pharmaceutical dosage forms (Hamad, 2010). Several formulation techniques are currently available to achieve such goals. These techniques can be classified into two main categories (Savjani et al. , 2012). I: physical modification such as particle size reduction, optimisation of microstructure, supercritical fluids or crystal habit (polymorphs and amorphous forms) II: Chemical modification such as salt formation and co-crystals, use of buffers or novel excipients (Adebisi et al., 2016; Al-Hamidi et al., 2015, 2013, 2010a, 2010b; Asare-Addo et al., 2018; Guillory, 2003;

He et al., 2017; Nokhodchi et al., 2017; Rabinow, 2004; Ramirez et al., 2017; Stahl and Wermuth, 2018; Šupuk et al., 2013). Each technique has its pros and cons. For example, the enhancement of solubility of a neutral, weakly acidic or weakly basic drug-using salt formation is not always feasible. Reducing the size can also be limited as generating very fine particles can pose safety issues during handling (Vasconcelos et al., 2007; Serajuddin, 1999). One of the attractive routes to overcoming these problems is by formulating poorly soluble drugs into amorphous solid dispersions (ASD). ASD systems are composed of amorphous drug stabilised by the presence of the polymer(Newman et al., 2015). Solid dispersions can be manufactured by either solvent evaporation techniques or melting methods. In the solvent evaporation technique, the drug and polymer are dissolved in a solvent followed by the evaporation of the solvent using spray drying (Ali and Lamprecht 2017; Sawicki et al., 2016; Paudel et al., 2013) or freeze-drying methods (Pas et al., 2018; Lian et al., 2014; Betageri and Makarla, 1995). Melting methods, especially hot-melt extrusion (HME), have many advantages, including scalability, being a solvent and dust-free method and has industrial applicability (Paudel et al., 2013). These examples emphasise the need for these formulation techniques to be studied more extensively using novel experimental techniques that can help both formulation scientists and regulatory bodies.

1.4 Aims and Objectives

This thesis aims to first study the effect of formulation properties such as polymer type and content on the performance of pharmaceutical powders produced by a hot melt extrusion process. Microstructure will be investigated using X-ray microtomography and a novel use of dynamic contact angle will be used to investigate the various parameter effects on wetting.

Secondly, the effect of particle properties, mainly size and shape, on the performance of pharmaceutical materials represented by the flow will be investigated. In this part, a multivariate data analysis technique will be used to investigate the main factors affecting flow. In addition, the sensitivity of different shape and size of excipients to the effect of lubricant at different levels will also investigated.

Thirdly, the effect of particle properties of commonly used excipients will be explored on the microstructure and further the mechanical behaviour of pharmaceutical compacts.

Fourthly, the effect of particle properties and formulation properties on disintegration behaviour will be investigated by coupling a novel surface dissolution imaging instrument (SDI2) with an online particle size analyser.

Lastly, this thesis will aim to utilise artificial intelligence and a neural network to predict the performance of pharmaceutical powders based on particle size and shape properties.

1.5 Materials selection

In order to achieve the above-mentioned aims, diverse materials with different material properties were used in this thesis. To assess particle properties on the performance of pharmaceutical powders, three commonly used pharmaceutical excipients were used in this thesis. These excipients were microcrystalline cellulose, dicalcium phosphate and lactose. Blends of these three commonly used excipients were also used in different ratios. Different grades with different particle properties were outsourced. Dicalcium phosphate was carefully selected over lactose and microcrystalline cellulose to run the disintegration testing as it is both insoluble in water and, as in the case of lactose and does not swell upon contact with water such as in the case of microcrystalline cellulose. Sodium starch glycolate (CSS), crospovidone (CP) and croscarmellose(CSS) were used as super disintegrants in this study. To study the effect of formulation properties on the performance of pharmaceutical dosage forms, glyburide was chosen as a model drug. Glyburide has a poorly soluble and high permeability profile. It represents an ideal example of BSC II compounds.

Chapter 2 - Experimental methods

Note to reader: This section explains the science behind the majority of the techniques used in this thesis. How the techniques are used are further described in each individual chapter where applicable.

2.1 Characterisation tools

2.1.1 Microscopy

Microscopy is considered one of the most commonly used analytical tools that complements other particle size and shape characterisation techniques. It is a powerful and easy to use technique that allows direct observation of both particle size and shape. Microscopical observations require a tiny amount of material, and therefore, it is one of the material sparing techniques that can be used in the early phases of drug development, where a minuscule amount of material is available.

Applications of microscopy in the pharmaceutical industry are enormous. These applications include crystallisation troubleshooting (Durbin & Feher, 1990), excipient & API identification and characterisation (Boiret et al., 2016), the homogeneity of the blend (Pfannmöller et al., 2011), granules shape and size evaluation (Fonner et al., 1966), and foreign particulate matter identification (Blanchard et al., 2004).

Microscopical tools can be divided into three main categories: optical, electron microscopy and the recently developed atomic force microscopy.

Optical microscopy is the simplest form of microscopy. A light source is used to observe the particle size and shape of particles.

Two major types of electron microscopy are available: scanning electron microscopy (SEM) and transmission electron microscopy (TEM). These two types are similar in

terms of samples being imaged under high vacuum conditions. However, the sample thickness used in TEM is limited to a few nanometres, whilst samples used in SEM are usually thick enough to view surface structure and morphology. In addition, samples used in TEM are usually biological in nature, and not all pharmaceutical samples can be used by TEM (Klang et al., 2013).

In this thesis, scanning electron microscopy is used extensively and thus discussed further.

2.1.1.1 Scanning electron microscopy (SEM)

SEM is a valuable technique in exploring surface topography, particle morphology and size. Using SEM, scientists can examine not only powders but also different pharmaceutical dosage forms such as granules, tablets or capsules. Advantages of scanning electron micrography over light microscopy include the ability to reach higher magnification, increased field depth, and a much higher lateral spatial resolution which can reach 1 nm. However, samples used in scanning electron microscopy needs to be carefully prepared to avoid contamination. Therefore, careful handling of the sample is very important as a light touching of the sample will be seen once the sample is analysed. Powders and particles are carefully dispersed onto a sample holder using double adhesive tape. The sample is then coated using a thin layer of metal to prevent the sample from acquiring a negative charge caused by emitted electrons which can cause the sample to glow. Moreover, this thin layer of metal can also help in maintaining the thermal stability of the sample studied. Platinum or gold

is usually used as the coating agent. However, if the samples cannot be coated for any reason, environmental scanning electron microscopy (ESEM) can be used in this case.

Coated samples are then transferred to the SEM chamber, which is maintained at a very high vacuum to prevent electron scattering due to colliding with gas molecules. **Figure 2.1** shows how SEM works. Electron beams are emitted from an electron gun located at the top of the electron column. Electrons are then accelerated using a high voltage. This voltage is usually between 100V and 30000 V. Depending on the sample studied, a suitable voltage is used to get all the desired information from the sample. Electrons are then condensed using a specific lens before they are passed through scan coils which deflect electrons toward the sample studied. These electrons pass through an objective lens which also helps to direct electrons toward the sample studied. Once primary electrons hit the sample, both secondary electrons and an X-ray emitted. These emitted electrons are detected using three main detectors: a backscattered electron detector, a secondary electron detector and an X-ray detector. Secondary electron detector gives the surface topography of the sample, while X-rays provides information about the elemental composition of the sample studied.

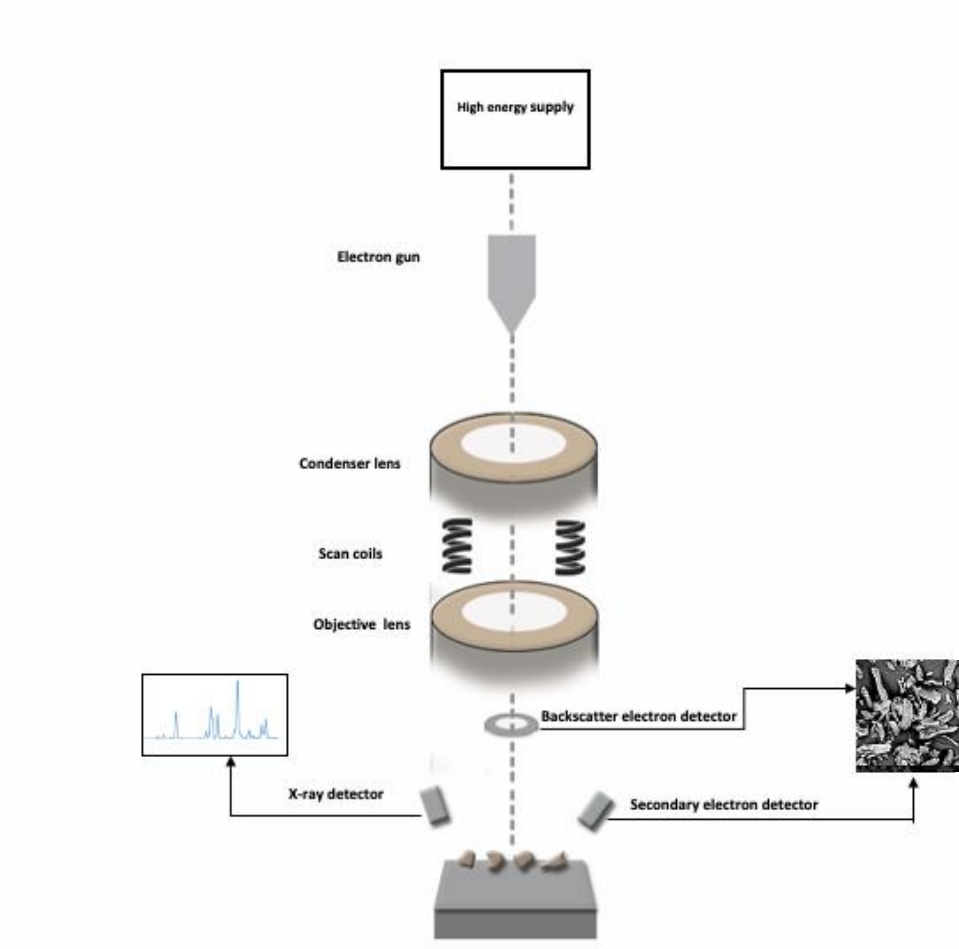

Figure 2.1 Schematic diagram of SEM adapted from (Storey & Ymén, 2011)

2.1.2 Particle size and shape characterisation techniques

2.1.2.1 Sieving:

Sieving is one of the traditionally used methods for particle size analysis of pharmaceutical powders. Sieving can be dry or wet. Wet sieving is usually used for hydrophobic and very cohesive powders. It is an uncommon method and only can be used when dry sieving is inapplicable. In this method, the hydrophobic powder is usually dispersed in water.

Dry sieving is achieved by mechanical shaking, sonication, or air-jet dispersion. Surface characteristics are affected by the way sieving is achieved. For example, particles produced from air-jet tend to be cleaner, and fewer fine fractions are produced using this method comparing with mechanical ones (Zeng et al., 2000).

Sieving involves the size fraction of powder using different sieves with different mesh sizes. Sieves are usually loaded above each other, with sieve mesh size decreasing from top to bottom. The sample is then loaded on the sieve with the largest mesh size. The sample is further subjected to mechanical, sonication or air-jet agitation. As agitation is applied, particles pass through sieves depending on their cross-sectional diameter, with the finest particles collected on the bottom pan. Fractions between each sieve are then collected and weighed. Data are then presented using particle size distribution graph or cumulative distribution (Storey & Ymén, 2011).

The advantages of sieving are enormous. It is an easy and straightforward method that does not require much training. Besides, sieving can serve as an early indication of the flowability of a powder. However, sieving needs to be validated and standardised in terms of the amount of sample used and shaking time used. If excessive material is used, a sieves mesh will be blocked, preventing fine particles from passing through the sieve. This will, in turn, give an inaccurate particle sizing distribution graph. Shaking time needs to also be standardised as too long of a shaking time will cause particles to break and give inaccurate results. Another disadvantage of sieving is that the technique requires a large amount of sample, which make it inappropriate as a tool in early drug development where a small amount of API is available. In addition, this method cannot be used with expensive APIs. Finally, sieving is a time-consuming method when comparing with other particle sizing techniques such as laser diffraction and image analysis (Aulton & Taylor, 2013; Storey & Ymén, 2011)

In this thesis, standard USP sieves were used. The sieve procedure was standardised in terms of the amount and time used. Size fractions were used for carrying future experimental work as detailed in later chapters (chapters 5 and 6)

2.1.2.2 Laser diffraction:

Laser diffraction is a technique that can be employed in both research and development (R&D) and quality control (QC) labs. It has the flexibility of operating in both wet and dry medium. Moreover, it is a robust, precise, reproducible and well-established method that has been used for a long time in the pharmaceutical industry.

Applications of laser diffraction can be found in dry powder inhaler formulations, tablet formulations & optimisations, powder mixing, segregation and many other pharmaceutical formulations. The basic concept of laser diffraction is that the diffracted angle of the laser is inversely proportional and correlated to the size of particles measured. Two main instruments are currently based on this concept: Malvern Mastersizer and Sympatec Heleos. These two instruments share the same concept mentioned above. However, the theory employed in calculating particle size is significantly different. Malvern Mastersizer uses Lorenz-Mie theory, wheras Sympatec uses a simpler form of the Lorenz-Mie theory called the Fraunhofer diffraction theory (Storey & Ymén, 2011).

The Lorenz-Mie theory requires a knowledge of the diffraction index of the material measured. This theory also takes into account reflection, absorption and refraction of particles as well as scattering. However, particles need to be isotropic, spherical and have smooth surfaces. In addition, this theory cannot be used in measuring powder blends that contain particles with different refraction indexes as a wide range of results that will be obtained from the same scattered light.

The Fraunhofer theory, on the other hand, assumes that all particles particle size is 40 times larger than the laser length used, which limits the minimum particle size to 25μm when using a He-Ne laser source. The theory also assumes that all particles are opaque and do not absorb, reflect or refract light. This theory does not require a pre-knowledge

of the refraction index of the material used as in Lorenz-Mie theory (Storey & Ymén, 2011).

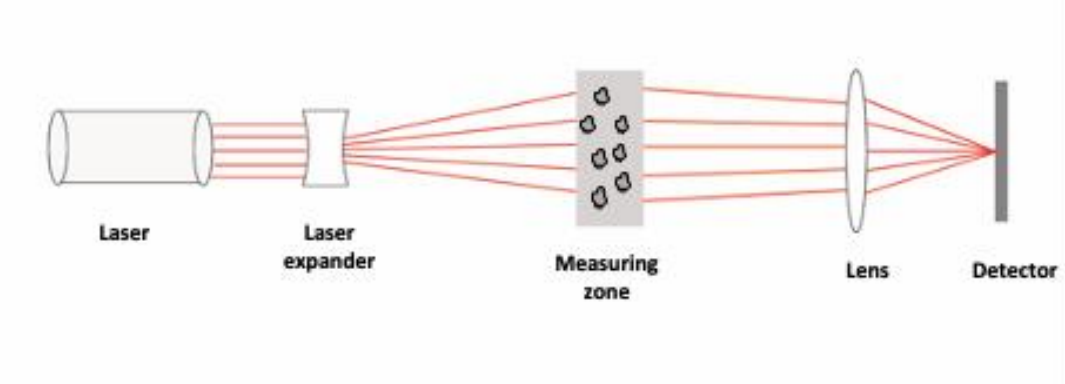

Figure 2.2 Illustrative diagram on the principle of laser diffraction adapted from (Storey & Ymén, 2011)

As depicted in **Figure 2.2**, the system is composed of a laser source, sampling zone where the sample is passed through, lens and a detector that measure the intensity of scattering. A software that converts these scattering into particle sizes is used based on Fraunhofer or the Lorenz-Mie theory. Different dosing systems are available, and they differ depending on the nature of the sample used. For example, a special dosing system can be used with the Sympatec Heleos in order to connect the dry powder inhaler to the system used (Storey & Ymén, 2011).

In this thesis, a combination of a wet and dry system to measure the particle size of powders is used, with the selection being merely based on the availability and access to these systems. The type of lens used in the study was chosen based on the light microscopy images, which gave an indication of the appropriate lens to use. In order to ensure the dispersing line was clean and free from contaminants, 2 spoonsful of

sand (40-100 mesh) was passed through the dispersing line prior to analysis. The primary sample container was thoroughly mixed by rolling and inverting by hand as well as mixing using a spatula. Approximately 200 mg of the material studied was transferred into an ASPIROS tube. Prior to running the measurement, the ASPIROS tube was gently inverted and agitated to ensure the sample was dispersed evenly and to reduce the loss of material in the vials. The sample for the wet method was treated the same. However, in the wet method, the Mastersizer was used in order to identify the particle size of the materials studied.

2.1.3 Image analysis

SEM and light microscopy are considered simple and direct methods for imaging particle shape. The USP general chapter (776) provides a qualitative description of particles shapes. This monograph classifies particles into six different shapes defined and illustrated in Figure 2.3 and Table 2.1(USP convention, 2020b)

Table 2.1 Different particle shape terminologies and description of these terminology

Particle shape	**Description**
Laths (blade) (A)	Particles that are long, thin and have a blade-like shape.
Equant (B)	Particles that have the same width, length, and thickness
Columnar (prismatic) (C)	Particles that similar to the needle but have greater width and thickness than needles.
Plates (tabular)(D)	Particles that have the same width and length but thinner than flakes.
Needles (acicular) particles (E)	Particles that have needle shape and same width and thickness.
Flakes (F)	Particles that have the same width and length but thicker than flakes.

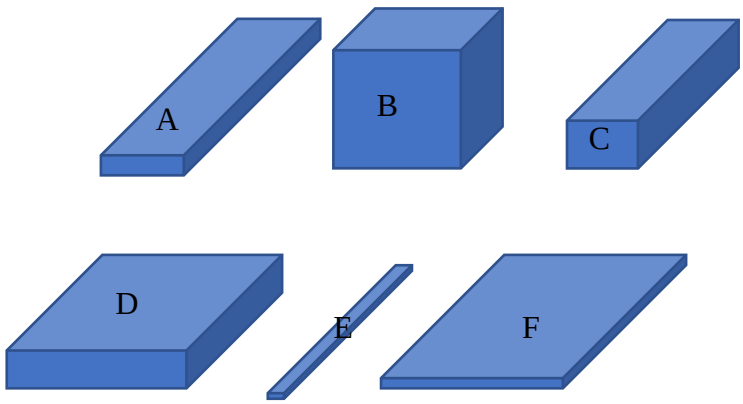

Figure 2.3 Illustration of different particle shapes (descriptions of each shape can be found in table 2.1)

Though qualitative descriptions provide a general idea about the shape of the particles, it is crucial to describe those particles in a more quantitative way. Therefore, a quantitative image analysis technique is required. Static and dynamic image analysis are two emerging technologies that have attracted much attention in recent years and can address limitations of both light and electron microscopy.

Static and dynamic image analysis are two main techniques that are currently used in the pharmaceutical. The differences between these techniques are mainly how particles are fed into the system:

- Static image analysis: the sample is dispersed on a plate or a slide and then imaged when particles are settled. Morphologi G3 is an example of an instrument that uses this principle in particle imaging.
- Dynamic image analysis: the sample is constantly fed into the system, and the particles are images while they are moving. QicPic is an example of a dynamic image analysis system.

Static imaging involves a pre-dispersed powder sample on a glass slide similar to the one used in light microscopy. Particles within the sample are then captured using a specific camera. This technique has many advantages, including capturing particles in a static and mechanically stable position. This will, in turn, result in a better image resolution. Also, this technique offers the ability to classify particles by a process called filtration. Filtration can offer the ability to monitor how sub-classes of particles

such as agglomerates will behave during a specific process (Gamble et al., 2015). However, there are many limitations and challenges when using static imaging. Firstly, this technique requires a long analysis time for each sample ranging from 20 min - 2 hours. This time could also be increased in the case of applying particle filtration. In addition, some particle can be challenging, such as highly three-dimensional samples, elongated and cohesive particles. This mainly because of the limitation in the depth of field (Gamble et al., 2015). Particle filtering can also be a subjective technique and will affect imaging results

Dynamic imaging overcomes drawbacks associated with static imaging by decreasing analysis time, imaging elongated, cohesive, and highly three-dimensional particles. Furthermore, this technique offers the ability of imaging a large number of particles which can statistically more representative of the sample studied when compared with static imaging. Also, using dynamic image analysis, no sample preparation is needed. In addition, dynamic imaging can serve as both in-line/on-line PAT tool (Gamble et al., 2015; Rabinski & Thomas, 2004). Moreover, comparing SEM micrograph with dynamic image analysis data obtained by QicPic system showed a semi-quantitative relationship (Yu & Hancock, 2008). The only limitation of dynamic image analysis is a lower resolution when compared with static image analysis, which provides better image quality (Gamble et al., 2015)

The system can be illustrated in Figure 2.4 A dispersing unit is used to inject the sample into the system. This dispersing system can work on both dry and wet mode

(Wilson, Wren, & Reynolds, 2012). Particles are then imaged using a high-speed camera supplied with a specific objective lens. The particles are subject to a pulsed light source in order to get a better quality of the picture (Witt, Köhler, & List, 2004).

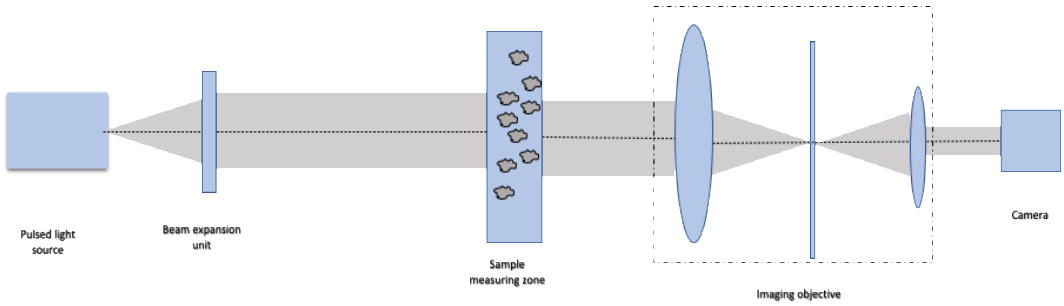

Figure 2.4 Dynamic image analysis principle (Gamble et al., 2015)

In our thesis, a dynamic image analysis system was used using a QicPic instrument (Sympatec, UK) to characterise the particles in terms of size and shape. In order to ensure that the dispersing line was clean and free from contaminants, two spoonsful of sand (40-100 mesh) were passed through it before analysis. The primary sample container containing each excipient grade was thoroughly mixed by rolling and inverted by hand as well as mixed using a spatula. Before starting the measurement, the sample, approximately 2g, was gently inverted and agitated to disperse it evenly and, thus, reduce the loss of material in the vials. The M7 lens was selected for this study, where each measurement was repeated three times. The WINDOX software was utilized to perform the statistical analysis of the obtained measurements.

2.1.4 X-ray microtomography

X-ray microtomography (XμCT) is a new promising technique that considered a non-invasive and direct method for evaluation of the microstructure of pharmaceutical tablets. Tablet microstructure has shown to have a definite role in affecting the performance of pharmaceutical tablets such as mechanical strength (Gong et al., 2015), drug releases (Hancock et al., 2003) and disintegration behaviour (Markl et al., 2016; Markl et al., 2017). Therefore, understanding the microstructure can give clues and guide formulators in drug product development and optimisation.

Figure 2.5 illustrates how x-ray microtomography works. Briefly, the system consists of four main components: x-ray source which diffracts x-ray toward the sample, a sample holder, x-ray detector that capture x-ray after interacting with the sample, and a computer system that control, capture and analyse data. X-ray scans the sample from side to side in lines from top to bottom. Consequently, a shadow image is produced. The sample is then rotated in a specific angle, and the same area is then scanned. Fourier transform algorithm is then used to produce a 3D image of the sample studied. These 3D images will have different density spots depending on the atomic composition of the sample studied (Hancock & Mullarney, 2005).

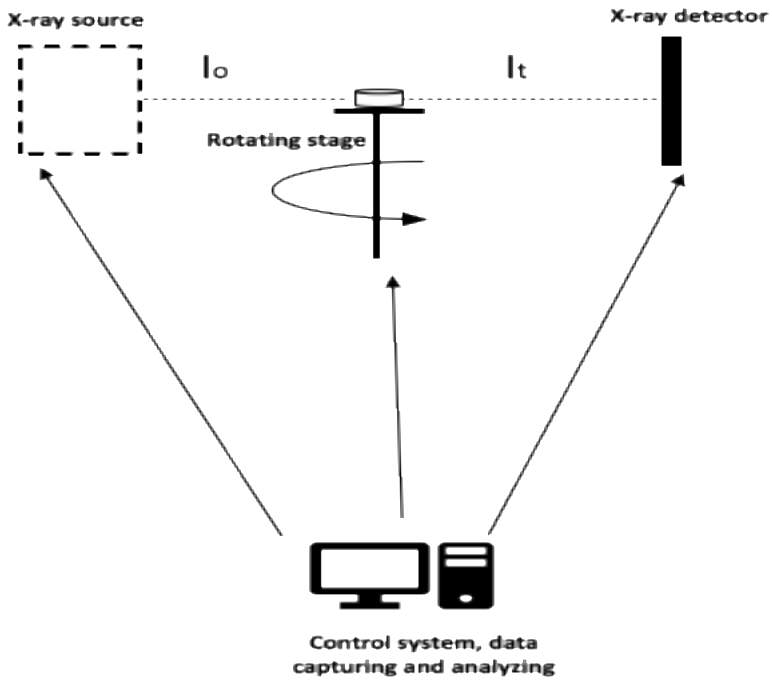

Figure 2.5 Schematic diagram of X-ray microtomography adapted from (Hancock & Mullarney, 2005)

Some interesting applications include real-time dissolution (Kašpar et al., 2013), tablets pore morphology evaluation (Markl et al., 2017), tablet coating evaluation (Perfetti et al., 2010), powder segregation investigation (Liu et al., 2013)

Kašpar et al. (2013) used X-ray tomography to observe changes in the microstructure of granules produced from high shear wet granulation during dissolutions. Paracetamol granules were produced with different porosities by varying processing parameters such as binder/ solid ratio, impeller speed and wetting time. X-ray microtomography showed that granules produced have a porosity ranging from 7% to 18%. UV dissolution showed that increasing porosity resulted in a decrease in dissolution time. In addition, X-ray tomography was used to visualise how

microstructure was changing during dissolution. The granule was firstly imaged using x-ray tomography. Then, the sample was partly dissolved in ethanol. Ethanol was selected as it will selectively dissolve paracetamol but not excipients used. The granule was placed for a specific time in ethanol and then immediately evaporate the ethanol under vacuum to stop the dissolution process. The granule was then reimaged and compared with the previous image in term of microstructure. This process was repeated at different time points, and images were then evaluated (Kašpar et al., 2013).

XμCT and terahertz spectroscopy were used to evaluate the pores within calcium carbonate tablets in order to study the disintegration behaviour of pharmaceutical tablets. XμCT was able to provide detailed information about every pore structure, their orientation and shape within calcium carbonate tablets (Markl et al., 2017).

XμCT was also used to evaluate tablet coating. The technique was usefully capable in identifying coating thickness, coating cracks, inside or outside damage of tablets studied. This of great importance during coating, and XμCT can be employed as a quality control test. In addition, it may serve as a tool for the improvement of the coating process (Perfetti et al., 2010).

XμCT has also been employed to investigate the segregation of pharmaceutical powders during blending (Liu et al., 2013). XμCT of microcrystalline and starch showed that the homogeneity of the blend increased as the time of rotation increased but decreased with an increase in the time of vibration. XμCT showed that large

spherical particles tend to stay at the top and small spherical particle migrate to the bottom of the container, causing segregation to occur (Liu et al., 2013). Other applications include the identifying of foreign matters and counterfeit products (Hancock & Mullarney, 2005).

Although there are enormous benefits of using XμCT in pharmaceutical industry, especially when coupled with other techniques, XμCT has many limitations and challenges. One of the main limitations is the long analysis time which is usually from 1-2 hours. In addition, reconstructing images also require extra time, which can range from 1-3 hours, depending on the sample studied. For these reasons, the technique cannot be applied as a routine test nor employed as a quality control test in pharmaceutical industry (Markl et al., 2017). Safety is another concern associated with the use of X-rays.

In this thesis, XμCT was used on many occasions to investigate the microstructure of tablets studied. To do so, pharmaceutical drug products were imaged by XμT (Nikon XT H 225, Nikon Corp. Tokyo, Japan) using a tungsten target with 75 kV accelerating voltage and 250 μA gun current using a copper filter (thickness 0.125 mm). Drug product was mounted using double-adhesive tape. A set of projections were collected with over 120 min XμT acquisition. The set of projection images were then reconstructed using CT-Pro and then examined using VG Studio 2.1 software.

2.1.5 Surface roughness analysis

Powders are usually composed of particles of different size and shape. Once compacted into a specific shape and size, the surface roughness of the resultant compact is determined by how these particles are distributed and configured. Particle orientation and, consequently, surface roughness will affect how the mechanical properties of pharmaceutical tablets (Narayan & Hancock, 2005).

SEM or light microscopy can provide a qualitative assessment of surface roughness. However, several challenges associated with the use of the previous techniques, including the working microscopic area, which can be limited to a small region of tablet study. In addition, SEM coating can change the surface characteristic significantly.

Therefore, it is important to evaluate surface roughness in a more quantitative method. Quantitative surface roughness evaluation methods fall into two main categories depending on the contact between the surface sensor and the surface studied. These methods include contacting surface characterisation, such as profilometry and atomic force microscopy. Non-contacting, on the other hand, can include non-contact optical profilometry. Contacting method, however, can cause damage on the surface of the compact studied. In addition, these techniques may require sample preparation and extensive training (Kapłonek et al., 2016). For this reason, a non-contact optical profilometry method was employed in our thesis.

Non-contact profilometry methods use light or laser source to image the surface in a three dimensional (3D) resolution in the submicron to micron range. They are direct, non-destructive, and suitable for characterising pharmaceutical compacts (Van der Jeught & Dirckx, 2015). Focus variation microscopy (FVM) is an example of a non-contact surface analysis method that was used in this thesis.

Figure 2.6 shows the operation principle of FVM. FVM works by projecting a white light source toward a small surface of the compact studied. The light then reflects from the surface toward a beam splitter. The beam splitter then directs the light toward a photoelectric detector where both photometric and geometric characteristics of the light are identified. This process will be repeated as the light scan through the sample on the x-axis (Kapłonek et al., 2016).

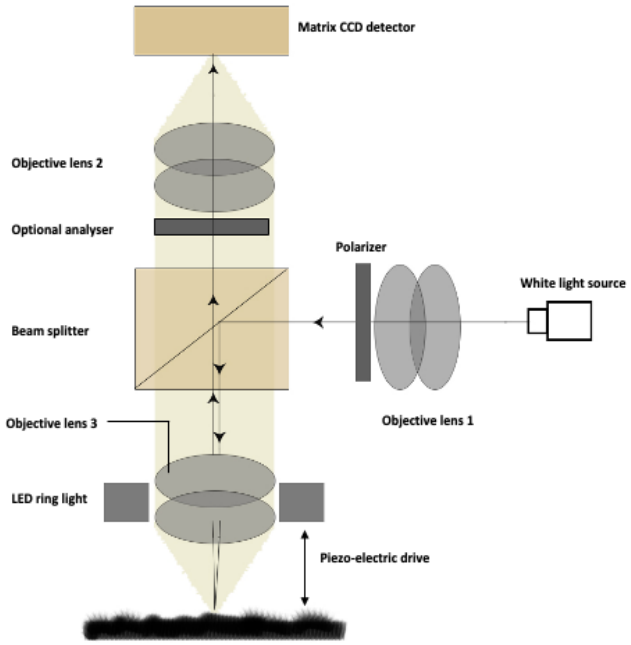

Figure 2.6 Operation principle of FVM adapted from (Kapłonek et al., 2016)

Surface roughness parameters arethen calculated from the surface roughness profile by calculating the total deviation of negatives and positives changes from the main plane that fit the surface studied. Different surface parameters can be used. These parameters can be classified as amplitude, spatial, hybrid or functional parameters (International Organization for standardisation, 2012). Table 2.2 explains these parameters in more details.

Table 2.2 Parameters calculated from surface roughness analysis (International Organization for standarisation, 2012)

Group	Parameter	Description
Amplitude	*Sa*	The arithmetic mean deviation of the surface
	St	Sum height of surface
	Sq	Root-mean-square (RMS) of the surface
	Sp	Maximum height of summits
	Sv	Maximum depth of valleys
	SsK	Skewness of height distribution
	Sku	Kurtosis of height distribution
Spatial	*Sds*	Density of summits of surfaces
Hybrid	*Sdq*	RMS slope of the surface
Functional	*Vmp*	Material volume of the peaks
	Vmc	Material volume of the cores
	Vvv	Void volume of valleys

In this thesis, a focus variation instrument (Contour LS 3D Optical Profiler (Bruker)) was used to assess the surface topography of pharmaceutical product using 5 x or 10 x objective and specific lateral resolution. The obtained images were further analysed

using the Surfstand™ software (Taylor Hobson, UK, and University of Huddersfield, UK) to obtain 2D and 3D profiles of the surfaces (Ward et al., 2017). The Sq parameter, which is defined as the root mean square value of the surface departures from the mean plane within the sampling area, was of interest with regards to the influence of the polymer concentration on the pellets produced. This parameter is represented by equation 2.1

$$Sq = \sqrt{\frac{1}{A}\iint_A z(x,y)\delta x \delta y} \qquad \textbf{Eq. 2.1}$$

Where: A = Sampling Area, Z (x, y) = surface departures

2.1.6 True density analysis

Density is defined as the mass of powder per unit of volume. The British Standards Institution distinguishes between two types of density:

- Absolute powder density (true density), which is defined as the mass of powder per unit of absolute powder volume.
- Apparent powder density, which is defined as the mass of powder divide by the apparent volume.

True density in pharmaceutical industry can be calculated from the crystal structure. This is can easily be calculated by knowing both the molecular weight and crystal lattice, which is determined by XRPD (Viana et al., 2002). Gas displacement is

another method that can be used. Helium pycnometer is a common and convenient method for calculating the true density of powders using gas displacement (USP convention, 2020a). In this method, it is very important to remove volatile containments by degassing the powder under vacuum before measuring density. The sample is weighed and then placed into a helium pycnometer cell. The gas is then purged under specific pressure. The volume of the gas occupied is compared with a reference cell volume within the pycnometer. By comparing the two volumes, the absolute volume, which is the volume that the powder occupies without any pores, is calculated. True density is then measured by dividing the weight of the sample by the absolute volume.

In this research, true density was calculated using Micrometrics AccPyc II 1340 Gas Pycnometer. True density was then used to evaluate the mechanical properties of pharmaceutical compounds using Heckle analysis.

2.1.7 Flow characterisation

Powder flow, along with powder compression properties, are two main important factors for the manufacturability of tablet dosage forms. Powders are complex materials that usually composed of three different phases components: solids which are the particles themselves, liquid which often exists on the surface of the particles and gas, which is existed between particles. The effect of the interaction of these three phases determines powder bulk properties. In addition, environmental or processing conditions also contributed to these properties. Powder can be processed under

consolidated, unconsolidatedd and aerated conditions. These processing conditions will have an effect on particle-particle interaction and, consequently, powder flow behaviour. Powder flow is a very crucial parameter in ensuring the robustness of a manufacturing process. Powders ranked as “poorly flowable” will have problems with die- filling before compression (Chattoraj & Sun, 2018). On the other hand, with “good powder flow” formulators can ensure uniform packaging and constant die-filling. Also, sufficient powder flow is vital to prevent tablet capping and lamination as poor powder flow can cause air trapping and consequently capping and lamination of produced tablets. Inconsistent powder flow may increase the number of fine particles, which will, in turns, result in an increase in die-wall friction, which will cause lubrication problems (Aulton & Taylor, 2013).

Particle properties are important parameters that are affecting particle powder flow. More discussion about the effect of these particle properties on flow can be found insection 1.1.2 .

Powder flow characterisation methods can be classified into two-three categories; static, dynamic and defined consolidation method (Hassanpour, Hare, & Pasha, 2019). Static methods, as the name implies, measure the flow behaviour of pharmaceutical powders in a static mode (Hassanpour et al., 2019). These methods require preparing the sample before further measuring the flow behaviour. The angle of repose and bulk density measurements are two common examples of static measurements that have been used in the pharmaceutical industry for a long time. They are easy,

straightforward method and inexpensive method. However, these methods are sample dependant and have low reproducibility. In addition, the angle of repose measurement scale is an arbitrary scale. Moreover, these methods lack the ability to differentiate between minor formulation changes, such as the source and the amount of magnesium stearate (Shah et al., 2008).

To address these limitations, dynamic flow methods are becoming more frequent in the pharmaceutical industry. Dynamic flow analysis has the advantages of measuring powders while they are moving, allowing a more realistic estimation of the flow behaviour. Common examples include flow through orifices, vibration-assisted methods, avalanche analysis method and powder rheometer (Hassanpour et al., 2019). Each of these tests has its advantages and disadvantages. Powder Rheometer, for example, is fast a reproducible method. However, data interpretation is difficult and more understanding of the blade role in testing still needed. Moreover, torque data need to be examined in depth in order to explain the data (Leturia et al., 2014).

Consolidation methods meaure the flow of pharmaceutical powder under packed bed conditions (Hassanpour et al., 2019). These methods can be time-consuming and require proper training. However, using consolidation methods, scientists can get more insights into the intrinsic properties of powders. In addition, they can quantify powder flow and provide more accurate measurements. Moreover, data generated from consolidation data can be used in design hoppers and problem-solving powder issues

in pharmaceutical industry (Leturia et al., 2014). For these reasons, a ring shear tester has been used in our research.

The ring shear tester uses an annular (ring-shaped) sample to measure the shear stress (the amount of pressure on a specific material) required to start the powder moving, i.e. make it “yield” at a range of normal stresses. The cell rotates very slowly taking the powder bed with it, but the lid is held in place by the two tie rods. The tie rods detect the movement of the lid as the powder moves against it and detects when the powder finally yields.

Before measuring the flow of the powder, pre-consolidation stress is applied to erase the powder history of the powder. Then, the powder bed is subjected to a series of pressure as a function of time. Once the shear stress is high enough, the powder will start to yield or flow. A plot of shear strength vs compressive force is called yield locus, where shear strength (Sf) the limiting value of the resistive shear stress or the extent to which a bulk solid resist being deformed.

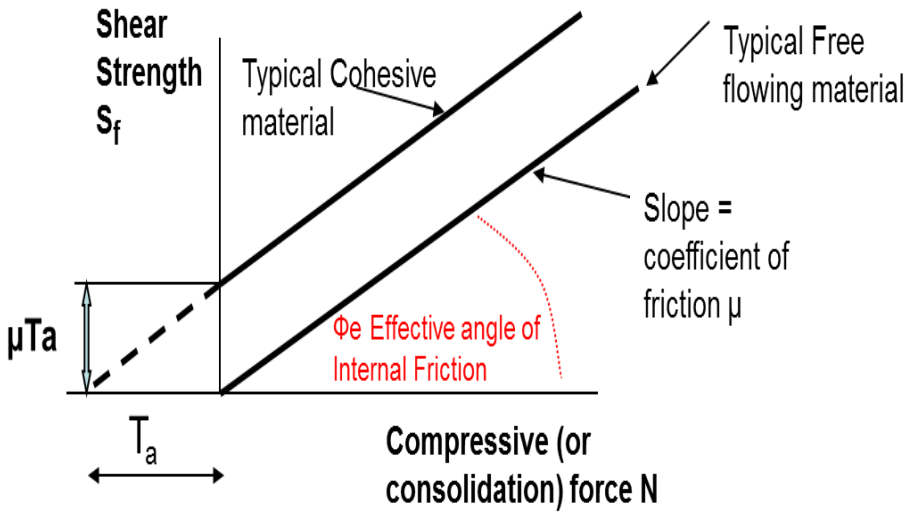

Figure 2.7 Shear strength vs compression force diagram (Schulze, 2008)

Figure 2.7 shows a Yield locus plot defined in the equation Sf = μ (N + Ta), where μ = coefficient of internal friction and Ta is the "apparent Tensile strength". Apparent tensile strength is defined as the value of N (-ve) where shear strength = 0.

When N=0, Sf is defined as "cohesivity" (μ Ta) or inherent ability to resist deformation. Unconfined Yield Stress is the strength of the material at the free surface. Each Yield Locus determines one point on the Flow Function. The Flow Function is a plot of the unconfined yield stress (σc) vs the major consolidating stress (σ1)

The Major Principal Stress σ1 (or consolidation stress) is the highest normal stress applied to the powder during testing: above this level, the powder will either yield (i.e., flow) or densify. Mohr circle tangential to the yield locus and passing through the origin gives σc the unconfined yield strength, which is the effective consolidation

strength OR the normal stress at which an unconfined powder column (like a cylindrical sandcastle) would flow. Flow Function is the relationship between the unconfined yield strength and the Major principal (or consolidation) stress: $\sigma C = f(\sigma 1)$

The usefulness of the Flow Function obviously increases with the number of data points used. The lower the slope the better the flow.

Rhodes classified powder flowability according to FFC values as follows; FFC<1 not flowing; 1<FFC<2 very cohesive; 2<FFC<4 cohesive; 4<FFC<10 easy flowing; and 10<FFC free-flowing (Rhodes, 2008).

In this research, a ring shear tester (RST-XS, Dietmar Schulze, Wolfenbuttel, Germany) was utilized to characterise the flow of the powders. The cell was over-filled with the sample powder of interest, and then a spatula was used to gently smoothen the surface. The weight of the shear cell and the sample was determined and recorded using the software provided. A pre-shear stress of 4,000 Pa was applied to erase the powder history. Normal loads applied were 25%, 38%, 51%, 65% and 25% of 4,000 Pa.

2.1.8 Differential scanning calorimetry (DSC)

DSC is a fast, user-friendly tool that can give insights into material behaviour of especially monitoring any solid form changes. The instrument work by measuring

energy changes that occur within the material under different thermal conditions. These changes will provide valuable information about any solid form changes such as melting or glass transition. The instrument measures heat flow which can be expressed as endothermic (into the sample) or exothermic (out of the sample). Once the heat flow is obtained, derivative curves can be obtained using a specific mathematical algorithm. These curves can provide information about glass transition, weight loss, and the resolution of the DSC method utilised (Storey & Ymén, 2011)

Sample preparation is essential for a good DSC measurement and usually performed by encapsulation of the sample in a tailored designed pan to prevent contamination of the sample within the furnace. The temperature range is then defined. The lower range usually starts below any expected transition to get a flat baseline. The higher range, on the other hand, should be below any decomposition of the sample to prevent any noise caused by sample decomposition. Scan rate is also another factor for setting-up a specific method. The scan rate (commonly 10°C/min) can greatly affect sensitivity, resolution and transition kinetic (Craig & Reading, 2006)

In this thesis, the main purpose of DSC was used to monitor crystal form changes within formulations produced from hot-melt extrusion (HME). It was expected that materials produced from HME was to be completely amorphous. These amorphous systems, however, pose the risk of being "unstable systems" and can therefore convert into its more stable crystalline form. This will, in turn, affect the dissolution performance of these systems.

2.1.9 X-ray powder diffraction (XRPD)

XRPD is a valuable analytical technique that is important in defining solid form changes, including polymorphs, solvate, salts, co-crystals and amorphous dosage forms. It provides useful information about the structure packaging of powders (i.e., crystal or amorphous) and, therefore, a possible indication of the stability of these materials (Storey & Ymén, 2011).

The system composed of an X-ray source, a sample holder and an X-ray detector. Sample is prepared and mounted in a specific disc. Then X-rays emitted from the X-ray source toward a sample where X-rays are diffracted depending on the packaging of molecules within the material. By identifying the arrangement of molecules within a specific material, patterns could be analysed and ultimately define the crystallinity of the material. These arrangements can be defined by using Bragg's law which relates the space between molecules (referred as d in equation 2.2) to the X-ray half scattering angle (θ) (Ivanisevic & Schields, 2010)

$$n\lambda = 2dsin(\theta) \qquad \textbf{Eq. 2.2}$$

Where n is an integer, λ is the wavelength of X-ray source, and d is the spacing parameter.

XRPD has many applications in pharmaceutical development and manufacturing. These applications include API characterisation(Egusa et al., 2017), material phase

identification (Morrison et al., 2009), structural analysis of crystalline material(Ivanisevic et al., 2010) or amorphous materials and characterisation of multicomponent analysis(Moore et al., 2009).

In this thesis, XRPD, along with DSC, was used to monitor any crystal form changes within formulations produced from hot-melt extrusion (HME). Samples produced from the HME process are expected to be amorphous, and therefore both DSC and XRPD were used to confirm these expectations.

2.1.10 Wettability measurement using contact angle

Wettability plays a vital role during all stages of development and processing of pharmaceutical dosage forms such as wet-granulation (Zhang et al., 2002) and coating (Lefebvre et al., 2011). It also has an important consequence on the performance of pharmaceutical oral dosage forms such as dissolution rate and consequently the bioperformance of the dosage form.

To characterise wettability, there are currently versatile techniques that are commonly used. These techniques include Sessile drop, Whilhelmy Plate, Column Wicking, Thin Layer Wicking, Capillary Pressure, Drop Penetration, Dynamic Contact Angle, Atomic Force Microscopy, Environmental Scanning Electron Microscopy, and Inverse Gas Chromatography. A reader can refer to a review article of Alghunaim et al., which provides an excellent summary of each technique (Alghunaim et al., 2016). In this thesis, the sessile drop technique was used to determine the contact angle. This

technique is simple, quick and easy to use. As illustrated in **Figure 2.8**, the contact angle is formed once a liquid gets into contact with a solid material. As the angle increases, the wettability is decreased.

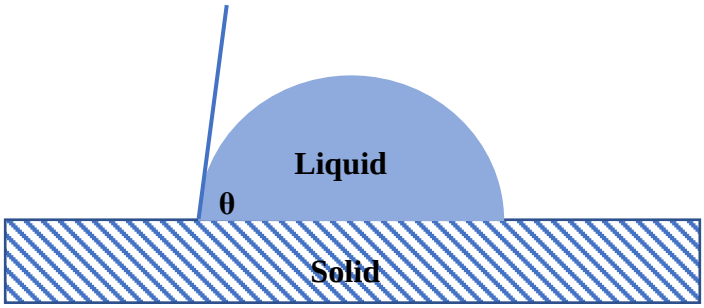

Figure 2.8 Illustration of interaction between solid phase and liquid phase and the resultant angle

The contact between the liquid and the solid is usually captured using a high-speed camera. By analysing images captured, the contact angle can be determined. This technique, however, poses some limitation, especially when liquid is absorbed by solid quickly, which make it difficult to measure the angle formed between the liquid and solid. To overcome this limitation, the elapsed time needed for the drop to disappear was recorded. That time for the drop to disappear was then used to compare between different formulations.

2.1.11 Compaction simulator

Tablet production involves compressing powder into a suitable compact with a predefined thickness and weight. Two main types of instruments can be chosen depending on the availability of the API and the purpose of the study. These include rotary press and single punch machines (Augsburger & Hoag, 2016).

Rotary press can be used in an industrial setting but require a large amount of materials. Due to the amount of the API required, the use of these type of machines can be limited in early stages of API discovery. Single punch tabletting machine is of great importance, especially in the early stages of API development. These machines can provide valuable details about the mechanical properties of pharmaceutical powders. Compaction simulators are an example of these machines that give accurate information about powder compaction properties. Moreover, these machines can be used in the pre-formulation, formulation and scale-up stages of drug product development. In pre-formulation, a single punch machine can be used to investigate the mechanical properties of different API batches and comparing between these batches. In addition, they can be used to give an early indication of deformability, plasticity, compressibility and sticking behaviour of API studied. In formulation stages, they can be used to investigate the effect of formulation changes on the mechanical properties of pharmaceutical compacts produced. In addition, they are of great value to establish a robust tablet production setting. Moreover, these machines

can serve as a valuable tool in scale-up and production, such as changes in API properties such as size and shape (Augsburger & Hoag, 2016).

In this thesis, a single punch mechanical testing machine attached to a compression platen (M500-50CT, Testometric Co, limited. Rochdale, UK) was used. Different compression forces were used in order to investigate the mechanical properties of different powders. Compaction speed was kept the same during the compression process. A linear variable differential transformer (LVDT) linked to the platens was used to record the displacement of the upper punch (Solartron AX/2.5/S, Solartron metrology limited, UK) (Laity et al., 2015; Laity & Cameron, 2008). Force was applied using the upper punch while the lower punch remains stationary. Once the compression cycle is completed, tablets were gently removed and further weighed and measured in terms of thickness and diameter. Upper, lower punches and dies were carefully lubricated before conducting any compression work using a suspension of 0.25% magnesium stearate in ethanol to minimise sticking and prevent capping (Khorsheed et al., 2019).

A typical force-displacement profile can be seen in Figure 2.9. Plastic work, elastic work, compression phase and decompression phase are highlighted in the figure. Elastic and plastic work were used to differentiate between powders in terms of plasticity (Aburub et al., 2007)

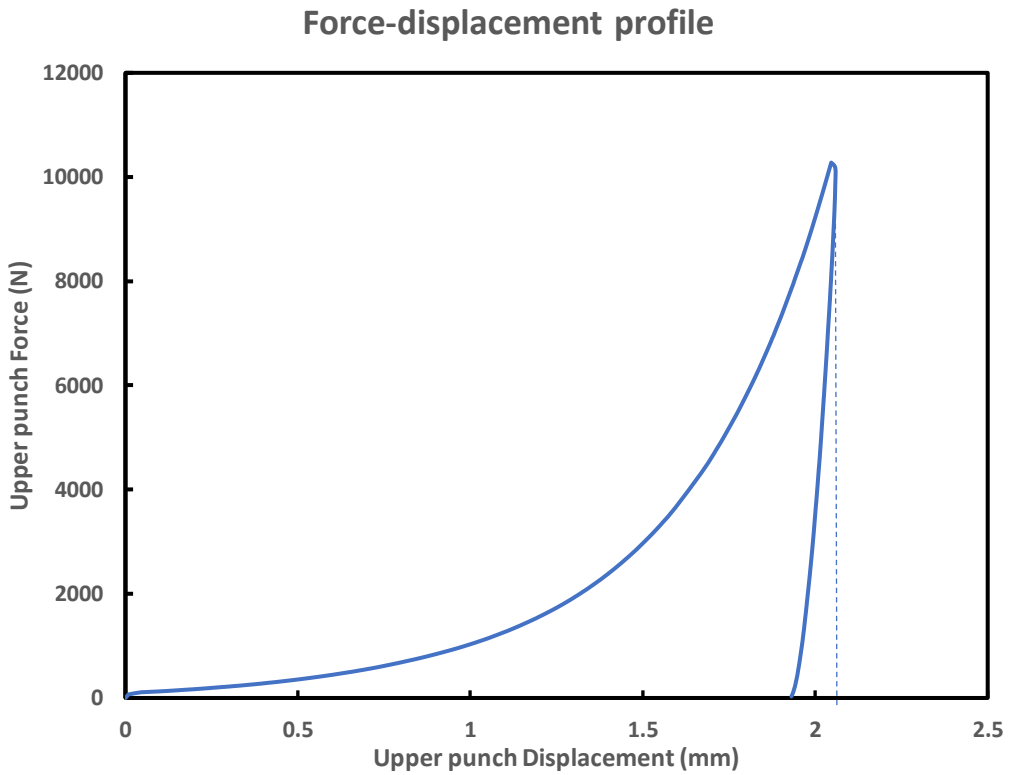

Figure 2.9 Typical force-displacement profile

Yield pressure was also used to compare between compressibilities of different batches. Yield pressure is the reciprocal value of the Heckel coefficient (Pitt & Sinka, 2007). Heckle coefficient (K) was calculated using equation 2.3:

$$Ln\left(\frac{1}{1-D}\right) = K.P + A \qquad \textbf{Eq. 2.3}$$

This equation is a linear equation with K (Heckle coefficient) is the slope, D is the relative density at any given compaction pressure P, and A is a constant (and the y-intercept).

2.1.12 Real time disintegration monitoring

Tablet disintegration is one of the primary key parameters affecting both in vitro and in vivo release of pharmaceutical tablets. Conventional compendial methods such as those used in both USP and British pharmacopoeias only provide qualitative information on the speed of disintegration of pharmaceutical tablets. It does not provide any insights into how disintegration works (Donauer & Löbenberg, 2007). Therefore, there is a growing interest in understanding tablet disintegration mechanism through a real-time process. Wilson et al. establish a new system that links the dynamic image analysis technique (QicPic) to USP dissolution media. This method allows monitoring both the number and size of particles produced after dissolution (Wilson et al., 2012). However, this method cannot separate disintegration from dissolution and does not account for what happens within the tablet itself. Rajkumar et al. designed a flow-through cell that can monitor the disintegration behaviour in real-time. This method allows monitoring changes in tablet disintegration and allows online imaging of the disintegration behaviour (Rajkumar et al., 2016). In this research, the effect of both particle size of starting materials and the type of disintegrant on the performance of pharmaceutical compacts was studied by utilising a flow through cell similar to the one designed by Rajkumar et al. and connecting this flow through the cell to a wet particle size analyser to observe both particle size changes and fragmentation of particles upon compression and disintegration.

The system used in this research utilises the whole-cell dosage form provided by Sirius Analytical in order to perform disintegration studies (Sirius, 2017). The cell used in this thesis was connected to a buffer reservoir. The buffer was pumped at a constant speed through the whole cell. The whole-cell was first flushed with water before it drained. Then the tablet was inserted into the system using a specific holder. Buffer solution was then pumped into the system. The disintegration behaviour of tablets was monitored using a specific camera connected to the system. After full disintegration, the system was connected to a wet particle size analyser where the particle size of disintegrated tablets was analysed.

Figure 2.10 illustrates this technique used in this research to monitor the disintegration behaviour of different compacts and particle size changes once the disintegration is complete.

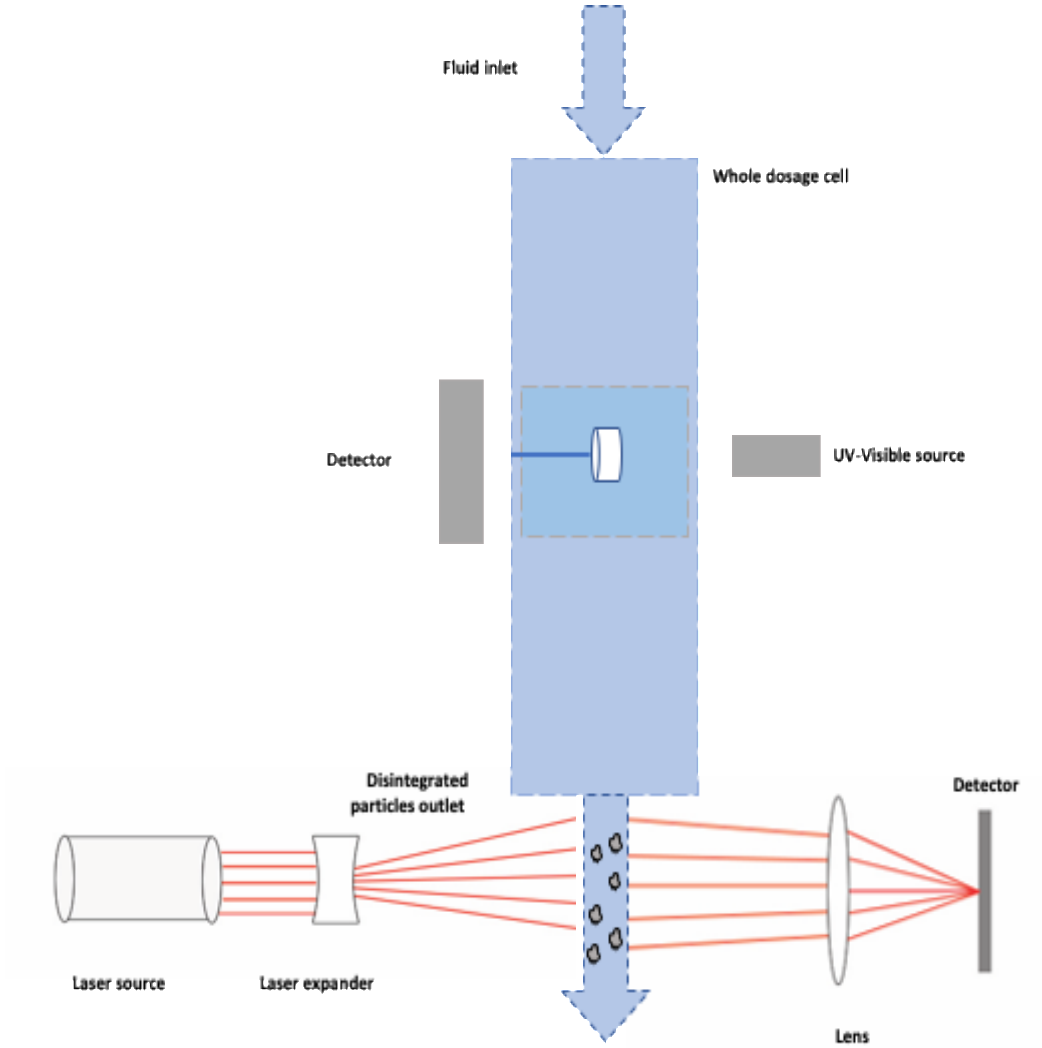

Figure 2.10 Schematic diagram of how tablet disintegration was measured by coupling SDI2 and laser diffraction (wet method)

Chapter 3 - Evaluating how formulation properties affect the microstructure and performance of solid dispersions: glyburide as a case study

Note to reader: Aspects of this chapter has been published under the title “Hot-melt extrusion process impact on polymer choice of glyburide solid dispersions: The effect of wettability and dissolution” in the International Journal of Pharmaceutics. https://doi.org/10.1016/j.ijpharm.2019.01.038

3.1 Introduction

As discussed in chapter 1 of this thesis, material science tetrahedron concept focuses on the effect of particle properties, processing properties, and formulation properties on the performance of pharmaceutical powders or dosage forms. Later chapters (Chapters 4, 5 and 6) focus on the effect of particle properties on the performance of pharmaceutical powders. In this chapter, the focus is on how formulation properties may impact on the performance of pharmaceutical formulations especially in terms of microstructure, wettability and dissolution performance. A poorly soluble model drug (glyburide) was used as an example to explain how formulation properties such as polymer type and level would affect the performance of formulations produced by hot-melt extrusion (HME). Poorly soluble drugs are very challenging during pharmaceutical development as solubility, and further dissolution tends to be the rate-limiting step for these compounds entering the systemic circulations and giving the desired therapeutic response (Adebisi et al., 2016; Conway and Asare-Addo 2016).

One of the attractive routes to overcoming these problems is by manufacturing amorphous solid dispersions (ASD). ASD systems are composed of amorphous drug stabilised by the presence of a polymer (Newman et al., 2015). Melting methods, especially HME have many advantages including scalability, being a solvent and dust free method and has industrial applicability (Paudel et al., 2013). The drug-polymer is blended then fed through hopper to a heated barrel of a twin-screw extruder. In the extruder, the drug-polymer blend experiences very high shear and temperature which leads to the formation of a homogenous dispersion of the drug into the polymer matrix. The formed solid dispersion is then pushed through the die to get the solid dispersion threads which are then subjected to pelletisation and the pellets collected as a

finished product. The physical properties and ultimately the performance of pellets can be controlled by either changing the processing parameters such as temperature, speed or twin-screw configuration or using different polymers (Van den Mooter, 2012). Choosing the right polymers for hot melt extrusion process depends on many factors. These factors include the target formulation required such as immediate-release or delayed release dosage forms, physicochemical properties of these polymers that are compatible with the active pharmaceutical ingredients used in solid dispersions and the processing conditions that drug-polymer will go through (Thakkar et al., 2020). Polymers used not only enhance the stability profile of APIs used, but also may play additional roles such as solubility enhancers as in the case of HPMC, HPMCAS, and PEG or controlling the release of the APIs as in the case of ethyl cellulose, Eduragit and chitosan formulations (Thakkar et al., 2020). Polyethyleneglycol–polyvinyl caprolactam–polyvinyl acetate grafted copolymer (PEG6000/vinylcaprolactam/vinyl acetate copolymer, Soluplus®, BASF, Germany) (Figure 3.1) is a promising polymer that has attracted a lot of attention over the last decade. Soluplus® possesses the advantages of improving both the process (Djuris, et al., 2013) and the dissolution rate of poorly soluble drugs (Nagy et al., 2012). The addition of PEG 6000 and the low glass transition temperature enhances the processability and eliminates the addition of a plasticiser. Soluplus® also improves the dissolution rates of poorly soluble drugs by forming a solid solution with the drug. Kollidon® VA 64 or PVP VA64 (polyvinylpyrrolidone-vinyl acetate copolymer) (Figure 3.1) is another polymer which has been demonstrated to enhance the dissolution rate of poorly soluble drugs (Ponnammal et al., 2018). PVP VA64 works by solubilising poorly soluble drugs and ultimately improving the dissolution rate. An

enhancement in mechanical properties and the production of flexible extruded pellets has been reported for the use of PVP VA64 (Solanki et al., 2018). Both polymers are considered as safe excipients and easy to handle with good flowability properties (Djuris et al., 2013; Nagy et al., 2012).

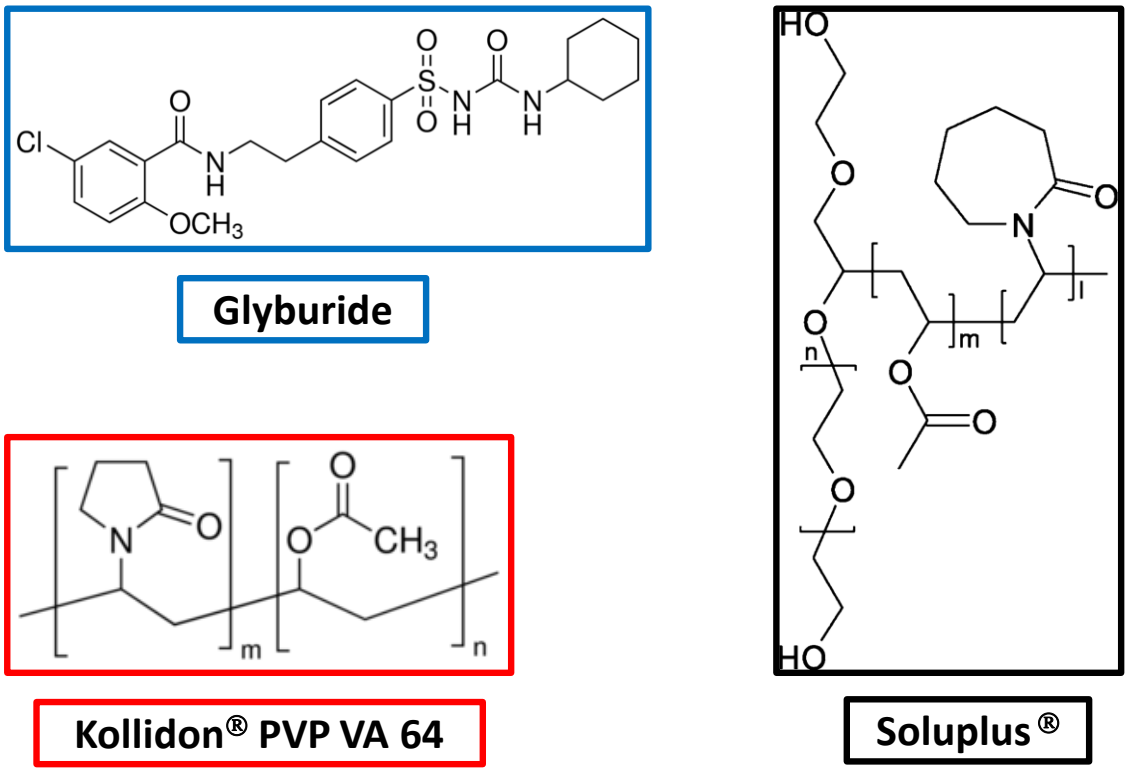

Figure 3.1 Structure of Glyburide, Soluplus® and Kollidon® PVP VA64 used in the manufacture of pellets from the hot-melt extrusion process for the formulations (Samples A-D)

3.2 Aims and objectives

The objective of this research was to evaluate the effect of formulation properties mainly polymer choice and concentration on the performance of the microstructure and wettability of a hot-melt extruded solid dispersion. Glyburide (Gly) was used as a model poorly soluble drug.

Solid dispersions were produced using a continuous twin screw extruder. Solid dispersion of Gly using Soluplus® (Sol) and PVP VA64 at two different polymer levels were prepared. The surface of resultant pellets was characterised using a focus variation instrument. Then the effect of both polymer type and level on wettability and microstructure was investigated. The purpose was to investigate if there is any correlation between the wettability of the solid dispersions (polymer level and type) and the performance of dissolution as to the best of our knowledge, there are no previous research that have studied this.

The manufactured solid dispersions were also characterised using scanning electron microscopy (SEM). SEM method is further described and detailed in section 2.1.1.1. Image analysis using a focus variation instrument (FVI). More information on (FVI) method can be found in section 2.1.5. Differential scanning calorimetry (DSC) (as described in section 2.1.8) and X-ray powder diffraction (XRPD) (as described in section 2.1.9) were also used to investigate if there was any changes in the solid form. X-ray microtomography (XμT) was used as detailed section 2.1.4 to investigate the changes in microstructure. Dynamic contact angle measurement and dissolution analysis using biorelevant dissolution media (FASSIF) were also used to compare between the resultant formulation in terms of dissolution behaviour. A laser diffraction method (section 2.1.2.2) was also used to investigate if there was any particle size differences between the obtained formulations. Preparation of hot-melt extruded (HME) solid dispersions

To prepare these solid dispersions, 16 mm twin screw extruder (Pharmalab, Thermo Scientific, UK) was used. Gly and either PVP VA64 or Soluplus® at two different ratios (1:1 and 1:2)

were firstly blended using a T2F Turbula Blender System (Willy A Bachofen AG) for 10 min in order to ensure uniformity of powder mixing. A plasticiser (PEG 4000) was added to the PVP VA64 samples to enhance the extrusion mechanism. HME barrel temperature is highlighted in Table 3.1 where care was taken to ensure the degradation temperature of Gly which has been reported to range between 195 - 200 ℃ (Wei et al., 2008b) was not reached by reading the actual temperature recorded during the HME process also. A mixture of conveying and kneading elements with a stagger angle of 60 degrees for the kneading elements was used. Screw rotation speed was fixed at 100 rpm for all four sample batches. The feeding rate of the powder was set at 5 g/min). The resultant extrudates were further pelletised using a Caleva multi lab machine. A small amount of the resultant pellets were saved for a further characterisation while the rest were further milled using a mortar and pestle and sieved to 250 µm undersize (to ensure the same size fractions were used for all analysis). These samples were used in the dissolution testing and labelled as samples A-D (Sample A is 1:1 Gly:Sol, Sample B is 1:2 Gly:Sol, Sample C is 1:1 Gly:PVP VA 64 and Sample D is 1:2 Gly:PVP VA 64) and their corresponding physical mixtures labelled as samples PMA-PMD. These physical mixtures were prepared in a gram scale by weighing suitable amount of Gly and blend it with the either Sol or PVP at (1:1) and (1:2) ratio.

Table 3.1 Zone number and corresponding temperature for conveying and kneading

Zone Number	1	2	3	4	5	6	7	8	9	Die
Temperature (°C)	45	70	90	175	175	175	175	175	175	175

3.3 Methods

3.3.1 Content uniformity of Gly in milled and sieved samples

Gly content was analysed using the HPLC method. A 50 mg of the milled and sieved samples A-D was dissolved each in 50 mL acetonitrile and an assay was performed to determine the content of Gly in each sample. The results from the assay were further used to determine the amount of powder needed to fill the gelatine capsules size 3 to ensure the same amount of Gly was present in each capsule.

3.3.2 Scanning electron microscopy (SEM)

Samples were sputter-coated with gold for 60 s using a Quorum SC7620. The scanning electron microscope (Jeol JSM-6060CV SEM) operating at 10 kV was used to generate electron micrographs images. Pellets (Samples A-D) were cross-sectioned and mounted onto a metal stub using a double-sided adhesive tape. Micrographs with different magnifications were taken to aid an understanding of the polymer ratios impact on the pellets produced. More information about this technique can be found in section 2.1.1.1 of this thesis.

3.3.3 Surface roughness analysis using focus variation instrument (FVI)

A focus variation instrument (Contour LS 3D Optical Profiler (Bruker)) was used to assess the surface topography of the pellets using 10 x objective and 2.9 μm lateral resolution. The obtained images were further analysed using the Surfstand™ software (Taylor Hobson, UK, and University of Huddersfield, UK) to obtain 2D and 3D profiles of the surfaces (Ward et al., 2017). Detailed discussion on the FVI can be found in section 2.1.5 of this thesis.

3.3.4 Differential scanning calorimetry (DSC)

Thermal studies for the milled samples and their corresponding physical mixture were investigated using the software obtained from Mettler-Toledo, Switzerland. 3-6 mg of the milled and seived samples (Samples A-D) or its physical mixture (Samples PMA-PMD) was placed in a standard aluminium pan with a vented lid and sealed. The crimped pans were heated from 20 to 250 °C at a scanning rate of 10 °C/min using nitrogen gas to purge the DSC (Mettler-Toledo, Switzerland). More information about the principles of theremal ananlysis can be found in section 2.1.8 of this thesis.

3.3.5 X-ray powder diffraction (XRPD)

Gly, the milled and sieved powder (Samples A-D) and their corresponding physical mixtures (Samples PMA-PMD) were scanned using Bragg–Brentano geometry, over a scattering (Bragg, 2θ) angle range from 5 to 100°, in 0.02° steps at 1.5° min^{-1} using a D2 Phaser diffractometer (Bruker AXS GmbH, Karlsruhe, Germany) (Laity et al., 2015). The XRPD signals were further analysed using Microsoft Excel. More information about the principles of XRPD can be found in section 2.1.9 of this thesis.

3.3.6 X-ray microtomography (XμT)

Pellets prepared early as described in section 3.3 were imaged by XμT (Nikon XT H 225, Nikon Corp. Tokyo, Japan) using a tungsten target with 75 kV accelerating voltage and 250 μA gun current using a copper filter (thickness 0.125 mm). Pellets were mounted using a double-adhesive tape. A set of projections were collected with over 120 min XμT acquisition.

The set of projection images were then reconstructed using CT-Pro and then examined using VG Studio 2.1 software. A detailed information on this method can be found in section 2.1.9.

3.3.7 Particle size analysis using laser diffraction:

Particle size analysis techniques are detailed and described in section 2.1.2.2. A laser diffraction instrument (Sympatec, UK) was utilized to particle size these samples supplied with R3 lens.The primary sample container containing each excipient grade was thoroughly mixed by rolling and inverted by hand as well as mixed using a spatula. Before starting the measurement, the sample was gently inverted and agitated to evenly disperse it and, thus, reduce loss of material in the vials. The WINDOX software was utilized to perform the statistical analysis of the obtained measurements.

3.3.8 Dynamic contact angle measurement:

Sample A-D were milled and sieved before conducted any contact angle measurements. The sessile drop method (Drop Shape Analysis System, DSA30, Krüss GmbH, Hamburg, Germany) was used to obtain the dynamic contact angle for each formulation (Figure 3.2). This was performed using 1 µL of either deionised water or a FASSIF medium. The liquid was dispensed from a needle to generate a drop and images of the droplet were recorded with a rate of 10 frames per second. The measurements were made at room temperature in triplicate and the average values and standard deviations were calculated. The initial contact angle was determined from the first ten images (measurement time of 1 s). More details about the principles of contact angle measurement can be found in section 2.1.10 of this thesis.

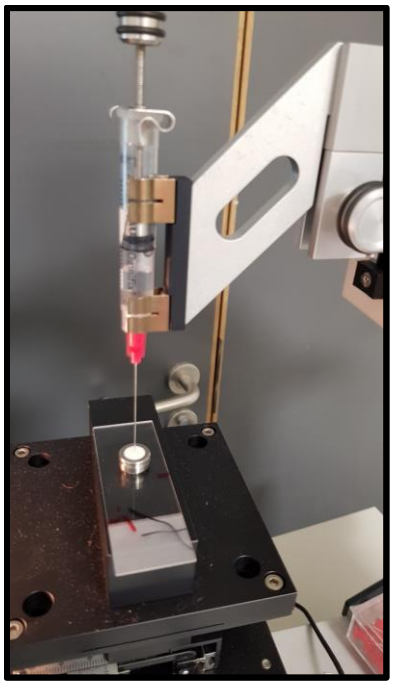

Figure 3.2 Contact angle testing instrumentation used in the study to determine the wettability and initial liquid imbibition of the solid dispersions produced

3.3.9 High performance liquid chromatography (HPLC) analysis:

A Shimadzu HPLC system equipped with a C18 column (250 mm x 4.6 mm ID, 4µm, Phenomenex) was used for the Gly analysis. An Isocratic elusion type with a mobile phase of ammonium acetate and acetonitrile (45:55) was used at a flow rate of 1 mL/min. A UV-Vis detector was utilised, and the absorption peak for Gly was investigated at a maximum wavelength of 254 nm. The retention time for Gly was around 2.8 min (Gedeon et al., 2008). Six concentrations of glyburide (1000, 200, 40, 20, 8, 4 µm/ml) were prepared. The calibration standards were injected in triplicates. The detector response was shown to be linear over the

range studied and gave a regression coefficient (R2) of 1 and Y=6951.3x+872.47. The calibration curve for the method is presented in Figure 3.3.

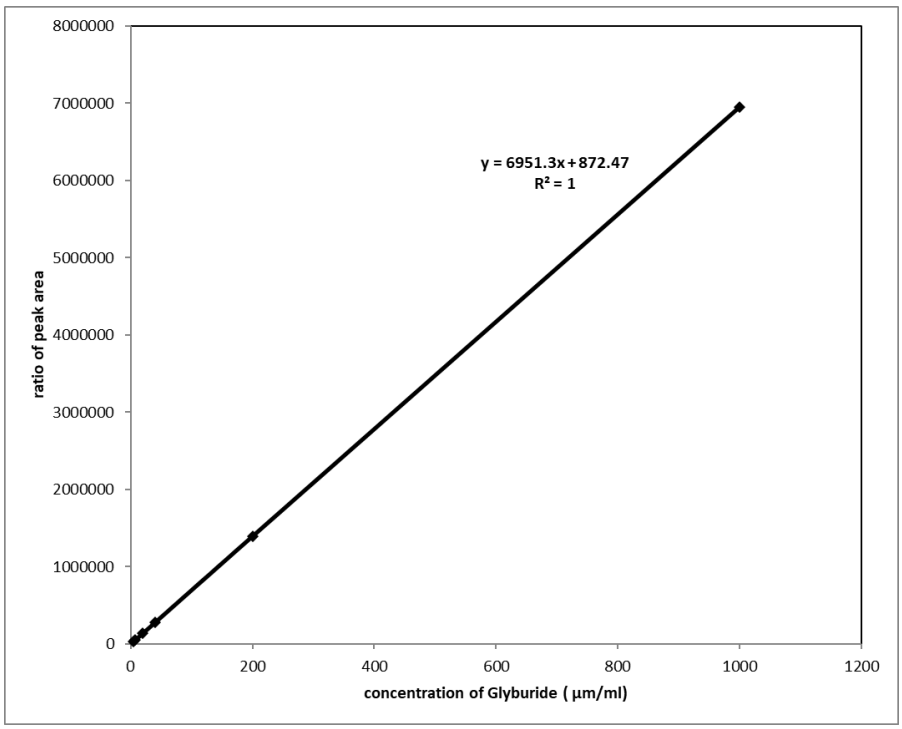

Figure 3.3 Calibration curve used to determine glyburide concentration

3.3.10 Dissolution analysis

3.3.10.1 Media preparation:

Fasted state simulated intestinal fluid (FASSIF) biorelevant dissolution media was prepared by dissolving 2.24 g of FASSIF powder for each 1 L of phosphate buffer (pH 7.4). The phosphate buffer was prepared using monobasic potassium phosphate and sodium hydroxide according to the USP pharmacopoeia (Wei & Obenberg, 2006).

3.3.10.2 Dissolution of the Gly solid dispersions:

A USP I (basket method) apparatus was used for the dissolution testing. 900 mL of dissolution media was filled in a 1L dissolution vessel. The media was heated to 37 ± 0.5 °C. The physical mixtures (PMA-PMD) as well as the milled and sieved powder samples (samples A-D) containing an equivalent of 20 mg Gly content (based on their content uniformity) were weighed and then used to fill a size 3 hard gelatine capsule before being transferred to the basket. A rotation speed of 100 rpm was used. The dissolution study was conducted for 2 h. 10 mL of the dissolution media was withdrawn and filtered at the 1, 5, 10, 20, 30, 45, 60, 90 and 120 min predetermined time points for HPLC analysis (section 3.4.9) of the Gly content. A preheated biorelevant media was used to replace the 10 mL media taken out after each time point to ensure the constant 900 mL volume. All dissolution studies were conducted in triplicate.

3.3.10.3 Dissolution parameters:

Mean dissolution time (MDT) (equation 3.1), defined as the mean time for the drug to dissolve under *in-vitro* dissolution conditions, is a model-independent method and is suitable for dosage forms that have different mechanisms of drug release (Al-Hamidi et al., 2013; Kaialy et al., 2016; Khan, 1975; Mu, Tobyn, & Staniforth, 2003; Nep et al., 2017)

$$MDT = \frac{\sum_{j=1}^{n} t_j \, \Delta M_j}{\sum_{j=1}^{n} \Delta M_j} \qquad \textbf{Eq. 3.1}$$

where j is the sample number, n is the number of dissolution sample times, $\boldsymbol{t_j}$ is the time at midpoint between $\boldsymbol{t_j}$ and $\boldsymbol{t_{j-1}}$ and $\Delta \boldsymbol{M_j}$ is the additional amount of drug dissolved between $\boldsymbol{t_j}$ and $\boldsymbol{t_{j-1}}$.

The dissolution efficiency (DE) (equation 3.2) is defined as the area under the dissolution curve up to a certain time *t*, expressed as a percentage of the area of a rectangle described by 100% dissolution in the same time *t* (Asare-Addo et al., 2015; Khan, 1975) was also calculated

$$DE = \frac{\int_0^t y \times dt}{y_{100} \times t} \times 100 \qquad \textbf{Eq. 3.2}$$

where y is the drug percent dissolved as a function of time t.

3.4 Results and discussions

3.4.1 SEM and focus variation analysis

SEM images are presented in Figure 3.4. As can been seen from images, the microstructure of the pellets vary in terms of its overall porosity (further analysed using XµT). Furthermore, some of the crystalline drug could be seen on the surfaces of some extrudates (highlighted by the yellow dashed circles). This has been further confirmed by solid state analysis. This was however not evident on the samples with increased polymer content (Samples B and D).

Focus variation analysis showed significant variation in the surface texture across all four extrudes in keeping with SEM (Figure 3.5). It has been observed that Sq value increased as polymer content increased through sample studied (Sample A, 1:1 Gly:Sol – Sq = 19.83 µm ;

Sample B, 1:2 Gly:Sol – Sq = 48.78 µm; Sample C, 1:1 Gly:PVP VA64 – Sq = 26.56 µm; Sample D, 1:2 Gly:PVP VA64 – Sq = 33.58 µm).

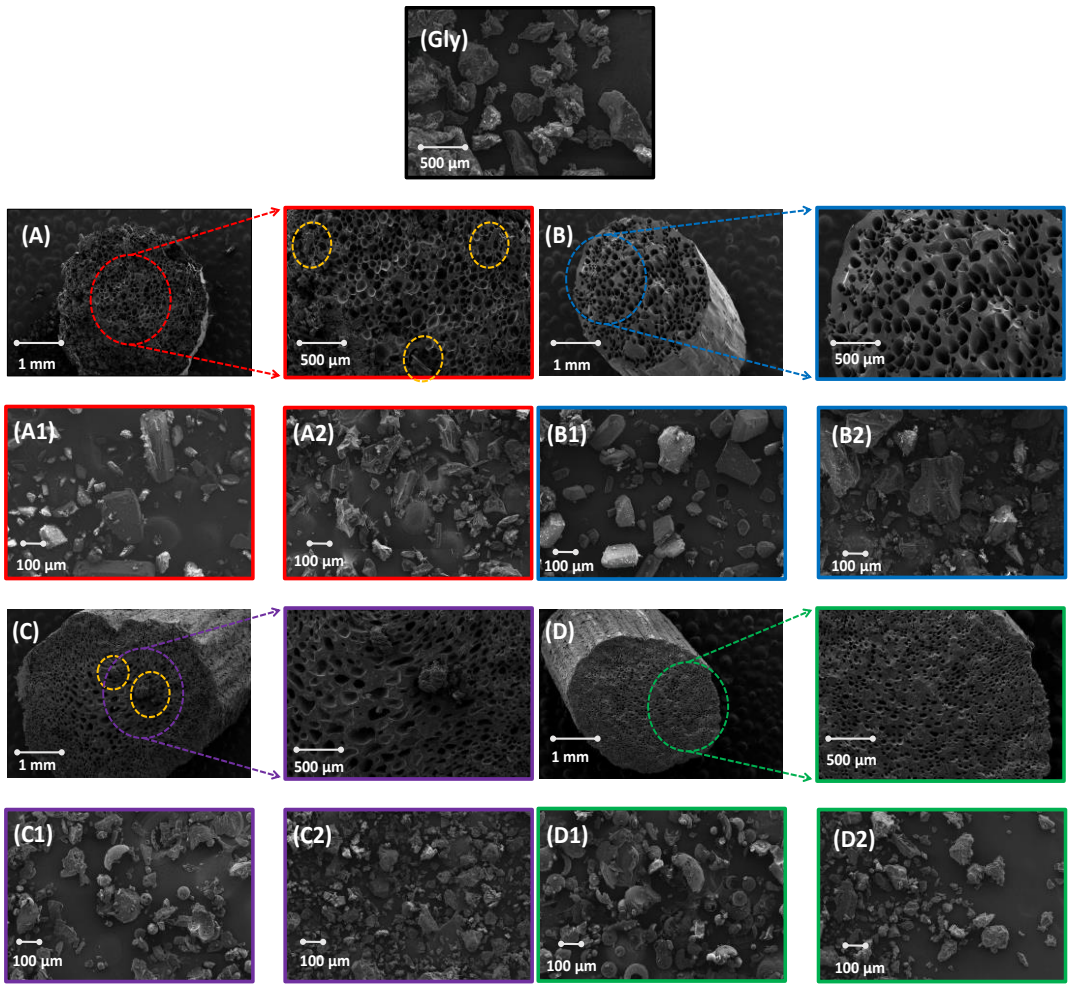

Figure 3.4 SEM images of Gly, (A) HME extrudate pellets of 1:1 Gly:Sol (sample A) formulation, (A1) physical mixture of 1:1 Gly:Sol, (A2) 1:1 Gly:Sol (milled and sieved sample from HME extrude pellets of A), (B) HME extrudate pellets of 1:2 Gly:Sol (sample B) formulation, (B1) physical mixture of 1:2 Gly:Sol, (B2) 1:2 Gly:Sol (milled and sieved sample from HME extrude pellets of B), (C) HME extrudate pellets of 1:1 Gly:PVP VA64 (sample C) formulation (C1) physical mixture of 1:1 Gly:PVP VA64 (C2) 1:1 Gly:PVP VA64 (milled and sieved sample from HME extrude pellets of C), (D) HME extrudate of 1:2 Gly:PVP VA64 (sample D) formulation, (D1) physical mixture of 1:2 Gly:PVP VA64 (D2) 1:2 Gly:PVP VA64 (milled and sieved sample from HME extrude pellets of D)

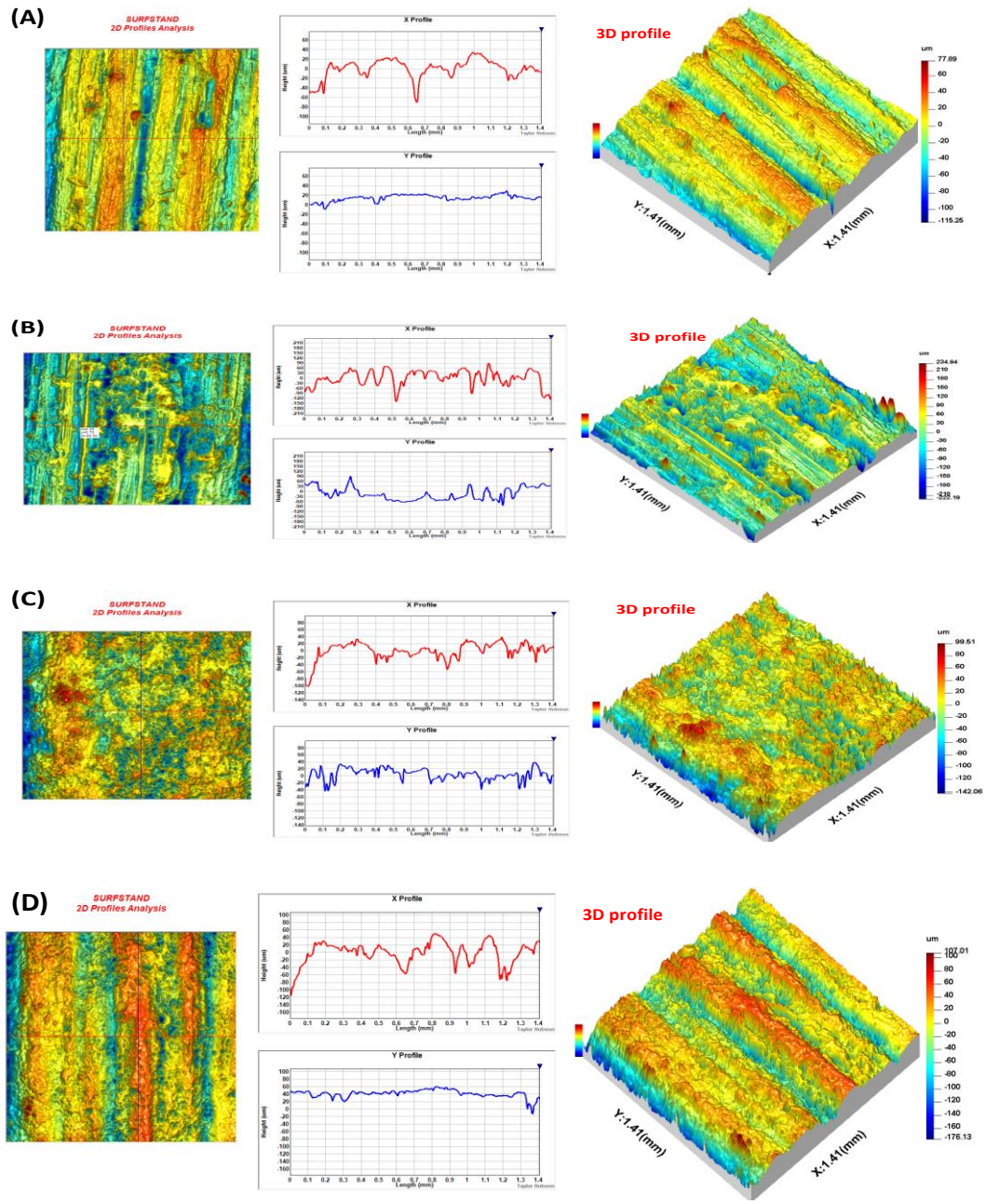

Figure 3.5 Focus variation images of (A) Sample A, 1:1 Gly: Sol (B) Sample B, 1:2 Gly: Sol (C) Sample C, 1:1 Gly: PVP VA64 (D) Sample D, 1:2 Gly: PVP VA64

3.4.2 X-ray computed microtomography

The reconstructed XµT cross-sectional images of the filaments confirmed the findings from the SEM images (Figure 3.6). As polymer content increased, a decrease in the porosity was observed. Sample A (1:1 Gly:Sol) showed a higher porosity (63.72 %) compared to sample B (1:2 Gly:Sol) (57.41 %). This was also evident for samples C (1:1 Gly:PVP VA64) and D (1:2 Gly:PVP VA64). The porosity values for samples C and D were 19.47 % and 14.22 % respectively suggesting also that an increase in polymer content decreases the porosity of pellets produced. Order of porosity values was as follow: A > B > C > D. These results suggest that the PVP VA64 makes denser pellets which may well have dissolution consequences.

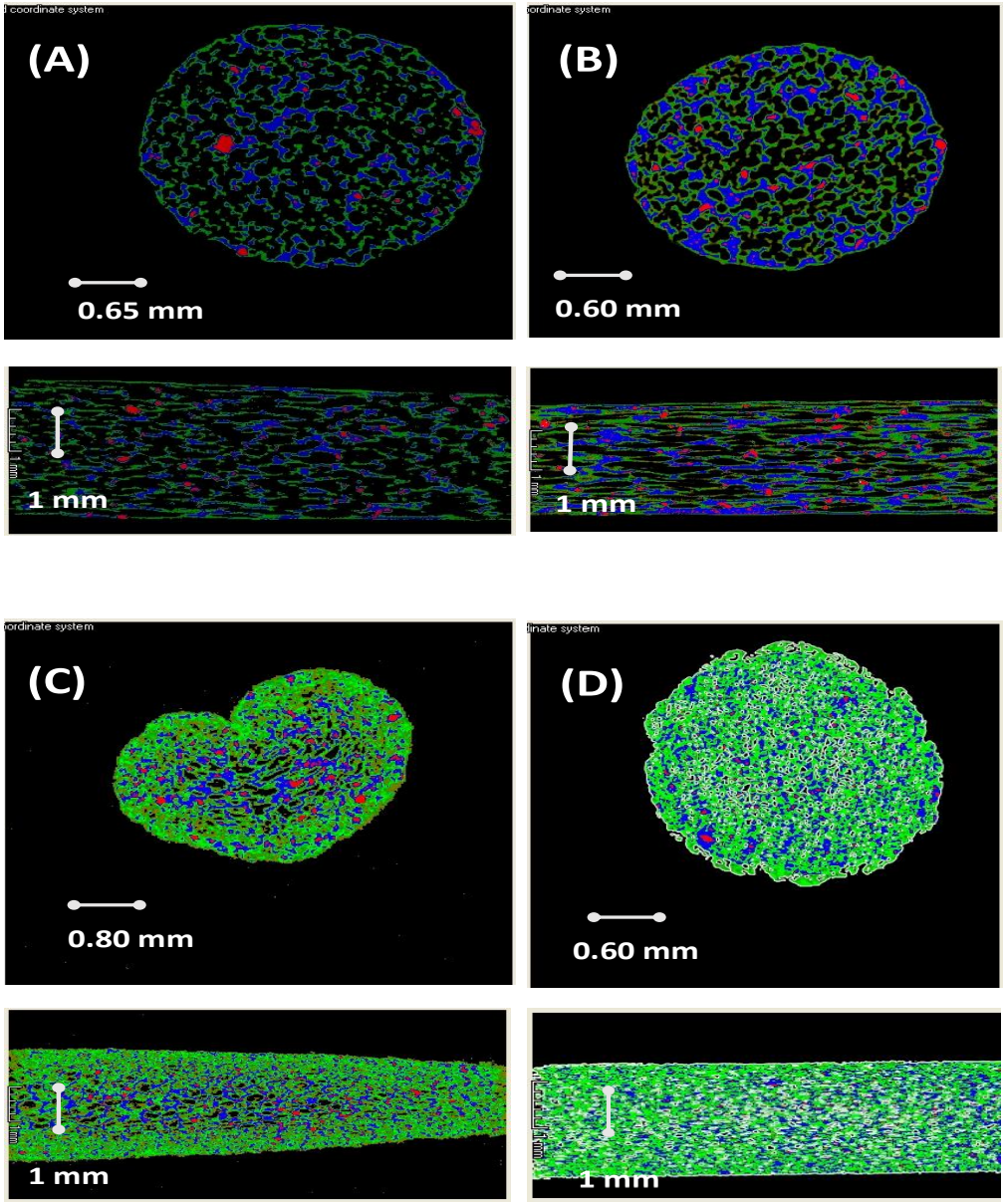

Figure 3.6 XμT of sagittal and diametric images of formulated HME extrudate pellet (A) HME extrudate pellet of 1:1 Gly:Sol (sample A), (B) HME extrudate pellet of 1:2 Gly:Sol (Sample B), (C) HME extrudate pellet of 1:1 Gly:PVP VA64 (sample C), (D) HME extrudate pellet of 1:2 Gly:PVP VA64 (sample D). Red colour is Gly, green and blue colour are polymer (Sol or PVP VA64) and black represents the pores

3.4.3 Solid-state analysis

DSC graphs showed Gly to have a sharp melting point at 175 °C confirming its crystallinity. This was similar to that reported by Cirri et al. (2004) . The physical mixtures of Gly with polymers showed a similar peak at the melting point of Gly with less intensity. An increase in the polymer content therefore brought about a general reduction in the melting point of Gly. This can be attributed to increased interactions between the polymer and also due to an increase in hydrogen bonding interactions between the drug and polymer (Huang and Dai, 2014; Rim and Runt, 1984) which results in a melting point depression. The physical mixture of Gly with PVP VA64 showed another peak at around 60 °C. This corresponds to the melting point of PEG4000 which was added to the formulations as a plasticiser (Sheskey et al., 2017). The resultant extruded products of Gly:Sol and Gly:PVP VA64 at the two drug loading levels showed no obvious melting point peak for Gly thereby suggesting that Gly had been molecularly dispersed within the polymers used (Figure 3.7). XRPD confirmed Gly to be completely crystalline (Figure 3.8). However, the samples that had been extruded (A-D) showed a significant reduction in the crystallinity of Gly. It was observed that an increase in the polymer content brought about a further decrease in the crystallinity of Gly. Interestingly, the XRPD data did reveal that samples A-D were not fully amorphous as suggested from the DSC data (Figure 3.7). Samples A and B however were observed to be more amorphous than C and D suggesting that with the process parameters used for the HME processing, Sol had the greater ability in converting crystalline Gly to its amorphous form which may potentially have implications for dissolution testing.

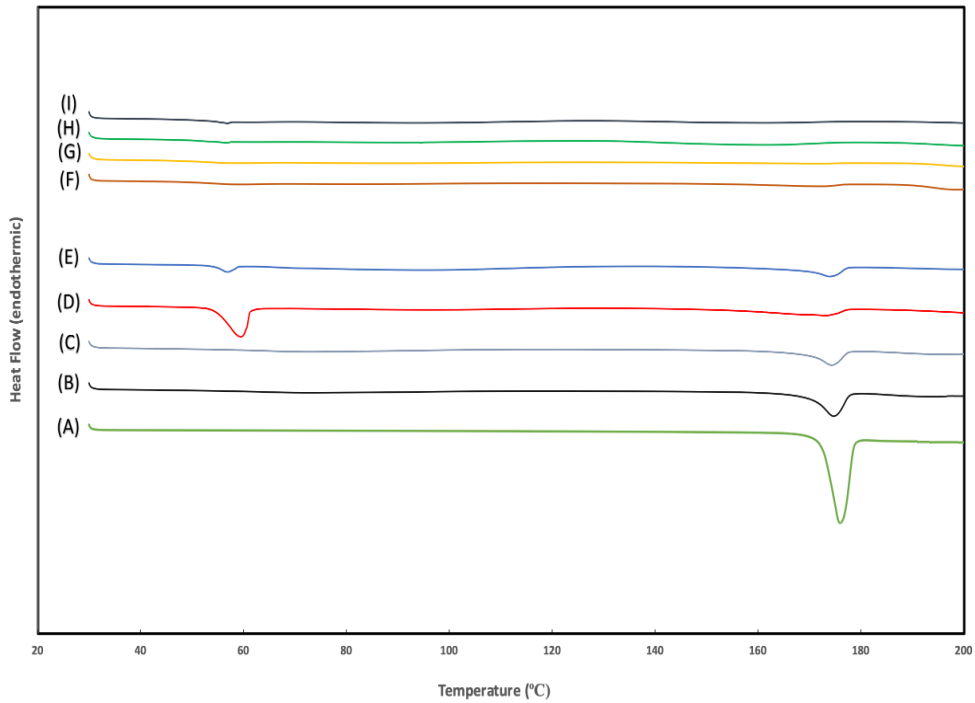

Figure 3.7 DSC thermograms of (A) crystalline Gly, the physical mixtures of (B) 1:1 Gly:Sol, (C) 1:2 Gly:Sol, (D) 1:1 Gly:PVP VA64, (E) 1:2 Gly:PVP VA64, and the hot-melt extruded samples of (F) 1:1 Gly:Sol, (G) 1:2 Gly:Sol, (H)1:1 Gly:PVP VA64 , (I) 1:2 Gly:PVP VA64

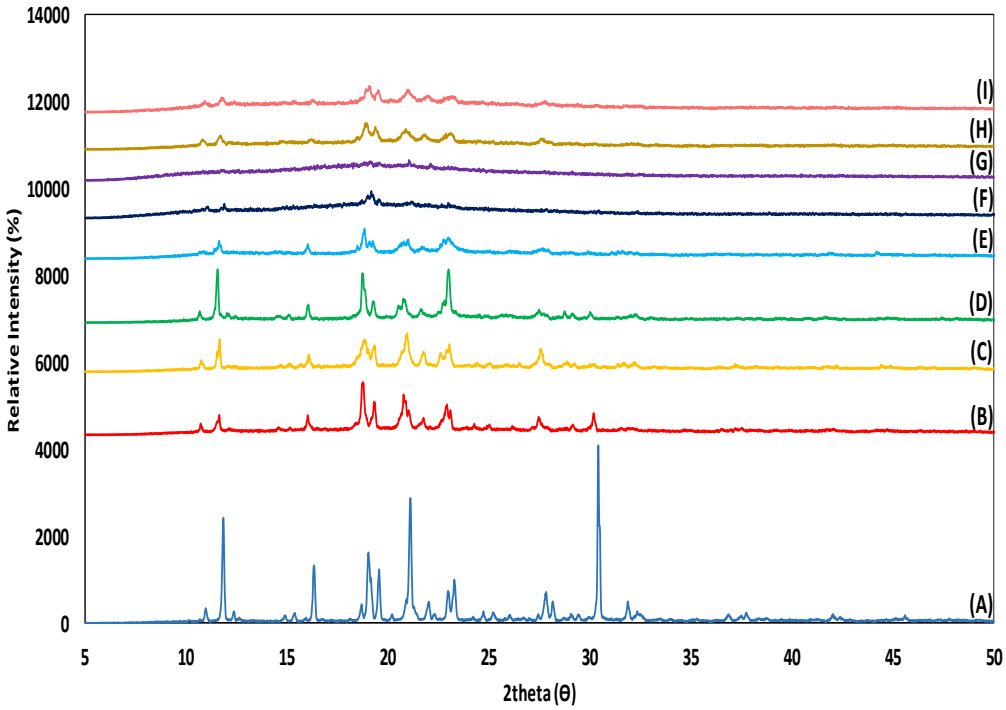

Figure 3.8 XRD of (A) crystalline Gly, the physical mixtures of (B) 1:1 Gly: Sol , (C) 1:2 Gly: Sol, (D) 1:1 Gly:PVP VA64, (E) 1:2 Gly:PVP VA64, and the hot-melt extruded samples of (F) 1:1 Gly:Sol, (G) 1:2 Gly:Sol, (H)1:1 Gly:PVP VA64 , (I) 1:2 Gly:PVP VA64

3.4.4 Contact angle measurement

Samples were sieved and analysed by laser diffraction to ensure a homogenous particle size distribution and to eliminate the effect of particle size. Table 3.2 showed particle size descriptors of these samples. As it shown in the table, similar values in these descriptors were observed indicating that particle size did not play a major role in the performance of these samples.

Table 3.2. Particle size distribution of Glyburide and its solid dispersions

Sample	D [0.1, v] µm	D [0.5, v] µm	D [0.9, v] µm
Sample A (Gly:Sol)(1:1)	13.11	58.30	79.79
RSD%	0.17	0.07	0.05
Sample B (Gly:Sol)(1:2)	11.43	55.35	78.53
RSD%	0.04	0.17	0.07
Sample C (Gly:PVP VA64)(1:1)	9.75	53.88	77.98
RSD%	0.17	0.37	0.17
Sample D (Gly:PVP K30)(1:2)	14.01	60.85	80.68
RSD%	0.79	0.10	0.04
Pure Drug (Glyburide)	4.09	35.02	72.09
RSD%	0.22	0.38	0.08

Contact angle measurements were performed using both deionised water and FASSIF. Using water, sample A (1:1 Gly:Sol) had the highest contact angle (90.65 ± 7.06 °). This was followed by sample B (1:2 Gly:Sol) with a contact angle of 84.41 ± 2.60 °. Sample C had the lowest contact angle (33.72 ± 1.24 °) followed by sample D with an angle of 41.11 ± 2.33 ° (Figure 3.9). This suggested samples C and D to be significantly more hydrophilic than samples A and B.

Dynamic contact angle measurements for the samples using FASSIF showed a different trend. The contact angles for samples A (1:1 Gly:Sol) and B (1:2 Gly:Sol) could not be measured as the droplet absorbed very quickly (within a few seconds). As such, the elapsed time for the droplet to be absorbed for these samples were taken into consideration. The mean time for sample A to be absorbed was 1.67 ± 0.50 s, whereas the mean time for sample B to be absorbed was 0.17 ± 0.05 s. This indicates that sample B wets slightly better than sample A. This was in contrast to the results from the deionised water suggesting that the presence of the various ions in the FASSIF media may have had a solubilising effect on the samples with an increase in polymer content having a greater effect. Samples C (1:1 Gly:PVP VA64) and D (1:2 Gly:PVP VA64) however had a lower absorption rate compared to samples A and B therefore the dynamic contact angle (Figure 3.10) could be determined. The data reveals that even though the initial contact angles for samples C and D were similar, sample D wets better than sample C over time. This was also similar to the trend observed for samples A and B where an increase in polymer content seemed to accelerate the ingress of media. In summary, the order of wetting for samples was: B > A > D > C. This change in contact angle order in comparison with deionised water may have implications again for dissolution testing and as such consideration should be made with regards to making appropriate predictions for dissolution based on the media for contact angle testing.

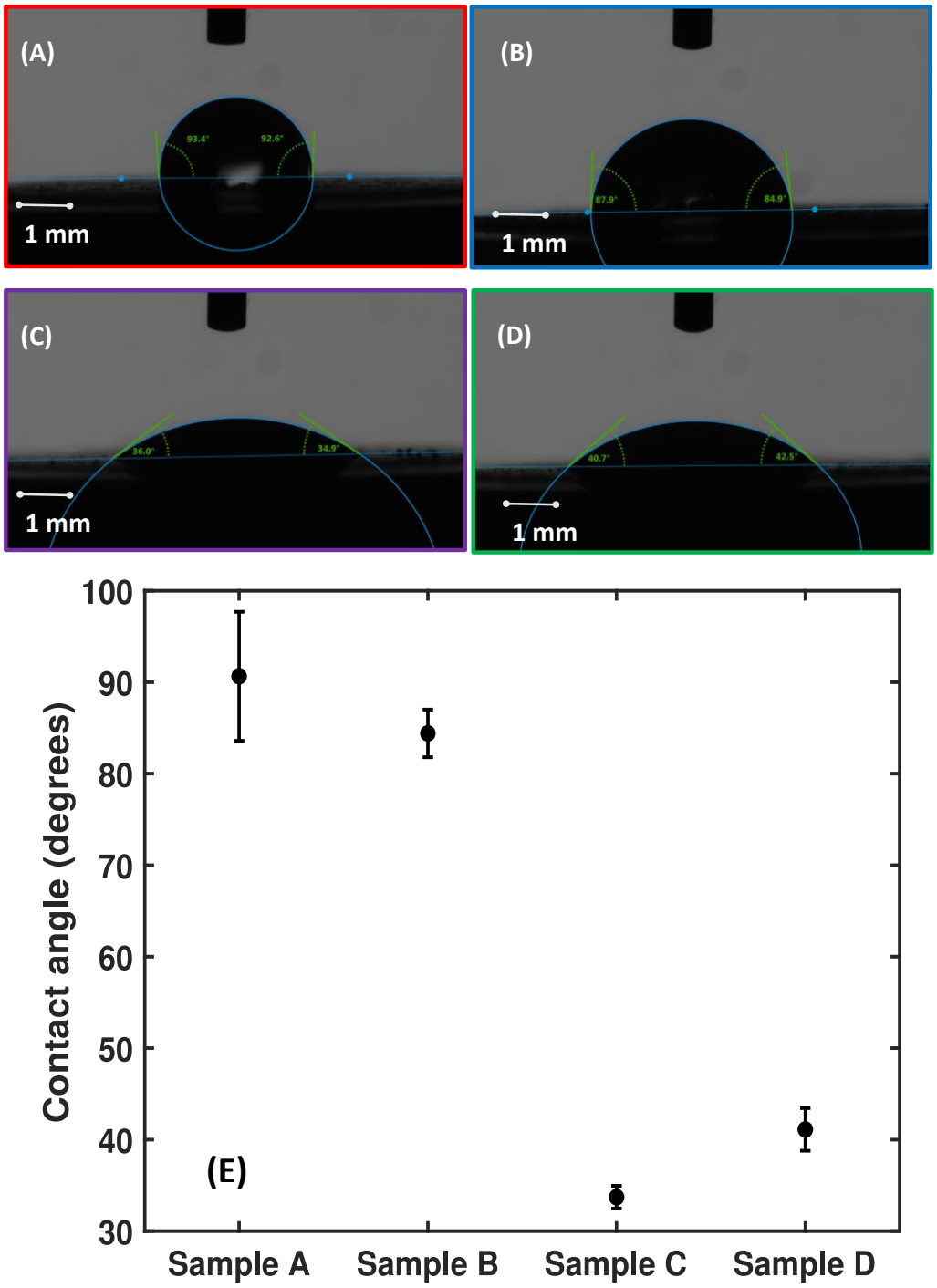

Figure 3.9 Contact angle testing of (A) 1:1 Gly:Sol (sample A), (B) 1:2 Gly:Sol (Sample B), (C) 1:1 Gly:PVP VA64 (Sample C), (D) 1:2 Gly:PVP VA64 (Sample D) and (E) a plot of all the contact angle degrees of samples A-D for comparison

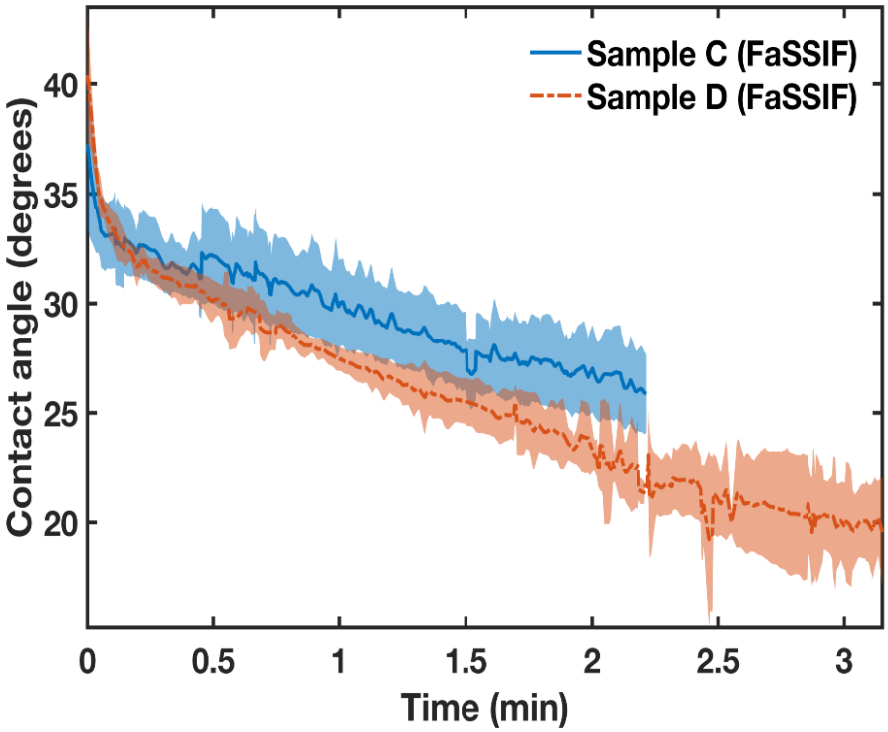

Figure 3.10 Dynamic contact angle measurement of samples C (1:1 Gly:PVP VA64) and D (1:2 Gly:PVP VA64) using FASSIF as the media

3.4.5 Dissolution analysis

Dissolution results can be observed in Figure 3.11. HME samples showed superior dissolution profiles to both crystalline Gly and their physical mixture counterparts. Samples containing Sol showed increased dissolution profiles to those containing PVP VA64. In addition, sample B, which contained 1:2 Gly:Sol, showed a higher dissolution rate in comparison to sample A (1:1 Gly:Sol). This indicates that increasing the level of polymer content enhanced the dissolution of Gly. A similar trend was observed with sample C and D, with sample D (1:2 Gly:PVP VA64) showing a higher dissolution rate in comparison to sample C (1:1 Gly:PVP VA64). This was confirmed by the MDT, MDR and DE values. Sample A had a DE value of 36.43%, MDT of 55.40 min and an MDR of 0.51% min^{-1} while sample B had a DE of 60.53%, MDT of 29.70

min and MDR of 0.91% min^{-1}. Sample C had a DE value of 10.17%, MDT of 66.28 min and MDR of 0.14% min^{-1} while sample D had a value of DE of 14.44%, MDT of 65.30 min and MDR of 0.19% min^{-1}. It was interesting to note that the dissolution results correlated with the wetting results from the contact angle measurement using the FASSIF media. This indicates that the initial liquid imbibition process as captured by the dynamic contact angle directly affects the dissolution performance. This dissolution behaviour can therefore be attributed to the nature of the polymers, its concentration as well as the degree of amorphorisation. This contributed to its increase in wettability as well as dissolution with sample B (higher in amorphous content) being the one with the highest dissolution).

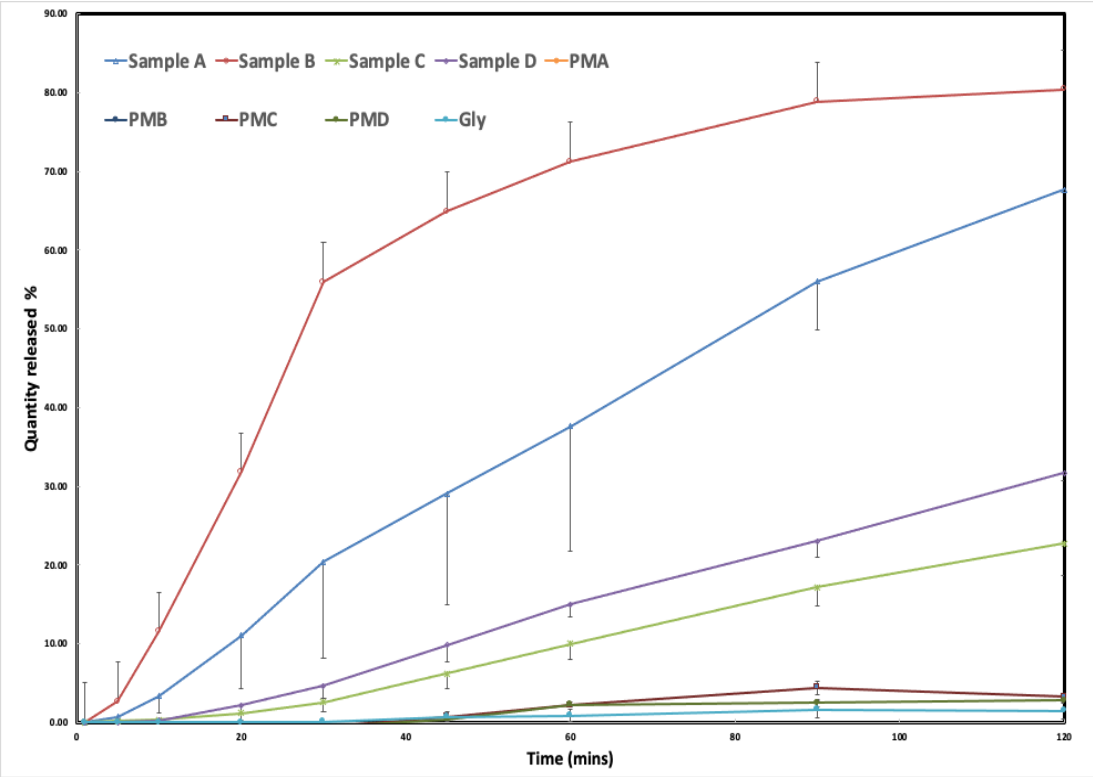

Figure 3.11 Dissolution profiles for 1:1 Gly:Sol (sample A), 1:2 Gly:Sol (Sample B), 1:1 Gly:PVP VA64 (Sample C), 1:2 Gly:PVP VA64 (Sample D) together with their corresponding physical mixtures PMA-PMD over 120 min

3.5 Conclusion

This chapter made it clear how formulation properties could play an important role in determining the performance behaviour of pharmaceutical formulations using novel characterisation techniques such as X-ray tomography and dynamic contact angle measurement. In this chapter solid dispersions of Gly with Sol and PVP VA64 were made at varying concentrations using a hot-melt extrusion process. Microstructure and surface morphology showed a significant variation observed by SEM and focus variation analysis. This was also confirmed by XµT which also showed an increase in polymer content decreased the porosity of the manufactured solid dispersions (Pellets) with PVP VA64 potentially making denser products which could have its own implications. Contact angle analysis correlated with the dissolution studies using FASSIF media indicating that the initial liquid imbibition process as captured by the dynamic contact angle directly affects the dissolution performance

Chapter 4 - Investigating the effect of particle size and shape of lubricated and unlubricated powders on the flow behaviour of pharmaceutical powders

Note to reader: Aspects of this chapter has been published under the title “A predictive integrated framework based on the radial basis function for the modelling of the flow of pharmaceutical powders” in the International Journal of Pharmaceutics. https://doi.org/10.1016/j.ijpharm.2019.118542

4.1 Introduction

Earlier in chapter 3, the effect of formulation properties on the performance of HME formulations were investigated. In this chapter, particle properties (size and shape) will be assessed against the flow performance of pharmaceutical powders. Powder flow, along with powder compression properties, are two main important factors for the manufacturability of tablet dosage forms. Powder flow is a very crucial performance parameter in ensuring the robustness of a manufacturing process. Aims and objectives

As the behaviour of APIs and pharmaceutical excipients/powders play a crucial role as to how they are formulated, it is important to fully undertand the inter-relationship between particle powder proerties and powder bulk properties such as flow. To this end, the aim of this work was to first characterise particle powder properties (size and shape) of different MCC, DCP and lactose and their corresponding blends.These grades were chosen because of their common use in pharmaceutical formulation and their differences in mechanical properties. Different grades were chosen in order to cover a wide range of pharmaceutical powders. Secondly, powder bulk properties (flowability) of these grades were also determined. A multivariate analysis was then conducted in order to assess which parameters affect powder flow most.
Finally, a lubrication study using two grades of MCC, lactose and DCP with different particle size and shape were conducted using different lubricant concentration and blending times to study the effect of both lubricant concentration and blending time on the flow properties of pharmaceutical powders. The data produced will also eventually feed into a neural network to

build novel robust model capable of predicting the performance of pharmaceutical powder based on particle powder properties and will be described and presented in chapter (7).

4.2 Material and methods

4.2.1 Materials

Three pharmaceutically relevant powder materials having different grades were investigated in this chapter. These powder materials are MCC, dicalcium phosphate dihydrate and lactose. Eight grades of MCC having different particle size and shape were supplied by JRS Pharma (UK). These grades are VivaPur® MCC PH101, VivaPur® MCC PH102, VivaPur® MCC PH105, VivaPur® MCC PH100, VivaPur® MCC PH200, VivaPur® MCC PH302, MCC Prosolv 50 and MCC Prosolv 90. Five dicalcium phosphate dihydrate grades, namely, DI-CAFOS A12, DI-CAFOS A60, DI-CAFOS A150, DI- DI-CAFOS D14 and DI-CAFOS D16, were supplied by Chemische Fabrik Budenheim KG (Germany). Seven lactose monohydrate grades were supplied by Meggle Group (Wasserburg, Germany). These are Flowlac 90, Flowlac 100, Granulac 70, Granulac 200, Inhalac 250, Inhalac 400 and Tablettose 80. In addition to being commonly used in the pharmaceutical industry, these powder materials were selected for this research work because of their different flow properties. The range of powder properties was further extended by mixing a combination of the different excipients at various ratios (3:1, 1:1, 1:3). The blending process was conducted using a Turbula blender for 30 min. Lubrication study was investigated using magnesium stearate Kosher Passover HyQual™ which was supplied by Mallinckrodt pharmaceuticals.

4.2.2 Methods

4.2.2.1 Particle size and shape characterisation

The QicPic instrument (Sympatec, UK) was used in the determination of particle size and shape. Vibri dispersing unit was used to feed powder into the system with a feed rate of 35 % and a gap width of 2.5mm (Sympatec, 2018). In order to ensure the dispersing line was clean and free from contaminants, 2 spoonful of sand (40-100 mesh) was passed through the dispersing line prior to analysis.

The primary sample container containing each grade was thoroughly mixed by rolling and inverting by hand as well as mixing using a spatula. Approximately 2 g of each sample was used. Prior to running the measurement, the sample was gently inverted and agitated to ensure the sample was dispersed evenly and to reduce loss of material in the vials. M7 lens was selected and used for this study.

WINDOX software was used for statistical analysis of the replicates using the full 11 decimal place values.

The particle size and shape properties of the binary blends were determined from the single component size and shape properties using a volume-based mixing rule. The physical property ($x_{\mathrm{mix},i}$) is calculated using equation 4.1 from the single component properties $x_{i,j}$ of material j:

$$x_{\mathrm{mix},i} = \sum_{j=1}^{N} f_{\varrho,j}\, x_{i,j} \qquad \textbf{Eq. 4.1}$$

with $N = 2$ as the number of components/materials. $f_{\varrho,i}$ is the volume based fraction considering particle true density, ϱ_i, and calculated by equation 4.2

$$f_{\varrho,i} = \frac{\varrho_i}{\sum_{j=1}^{N} \varrho_j} f_i \qquad \textbf{Eq. 4.2}$$

with f_i as the weight-based fraction of material i.

4.2.2.2 Scanning microscopy

Electron micrographs of all MCC, lactose, DCP grades were obtained using a scanning electron microscope (SEM) (Joel JSM-6060CV) operating at either 2 or 5 kV. The samples were mounted on a metal stub with double-sided adhesive tape and coated under vacuum with carbon in a nitrogen atmosphere before observation. Several magnifications (×100–3000 magnifications) were used to observe the shape and surface topography of particles of the different grades.

4.2.2.3 True density

The true density of all the excipients, as detailed in section 2.1.6, was determined using a Micromeritics Accupyc II pycnometer 100 (Micromeritics, USA). The test was carried out using a multi-run system (10 runs) with a standard deviation of 0.005 % for all the excipients.

4.2.2.4 Flow measurement using ring shear tester

A Ring shear tester (RST-XS, Dietmar Schulze, Wolfenbuttel, Germany) was used to characterise the flow of MCC, lactose, DCP, blends and lubricated grades. The general theoretical background about this method is described in section 2.1.7. The cell used was the medium cell as shown in Figure 4.1

Figure 4.1 Ring shear tester cell

The cell was over-filled with each sample tested and then a spatula was used to smoothen the surface. The shear cell along with the material used was weighed and recorded in the software used. A pre-shear stress of 4000 Pa was used to erase the powder history. Normal loads applied were: 25 %, 38 %, 51 %, 65 % and 25 % of 4000 Pa. The flow function coefficient (FFC) is defined as in equation 4.3

$$FFC = \sigma_c / \sigma_u \qquad \textbf{Eq. 4.3}$$

where σ_u is the unconfined yield stress-stress that makes the powder bed to flow and σ_c is the consolidation stress is the stress that compacts the beds (Yu et al., 2011).

As FFC values increases, the better flow a powder will have. Rhodes classified powder flowability according to FFC values as presented in **Table 4.1** (Rhodes, 2008).

Table 4.1 Flow categorisation according to Rhodes (2008)

Flow category	FFC range
not flowing	FFC < 1
very cohesive	1 < FFC < 2
cohesive	2 < FFC < 4
easy flowing	4 < FFC < 10
free flowing	10 < FFC

4.2.2.5 Lubrication study

Two grades of MCC were firstly chosen to conduct a lubrication study using magnesium stearate. These grades have different shape and size profiles (MCC 101 and MCC microsphere 100). MCC100 have spherical particles whereas MCC101 contain elongated particles. Two levels of magnesium stearate (0.25 % and 2 %) at 4, 10 and 30-min blending times were investigated. Blending study was conducted using a Turbula blender at a speed of 49 rpm as depicted in Figure 4.2. The same study design was then conducted on two grades of DCP (A60 and D14) and two grades of lactose (Flowlac 100 and Tablettose 80) using two levels of magnesium stearate at 3 different blending times. DCP and lactose are commonly used as fillers in pharmaceutical formulation hence it would be very important to determine if there is any interaction between DCP or lactose and magnesium stearate in terms of flow.

Figure 4.2 Turbula blender

The lubrication coefficient (K-values) was calculated using equation 4.4 (Kushner & Moore, 2010)

$$\mathrm{K-Value} = \left(\mathrm{V}^{\frac{1}{3}} * \mathrm{HS} * \mathrm{N}\right) \qquad \textbf{Eq. 4.4}$$

Where V: is the volume of container used, HS: the headspace of the space left in the container used, N is the number of rotations= rotation speed (rpm)*time.

V, HS and rotation speed were all kept constant. The blending-time was changed however and for each time point, a K-value was calculated as Table 4.2

Table 4.2 DOE (Design of Experiment) of the proposed study

Excipient	Magnesium Stearate (Mg St) conc. (%)	Time (min)	K-value	Batch Number
MCC 1001	Mg stearate 0.25%	4	40	MCC PH101_MgSt 0.25_4
		10	100	MCC PH101_MgSt 0.25_10
		30	300	MCC PH101_MgSt 0.25_30
	Mg stearate 2%	4	40	MCC PH101_MgSt 2_4
		10	100	MCC PH101_MgSt 2_10
		30	300	MCC PH101_MgSt 2_30
MCC microsphere 100	Mg stearate 0.25%	4	40	MCC PH101_MgSt 0.25_4
		10	100	MCC PH101_MgSt 0.25_10
		30	300	MCC PH101_MgSt 0.25_30
	Mg stearate 2%	4	40	MCC PH101_MgSt 2_4
		10	100	MCC PH101_MgSt 2_10
		30	300	MCC PH101_MgSt 2_30

Note: With a batch number like "MCC PH101_Mg St 0.25_4", MCC PH101 is the grade of MCC used, Mg St, is magnesium sterate, 0.25 signifies the concentration of Mg St used and 4 is the mixing time in min.All experiments were conducted in triplicates.

4.2.2.6 Multivariate data analysis (MVA)

Multivariate data analysis is a statistical method that allows exploring the effect of different variables (Xs) relating to a specific response (Y) (Ferreira & Tobyn, 2015). It is a useful statistical tool to explore patterns among data. The method was first used in chemical industry back in 1975 (Kowalski, 1975) and has recently been used in pharmaceutical industry applications in both drug development and improving current commercial processes (Lourenço et al., 2012; Yacoub et al., 2011). Pharmaceutical development applications include drug

substance development (Shi, Zaborenko, & Reed, 2013) , drug product development (J. Huang et al., 2009), material science (Sandler & Wilson, 2010), process control and monitoring (Machin, Liesum, & Peinado, 2011) , biopharmaceutical (Mercier et al., 2013), and investigational studies (Huang et sl., 2011) . In this thesis, MVA was used to establish correlations between different particle size and shape descriptors and to investigate how that can be related to the flow properties of pharmaceutical excipients. Multivariate analysis was conducted using jmp software. More information on the software and its capability is reported elsewhere (https://www.jmp.com/en_gb/home.html).

4.3 Results & discussion

4.3.1 Particle size data of MCC grades

Figure 4.3shows the particle size overlays of the different MCC grades. A comparison between the three main particle size descriptors (D [0.1, v], D [0.5, v] and D [0.9, v]) of MCC grades is presented in

Figure **4.4** . Raw data are presented in the appendix of this thesis in Table A 1. MCC PH200 had the largest particle size with a D [0.9, v] of 393.44 µm followed by MCC PH100 and MCC PH302. MCC PH105 was the finest grades with a D [0.1, v] of 13.63 µm though D [0.9, v] was 239.31 µm which is attributed to the agglomerate peak seen in the particle size distribution. MCC PH102 has a larger particle size descriptor in comparison with MCC PH101 (Table 4.2). Furthermore, MCC Prosolv 90 showed a larger particle size compared to Prosolv 50 with the latter having more fines (smaller D [0.1, v] value). These data will be further fed into a neural network model to predict the flow performance of pharmaceutical powders.

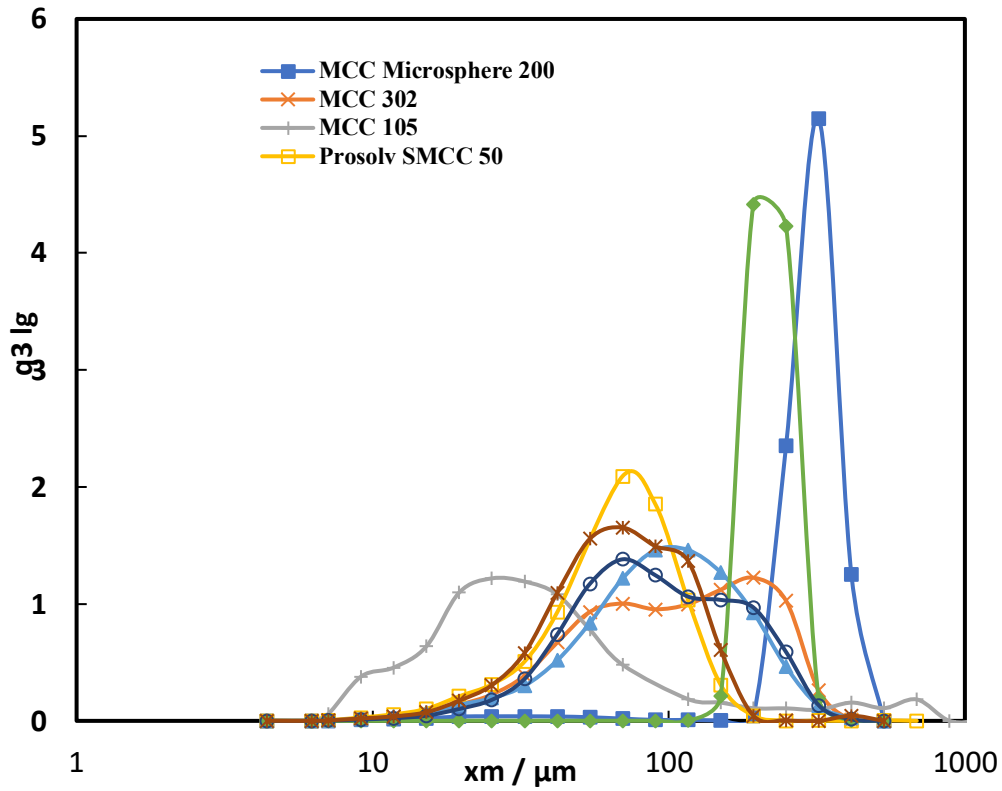

Figure 4.3 Particle size overlays of different MCC grades

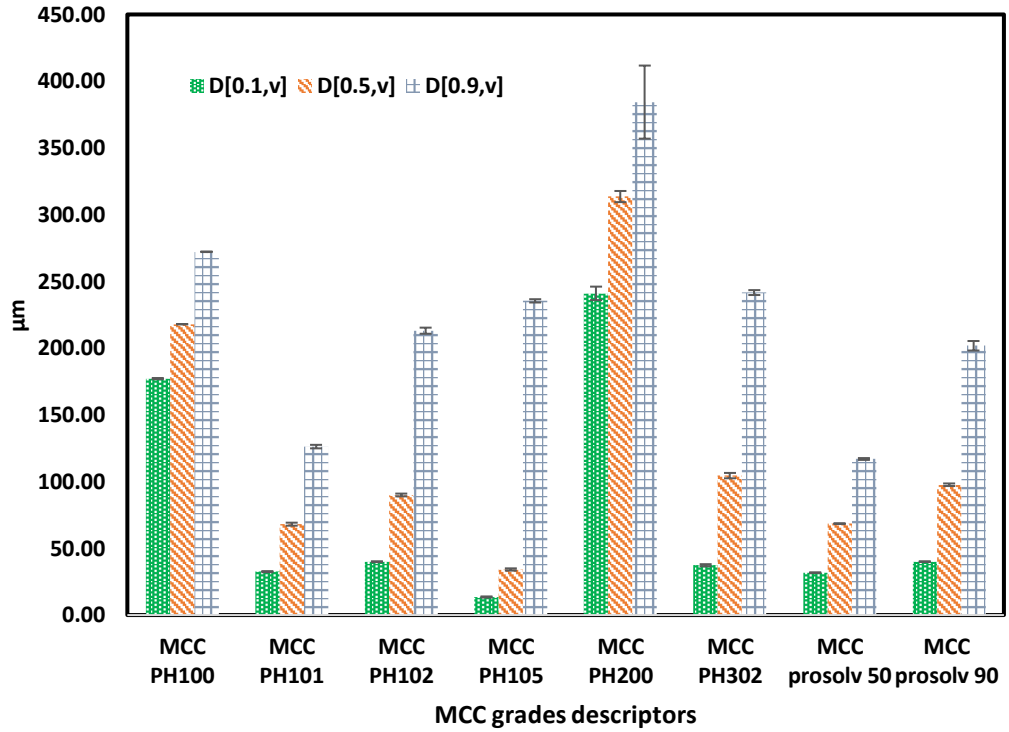

Figure 4.4 Comparison between particle size descriptors of MCC grades

4.3.2 Particle Shape of MCC grades

Figure 4.5 shows the particle shape descriptors generated by the QicPic. Raw data can be found in the appendix of this thesis in the appendix section (Table A 2). S50, 3 of sphericity and aspect ratio were used to compare between grades. Results showed that MCC PH100 and MCC PH200 are the most spherical particles with MCC PH200 had the largest s50,3 value (0.89) followed by MCC PH100 with an s50,3 value of (0.88). MCC PH101 showed a more spherical particle than MCC PH102 with s50, 3 of 0.70 and 0.69, respectively. MCC PH105 showed the least spherical particles with s50, 3 of 0.66. (Table A.2 and Figure 4.5). Particle size and shape results suggest that MCC 200 may potentially have a superior flow based on the findings of a

larger particle size (higher values of D [0.1, v], D [0.5, v] and D [0.9, v]) and more spherical particle shape (higher values of s50,3 and s10,3). In addition, similar particle size and shape data may suggest that the flow of these grades could be similar (comparing the particle size and shape descriptors of MCC 101 and Prosolv 50). To prove this hypothesis or reject it, the flow of these grades was further evaluted as detailed in section 4.4.10.

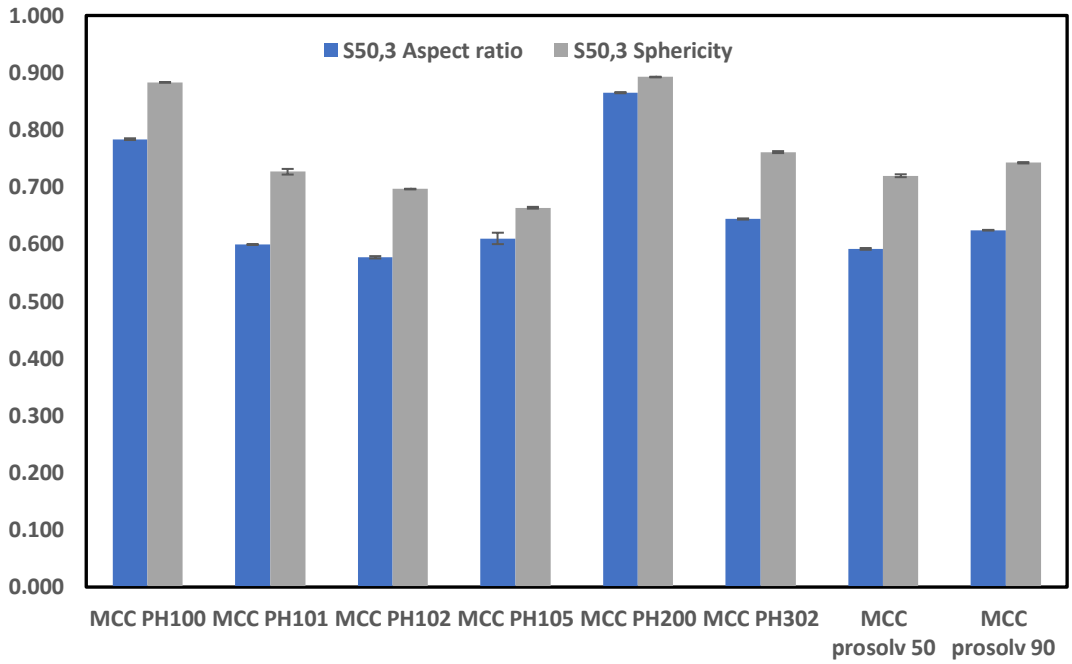

Figure 4.5 Particle shape descriptor s50,3 of MCC grades

4.3.3 Particle size data of lactose grades

Figure 4.6 shows the particle size overlays of the different lactose grades. Raw data are presented Table A 3 in the appendix section. A comparison between the three main particle size descriptors (D [0.1, v], D [0.5, v] and D [0.9, v]) of lactose grades is presented in Figure 4.7. Tablettose 80 had the largest particle size with a D [0.9, v] of 433.12 µm followed by Flowlac 100, Flowlac 90 and Granulac 70. Inhalac 400 was the finest grades with a D [0.1, v]

of 8.44 µm. Furthermore, Inhalac 250 diplayed a larger particle size compared to Inhalac 400 with the former having more fines than the Inhalac 400 (smaller D [0.1, v] value). These data will be further fed into a neural network model along with flow data to predict the flow performance of pharmaceutical powders in Chapter 7.

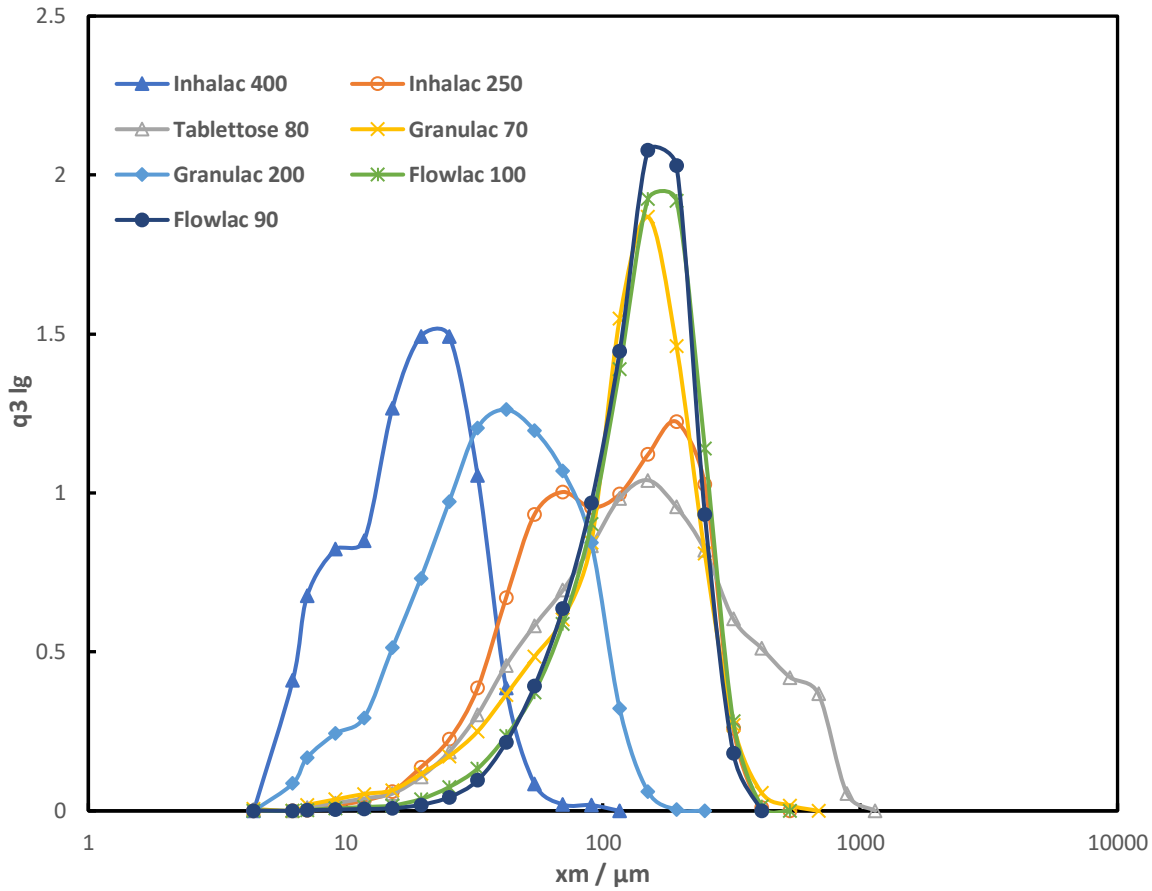

Figure 4.6 Particle size overlays of lactose grades

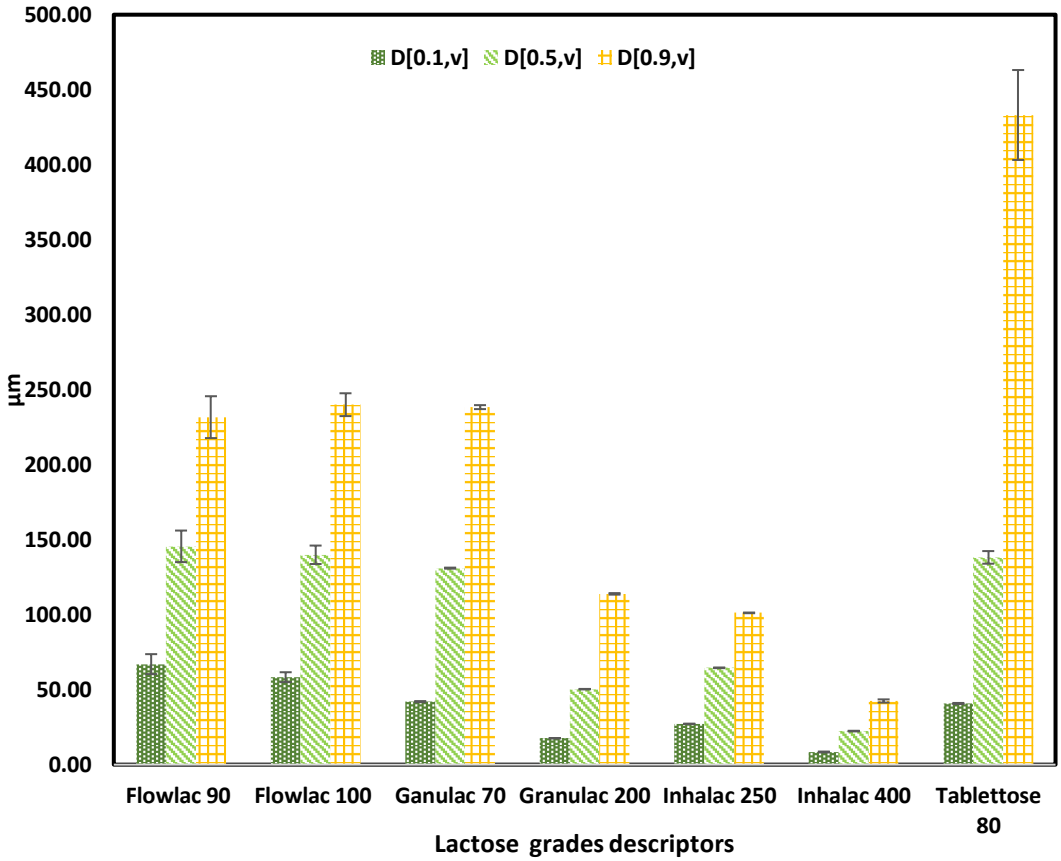

Figure 4.7 Comparison between particle size descriptors of lactose grades

4.3.4 Particle shape data of lactose grades

Figure 4.8 shows the particle shape descriptors generated by QicPic. Raw data are presented in Table A 4 of this thesis in the appendix. As with MCC grades, s50, 3 of sphericity and aspect ratios were used to compare between the different grades. Results showed that Flowlac 100 and Flowlac 90 were the most spherical particles. Flowlac 90 had the largest s50,3 value (0.88) followed by Flowlac 90 with an s50,3 value of (0.87). Tablettose 80 had more spherical particle than Granulac 70 and Granulac 200 with s50, 3 values of 0.74, 0.71 and 0.68 respectively. Inhalac 400 was the least spherical with s50, 3 value of 0.67 (Table A 4and Figure 4.8). These

data along with particle size data suggested that both Flowlac 90 and 100 may tend to flow better when compared with the smallest and less spherical grades such as Inhalac and Granulac grades. Particle size data could also suggest that Tablettose had s superior flowability. However, this higher flowability is less than Flowlac 90 and 100 which had a higher amount of spherical particles suggesting that not only size is critical to flow but also shape of the particles that powder is consisting of. More flow evaluation was conducting in section 4.4.11 to see how particle size and shape properties can be related to the flow behaviour of lactose grades.

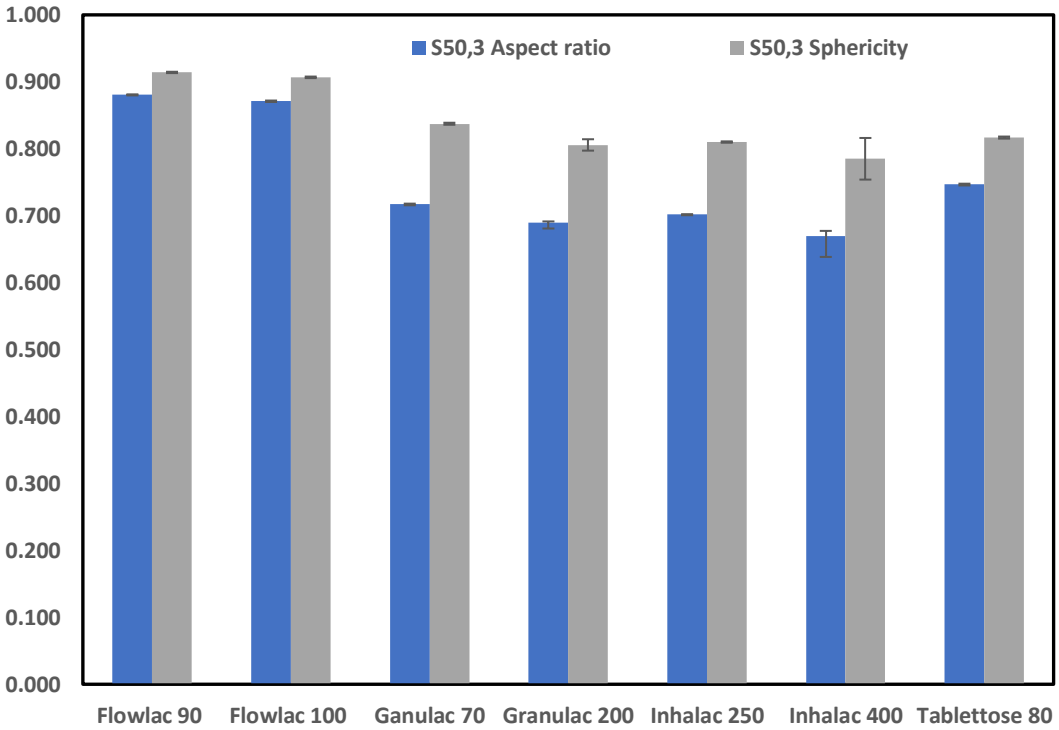

Figure 4.8 Particle shape descriptor s50,3 of lactose grades

4.3.5 Particle size data of DCP grades

Figure 4.9shows the particle size overlays of the different DCP grades. Raw data are presented in the appendix of this thesis in Table A5. A comparsion between the three main particle size descriptors (D [0.1, v], D [0.5, v] and D [0.9, v]) of DCP grades is presented in Figure 4.10. A150 had the largest particle size with a D [0.9, v] of 269.03 µm followed by D160 and D14 and A12. A12 and D14 were the finest grades with a D [0.1, v] of ~8.14 µm. These data will be further fed into a neural network model along with flow data to predict the flow performance of pharmaceutical powders in Chapter 7.

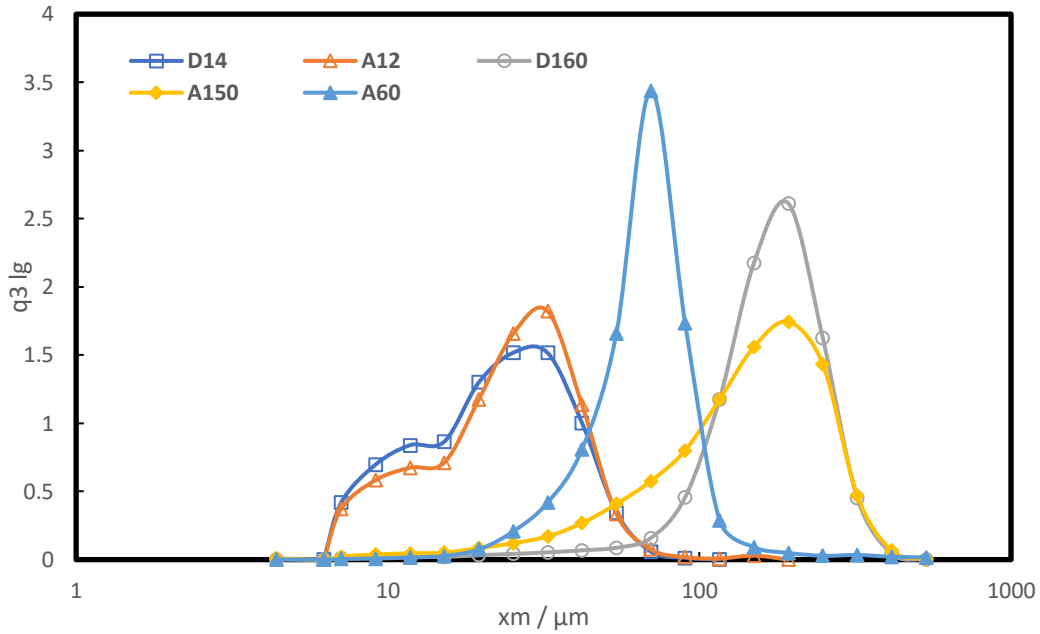

Figure 4.9 Particle size overlays of different DCP grades

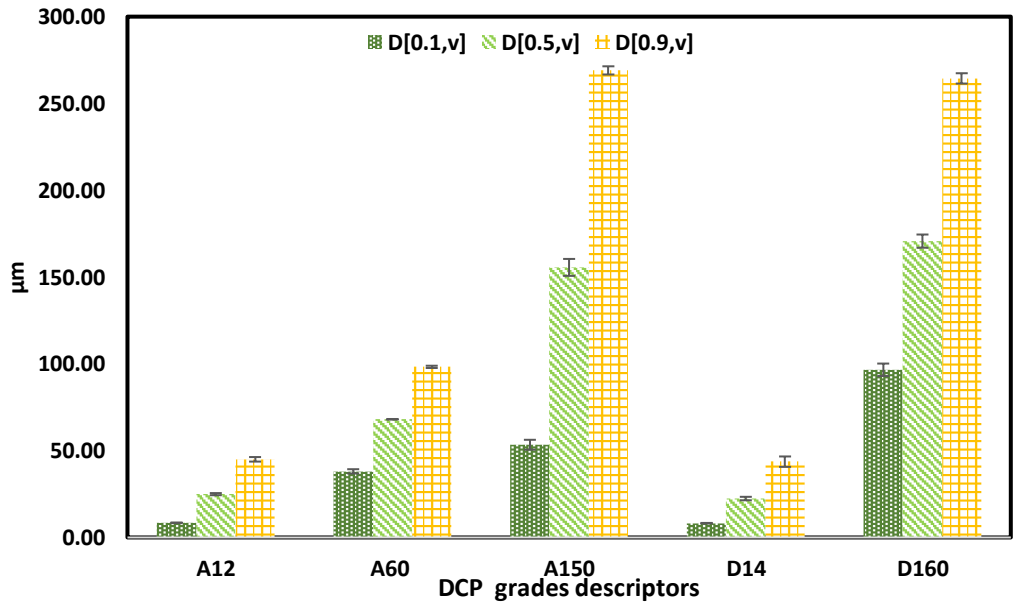

Figure 4.10 Comparison between particle size descriptors of DCP grades

4.3.6 Particle shape data of DCP grades

Figure 4.11shows the particle shape descriptors generated by QicPic. S50, 3 of sphericity and aspect ratio were used to compare between the different DCP grades. Results showed that A60 was the most spherical with A60 having the largest s50,3 value followed by A150 and D160 Although particle size distributions for both A12 and D14 are similar, particle shapes were significantly different as S50,3 was higher in the case of A12 indicating the presence of more spherical particles. A150 and D160 had similar particle shape descriptor although the amount of fines were significantly different between these grades. D14 was the least spherical with s50, 3 of 0.68 (Table A6 (Appendix) and Figure 4.11. Particle size and shape data may suggest that A150 and D160 have a better flow when comparing with other grades. This is on the basis that larger particle and more spherical grades may flow better than smaller and less spherical particles. This hypothesis was tested further in section 4.4.12.

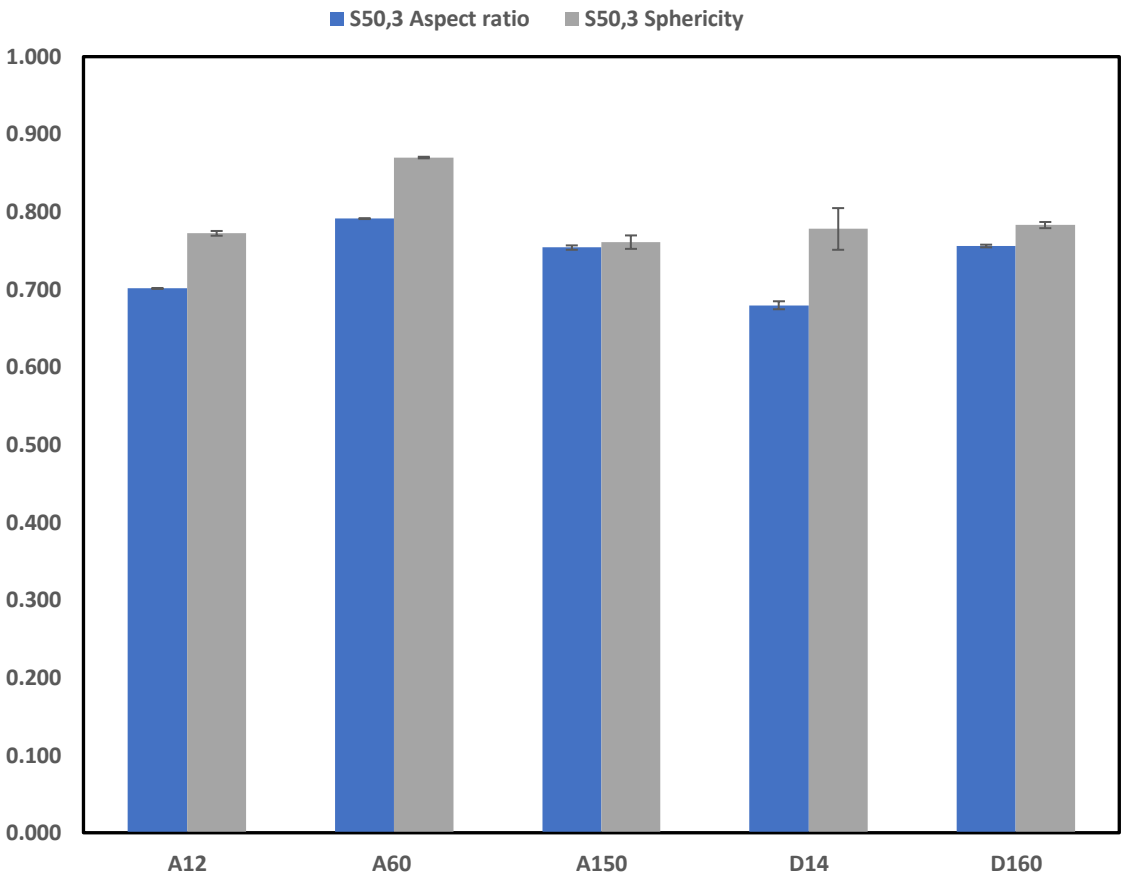

Figure 4.11 Particle shape descriptor s50,3 of t DCP grades

4.3.7 Particle size and shape data of blends

Particle size and shape of blends could not be obtained using the QicPic as segregation occurred after the powder was blended. As a result, a volume mixing rule was adopted as described in section 4.3.2.1. Binary mixtures of 1:1, 1:3 and 3:1 were used (Tables 4.3– 4.7). True density of the single components was measured using helium pycnometer as described in section

4.3.2.3. It is worth noting that the particle size and shape descriptors are increased when a specific component with a larger particle size is increased and vice versa.

For the MCC blends, 3:1 (MCC200: Prsolov 90) had the largest particle size with D [0.9, V] of 165 µm, whilst 3:1 blend of (Prsolov 90: MCC102) had the smallest particle size with D [0.9, V] of 73 µm (Table 4.3). DCP grades blend of 3:1 (A150: D14) displayed the largest particle size whilst the 1:3 blends of (A60: D14) had the smallest particle size distribution (Table 4.4). The lactose blend of 3:1 (Tablettose 80: Inhalac 400) had the largest particle size distribution wheras the 3:1 mixture of (Inhalac 400: Granulac 200) has the smallest particle size distribution (Table .4.5).

When blending MCC and lactose grades together (Table 4.6), the 1:3 mixture of (MCC101: Inhalac 400) had the smallest particle size distribution with D [0.9, V] = 31.70 µm, whilst the 1:3 blend of (MCC101: Tablettose 80) had the largest particle size with D [0.9, V] = 177.38 µm.

When blending MCC and DCP together (Table 4.7), the 1:3 blend of (A12: Inhalac 400) had the smallest D [0.9, V] value, whilst the 1:3 blend of (A12: Tablettose 80) had the largest value of D [0.9, V]. These data will be used in Chapter 7 to build a neural network predictive model.

Table 4.3 Particle size and shape descriptors of blends of MCC grades; C1 is MCC200, C2 is MCC101, C3 is Prsolov 90, C4 is MCC102 and C5 is MCC105

Mixture Code	D [0.1, V] (µM)	D [0.5, V] (µM)	D [0.9, V] (µM)	D [4,3] (µM)	S10,3	S50,3
C1_1_C2_1	67.64	94.54	126.72	95.74	0.274	0.367
C1_1_C2_3	42.06	64.53	95.36	66.97	0.236	0.335
C1_3_C2_1	93.22	124.55	158.08	124.52	0.312	0.398
C1_1_C3_1	68.45	100.85	144.88	103.74	0.277	0.370
C1_1_C3_3	44.60	75.72	124.70	80.66	0.245	0.346
C1_3_C3_1	92.31	125.99	165.05	126.81	0.310	0.395
C2_1_C4_1	18.13	39.53	84.88	46.62	0.187	0.295
C2_1_C4_3	19.09	42.32	95.85	51.16	0.184	0.293
C2_3_C4_1	17.17	36.74	73.90	42.09	0.191	0.297
C2_1_C5_1	10.97	24.59	93.51	45.85	0.209	0.303
C2_1_C5_3	9.25	21.81	112.30	52.09	0.227	0.321
C2_3_C5_1	9.25	21.81	112.30	52.09	0.227	0.321

Table 4.4 Particle size and shape descriptors of blends of DCP grades; D1 is A150, D2 is D14, D3 is D160, D4 is A12 and D5 is A60

Mixture Code	D [0.1, V] (µM)	D [0.5, V] (µM)	D [0.9, V] (µM)	D [4,3] (µM)	S10,3	S50,3
D1_1_D2_1	15.91	46.00	80.73	47.94	0.262	0.358
D1_1_D2_3	9.91	28.35	50.78	30.02	0.238	0.341
D1_3_D2_1	21.91	63.66	110.67	65.85	0.285	0.375
D3_1_D4_1	24.00	45.19	71.76	43.40	0.266	0.363
D3_1_D4_3	14.32	29.47	48.28	29.11	0.263	0.375
D3_3_D4_1	33.68	60.91	95.24	57.70	0.270	0.352
D5_1_D2_1	11.92	23.15	36.12	25.96	0.275	0.369
D5_1_D2_3	7.91	16.92	28.46	19.03	0.245	0.346
D5_3_D2_1	15.92	29.39	43.78	32.90	0.305	0.391

Table 4.5 Particle size and shape descriptors of lactose blends; M1 is Granulac 70, M2 is Granulac 200, M3 is Inhalac 400, M4 is Flowlac 100, M5 is Tablettose 80, M6 is Inhalac 250 and M7 is Flowlac90

Mixture Code	D [0.1, V] (µM)	D [0.5, V] (µM)	D [0.9, V] (µM)	D [4,3] (µM)	S10,3	S50,3
M1_1_M2_1	14.90	45.32	88.04	49.03	0.270	0.352
M1_1_M2_3	11.85	35.25	72.50	39.25	0.265	0.349
M1_3_M2_1	17.95	55.40	103.58	58.82	0.275	0.356
M1_1_M3_1	12.57	38.21	69.95	40.32	0.252	0.347
M1_1_M3_3	8.41	24.73	45.65	26.34	0.239	0.342
M1_3_M3_1	16.74	51.69	94.25	54.30	0.265	0.353
M4_1_M2_1	18.99	47.59	88.50	51.13	0.300	0.390
M4_1_M2_3	13.89	36.36	72.69	40.27	0.280	0.367
M4_3_M2_1	24.10	58.81	104.32	61.98	0.320	0.413
M5_1_M3_1	12.28	40.07	118.67	53.94	0.262	0.355
M5_1_M3_3	8.26	25.64	69.98	33.13	0.244	0.345
M5_3_M3_1	16.31	54.50	167.37	74.74	0.281	0.365
M6_1_M7_1	23.96	53.34	84.53	54.30	0.304	0.397
M6_1_M7_3	29.41	64.52	102.51	65.77	0.329	0.427
M6_3_M7_1	18.52	42.16	66.55	42.83	0.279	0.366
M4_1_M1_1	25.09	67.74	119.59	70.70	0.310	0.398
M4_1_M1_3	23.03	66.57	119.28	69.61	0.295	0.378
M4_3_M1_1	27.15	68.91	119.90	71.79	0.325	0.417
M3_1_M2_1	6.50	18.14	39.00	20.83	0.242	0.404
M3_1_M2_3	7.63	21.59	47.83	25.07	0.251	0.407
M3_3_M2_1	5.37	14.69	30.16	16.60	0.234	0.410

Table 4.6 Particle size and shape descriptors of MCC and lactose blends; C2 is MCC101, M1 is Granulac 70, M2 is Granulac 200, M3 is Inhalac 400, M5 is Tablettose 80, and M7 is Flowlac90

Mixture Code	D [0.1, V] (µM)	D [0.5, V] (µM)	D [0.9, V] (µM)	D [4,3] (µM)	S10,3	S50,3
C2_1_M7_1	25.18	54.08	90.37	56.59	0.270	0.372
C2_1_M7_3	29.92	64.68	105.09	66.69	0.311	0.414
C2_3_M7_1	20.44	43.48	75.66	46.48	0.229	0.331
C2_1_M1_1	18.61	49.64	90.90	53.02	0.237	0.330
C2_1_M1_3	19.72	57.30	104.54	60.53	0.257	0.343
C2_3_M1_1	17.50	41.99	77.27	45.50	0.217	0.316
C2_1_M5_1	18.31	51.47	139.41	66.55	0.247	0.337
C2_1_M5_3	19.29	60.09	177.38	80.89	0.273	0.355
C2_3_M5_1	17.33	42.85	101.43	52.21	0.222	0.319
C2_1_M3_1	10.26	22.65	42.24	25.02	0.210	0.317
C2_1_M3_3	7.23	16.90	31.70	18.64	0.217	0.326
C2_3_M3_1	13.28	28.41	52.77	31.40	0.203	0.309

Table 4.7 Particle size and shape descriptors of MCC and DCP blends; D4 is A12 , M1 is Granulac 70, M2 is Granulac 200, M3 is Inhalac 400, M5 is Tablettose 80, and M7 is Flowlac90

Mixture CODE	D [0.1, V] (µM)	D [0.5, V] (µM)	D [0.9, V] (µM)	D [4,3] (µM)	S10,3	S50,3
D4_1_M7_1	14.91	34.50	56.59	35.65	0.273	0.383
D4_1_M7_3	19.70	43.83	70.60	44.94	0.261	0.352
D4_3_M7_1	10.13	25.16	42.58	26.35	0.286	0.414
D4_1_M1_1	10.02	30.80	55.92	32.51	0.251	0.353
D4_1_M1_3	12.27	38.04	69.15	39.98	0.222	0.301
D4_3_M1_1	7.77	23.56	42.69	25.05	0.279	0.406
D4_1_M5_1	9.83	32.12	89.84	42.00	0.258	0.359
D4_1_M5_3	11.99	40.03	120.06	54.23	0.233	0.309
D4_3_M5_1	7.67	24.20	59.61	29.77	0.282	0.408
D4_1_M3_1	4.22	12.02	22.06	13.04	0.232	0.345
D4_1_M3_3	3.58	9.91	18.42	10.80	0.194	0.289
D4_3_M3_1	4.86	14.14	25.70	15.28	0.269	0.401

4.3.8 Scanning electron microscopy

The electron micrographs obtained by SEM for the different grades of MCC, DCP and lactose are depicted in Figures 4.12 - 4.14 respectively. As shown in Figure 4.12, the MCC microsphere 100 has, as expected, spherical particles with diameter values that are in the range of approximately 150 µm to 300 µm. It is worth mentioning that a similar morphology can also be observed for the MCC microsphere 200 sample, however, the particle diameter values are in the range of approximately 200 – 300 µm. These results were further confirmed by the QicPic analysis. It was also observed that the MCC PH101 and MCC PH102 have elongated plate-like particles with size in the range (40 – 350 µm). It is worth emphasizing at this stage that the former has a smaller particle size when compared to the latter. A similar particle shape can also be observed for the MCC PH105 and MCC PH302. The silicified grades of MCC have also elongated plate-like particles (Figure 4.12).

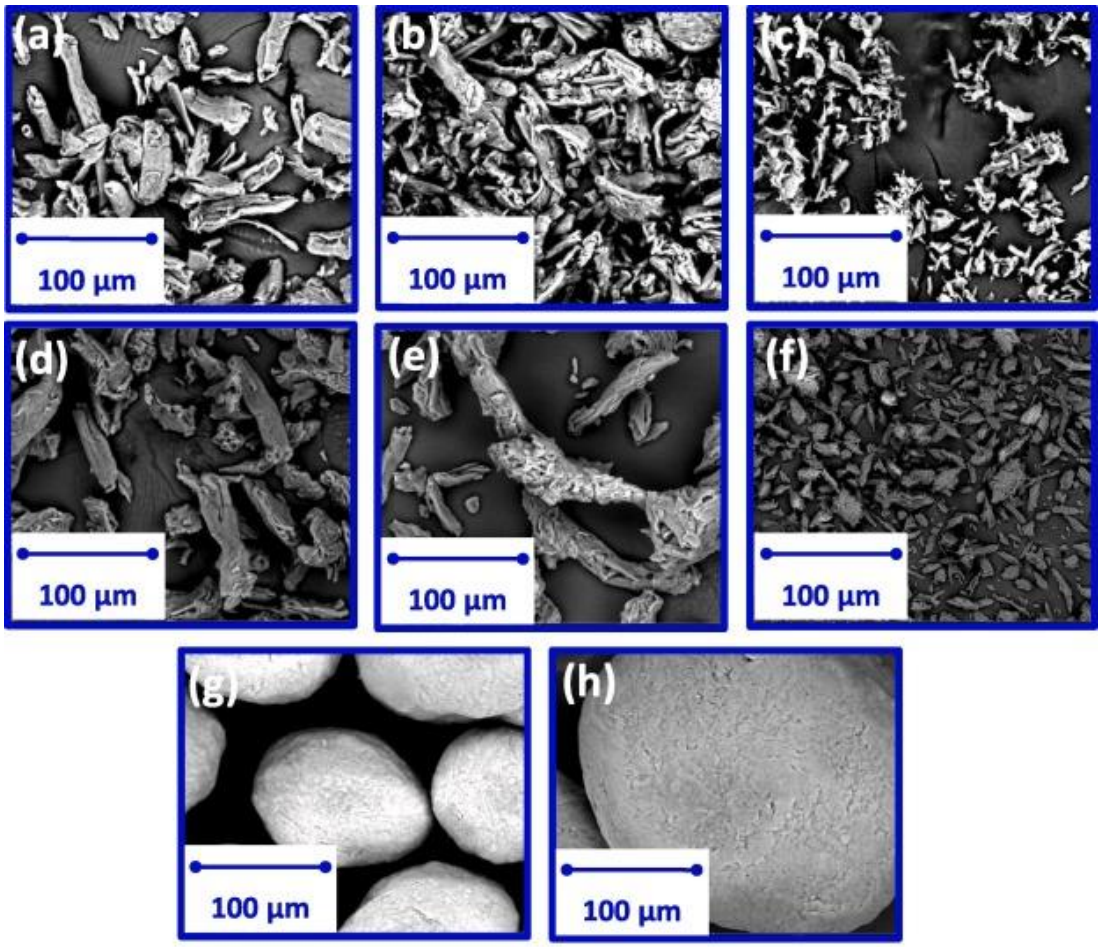

Figure 4.12 SEM images of MCC grades: (a) PH101, (b) PH102, (c) PH105, (d) PH302, (e) SMCC 50, (f) SMCC 90, (g) Microsphere 100 and (h) Microsphere 200

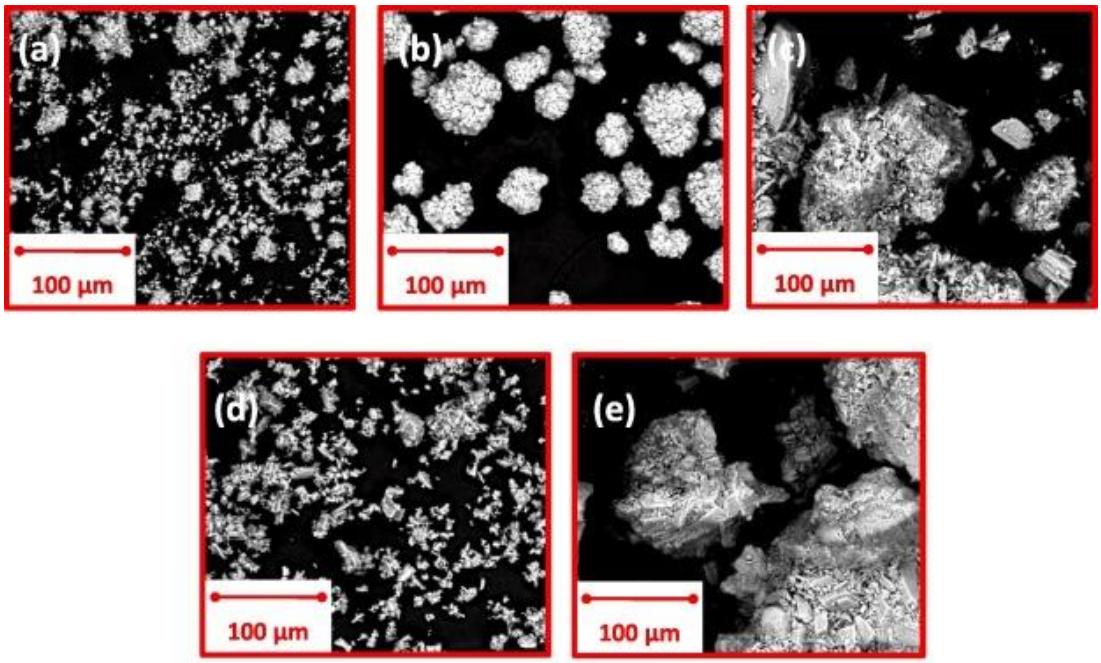

Figure 4.13 SEM images of dicalcium phosphate grades: (a) A12, (b) A60, (c) A150, (d) D14 and (e) D160.

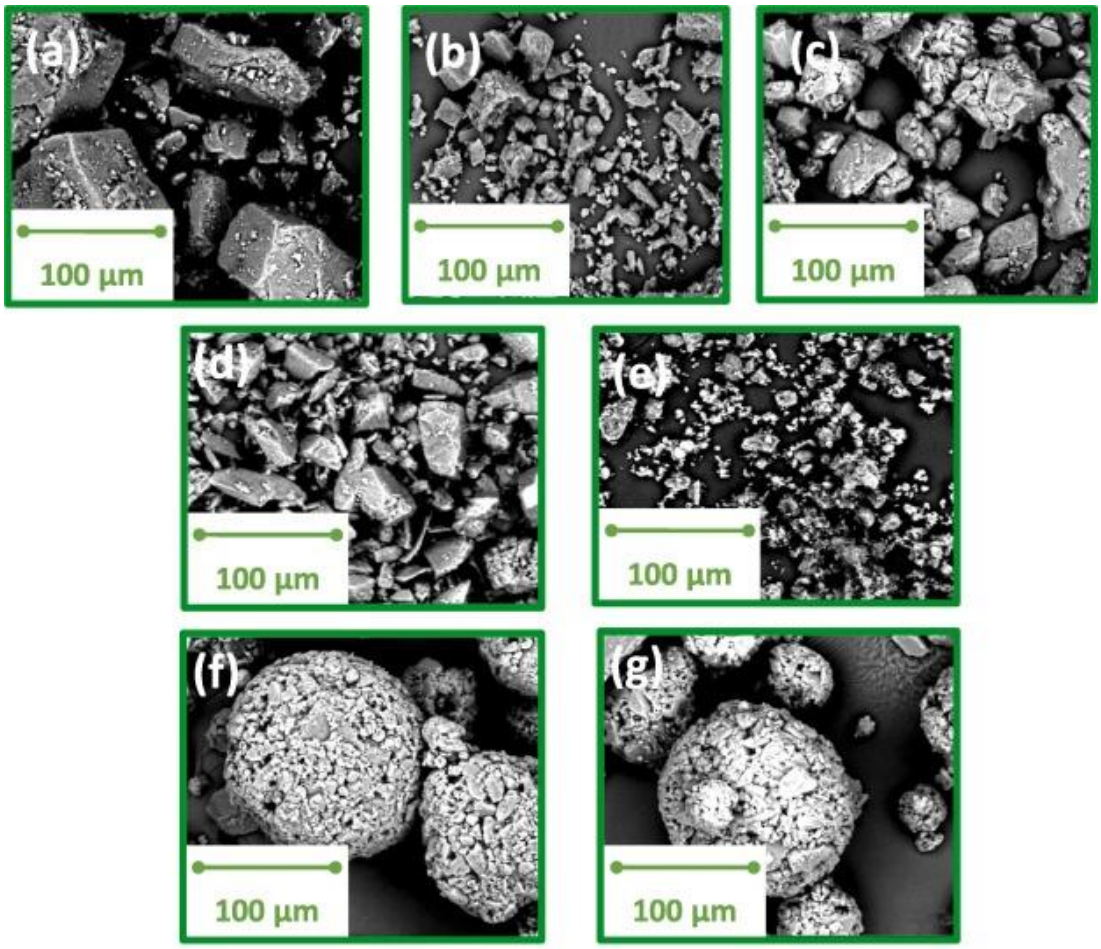

Figure 4.14 SEM images of lactose grades: (a) Granulac 70, (b) Granulac 200, (c) Tablettose 80, (d) Inhalac 250, (e) Inhalac 400, (f) Flowlac 90 and (g) Flowlac 100.

Different particle morphologies can also be observed for the DCP grades, as presented in Figure 4.13. For example, the D160 and A150 grades show an aggregated plate-like morphology with relatively large particle size (i.e. $D_{4,3}$ is approximately 160.3 µm). A similar morphology is noticeable for the D14 and A12, but the particle size is less than 100 µm. In contrast to these grades, the A60 grade has the most spherical particle shape with uniform size distribution ($D_{4,3}$ is approximately 76.12 µm). In Figure 4.14, it can be seen that lactose shows versatile morphologies ranging from cubical to

complete spherical particles. For instance, Flowlac 90 and Flowlac 100 have completely spherical morphologies with quite similar particle size distributions. Granulac 70 and Granulac 200 show cubical morphology with different particle sizes.

4.3.9 True density

The true densities values were needed to calculate the particle size and shape descriptors of the blend as described in section 4.3.2.1. Table 4.12 highlights the results from the true density calculations. DCP grades showed a higher true density due to the inorganic properties of these grades (>2 g/cm^3) while MCC and lactose have a lower value of true densities (<2 g/cm^3). This is was consistent with previous observation by Hancock et al (2003). The results obtained showed that lactose grades (with the exception of Flowlac 90) showed similar true densities values. As these grades are mainly different in particle size, particle size could have a minimal effect on true density measurements of pharmaceutical powders. This was consistent with previous studies which showed that particle size has no effect on the values of true densities. Cao et al examined two ibuprofen batches with two mean diameters (91 and 26 µm). Results showed true densities for these two different batches were similar between 1.117 and 1.115 g/cm^3 (Cao et al., 2008). A trend was observed with the DCP grades. However, some MCC grades showed a different trend. For example, prosolv 50 and prosolv 90 (different in particle size) showed a different true densities measurement (1.40 and 1.60, respectively). This can be attributed probably to the particle packages of these two excipients. Particle shape measurement previously

found that these two grades are slightly different in terms of particle shape (section 4.4.2) with prosolv 50 is less spherical than prosolv 90 which could explain why these grades are different in terms of densities.

Table 4.8 True densities of MCC, DCP and lactose grades (n=3)

Powders	Grades	True density (g/cm^3)	RSD%
Microcrystalline Cellulose	MCC PH100	1.56	0.0026
	MCC PH101	1.57	0.0005
	MCC PH102	1.58	0.0005
	MCC PH105	1.97	0.0008
	MCC PH200	1.52	0.0001
	MCC PH302	1.56	0.0015
	MCC prosolv 50	1.40	0.0008
	MCC prosolv 90	1.64	0.1153
Dicalcium Phosphate Dihydrate	A12	2.92	0.0014
	A60	2.86	0.0009
	A150	2.85	0.0013
	D14	2.60	0.0016
	D160	2.38	0.0004
Lactose Monohydrate	Flowlac 90	1.68	0.0012
	Flowlac 100	1.55	0.0004
	Ganulac 70	1.54	0.0004
	Granulac 200	1.54	0.0015
	Inhalac 250	1.55	0.0006
	Inhalac 400	1.56	0.0009
	Tablettose 80	1.55	0.0008

4.3.10 Flow data of MCC grades

Figure 4.15 displays the FFC values for MCC grades. Raw data can be found in the appendix of this thesis in table A 7 (Appendix). MCC PH200 has the highest FFC

value indicating this grade has the best flow among these grades. On the other hand, the MCC PH105 has the worst flow characteristic with an FFC value of 2 indicating that the powder falls in the cohesive category discussed in section 4.3.2.4. MCC PH105 and MCC PH101 fall in the cohesive flowability category as FFC value were 3.83 and 2 respectively. MCC PH102, MCC Prosolv 50 and MCC Prosolv 90 on the other hand, fall in the easy flowing category with FFC values of 4.97, 5.34 and 7.27, respectively. Further analysis of the data (Figure 4.16 (a,b,c and d)), shows a good correlation between the particle size descriptors and FFC. D [0.5, v] correlated well with FFC with an R^2 value 0.974 (Figure 4.16 b). D [0.1, v] also showed a good correlation with FFC with an R^2 value of 0.9573 (Figure 4.16 a).

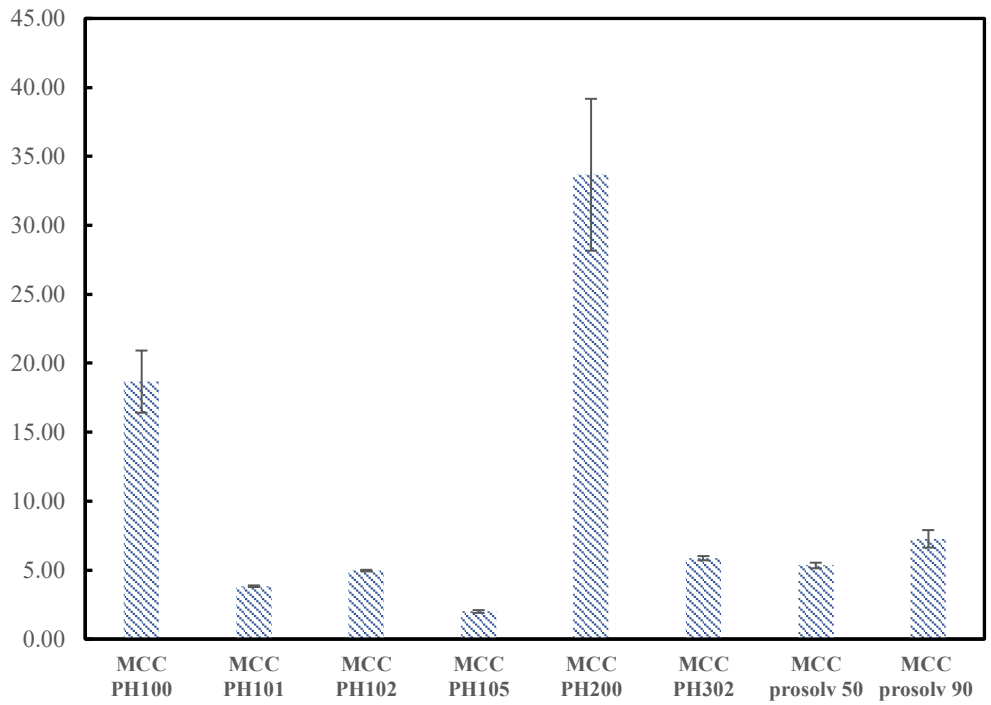

Figure 4.15 FFC values of different MCC grades

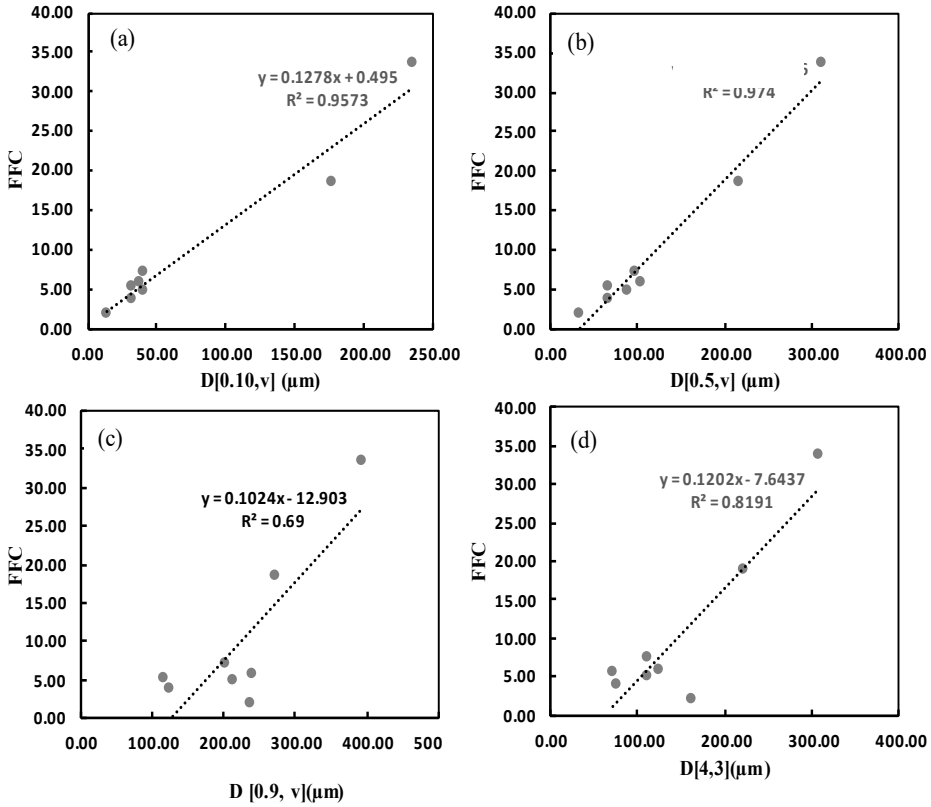

Figure 4.16 FFC of MCC grades vs (a) D [0.10,v] (b) D[0.50,v] (c) D[0.90,v] and (d) D[4,3]

4.3.11 Flow data of lactose grades

FFC values for the lactose grades are presented in Figure 4.17. Raw data used can be found in the appendix of this thesis in Table A 8. Flowlac 100 had the highest FFC value indicating this grade has the best flow among these grades. On the other hand, Inhalac 400 had the worst flow characteristic with FFC value of 0.99 indicating that the powder falls in the "not flowing" category as discussed in section 4.3.2.4. Flowlac 90 and Tablettose falls in the "free-flowing" category with FFC values of 13.73 and 10.50. Granulac 70 and Inhalc 250 fall in the "easy flowing" category as FFC value

were 7 and 4.23, respectively. Granulac 200 falls in the cohesive category with FFC values of 3.72. Further analysis of the data was conducted (Figure 4.18) to establish correlations between the particle size descriptors and FFC. Correlation graphs are depicted in Figure 4.18.

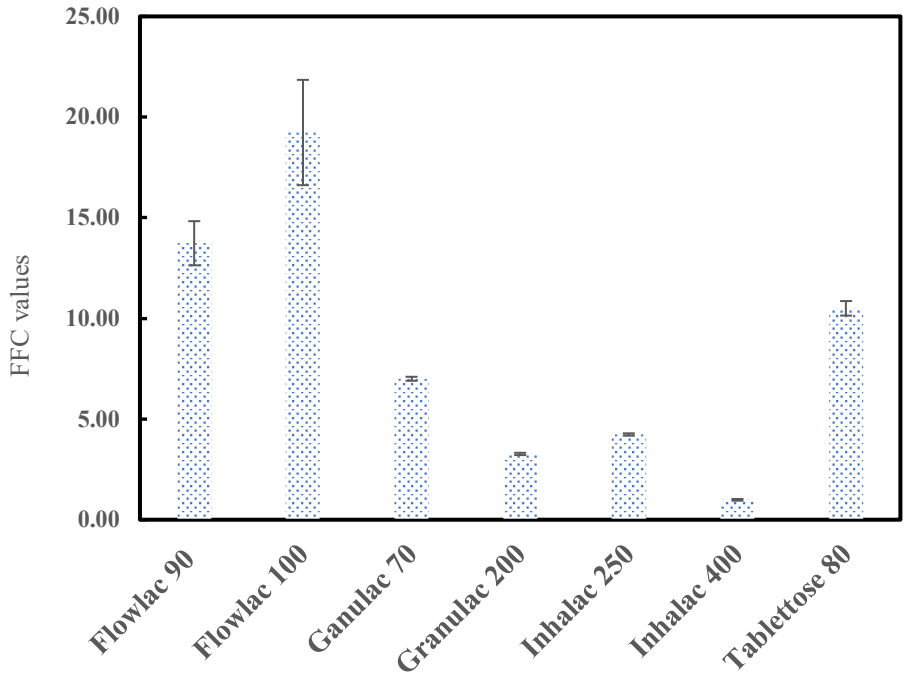

Figure 4.17 FFC values of different lactose grades

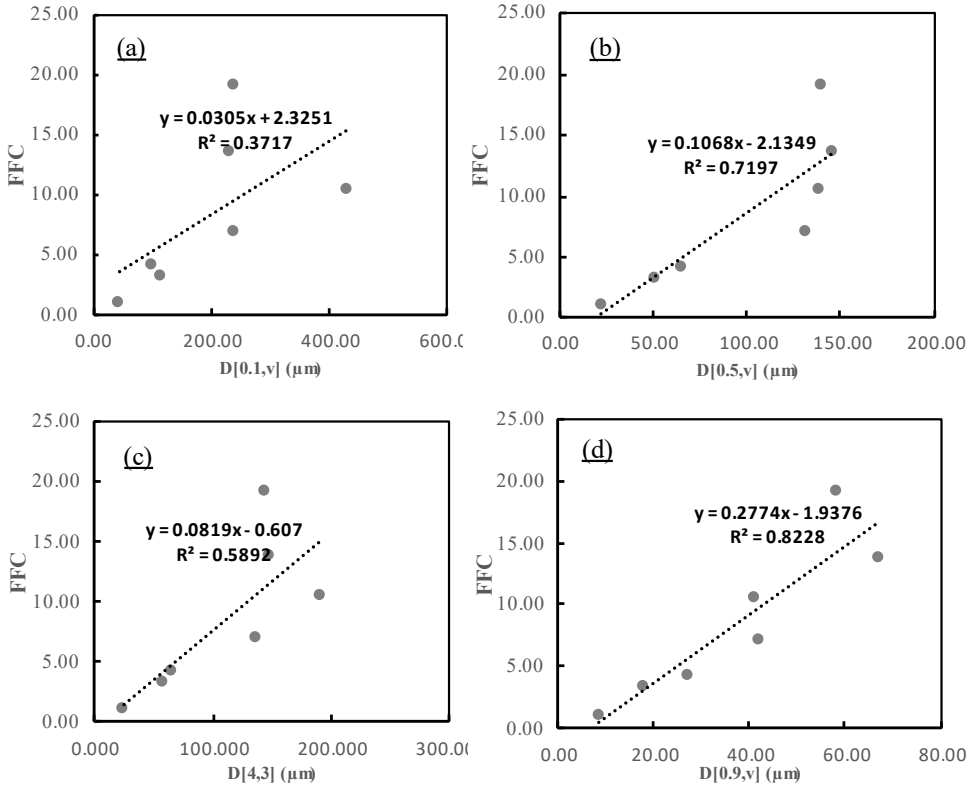

Figure 4.18 FFC of lactose grades vs (a) D[0.10, v] (b) D[0.50,v] (c) D[0.90,v] and (d) D[4,3]

4.3.12 Flow data of DCP grades

Figure 4.19 shows the FFC values for DCP grades. Raw data are presented in Table A9 in the Appendix of this thesis. D160 has the highest FFC value indicating this grade has the best flow amongst the DCP grades. D14 and A12 had the worst flow characteristic with FFC values of 2.10 and 2.40 respectively. These values indicate that these powders fall in the cohesive category as discussed in section 4.3.2.4. A60 and A150 both fall in the "free-flowing" category as FFC values were 20.70 and 32.0 respectively. The MCC PH102, MCC Prosolv 50 and MCC Prosolv 90 on the other

hand fall in the “easy flowing” category with FFC values of 4.97, 5.34 and 7.27 respectively. Further analysis of the data (Figure 4.20) shows a good correlation between the particle size descriptors and FFC. D [0.10, v] correlated well with FFC with an R^2 value 0.995 (Figure 20a). D [0.5, v] also showed a good correlation with an R^2 value of 0.843 (Figure 20b).

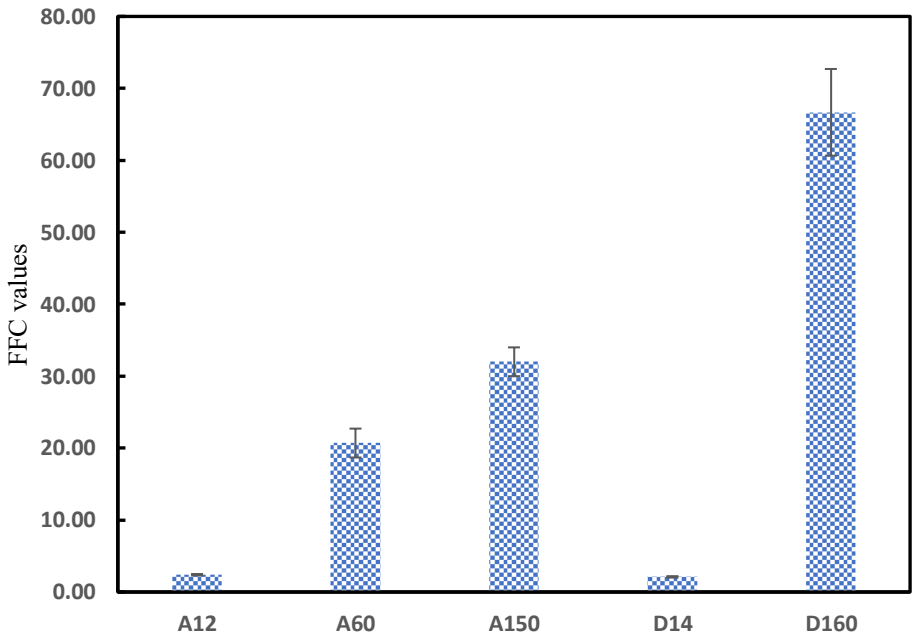

Figure 4.19 FFC values of different DCP grades

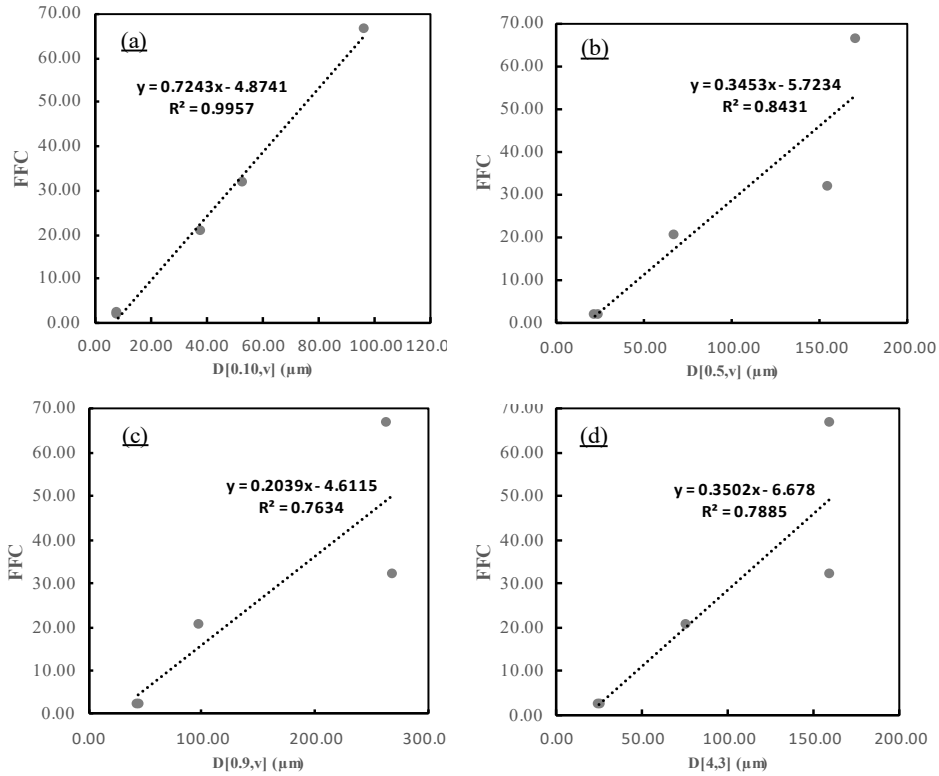

Figure 4.20 FFC of lactose grades vs (a) D[0.10,v] (b) D[0.50,v] (c) D[0.90,v] and (d) D[4,3]

4.3.13 Flow behaviour of the blends

Figure 4.21 showed FFC values along with the D [4,3] values for each of these blends.

For MCC only blends, It can be seen that increasing the ratio of MCC 101 in the (MCC101: MCC 200) mixture resulted in a slightly increase in the FFC (FFC value for 1: 1 ratio was 5.11 while 1:3 value was 5.33). D[4,3] value, however, decreased from 96µm to 67µm. This may be attributed to the fine particle of MCC101 distrbuted on the surface of MCC200 particles which may result in enhancing the total

flowability of the blend. The difference in D[4,3] value could be attributed to the dominant part of the excipient which is dominant within the blend.

What was interesting in the flow observations of MCC mixtures is the addition of prosolv90. Replacing MCC101 with prosolv90 at the same ratio has resulted in significantly increase in the FFC values for MCC200: prosolv900 when compared with MCC200:MCC101 mixtures (FFC value for MCC200:MCC101 was around 6 while FFC value for MCC200: prosolv90 was around 12). Changing the ratio of MCC101:MCC102 (C2:C4 mixture) did not show significant changes in the FFC value (FFC values were around 5 in all blends studied. In terms of D [4,3], the value for the mixtures of MCC101:MCC102 were around 50µm. Adding MCC105 to the MCC101 showed a dramatic decrease with the FFC value resulting in FFC value of around 2 in all mixture ratio studied (1:1, 1:3 and 3:1). D [4,3], in the other hand, was around 50 µm in all mixture studied.

In terms of DCP only blends, most of the blend studied showed an FFC value of less than 5 except in the case of using D160:A12 mixture (3:1 ration) where the value of FFC of that mixture was around 8. This was accompanied with value of D [4,3] of around 58µm.

In terms of lactose only blend, the majority of the mixtures showed a poor flowability with FFC less than 4 for Granulac 70: Granulac 200 ratios and Granulac 70: Inhalac 400. The FFC for lactose-based blends has increased when using Flowlac based formulations. For example, Granulac 200: Flowlac 100 showed an FFC value of

around 5. A combination of Inhalc 250 and Flowlac 90 showed an FFC values between (6-9). While a combination of Flowlac 100 and Granulac 70 showed the highest values of FFC for lactose-based formulation (11 ration has FFC=10, 1:3 ratio has FFC=8, and 3:1 ratio has FFC value of 12). Granulac 200: Inhalc 400 had the lowest values of FFC with FFC<2 for all ratios studied.

In terms of MCC: lactose blends, the highest value for FFC was observed with 1:3 ratio MCC101: Flowlac 90 with FFC value of 10. This can be attributed to the MCC101 fine and elongated particles being distributed on the surface of Flowlac 90 causing a reduce in particle frictions and ultimately enhance the flow performance of these blends. A combination of MCC101 and Inhalc 400 showed the lowest values of FFC.

For DCP: lactose, Flowlac 90 also showed to improve the flowability these blends, with 1:3 ratio of A12:Flowlac 90 has the highest value of FFC (FFC=10). A12:Inhalc 400, on the other hand, had the lowest values of FFC with FFC value of around 2 for all ratios.

The blends for the MCC, DCP and lactose grades displayed a range of FFC values which correlated to their particle size descriptors (i.e. $D_{4,3}$ values) (Figure 4.21 a-e). It was noticeable that an increase or a decrease in one of the ratios of the blends (3:1, 1:1 or 1:3) had a significant influence on the FFC values. This was correlated directly to the calculated particle size descriptors of the blend under investigation.

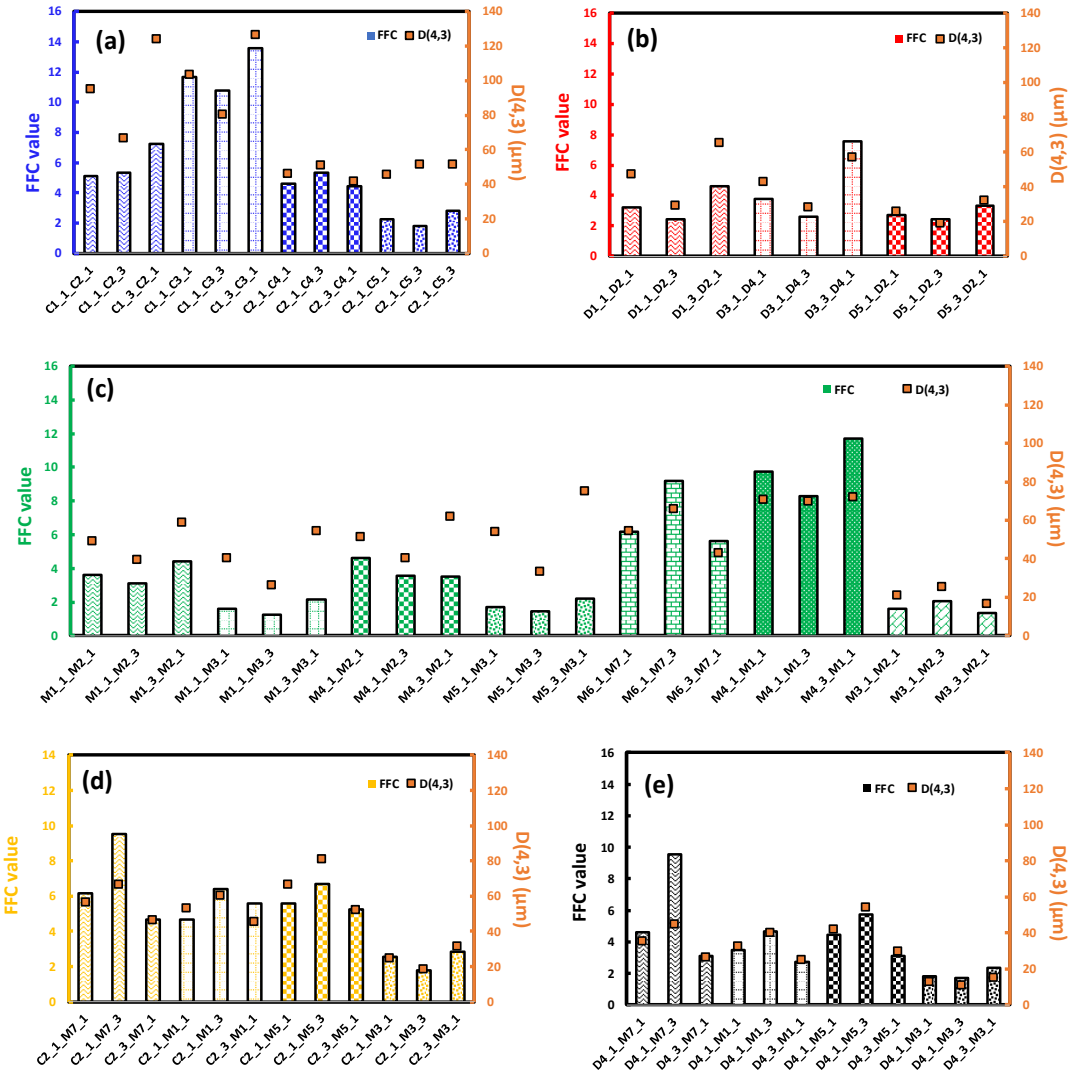

Figure 4.21. FFC values for (a) Blends of MCC grades; C1 is MCC200, C2 is MCC101, C3 is Prsolov 90, C4 is MCC102 and C5 is MCC105; (b) Blends of DCP grades; D1 is A150, D2 is D14, D3 is D160, D4 is A12 and D5 is A60; (c) Blends of lactose grades; M1 is Granulac 70, M2 is Granulac 200, M3 is Inhalac 400, M4 is Flowlac 100, M5 is Tablettose 80, M6 is Inhalac 250 and M7 is Flowlac 90; (d) Blends of MCC and lactose grades; (e) Blends of MCC and DCP.

4.3.14 Multivariate statistical analysis of data

Figures 4.22 - 4.25 showhow particle size, particle shape and flow parameters change within the powders studied. In terms of the particle size descriptors, it can be observed from the Figure 4.22 that D [0.9, v] varies from 10 µm to around 300 µm. This covers most pharmaceutical powder used in industrial setting and ensures the applicability of the potential model developed. For single component powders, MCC powders has the largest D [0.5, v] value followed by DCP and then lactose blends. It is also worth noting that the corresponding blend values for D [0.5, v] were always smaller than those of corresponding single components. This can be attributed to the effect of attrition during blending which may reduce the particle size value of D [0.5, v]. This was aligned with previous findings of Gamble et al who found that blending process parameters may result in a decrease in the mean particle assize of the formulation studied due to the attrition of the API within the formulation (Gamble et al., 2017)

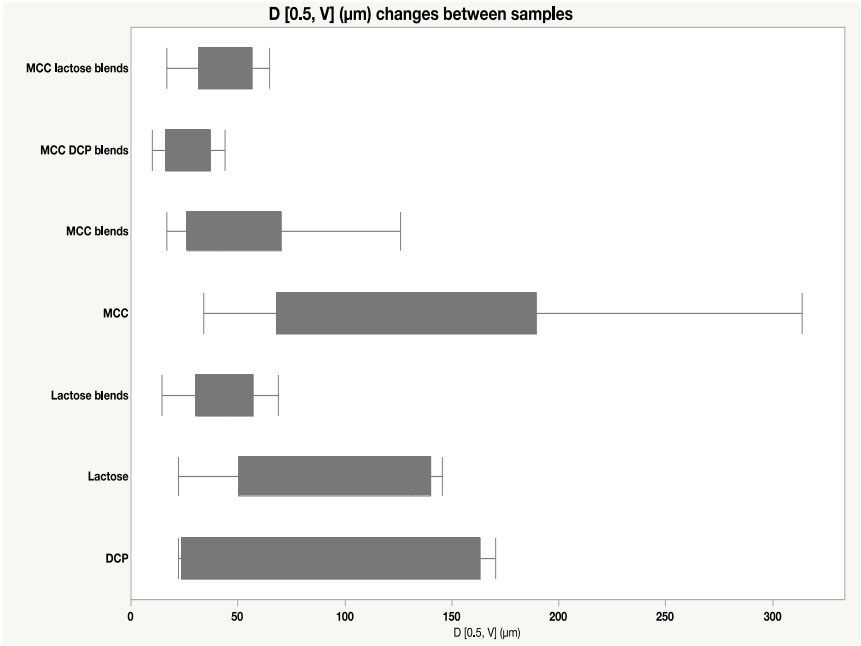

Figure 4.22 Changes of D [0.5, V] between samples

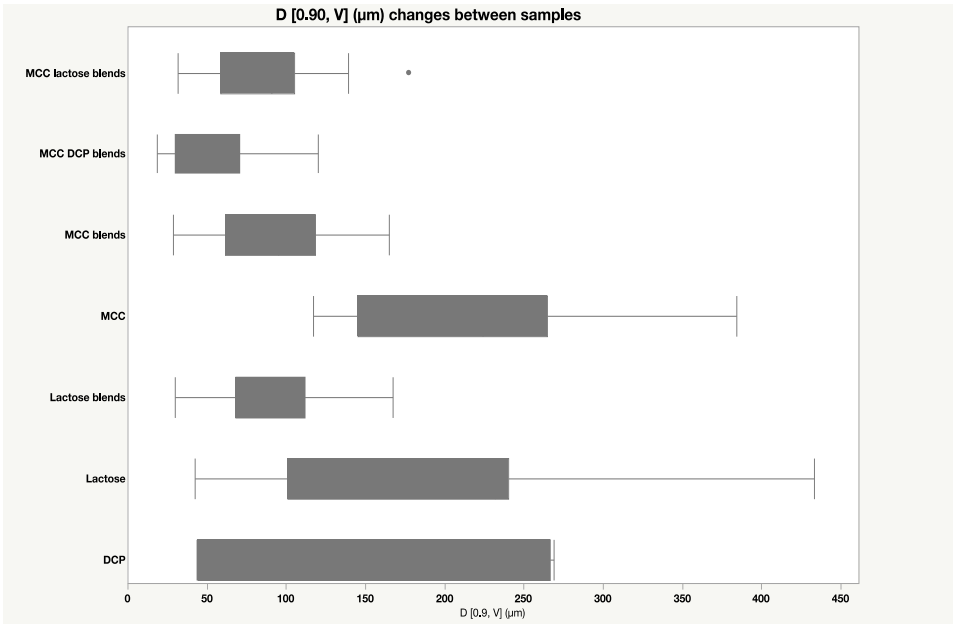

Figure 4.23 Changes of D [0.90, V] between samples

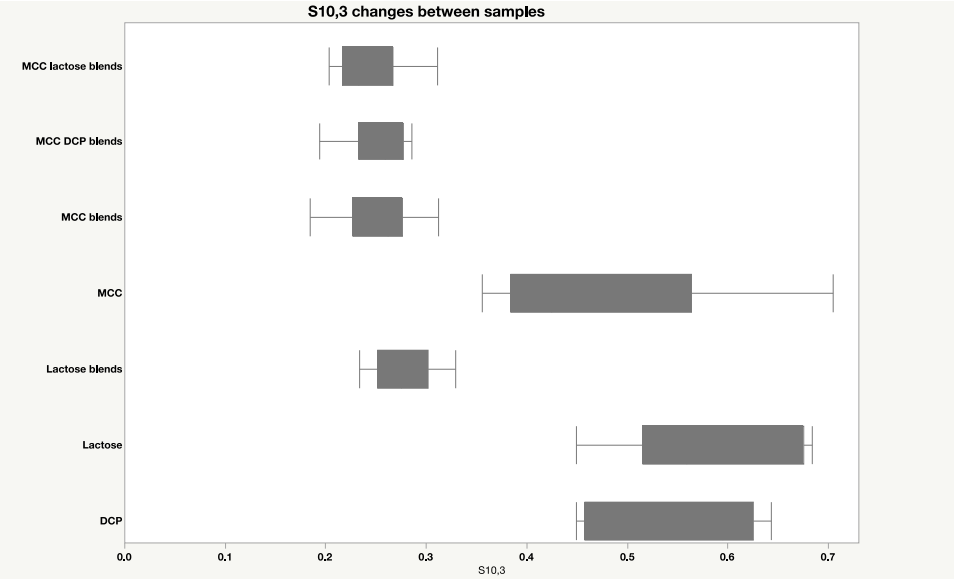

Figure 4.24 Changes of S10,3 between samples

In terms of particle shape, Figures 4.24 and 4.25 provides an overall overview on the values of particle shape descriptors of all powder studied. Particle shape descriptors range between 0-1. Lactose grades have a higher value of sphericity than MCC and DCP.

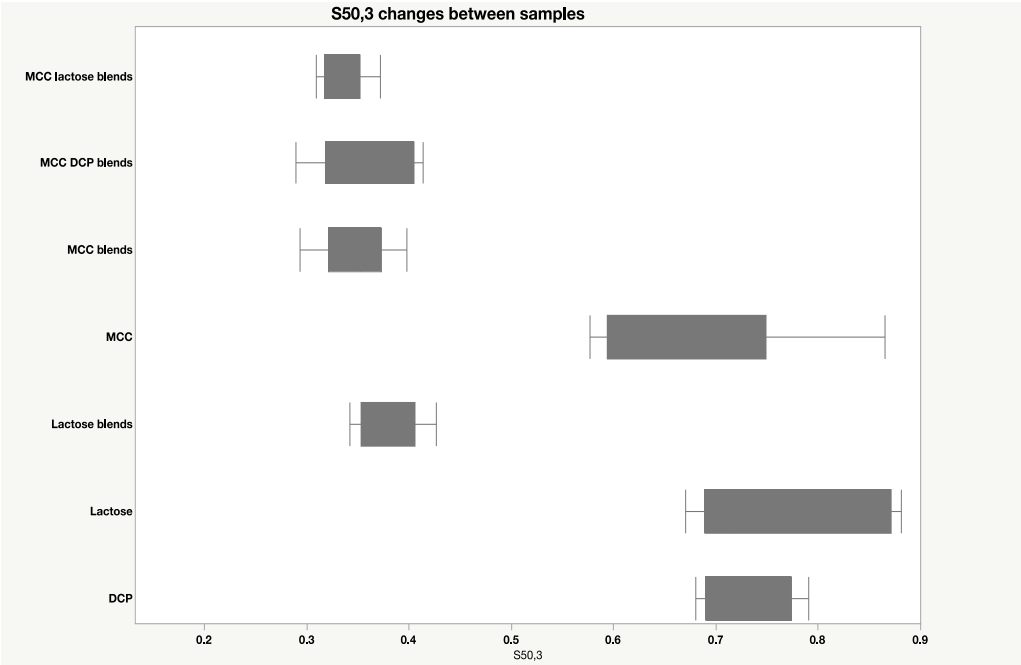

Figure 4.25 Changes of S50,3 between samples

FFC values range between 2 and 50 (Figure 26). This range ensured that powder studied covered a whole range of flow for pharmaceutical powders. DCP grades tend to have higher values than both MCC and lactose grades. Binary blends tend to flow less when comparing with the single corresponding blends. This might be justified as there may be a mechanical interlocking or fine particles distributed over on the surface of larger particles causing the surface to be smoother and ultimately enhancing the flow. These findings were aligned with previous study which showed that the flow behaviour may enhanced by an addition of fine particles such as silicone dioxide which distribute over the host particles and improving the flow by reducing mechanical interlocking and altering roughness of the host particles (York, 1975a).

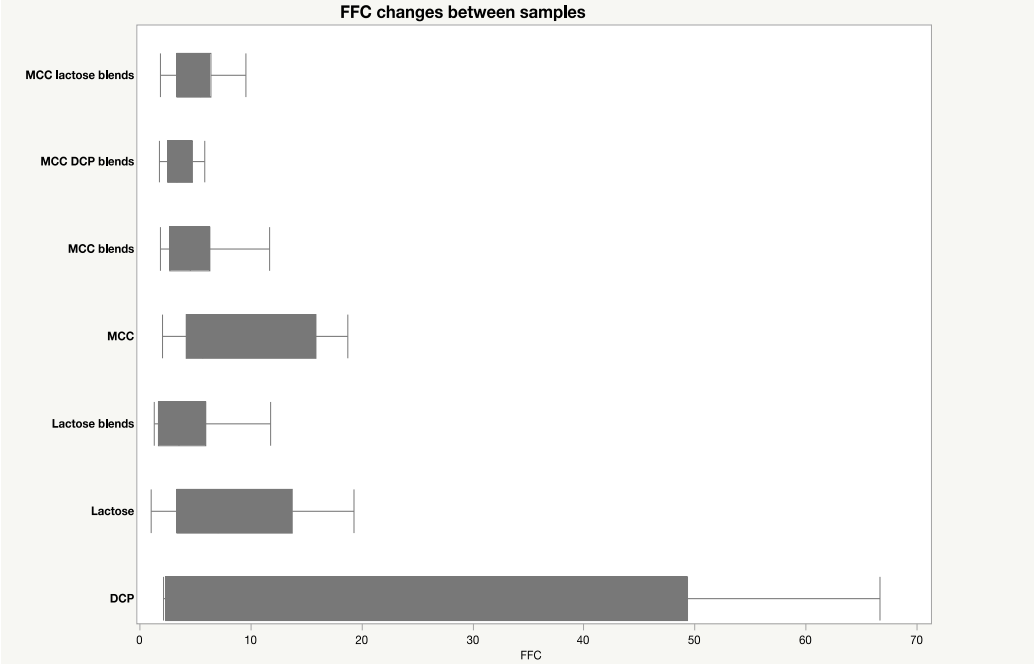

Figure 4.26 Changes of FFC between samples

Multivariate statistical analysis was then conducted to assess the interrelationship between particles and to study the effect of these parameters on the flow behaviour. The study was conducted on both single powders with blends and single powders alone to see if the analysis will be affected by the presence of binary mixtures. As it can be seen from Figures 4.27- 4.29 and Table 4.13, a good correlation was observed between particle size, shape descriptors and FFC values. Figures 4.27- 4.29 and Table 4.17 showed that D[0.5,v] has the greatest effect with a correlation value of 0.73. However, this correlation was conducted with scaling and centring the data studied. A partial least square (PLS) method was further used to enhance an understanding of these systems. Figure 4.29 highlight these findings and as it can be seen, both D [0.50, v] and S50,3 were positively correlated with FFC. D [0.10, v], D [0.90, v], and D [4,3]

were negatively correlated with FFC. This implies that controlling these descriptors is very essential to optimise the flow of pharmaceutical powders. For examples, in early in chemical development of pharmaceutical powder, it would be important to control D [0.10, v] in order to control the amount of fines representing by D [0.10, v]. This could be of great importance to ensure an optimised flow property. These findings also suggest that to increase FFC, particle engineering scientists can try to increase D [0.50, v] or decrease D [0.10, v] or D [0.90, v]. In terms of particle shape, our findings showed that controlling particle shape properties is also of great importance. S10,3 positively affect the FFC value while S50,3 can negatively affect the flow. Theses detailed findings has not observed before and would be an essential finding for particle engineering scientists.

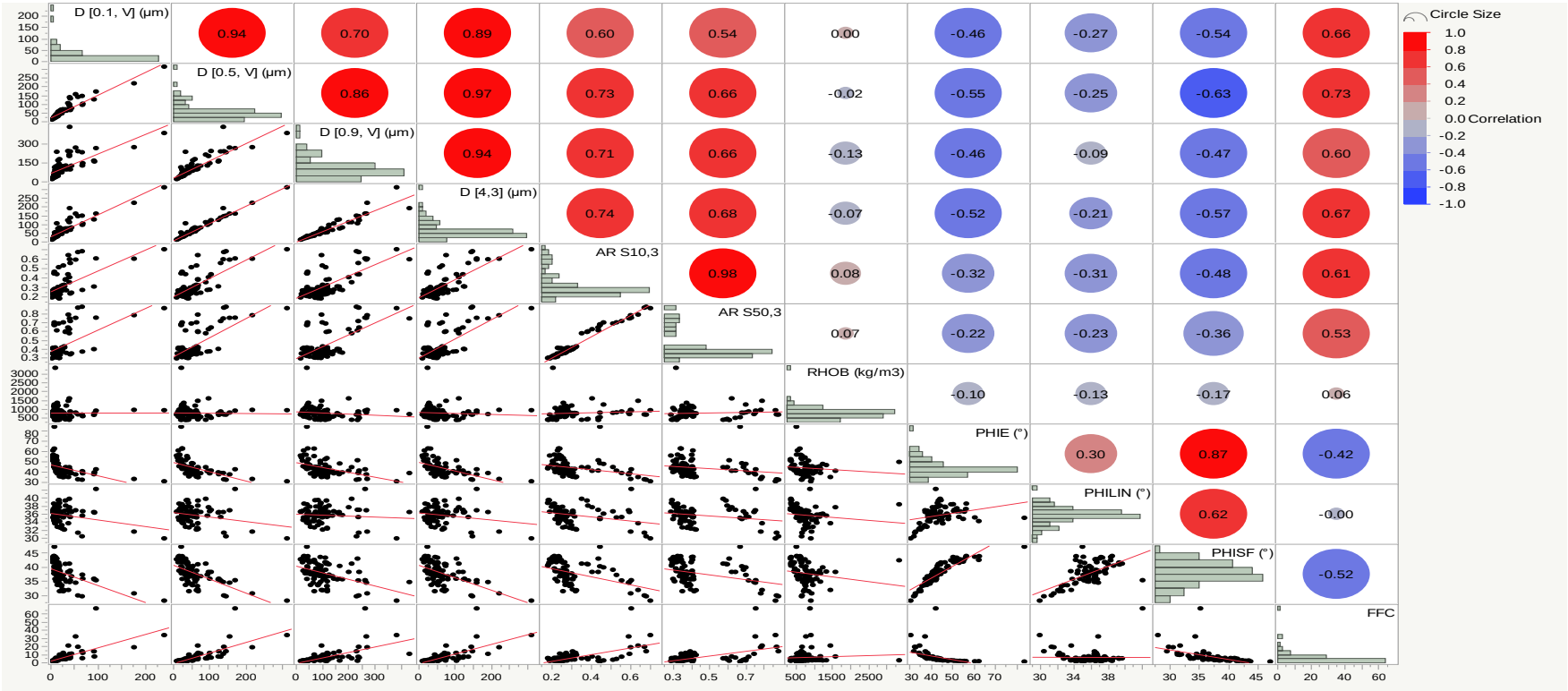

Figure 4.27 Matrixplot of particle size, shape descriptors and flow parameters along with correlation circles for each parameter for all powder including blends

Table 4.5 Correlation values of particle size, shape and flow parameters for all powder including blends

	D [0.1, V] (µm)	D [0.5, V] (µm)	D [0.9, V] (µm)	D [4,3] (µm)	S10,3	S50,3	RHOB (kg/m^3)	PHIE (°)	PHILIN (°)	PHISF (°)	FFC
D [0.1, V] (µm)	1.0000	0.9353	0.6968	0.8900	0.5966	0.5352	0.0026	-0.4649	-0.2678	-0.5442	0.6553
D [0.5, V] (µm)	0.9353	1.0000	0.8618	0.9749	0.7327	0.6640	-0.0217	-0.5495	-0.2544	-0.6273	0.7269
D [0.9, V] (µm)	0.6968	0.8618	1.0000	0.9421	0.7123	0.6573	-0.1303	-0.4589	-0.0865	-0.4726	0.5970
D [4,3] (µm)	0.8900	0.9749	0.9421	1.0000	0.7427	0.6784	-0.0743	-0.5215	-0.2061	-0.5700	0.6748
AR S10,3	0.5966	0.7327	0.7123	0.7427	1.0000	0.9795	0.0848	-0.3216	-0.3090	-0.4832	0.6082
AR S50,3	0.5352	0.6640	0.6573	0.6784	0.9795	1.0000	0.0657	-0.2184	-0.2343	-0.3578	0.5321
RHOB (kg/m3)	0.0026	-0.0217	-0.1303	-0.0743	0.0848	0.0657	1.0000	-0.1050	-0.1337	-0.1685	0.0564
PHIE (°)	-0.4649	-0.5495	-0.4589	-0.5215	-0.3216	-0.2184	-0.1050	1.0000	0.3023	0.8733	-0.4155
PHILIN (°)	-0.2678	-0.2544	-0.0865	-0.2061	-0.3090	-0.2343	-0.1337	0.3023	1.0000	0.6217	-0.0048
PHISF (°)	-0.5442	-0.6273	-0.4726	-0.5700	-0.4832	-0.3578	-0.1685	0.8733	0.6217	1.0000	-0.5160
FFC	0.6553	0.7269	0.5970	0.6748	0.6082	0.5321	0.0564	-0.4155	-0.0048	-0.5160	1.0000

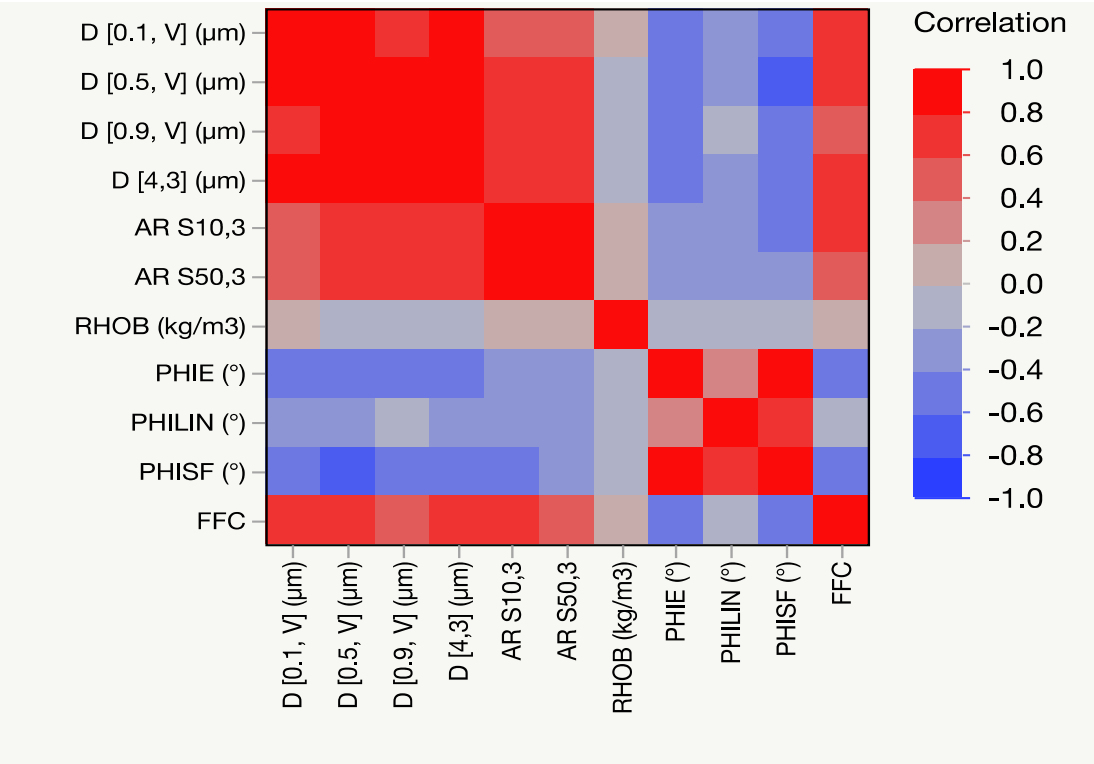

Figure 4.28 Colour map of correlation between parameter studied for all powder including blends

Coefficient	FFC
Intercept	0.0000
D [0.1, V] (µm)	-0.2984
D [0.5, V] (µm)	1.3896
D [0.9, V] (µm)	-0.1330
D [4,3] (µm)	-0.4794
AR S10,3	0.9684
AR S50,3	-0.7664

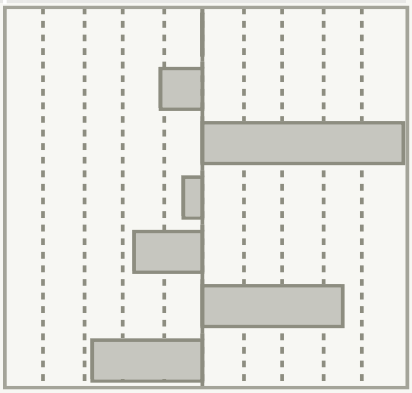

Figure 4.29 Correlation coefficients of partial least square method

4.3.15 Effect of magnesium stearate on the flow of MCC PH101 and MCC microsphere 100

The effect of adding magnesium stearate which commonly used as a lubricant in pharmaceutical oral dosage forms was examined. Previous studies showed that adding magnesium stearate would result in enhancing the flow behaviour of spray-dried lactose by reducing the friction points between lubricated particles which become more spherical and smoother once lubricated (Morin & Briens, 2013). The effect of reducing friction point was also observed with dry powder inhalation formulations where magnesium stearate improves the dispersion profile of salbutamol formulations. In fact, magnesium stearate showed to reduce the agglomeration of salbutamol particles (Tay et al., 2010). Moris and Briens study, however, was conducted on only one type of particles which was Flowlac 100 which is spherical in nature. More understanding of the effect of interaction of magnesium stearate with different particle size and shape particle is hence required. The findings showed that depending on the grade and specifically the particle properties, different findings could be obtained. In this study, two different grades of MCC PH101 (non-spherical) and MCC100 (spherical) were chosen to illustrate the effect of lubricant on the flow behaviour of spherical and non-spherical particles.

The flow of non-lubricated grades were compared to its corresponding lubricated grades. MCC101 and MCC100 were previously reported in section 4.4.10 to have FFC value of 3.83 and 18.67, respectively. When lubricated using 0.25% and 2%, it was noticed there were two different trends in terms of flow. FFC value of MCC101 increased slightly once lubricated to reach 7.37 at 2% of magnesium stearate using 30 min of blending time. This is aligned with previous studies conducted by Moris and

Brains (Morin & Briens, 2013) which showed that adding magnesium stearate resulted in an increase in the flow of pharmaceutical powder. However, for MCC100 (spherical particles) which has FFC value of 18.67, adding magnesium stearate resulted in a decrease in the FFC value especially at the higher concentration of magnesium stearate. This may be explained with magnesium stearate forming agglomerated particles rather than distributed on the smooth surface hindering the flow and consequently decreasing the FFC value.

The effect of magnesium concentration was then investigated to see if this may affect the flow performance of both MCC101 and MCC100. For MCC PH101 and using both low concentration and high concentration of Mg St, no noticeable change was observed in the flow characteristics of MCCPH101 (Table 4.14, Figure4.30). T-test was conducted in order to examine the significance of magnesium concentration on the FFC values between MCC101 and MCC100 grades. Increasing Mg St in MCC101 grades did not result in any significant differences in the flow behaviour. T-test shows that the p-value (0.128) was larger than 0.05 indicating that there are no significant differences between the two groups (High and low levels of Mg St). However, for MCC100 (spherical particles), increasing Mg St resulted in a higher FFC values with a p-value of (0.01876 <0.05), indicating that there is a significant difference in the FFC values as Mg St concentration increased. This strengthens the hypothesis that magnesium stearate in the spherical particles may form agglomerates among spherical particle and hence may affect the flow behaviour.

To examine these the reasons behind these findings, SEM imaging was conducted to get an idea how the Mg St particles are distributed among both MCC101 and MCC100 grades.

Table 4.6 DOE study and the resulted FFC values for MCC grades

		TIME (MIN)	K-VALUE	BATCH NUMBER	FFC	RSD %
MCC101		-	-	MCC101-no lubricant	3.83	0.06
MCC100		-	-	MCC100-no lubricant	18.67	2.25
MCCPH101 (FFC 3.83)	Mg stearate 0.25%	4	40	MCC PH101_MgSt 0.25_4	4.1	0.26
		10	100	MCC PH101_MgSt 0.25_10	4.27	0.12
		30	300	MCC PH101_MgSt 0.25_30	4.57	0.31
	Mg stearate 2%	4	40	MCC PH101_MgSt 2_4	4.7	0.2
		10	100	MCC PH101_MgSt 2_10	5.7	0.44
		30	300	MCC PH101_MgSt 2_30	7.37	0.38
MCC MICROSPHERE 100 (FFC 18.7)	Mg stearate 0.25%	4	40	MCC PH100_MgSt 0.25_4	17.9	0.66
		10	100	MCC PH100_MgSt 0.25_10	16.2	0.85
		30	300	MCC PH100_MgSt 0.25_30	16.5	0.5
	Mg stearate 2%	4	40	MCC PH100_MgSt 2_4	10.2	0.26
		10	100	MCC PH100_MgSt 2_10	10.1	0.1
		30	300	MCC PH100_MgSt 2_30	11.77	0.42

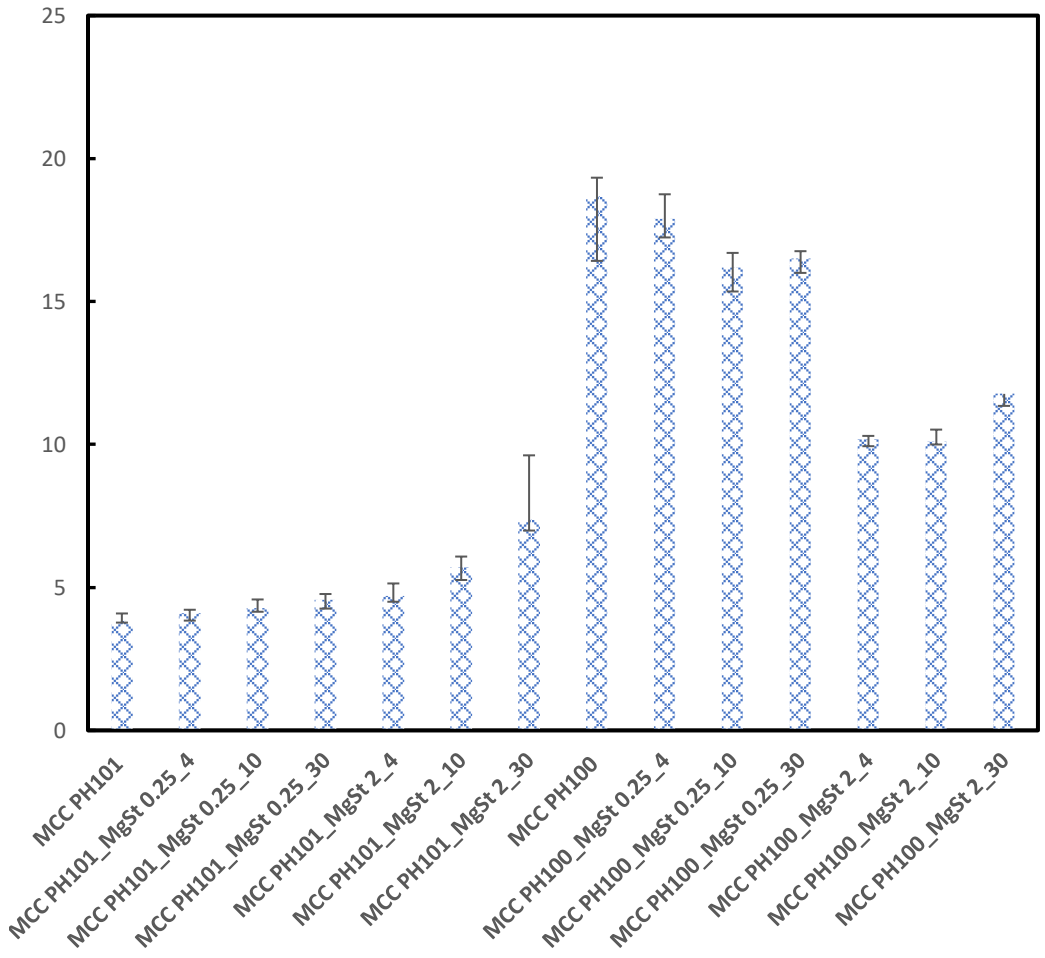

Figure 4.30 FFC values of lubricated and unlubricated grades

As SEM images for the two grades of MCC compared are discussed earlier, the focus is on the lubricated samples. Figure 4.32 depicts the images of the MCC PH100 at both the low and high concentrations of Mg St at the various mixing times of 4, 10 and 30 min. These images confirmed that Mg St had coated the surfaces of the MCC. The excess Mg St is evident in Figure 4.32 d-f. This excess of Mg St thus affects the surfaces of the spherical MCC and this change in the surface properties of the spheres thus resulted in a change in the flow behaviour of MCC PH100. The irregular particle shapes of MCC grades (i.e., MCC PH101) however were more sensitive to changes in lubrication parameters. This can be attributed to Mg St particles being impeded in the

irregular structure of MCC PH101 and is thus represented schematically as Figure 4.31.

Figure 4.31 Illustrative representation of the distribution of Mg St on the surface of MCC PH100 (A) and MCC PH101 (B)

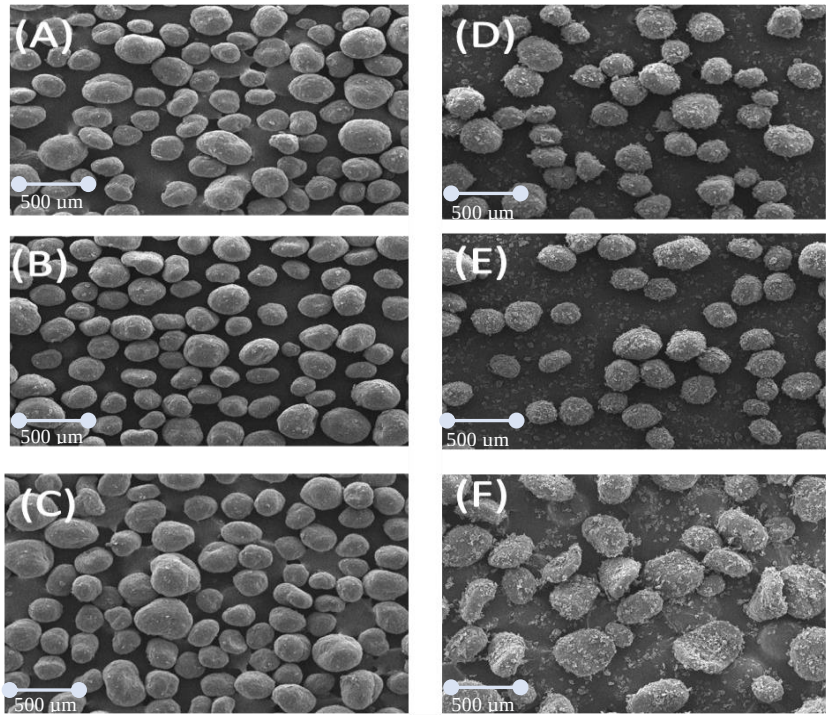

Figure 4.32 SEM images of (A) MCC PH100 with 0.25 % Mg St after 4min blending time, (B) MCC PH100 with 0.25% Mg St after 10 min blending time, (C) MCC PH100 with 0.25 % Mg St after 30 min blending time, (D) MCC PH100 with 2 % Mg St after 4 min blending time (E) MCCMCC PH100 with 2 % Mg St after 10 min blending tim(F) MCC PH100 with 2 % Mg St after 30 min blending time. Note: Mg ST is magnesium sterate

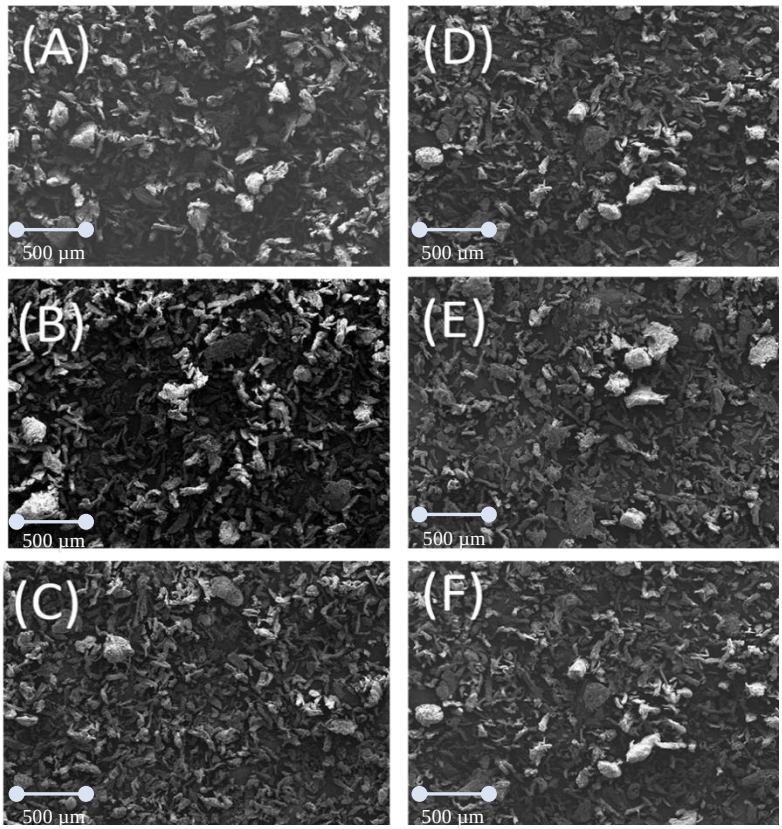

Figure 4.33 SEM images of (A) MCC PH101 with 0.25 % Mg St after 4 min blending time, (B) MCC PH101 with 0.25 % Mg St after 10 min blending time, (C) MCC PH101 with 0.25 % Mg St after 30 min blending time, (D) MCC PH101 with 2 % Mg St after 4 min blending time (E) MCC PH101 with 2 % Mg St after 10 min blending time (F) MCC PH101 with 2 % Mg St after 30 min blending time. Note: Mg St is magnesium stearate

4.3.16 Effect of magnesium stearate on the flow of lactose grades

Table 4.19 and Figure 4.34 show results of Flow characterisation for two grades of lactose specifically Tablettose 80 and Flowlac 100. Both these grades exhibit good FFC values with Flowlac 100 (FFC=19.23) had a superior flow property compared to Tablettose 80 (FFC=10.5) due to the more spherical particles Flowlac100 contained. When these two grades are lubricated using 0.25% and 2%, it was noticed that there were two different trends in terms of flow.

FFC value of Tablettose 80 did not change significantly once it is lubricated. FFC values for lubricated particles were between (9.30-11.17). This may be attributed to the surface nature of Tablettose particles (Figure 4.13) which as it can be seen is very smooth in nature which in turn may prevent magnesium stearate from being attached to the surface of Tablettose 80 grades and hence does not affect the flow of these particles opposite to observed in MCC101 grades. However, for Flowlac 100 (spherical particles) which has FFC value of 19.23, adding magnesium stearate resulted in a decrease in the FFC value especially at the higher concentration of magnesium stearate. This was aligned with our previous observation with MCC100. This can be attributed to the assumption that magnesium stearate forming agglomerated particles rather than distributed on the smooth surface hindering the flow and consequently decreasing the FFC value.

The effect of magnesium concentration was then investigated to see if this may affect the flow performance of both Tablettose 80 and Flowlac 100. For Tablettose 80, no

noticeable change was observed in the flow characteristics of lubricated Tablettose 80 grade when increasing the concentration of magnesium stearate (Table 4.15, Figure 4.34). T-test was conducted in order to examine the significance of magnesium concentration on the FFC values between Tablettose 80 and Flowlac100 grades. Increasing Mg St in Tablettose 80 grades did not result in any significant differences in the flow behaviour. T-test showed that the p-value was 0.345, which indicated that there were no significant differences between the two groups (High and low levels of Mg St for Tablettose 80 grades). However, for Flowlac 100 (spherical particles), increasing Mg St resulted in a lower FFC values with a p-value of ($0.01928 < 0.05$), indicating that there is a significant difference in the FFC values as Mg St concentration increased.

Table 4.7 DOE study and the resulted FFC values for lactose grades

		Time (min)	K-value	Batch Number	FFC	RSD %
Tablettose 80		-	-	Tablettose 80 -no lubricant	10.5	0.36
Flowlac 100		-	-	Flowlac100-no lubricant	19.23	0.75
Tablettose 80	Mg stearate 0.25%	4	40	Tablettose 80_MgSt 0.25_4	9.30	0.75
		10	100	Tablettose 80_MgSt 0.25_10	11.17	0.71
		30	300	Tablettose 80_MgSt 0.25_30	10.57	0.29
	Mg stearate 2%	4	40	Tablettose 80_MgSt 2_4	9.37	1.19
		10	100	Tablettose 80_MgSt 2_10	9.93	0.81
		30	300	Tablettose 80_MgSt 2_30	10.30	0.10
Flowlac 100	Mg stearate 0.25%	4	40	Flowlac 100_MgSt 0.25_4	7.47	0.15
		10	100	Flowlac 100_MgSt 0.25_10	8.73	0.15
		30	300	Flowlac 100_MgSt 0.25_30	9.03	0.15
	Mg stearate 2%	4	40	Flowlac 100_MgSt 2_4	12.20	0.20
		10	100	Flowlac 100_MgSt 2_10	11.90	0.10
		30	300	Flowlac 100_MgSt 2_30	12.20	0.10

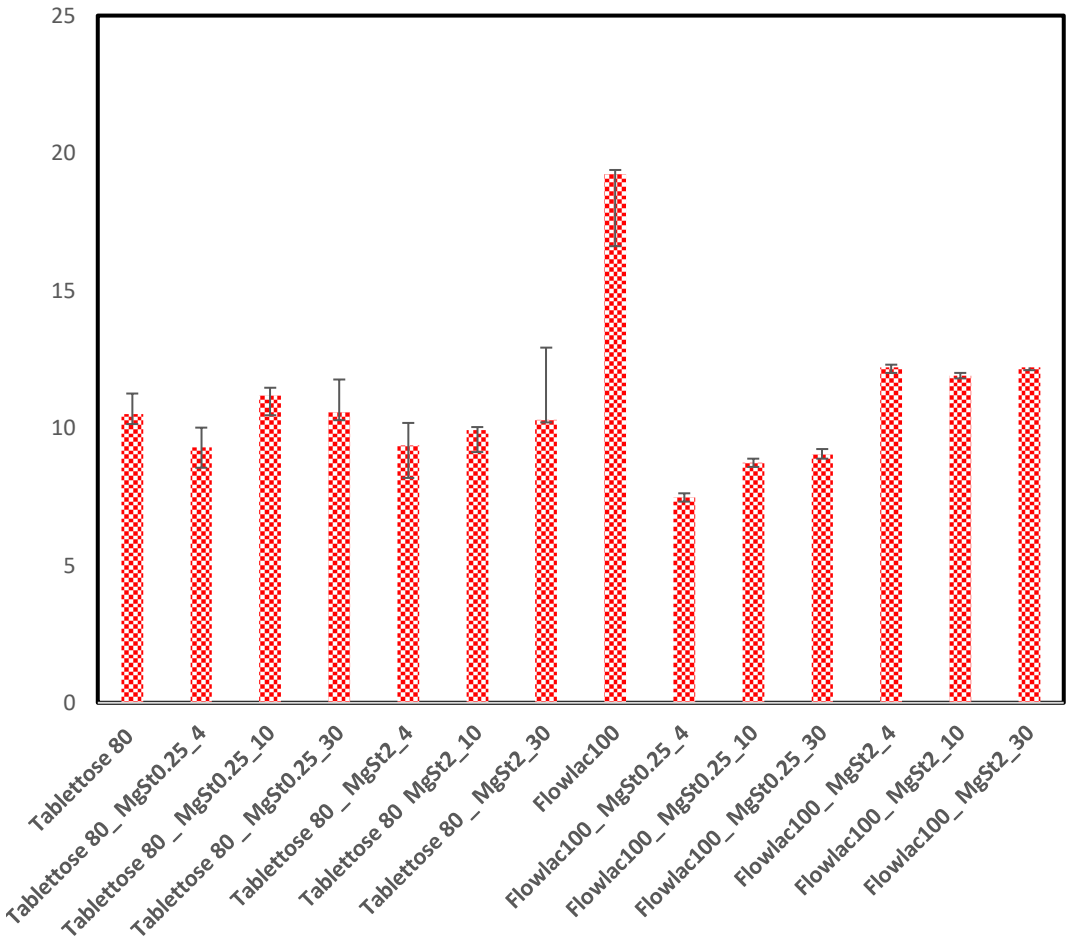

Figure 4.34 FFC values of lubricated and unlubricated grades of lactose

4.3.17 Effect of magnesium stearate on the flow of DCP grades

Table 4.16 and Figure 4.35 show results of flow characterisation for two DCP grades (A60 and D14). These two grades were chosen because of the differences in particle size and shape profiles and the willing to see if these grades will behave differently in terms of flow once they are lubricated. DCP A60 has an excellent flow profile with FFC=20.7 while DCP D14 has a very poor flowability with FFC= 2.10. When these two grades are lubricated using 0.25% and 2%, It was noticed there were two different trends in terms of flow.

In terms of DCP A60, FFC increased slightly using 0.25% concentration of Mg St. For example, FFC value for DCP A60 reached 22.30 using 0.25% Mg St concentration with 10 min blending time. This increase was more noticeable using 2% Mg St. FFC increased by about 6 to reach 26.43 for the lubricated grades of DCP A60 using 10 min blending time. This can be attributed to what was observed previously with MCC and lactose grades where magnesium stearate smoothed the surface of host particles and ultimately enhanced the flow properties of these grades. D14 grade, however, did not change significantly once lubricated with FFC value was around 2 for both the lubricated and unlubricated grades. This may be attributed to the size of D14 particles which does not allow enough attachment of magnesium stearate to the surface and hence does not affect the flow of the lubricated grades.

The effect of blending magnesium stearate concentration was also investigated to see if magnesium stearate concentration would result in a significant change in terms of flow. For A60 grade, T-test for (0.25% and 2% groups) shows that the p-value (0.011 <0.05) indicating that there is significant difference between the two groups (High and low levels of Mg St for A60 grades). However, for D14 grade, increasing Mg St did not result in any significant change in FFC values with a p-value of (0.1287 >0.05), indicating that increasing Mg St concentration did not show any significant difference in terms of flow.

Table 4.8 DOE study and the resulted FFC values for DCP grades

		Time (min)	K-value	Batch Number	FFC	RSD %
A60		-	-	A60-no lubricant	20.7	2.01
D14		-	-	D14-no lubricant	2.10	0.1
A60	Mg stearate 0.25%	4	40	A60_MgSt 0.25_4	22.40	0.20
		10	100	A60_MgSt 0.25_10	23.33	0.21
		30	300	A60_MgSt 0.25_30	22.30	0.20
	Mg stearate 2%	4	40	A60_MgSt 2_4	25.70	1.04
		10	100	A60_MgSt 2_10	26.43	0.06
		30	300	A60_MgSt 2_30	26.63	0.21
D14	Mg stearate 0.25%	4	40	D14_MgSt 0.25_4	2.47	0.15
		10	100	D14_MgSt 0.25_10	2.40	0.20
		30	300	D14_MgSt 0.25_30	2.13	0.49
	Mg stearate 2%	4	40	D14_MgSt 2_4	2.47	0.21
		10	100	D14_MgSt 2_10	1.95	0.22
		30	300	D14_MgSt 2_30	1.90	0.37

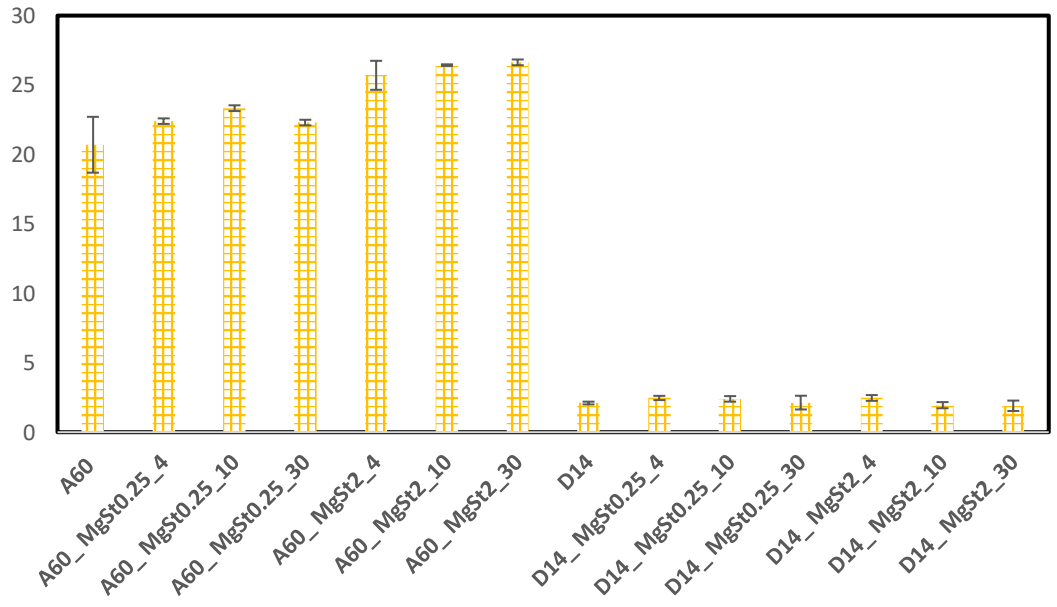

Figure 4.35 FFC values of lubricated and unlubricated grades of DCP grades

4.4 Conclusion

Particle size and shape play a significant role in the flow of pharmaceutical materials. A strong correlation was found between particle size descriptors and the flow function coefficient. Results also showed a good correlation between D [0.5, v] and FFC with an R^2 value 0.974 for MCC powders. D [0.1, v] also showed good correlation with an R^2 value of 0.9573 for the same powder. However, different correlation values between particle size descriptors and FFC values were observed with MCC, lactose and DCP. In addition, particle shape also played an important role on the flow especially for lubricated and unlubricated powders. Spherical particles were more sensitive to increased lubrication changes. Therefore, controlling particle size and shape is very important during pharmaceutical material development and manufacturing. Controlling these critical quality materials attributes will be very important in the manufacturability of dosage forms, especially with the ongoing trend toward continuous processing and manufacturing. This study has focused on three common pharmaceutical powders that are used in tablet pharmaceutical dosage form design. The effect of particle properties on flow behaviour using multivariate statistical analysis was investigated. In all powder studied, it was found that both D [0.5, v] and s10,3 positively affect powder flow. On the other hand, D [0.10, v], D [0.90, v] and S90 negatively affect powder flow. In the later stage of the study, the interaction of two grades of microcrystalline cellulose (different particle and bulk powder properties) with magnesium stearate as lubrication with the magnesium stearate is a crucial step on pharmaceutical dosage form production. It was found that a change in particle powder properties may result in a change in the flow of these

pharmaceutical materials which ultimately will have an effect on the handling and manufacturability of these excipients.

Chapter 5 - Investigating the effect of particle size and shape of pharmaceutical powders on the mechanical properties of produced tablets

5.1 Introduction

This chapter will evaluate the effect of particle properties mainly particle size and shape on the mechanical properties of the resultant compacts. The mechanical properties of tablets are considered one of the main properties that determine the success or failure of tabletting process (Hiestand, 1997). A deformation process should occur within the powder bed to get a tablet with a specific shape and geometry. This deformation usually occurs by applying a specific compression force upon a powder bed. Two main processes can occur during the tabletting process. These processes are compression and compaction. Each of these processes will have a direct effect on the critical properties of pharmaceutical tablets. Understanding these processes is essential for successful tablet manufacturing and is discussed in detail in section 1.2.1.2.4 of this thesis

5.2 Aims and objectives

As shown in the previous chapter, particle properties have significant implications on the flow of pharmaceutical materials. In this chapter, the aim is to understand the effect of these properties on the mechanical properties and, ultimately, on the pharmaceutical performance of powders during tabletting. Particle properties such as particle size and shape was firstly quantified using image-based particle characterisation techniques. These properties were also investigated using traditionally techniques such as the scanning electron microscopy. Image-based analysis techniques were used to overcome the limitation of static image analysis by allowing to capture a 3D image of the particle moving and overcoming the statistical limitation associated with static

imaging where a small quantity of sample is used to conduct analysis (Gamble et al., 2015; Löbenberg et al., 2000; Yu & Hancock, 2008).

5.3 Materials and methods

5.3.1 Materials

Three commonly used pharmaceutical excipients with different mechanical properties were chosen to investigate the effect of particle shape on the mechanical properties of the final compacts. These include two grades of lactose (Tablettose 80 and Flowlac 90), two grades of dicalcium phosphate (A60 and A150) and two grades of microcrystalline cellulose (MCC 101 and MCC200).

5.3.2 Tablet preparation

A computer-controlled mechanical testing machine (M500-50CT, Testometric Co, limited. Rochdale, UK) was used to prepare tablets using stainless-steel flat-face punches (10 mm). Both dies and punches were pre-lubricated using a suspension of magnesium stearate in ethanol (1% w/w). A pre-lubrication was carried out in order to minimise the sticking of powders to the surfaces of tooling. Powders were further compressed at 5, 10, 7.5 and 15 kN (Laity et al., 2015; Laity & Cameron, 2008). Prepared tablets were gently ejected and characterised in terms of thickness and diameter, and mechanical properties. A more detailed discussion on the principle of the compaction process can be found in section 2.1.11.

5.3.3 Tablet tensile strength and porosity

Tablets dimensions were calculated in terms of thickness (T) and diameter (H). Tensile strength was then calculated using equation 5.1

$$\sigma_T = \frac{2F}{\pi HT} \qquad \textbf{Eq. 5.1}$$

Where $\sigma_T$the tablet tensile strength (MPa), H is the diameter (mm), and T represent the thickness of the tablet (mm).

The porosity of tablets was calculated from the X-ray tomography images (section 5.3.6).

5.3.4 Work of compaction:

Work of compaction of powders used in this study was done by analysing data obtained from the mechanical testing machine using a compression-decompression method. This method involves compressing the tablet to a maximum compression force (10 kN) and then decompressing back to 0 kN. A force-displacement profile was then obtained. The area under the curve was calculated using a trapezoidal method using a simple Excel function. Total work of compaction, elastic work and plastic work was further calculated according to the following literature (Khorsheed et al., 2019)

5.3.5 Morphology and topography analysis

Powders were characterised in terms of morphology using both a static and dynamic method. SEM images were obtained using a scanning electron microscope (Jeol JSM-6060CV SEM) operating at 10 kV. Powders were dispersed into a metal stub with an adhesive tape and then sputter-coated with gold for 60 seconds. Micrographs with

different magnifications were taken to aid an understanding of the particle shape of each grade of excipient. More information about the SEM technique as well as the principle behind how it works can be found in section 2.1.14.2 of this thesis. Dynamic image analysis using a QicPic instrument (Sympatec, UK) was utilised to characterise particle shape. Two spoonsful of sand were first introduced to the system to ensure that the system was clean and free from contaminants. The primary sample container containing each excipient grade was thoroughly mixed by rolling and inverted by hand and mixed using a spatula. Before starting the measurement, the sample, approximately 2g, was gently inverted and agitated to disperse it evenly and reduce the loss of material in the vials. The M7 lens was selected for this study, where each measurement was repeated three times. The WINDOX software was utilised to perform the statistical analysis of the obtained measurements. For more information on the principle of image analysis, the reader can refer to section 2.1.3.

Surface roughness of tablets was studied using a focus variation instrument (Contour LS 3D Optical Profiler (Bruker) using 10x objective and 2.9 μm lateral resolution. Surfstand software (Taylor Hobson, UK, and University of Huddersfield, UK) was then used to obtain both 2D and 3D dimensions profiles of tablet surfaces (Ward et al., 2017). More information on the principle of focus variation analysis can be found in section 2.1.5.

5.3.6 X-ray microtomography (XμT)

Tablets (as obtained from section 5.3.2) were imaged by XμT (Nikon XT H 225, Nikon Corp. Tokyo, Japan) using a tungsten target with 75 kV accelerating voltage and 250 μA gun current using a copper filter (thickness 0.125 mm). A tablet was

placed on a plastic tube, and a set of projections were calculated with over 120 min XμT acquisition.2D, and 3D images were acquired using CT-Pro and then further examined using VG Studio 2.1 software. A more detailed discussion on the operational principles of X-ray microtomography can be found in section 3.4.6 of this thesis.

5.3.7 True density measurement

True density was measured using a helium Pycnometer (AccuPyc II) (Micromeritics, UK). 1.5 grams of each grade were dried to eliminate water presence from the sample as water interacts with helium and produces an inaccurate estimate of true density. The dried sample was placed in a 10 cm^3 cell, and the system is sealed. Helium was then purged in cycles until the pressure equilibrated. True density was also calculated for the compacts produced at 5, 7.5, 10, 15 kN. The reader is referred to section 2.1.6, for more discussion on the operational principles of true density analysis.

5.4 Results and discussions

5.4.1 Morphology analysis

5.4.1.1 Scanning electron microscopy

Figure 5.1 shows particle size and shape of grades studied. As can be seen from the figures, two distinctive shape morphologies were observed for each material. MCC 200 shows spherical particle shapes with an equidimensional shape. MCC particles indicated a particle size of around 200-300 μm. On the other hand, MCC101 displayed elongated needle-like particles with a particle size of around 100-150 μm. In terms of DCP particles, A60 particles were spherical with a particle size of around 100-125μm, while A150 showed elongated prismatic crystals with greater length and width than

the corresponding needle-like particles. Lactose particles have two distinctive structures. Flowlac 90 particles were sphere-like with a mean particle size of 200-300 µm, while Tablettose 80 grade showed prismatic like particles with particle size ranging from 200-300µm.

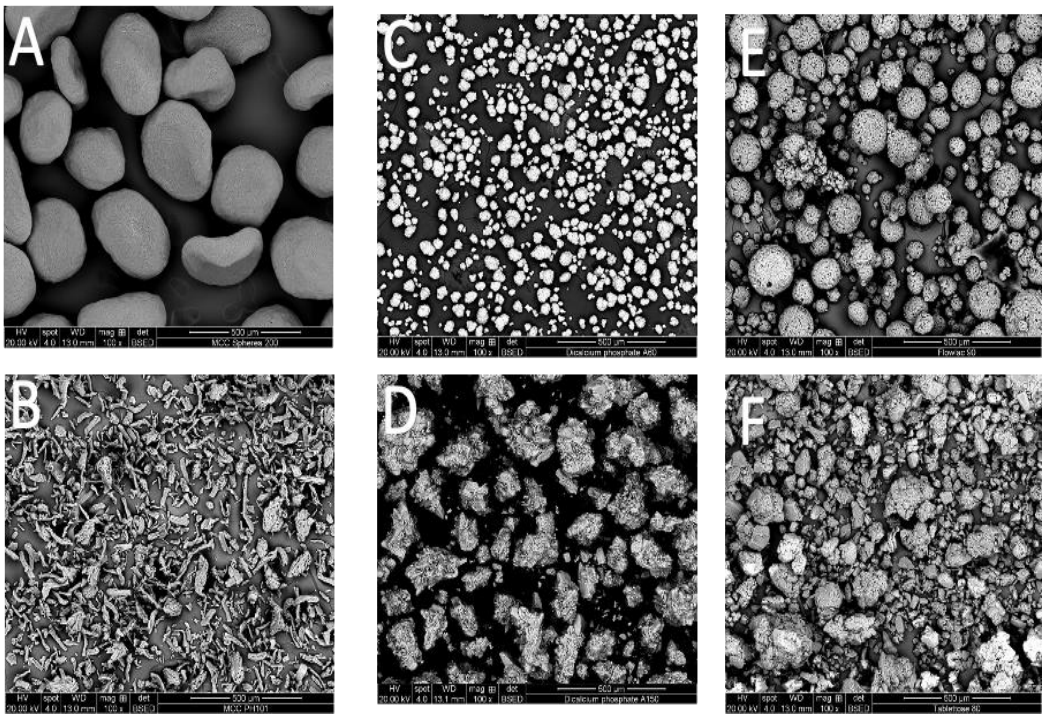

Figure 5.1 SEM images of A: MCC200 (Spherical microcrystalline grade), B: MCC101 (non-spherical microcrystalline grade), C: A60 (Spherical dicalcium phosphate), D: A150 (non-spherical DCP), E: Flowlac 100 (spherical lactose) and F: Tablettose (non-spherical lactose)

5.4.1.2 Particle size and shape analysis:

Results of particle and shape analysis of these grades are presented and discussed extensively in chapter 4, sections (4.4.1, 4.4.2, 4.4.3, 4.4.4, 4.4.5, 4.4.6 and 4.4.7). Table 5.1 and 5.2 briefly highlights these findings for the avoidance of repetition.

Table 5.1 particle size descriptors of MCC, DCP and lactose grades

GRADE/PARTICLE SIZE DESCRIPTORS	D [0.1, V] (µM)	D [0.5, V] (µM)	D [0.9, V] (µM)	D [4,3] (µM)	D [0.16, V] (µM)	D [0.84, V] (µM)	D [0.99, V] (µM)	SMD (µM)
MCC PH101	32.51	68.09	126.21	75.32	39.15	113.94	170.28	74.32
RSD %	0.41	1.13	1.32	1.47	0.44	1.76	3.75	2.20
MCC PH200	241.02	313.56	384.33	311.00	256.65	358.66	429.68	273.25
RSD %	5.06	4.17	27.38	9.07	5.89	10.55	57.46	39.22
A60	38.08	68.06	98.27	76.12	45.83	91.13	299.78	59.81
RSD%	1.23	0.18	0.65	5.58	0.31	0.60	12.57	0.45
A150	53.40	155.56	269.03	160.27	72.61	258.47	360.55	94.06
RSD%	2.85	4.87	2.36	3.92	4.16	22.57	2.03	3.78
FLOWLAC 90	67.02	145.56	231.67	148.51	82.11	210.28	325.84	137.07
RSD%	6.66	10.52	13.96	9.75	8.99	7.60	7.11	22.65
TABLETTOSE 80	40.77	138.18	433.12	191.53	53.31	334.80	756.42	87.33
RSD%	0.36	4.21	29.98	8.92	0.68	21.11	7.22	1.54

Table 5.2 Particle shape descriptors of MCC, DCP and lactose grades

GRADE/PARTICLE SHAPE DESCRIPTORS	ASPECT RATIO						SPHERICITY					
	S10,3	S50,3	S90,3	s16,3	s84,3	s99,3	S10,3	S50,3	S90,3	s16,3	s84,3	s99,3
MCC PH101	0.388	0.599	0.792	0.432	0.756	0.887	0.556	0.727	0.847	0.592	0.827	0.904
RSD%	0.001	0.001	0.001	0.001	0.001	0.002	0.005	0.005	0.002	0.005	0.003	0.001
MCC PH200	0.705	0.865	0.936	0.767	0.928	0.965	0.864	0.892	0.906	0.871	0.902	0.916
RSD%	0.003	0.001	0.001	0.001	0.001	0.002	0.002	0.001	0.001	0.002	0.002	0.001
A60	0.643	0.791	0.886	0.684	0.869	0.932	0.712	0.870	0.922	0.758	0.914	0.946
RSD%	0.005	0.001	0.000	0.002	0.001	0.000	0.001	0.001	0.001	0.002	0.001	0.001
A150	0.595	0.754	0.869	0.633	0.848	0.924	0.596	0.761	0.855	0.640	0.837	0.911
RSD%	0.002	0.003	0.002	0.001	0.002	0.001	0.017	0.009	0.005	0.015	0.006	0.003
FLOWLAC 90	0.684	0.881	0.942	0.737	0.933	0.966	0.806	0.914	0.939	0.836	0.935	0.950
RSD%	0.006	0.001	0.001	0.008	0.001	0.001	0.004	0.001	0.001	0.004	0.000	0.000
TABLETTOSE 80	0.599	0.747	0.861	0.634	0.839	0.917	0.708	0.817	0.887	0.741	0.873	0.929
RSD%	0.003	0.001	0.002	0.002	0.002	0.001	0.001	0.002	0.001	0.003	0.002	0.001

5.4.2 Surface roughness analysis

Figure 5.2 shows the surface topography images of tablets compressed at 10 kN produced using spherical and non-spherical particles of MCC, DCP and lactose grades. Figure 5.3 shows Sq values obtained at 10 kN force for each of these grades As shown from the two figures, spherical grades of the same material produced smoother surfaces when compared to the non-spherical grades (higher Sq values of spherical grades compared with non-spherical grades). This trend was observed in all materials studied (MCC, DCP and lactose). This study was aligned with previous findings by Naryan and Hancock where irregular shapes of MCC contributed to a higher roughness of tablet surfaces (Narayan & Hancock, 2003).

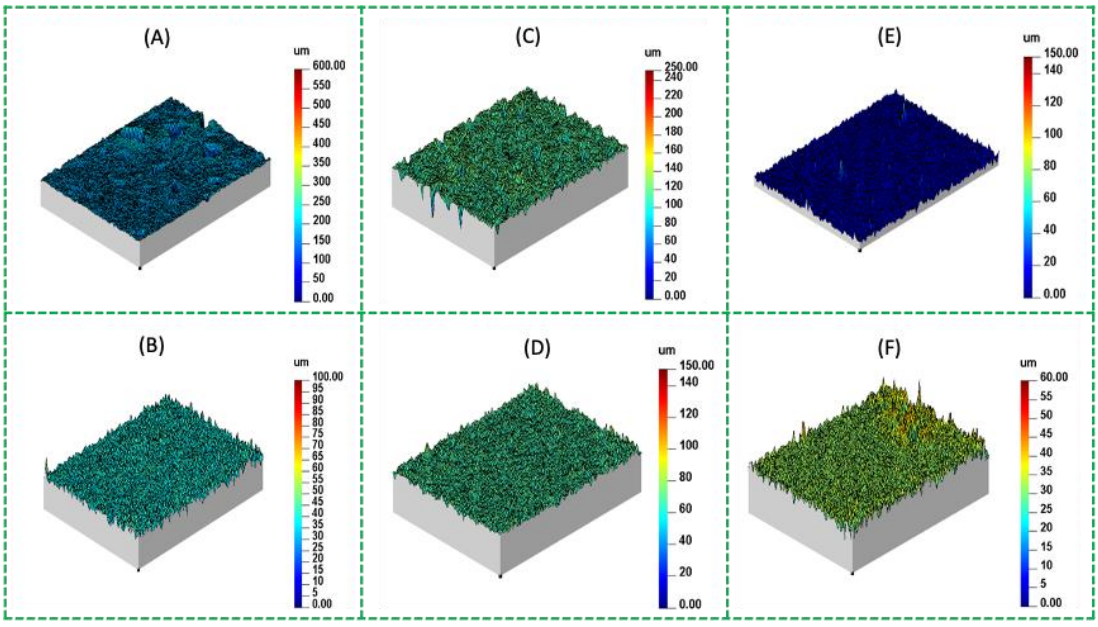

Figure 5.2 Surface roughness analysis of MCC -A:MCC200 (spherical), B: MCC101 (non-spherical)-, DCP -C:A60 (spherical), D:A15 (non-spherical)-and lactose -E: Flowlac90 (spherical), F: Tablettose 80 (non-spherical))-tablets compressed at 10 kN

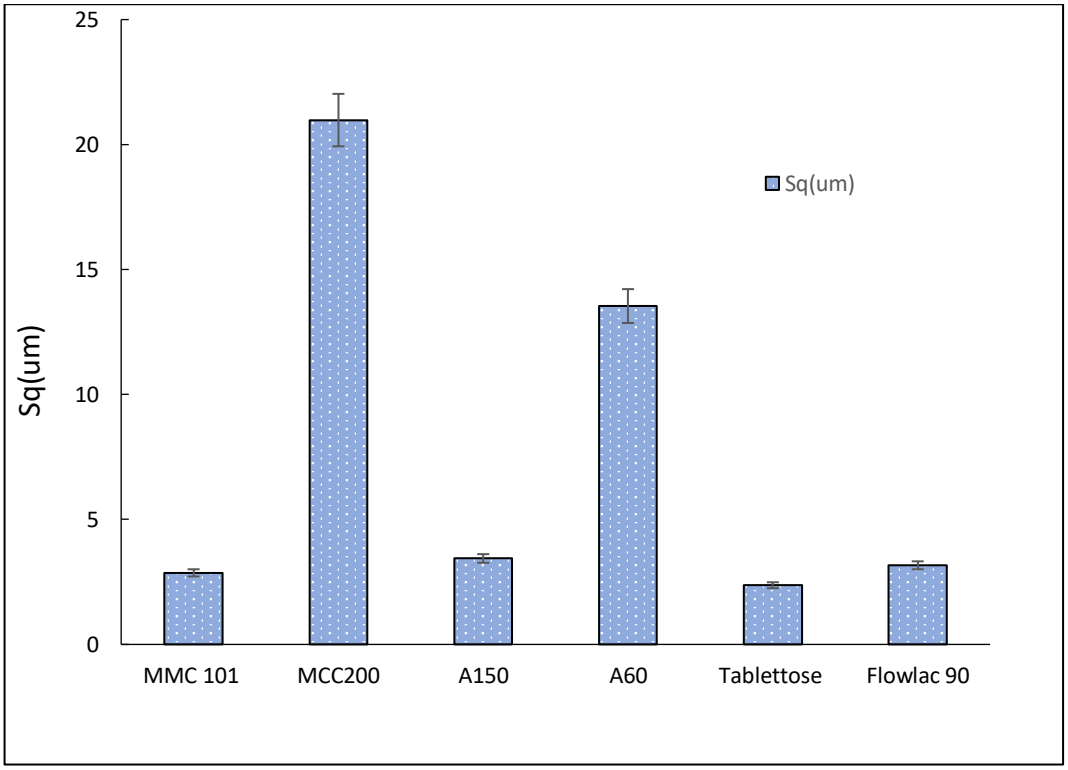

Figure 5.3 Sq of tablets compressed at 10 kN for MCC101 (non-spherical), MCC200 (spherical), A15 (non-spherical), A60 (spherical), Tablettose 80 (non-spherical) and Flowlac90 (spherical)

5.4.3 X-ray computed microtomography

X-ray microtomography was used in order to qualitatively assess how the porosity of compacts will be affected by changes in particle shape. Figure 5.4 shows the microstructure of these compacts made at 10 kN. As it can be seen from the figure that spherical grades of MCC, DCP and lactose tend to have a higher porosity when compared with their corresponding non-spherical grades. This can be attributed to the shape of the non-spherical particles resulting in mechanical interlocking which in turn, causes porosity values to decrease due to higher densification (He et al., 2019). On the other hand, spherical particles will not form such a type of interlocking, which will cause a higher porosity value of their corresponding compacts. These observations could provide more insights into the role of particle size and shape in determining the

internal structure of tablets and possibly future industrial defects such as capping or lamination of tablets. The application of X-ray tomography in determining possible internal tablet defects was previously reported by Yost et al. (2019), where X-ray tomography was used to quantitively assess a possible occurrence of lamination and capping tablet structure. However, this study was focused on the effect of formulation parameters such as roller compaction and the ratio of MCC: lactose within the formulation and processing parameters such as roller compression force on the possible internal defects within tablets. The X-ray tomography findings in this study highlights the importance of particle size and shape on determining the internal structure of corresponding tablets and, therefore, possible prediction of industrial defects that could occur, such as lamination and capping with different morphological grades of excipients. Spherical grades pose the risk of higher porosity compared with non-spherical grades and therefore pose the risk of future defects within tablets.

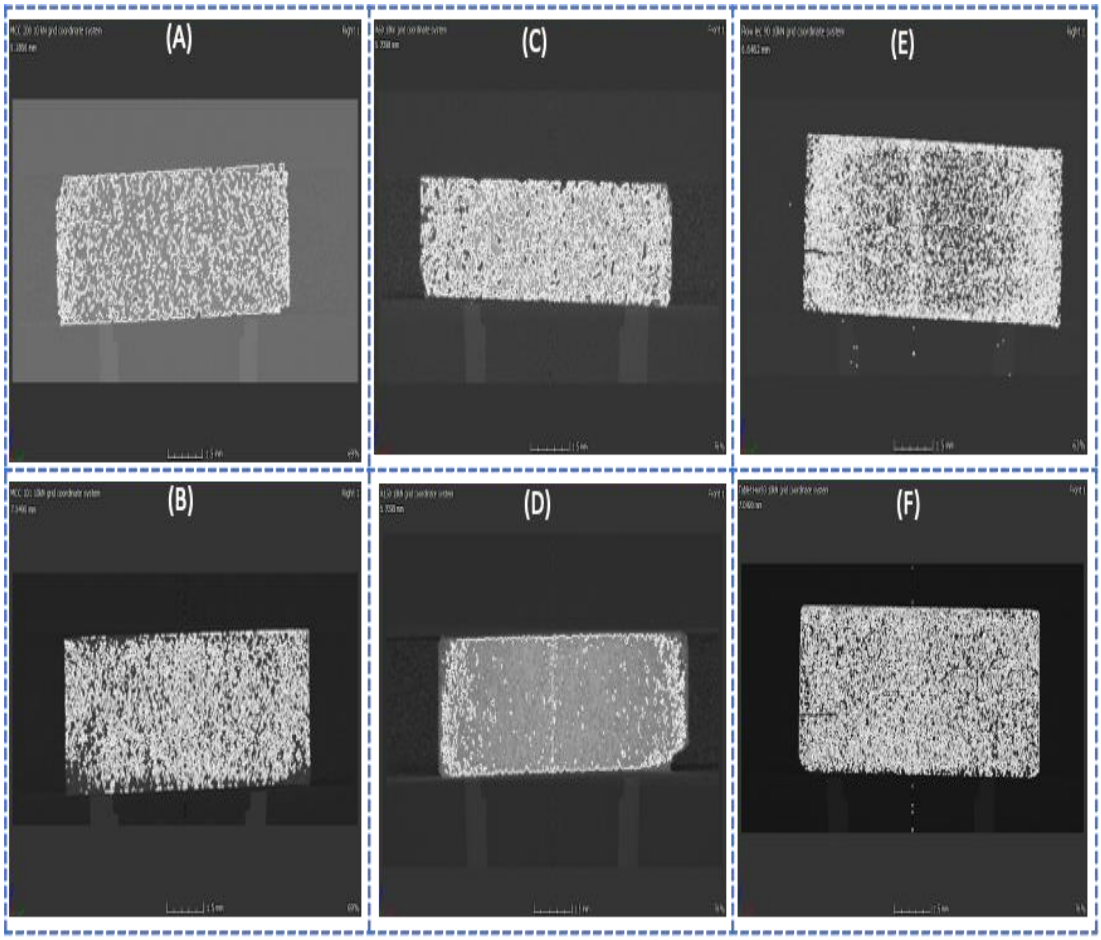

Figure 5.4 X-ray tomography of, A:MCC200 (spherical), B: MCC101(non-spherical), DCP C:A60 (spherical), D:A15 (non-spherical) and lactose E:Flowlac90 (spherical), F: Tablettose 80 (non-spherical) tablets compressed at 10 kN

5.4.4 True density results

Figure 5.5 and Table 5.3 summarises the true density values of different grades studied. As can be seen from the table and graph, no differences between the values of true densities observed for the same material. This indicates that particle shape and size have no effect on the value of true density of the same material. When comparing materials, DCP has the highest values of true density, followed by the lactose grades. These differences can be related to the differences in crystal structures, which could be one of the critical factors affecting the true density. As previously mentioned in

section 4.4.9, DCP grades tend to have a higher value of true densities when compared with MCC and lactose grades. These findings are aligned with previous findings (Cao et al., 2008; Hancock et al., 2003).

Table 5.3 True densities for MCC, DCP and lactose grades

Material	True density (g/cm^3)	SD
MCC101	1.744167	0.002648
MCC200	1.588867	0.005364
A60	2.848567	0.004567
A150	2.812867	0.008756
Tablettose 80	1.546267	0.007564
Flowlac 90	1.543067	0.004512

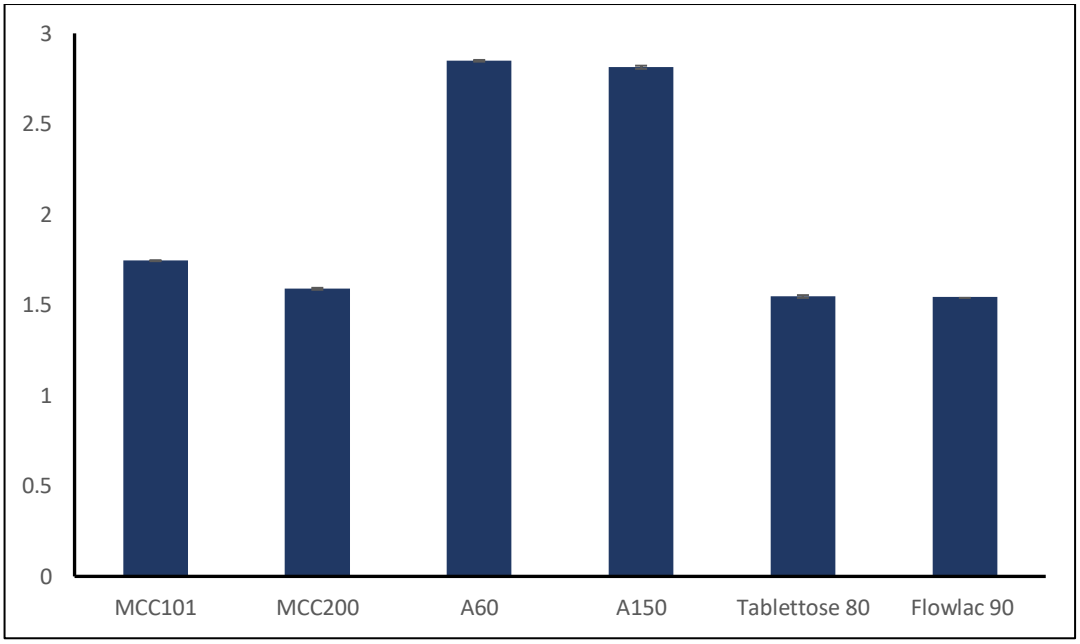

Figure 5.5 True densities of MCC, DCP and lactose grades

5.4.5 Mechanical analysis

5.4.5.1 Powder characterisation by Heckle analysis and work of compaction

Heckle analysis and work of compaction were used to assess how the mechanical properties will be affected by initial particle size and shape properties (Khorsheed et al., 2019). Yield pressure (Y*p*) was calculated using out-of-die Heckle analysis. The results of this analysis are reported in Table 5.4. For MCC grades, spherical particles showed a higher value of yield pressures when compared with non-spherical grades indicating that non-spherical grades have more plastic deformation than the corresponding spherical grades of MCC. This implies that the deformation behaviour for non-spherical grades could occur at a lower compression forces. This can be attributed to the mechanical interlocking that can be formed when compressing non-spherical particles. On the other hand, spherical particles could not possibly form any kind of mechanical interlocking between particles, resulting in higher yield pressure values. This was also reflected in the x-ray tomography images shown in Figure 5.4.

For DCP, a similar trend was observed when comparing between the spherical and non-spherical grades. DCP A150 (non-spherical grade) gave a yield pressure value similar to MCC 101 and much higher than the spherical grade (A60), indicating that non-spherical grade has more ability to form tablets due to the brittle nature of DCP. Also, the fragmentation behaviour of DCP may result in more interlocking when compared with the spherical grade. Lactose grades also showed a similar trend with non-spherical grade (Tablettose 80). However, it has a much lower yield pressure value indicating that this grade has more plastic deformation ability than the non-spherical grade and highlight this grade as a better choice for tablet manufacturing.

Table 5.4 Yield pressure, plastic work and elastic work of tablets studied

	Yield Pressure	R2 (Yp)	Plastic work (%)	SD (plastic work)	Elastic work (%)	SD (elastic work)
MCC 101	12.43	0.996	93.31	0.002	6.68	0.32
MCC 200	36.363	0.958	92.47	0.004	7.52	0.54
A150	12.360	0.910	91.69	0.154	8.30	0.43
A60	32.786	0.912	88.78	0.220	11.21	1.45
Tablettose 80	3.412	0.962	89.99	0.142	10.00	0.84
Flowlac 90	31.25	0.996	86.40	0.465	13.59	1.12

Force-displacement data was used to assess if the plasticity of formulations will change as a function of particle properties. Results of plasticity work and elastic work can be found in Table 5.1. As it can be observed from the table that, MCC and lactose have higher plasticity when comparing it to DCP. As discussed earlier in the introduction, MCC has plastic deformation behaviour. In contrast, lactose has brittle-plastic deformation, and our findings from the plastic work indicate that the compression force used (10 kN) is enough for plastic deformation to occur in lactose powder. These findings confirm that particle size and shape affected yield pressure rather than the deformation behaviour between lactose and dicalcium phosphate.

5.5 Conclusions

This chapter explores how particle properties will affect the tabletability performance of different grades of MCC, DCP and lactose. These grades were chosen in this chapter for two main reasons; A) they are the most commonly used pharmaceutical excipients used in tablet formation B) they are known to have different mechanical properties. Particle size and shape characterisation using SEM revealed that there are significant differences between particle properties of grades used of MCC, DCP and lactose. Tablet microstructure was examined using X-ray tomography. Results of X-ray microtomography showed that spherical particles form more porous tablets than their corresponding non-spherical grades. These findings have reflected on the values of yield pressure, with the spherical grades having a higher value of yield pressure than the non-spherical grade of the same excipient. These findings may explain that mechanical interlocking is the main mechanism mediated in the formation of tablets with non-spherical particles being better in tablet formation than the corresponding spherical ones.

In summary, this chapter highlights how important it is to control particle properties such as shape and size during manufacturing pharmaceutical tablets. It gives insights into how the microstructure of tablet will be affected by changes in particle properties. It also highlights mechanical interlocking as the primary mechanism affecting tablet formation.

Chapter 6 - Investigating the effect of formulation properties on the particle size of disintegrated tablets using a novel on-line particle sizer analyser

6.1 Introduction

Earlier in Chapter 4 and 5, the effect of particle properties on the flow performance and mechanical properties were evaluated. In this chapter, the effect of formulation properties on the disintegration behaviour of pharmaceutical compact will be investigated. For active pharmaceutical ingredients within tablets to exert any biological response, tablets should first disintegrate into particles before they dissolve and then absorbed through the gastrointestinal tract (Markl & Zeitler, 2017). Tablet disintegration is therefore one of the critical tests that should be monitored and evaluated. Tablet disintegration and subsequent dissolution are considered one of the main indicators of *in vivo* performance and subsequent biological activity (Rajkumar et al., 2016). Without enough disintegration and dissolution, active pharmaceutical ingredients within tablets will not reach the bloodstream nor exert any therapeutic response. Studying and monitoring disintegration behaviour is, therefore, of great importance. Factors affecting disintegration behaviour can be particle related or formulation related factors. Typical excipients used in the formulation of oral solid dosage forms can be filler, disintegrant, binders, and lubricant. Each of these excipients may affect disintegration behaviour either positively or negatively. Disintegration time, for example, can vary depending on the type and concentration of disintegrant used (Aulton & Taylor, 2013). The type and amount of binder could also affect the disintegration behaviour. Herting et al.(2007) for example, studied the differences in term of disintegration time between tablets produced using copovidone polymers (VA64) and HPMC polymers. Their findings showed that there were significant differences with the tablets produced using these two polymers. Tablets produced using the HPMC polymer showed a disintegration time twice as long as

those produced using the copvidone VA64 polymer. Lubricants are another formulation component that could affect the disintegration behaviour of tablets. Wang et al. showed that magnesium stearate as lubricant delayed the disintegration time due to its hydrophobicity. This causes a delay in water penetration and subsequent disintegration (Wang et al., 2010). He et al. (2007) found that the addition of magnesium stearate as a lubricant can decrease the disintegration time due to due to the tablet have a relatively low mechanical strength. Otsuka et al. (2004) showed the effect of lubricant on the disintegration time depended on both the lubricant used and the type of excipient used in the production of tablets .

6.2 Aims and objectives

This chapter will aim to develop a new novel method to investigate how particle size of disintegrating tablets may change by coupling a surface dissolution imager (SDI2) dosage form cell with an inline particle size analyser in the wet phase. Formulation properties effects on the disintegration behaviour of these tablets will then be investigated. To carry out these objectives, an insoluble filler was chosen to produce tablets using different compression forces at a different level of magnesium stearate concentration. Using soluble fillers such as lactose will not enable the visualisation of how formulation properties will affect the disintegration as the disintegrated particles will dissolve and will thus not be captured using the particle size analyser. Swellable materials will also not be suitable as their particle size will change upon contact with water/media.

6.3 Materials and methods

6.3.1 Materials

Dicalcium phosphate dihydrate (EMCOMPRESS ®) was purchased from JRS pharma and used in the study mainly because it is an insoluble filler. Three functional superdisintegrants were used in the study; CSS (Ac-Di-Sol) was supplied by DuPont (USA), Crospovidone (CP) (Kollidon CL) was donated from BASF Plc (UK), and Sodium starch glycolate (SSG) (Expoltab) was donated from JRS pharma (USA). Magnesium stearate (Kosher Passover HyQualTM) was supplied by Mallinckrodt pharmaceuticals.

6.3.2 Method

6.3.2.1 Tablet preparation

Tablets were prepared by mixing the dicalcium phosphate dihydrate powder with the corresponding percentage of disintegrant and lubricant as highlighted in Table 6.1. The various mixtures were blended using a Turbula blender for 30 min to ensure that a homogenous mixture are obtained.

Table 6.1 Sample IDs, Disntegrant used and magnesium stearate level for dicalcium phosphate dihydrate formulations

Sample ID	Disintegrant used (Conc.%)	Magnesium stearate Level
SSG (0.25%)	SSG (2%)	0.25%
SSG (2%)	SSG (2%)	2%
SSG (5%)	SSG (2%)	5%
CSS (0.25%)	CSS (2%)	0.25%
CSS (2%)	CSS (2%)	2%
CSS (5%)	CSS (2%)	4%
CP (0.25%)	CP (2%)	0.25%
CP (2%)	CP (2%)	2%
CP (5%)	CP (2%)	5%

A computer-controlled mechanical testing machine (M500-50CT, Testometric Co, limited. Rochdale, UK) attached to an extensometer was used to prepare tablets. Tablets were compressed using stainless steel die (Specac limited, Kent, England). Compaction was applied to three pre-set peak force of (5, 10,15 kN). A pre-weighed powder was placed into the die. The compaction speed was set at 3 mm min^{-1} throughout the compression period to the chosen maximum loading. A compression force was applied between the upper punch and the load cell. Whilst, the lower punch remained stationary. The upper punch displacement was recorded using a linear variable differential transformer (LVDT) position gauge probe (Solartron AX/2.5/S, Solartronmetrology limited, UK). This probe was further linked to the platens. (Laity et al., 2015; Laity & Cameron, 2008).

The compressed tablet was gently ejected from the die. The thickness and diameter of tablets were calculated using an electronic digital calliper (Mitutoyo, Japan) after 1 min of tablet ejection from the die. The mass of the tablet was calculated subsequently. More information about the compaction simulation process can be found in chapter 3, section 2.1.11 of the thesis.

6.3.2.2 Evaluation of mechanical properties

After compression, thickness (T) and diameter (H) of tablets were calculated. Tensile strength was then calculated as described previously in chapter 5 using equation 5.1

Work of compaction of powders used in this study was done by analysing data obtained from the mechanical testing machine using a compression-decompression method. This method involves compressing the tablet to a maximum compression force (10 kN) and then decompressing back to 0 kN. A force-displacement profile was then obtained. The area under the curve was calculated using a trapezoidal method. Total work of compaction, elastic work and plastic work has been further calculated according to the following literature (Khorsheed et al., 2019)

Yield pressure was also used to compare between compressibilities of different batches. Yield pressure is the reciprocal value of the Heckel coefficient (Pitt & Sinka, 2007). Heckle coefficient (K) was calculated using equation 3.5 which is detailed in section 2.1.11 of this thesis.

6.3.2.3 Real-time disintegration monitoring

This novel technique is discussed in more details in section 2.1.12. In summary, the method involves coupling the dissolution imaging instrument (SDI2) system with a Mastersizer. Before mounting the tablet within the full dosage cell of the SDI2, the cell was flushed using deionised water to ensure the system was clean. Tablet was then mounted within the cell using a metal wire designed specifically to hold the tablet in place. Water was used as a disintegration media. The flow rate was kept at 8.2 ml/min, and the temperature of the media (water) used was 37 ± 0.5 ºC

(Asare-Addo et al., 2019). After the disintegration of the tablets in the dissolution imaging instrument, the particles size of disintegrated particles was captured using the Mastersizer. Dicalcium phosphate is considered insoluble materials. Therefore, how formulation properties such as magnesium stearate and disintegrant type affect the particle size of resulted particles was investigated. All experiments were conducted in triplicate.

6.3.2.4 Particle size analysing

A mastersizer 3000 (Malvern) in a wet mode was used to analyse the particle size of disintegrant particles produced by the disintegration cell (section 6.3.3). Before running an experiment, the sample cell for the mastersizer was cleaned using deionised water, and the diffraction index of dicalcium phosphate (1.55) (PubChem) in water was entered into the software. A sample was then fed into the system until and the particle size measurement was calculated in triplicates. More information about particle size analysis can be found in section 2.1.2.2.

6.3.2.5 SEM

The particles obtained from the disintegration process (section 6.3.2.3) and dried were then examined using SEM. More information on the SEM method can be found in section 2.1.2. Briefly, a scanning electron microscope (Jeol JSM-6060CV SEM) operating at 10 kV was used to generate electron micrographs images. Samples were mounted onto a metal stub using double-sided adhesive tape. Samples were then coated with gold for 60 seconds using a Quorum SC7620. Micrographs with different magnifications were then taken.

6.3.2.6 Tablet surface analysis

A focus variation instrument (Contour LS 3D Optical Profiler (Bruker)) was used to assess the surface topography of pharmaceutical product using either 5 x or 10 x objective and specific lateral resolution. The obtained images were further analysed using the Surfstand™ software (Taylor Hobson, UK, and University of Huddersfield, UK) to obtain 2D and 3D profiles of the surfaces (Ward et al., 2017). The Sq parameter defined as the root mean square value of the surface departures from the mean plane within the sampling area. This parameter was previously used to compare between tablets surface and it is known to be sensitive to any changes of surface roughness of tablets (Narayan & Hancock, 2005). Sq parameter is calculated as previously mentioned in section 2.1.5 of this thesis.

6.4 Results and discussions

6.4.1 Powder characterisation by Heckle analysis and work of compaction

Heckle analysis and work of compaction were used to assess how the mechanical properties of the DCP changes by adding both the disintegrant and magnesium stearate at different levels. DCP is reported to be a brittle material and could fragment upon compression (Khorsheed et al., 2019). In this study, the Yield pressure (Y*p*) of DCP was calculated using out-of-die Heckle analysis. The results of this analysis are reported in Table 6.2. As shown from the table, adding sodium starch glycolate increased the yield pressure for DCP compared with other disintegrants at the same level of magnesium stearate. However, increasing the magnesium stearate in a formulation containing SSG resulted in a significant drop in yield pressure values. Y*p* value for the formulation containing (0.25 % of magnesium stearate) was 163.94 MPa, whereas Y*p* values for formulations containing 2 % and 5 % were 69.93 and 55.55 MPa respectively. This may be explained as a possible interaction between magnesium stearate and SSG that leads to a decrease in Yield pressure values as magnesium stearate level increases with increasing bonding between particles.

Formulations containing CSS and CP were insensitive to Y*p* changes as magnesium stearate content increased. Y*p* values of formulation which contain CSS were 65.35, 68.49 and 71.42 MPa whereas the samples containing CP were 71.42, 77.51 and 74. 04. This may be due to minimal interactions between the magnesium stearate and CSS and CP.

Table 6.2 Heckle analysis and Yield pressure values for DCP upon the addition of SSG, CSS and CP

	Yield Pressure (Yp) (MPa)	R2 (Yp)	Plastic work (%)	SD (plastic work)	Elastic work (%)	SD (elastic work)
SSG (0.25%)	163.94	0.95	91.40	0.032	8.6	0.29
SSG (2%)	69.93	0.93	93.51	1.652	6.45	0.03
SSG (5%)	55.55	0.94	89.65	0.362	10.35	1.64
CSS (0.25%)	65.35	0.86	91.95	0.362	8.05	0.36
CSS (2%)	68.49	0.86	90.44	0.392	9.56	0.39
CSS (5%)	71.42	0.88	89.66	1.062	7.02	6.47
CP (0.25%)	77.51	0.86	90.60	1.794	9.4	1.79
CP (2%)	74.07	0.90	91.33	0.681	8.67	0.68
CP (5%)	73.02	0.90	91.21	0.619	8.78	0.61

Force-displacement data was also used to assess if the plasticity of the formulation changes as formulation parameters (disintegrant type, disintegrant level, magnesium stearate level) changes (Aburub et al.,2007; Khorsheed et al., 2019). Results of plasticity work and elastic work can be found in Table 6.2. Percentage of plastic work and elastic work did not change between formulations studied (89.44-91.40%) while values of elastic work remained between (6.45-10.35). These findings indicated that changing these formulation parameters does not lead to a change the plasticity of DCP.

This can be attributed to the percentage of DCP within these formulations, which may be responsible for determining the plasticity of formulation as a whole.

6.4.2 Tablet characterisation

6.4.2.1 Tabletability profiles

Tabletability is defined as a relationship between tablet tensile strength and compression force. It is a good indication of the robustness of tablets produced and an indication that these tablets will have the required strength to withstand future handling and transport (Qiu et al., 2016). Tabletability profiles are obtained by compressing tablets at different compression points (three in this case). Figures 6.1-6.3 depicts tabletability profiles for formulations that contain SSG, CSS and CP respectively. In each graph, different levels of magnesium stearate are presented for each formulation.

For formulations containing SSG (Figure 6.1), decreasing the concentration of magnesium stearate from 5 % to 2% resulted in a decrease in tabletability. However, further decrease of magnesium stearate did not result in any significant loss in tabletability. Similar trends were observed with formulations that contained CSS (Figure 6.2) and CP (Figure 6.3). However, the loss of tabletability with these formulations when decreasing the magnesium stearate levels from 5 % to 2% was less compared to the corresponding formulations containing SSG. As DCP is classified as a material with a low bonding area but high bonding strength (C. C. Sun, 2011), the loss of tabletability as magnesium stearate level decreases may be attributed to the possibility of magnesium stearate enhancing the bonding strength between these particles and therefore increasing tabletability of the resulted formulation.

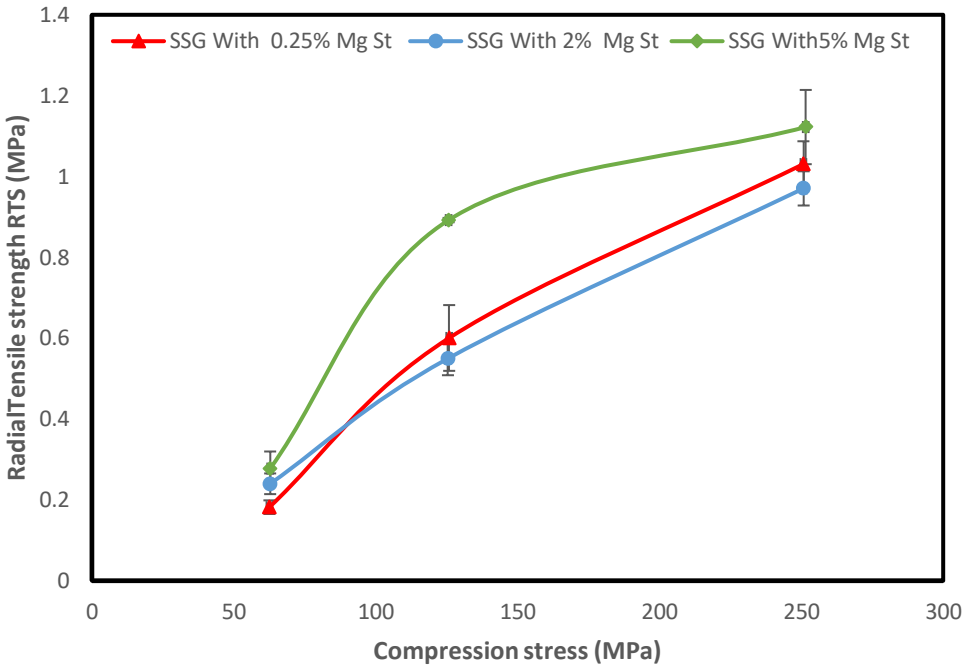

Figure 6.1 Tabletability profiles for SSG formulations

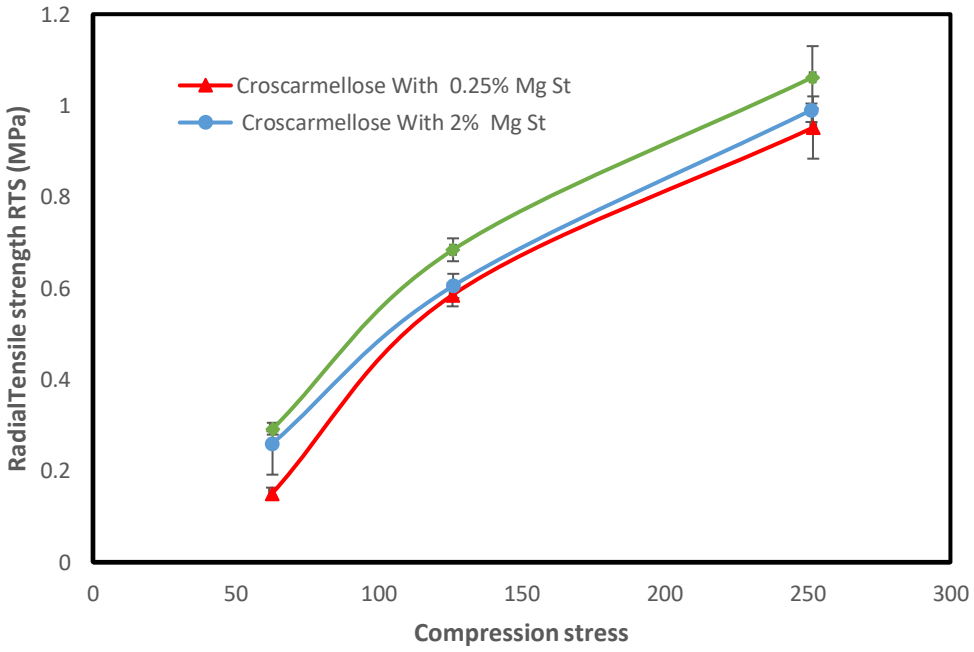

Figure 6.2 Tabletability profiles for CSS formulations

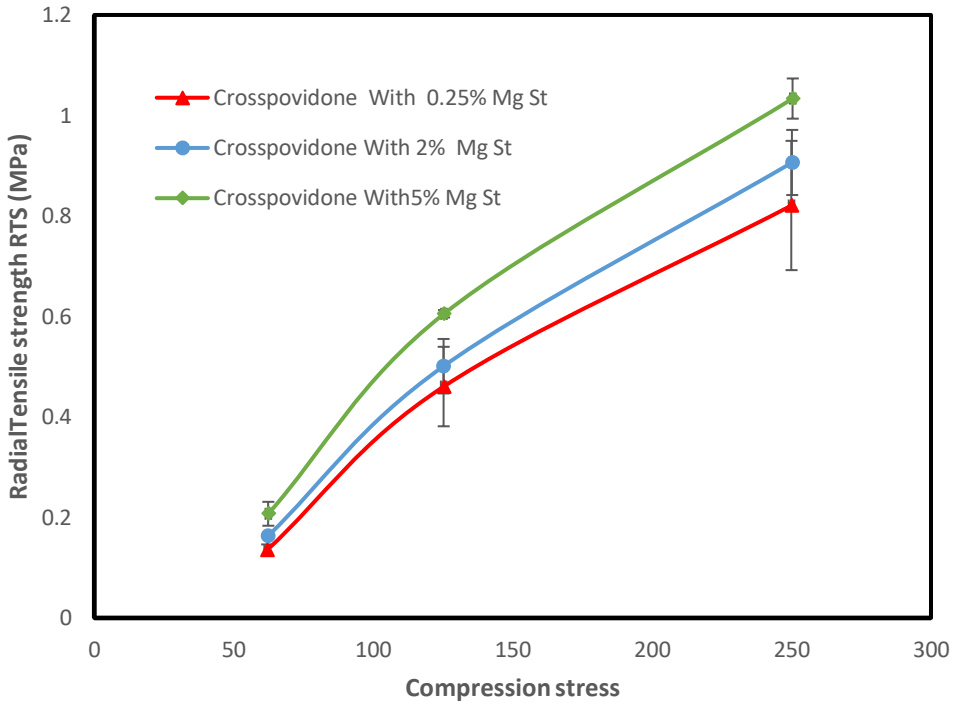

Figure 6.3 Tabletability profiles for CP formulations

6.4.2.2 Compactibility profiles

Compactibility profile is defined as a relationship between radial tensile strength and a solid fraction (Qiu et al., 2016). Low solid fraction results in fragile tablets. Figures 6.4-6.6 shows the compactibility profiles for the formulations containing SSG, CSS and CP, respectively. Solid fractions values for these formulations remained between 0.6-0.8. It is worth noting that increasing magnesium stearate level resulted in an increase in the solid fraction for all formulation studied (SSG, CSS and CP containing formulation). This increase in solids within tablets can be an indication of stronger tablets (Leuenberger et al., 1982). These findings were aligned with tabletability profiles where stronger tablets were observed as magnesium stearate level was increased. Another possible explanation may be that magnesium resulted in an increase in bonding between particles of dicalcium phosohate. However, this was

previously studied and highlighted that dicacium phosphate bonding would be uninfluenced by the presence of magnesium stearate (De Boer et al., 1978). Another possible explanation for increasing in compactibility can be attributed possibly to an interaction between magnesium stearate and disntegrants that lead to an enhanced bonding within powder beds and therefore increase solid fraction. These findings, however, contradict previous studies where the assumption that lubrication in general may lead to a weaker tablet (Paul & Sun, 2017).

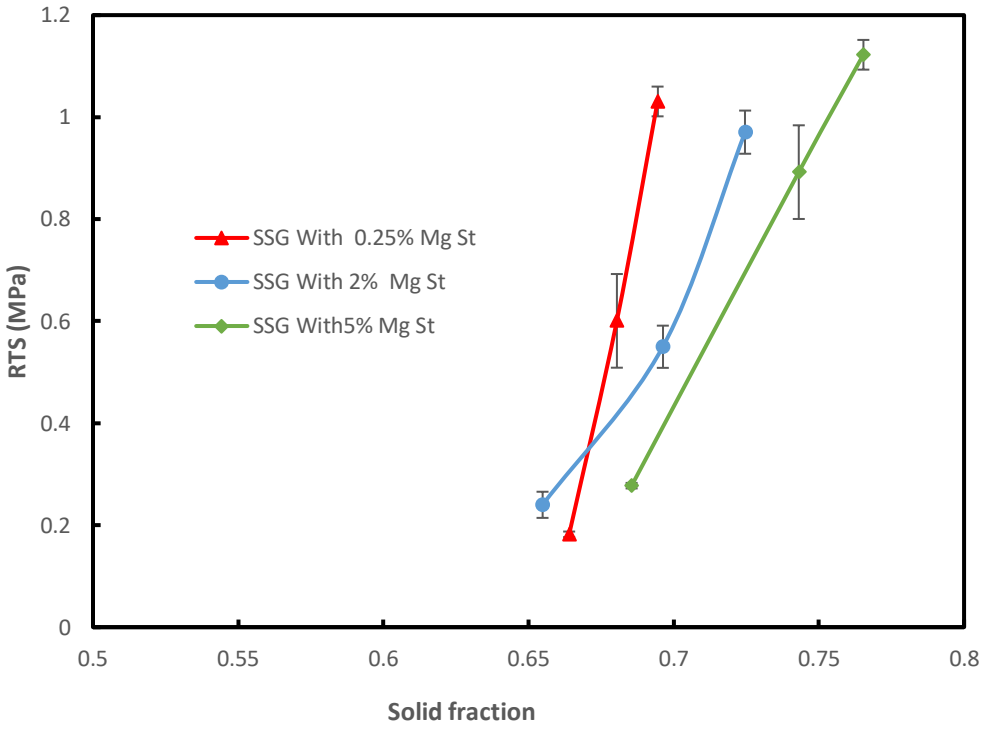

Figure 6.4 Compactibility profiles for SSG formulations

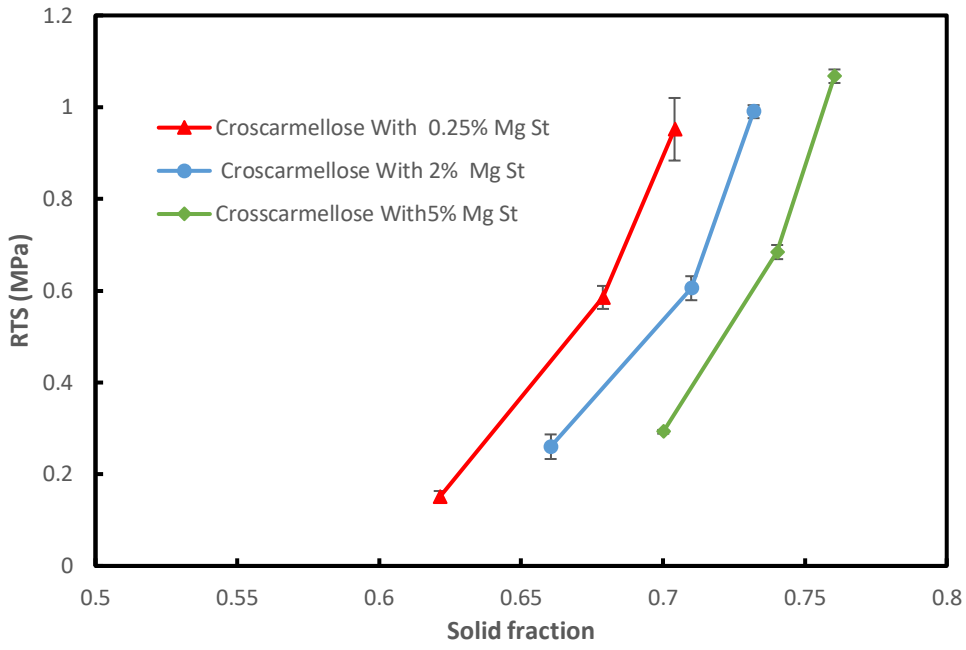

Figure 6.5 Compactibility profiles for CSS formulations

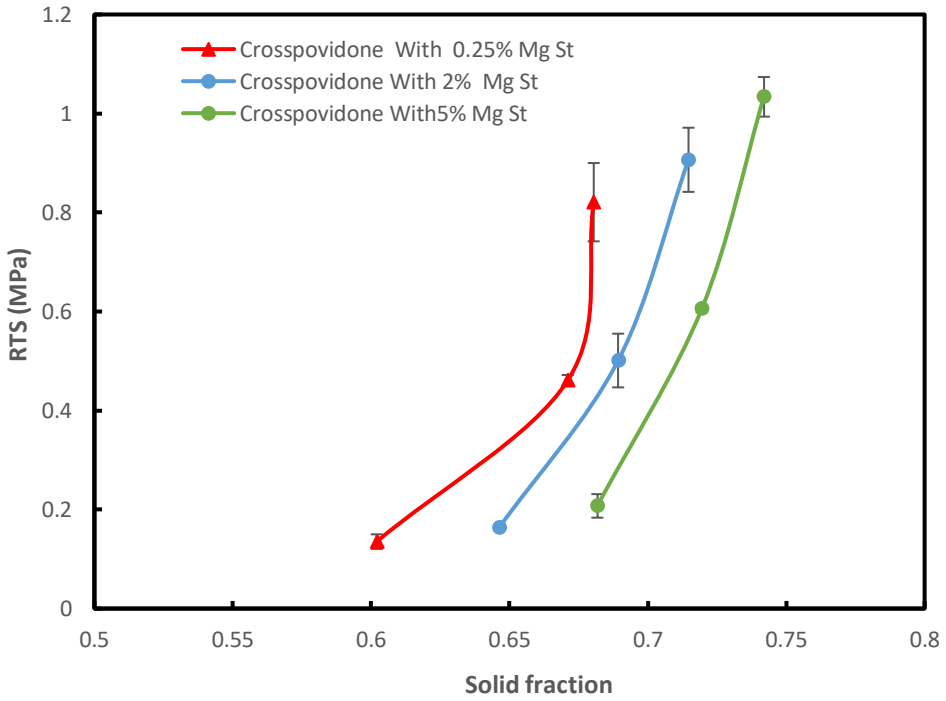

Figure 6.6 Compactibility profiles for CP formulations

6.4.2.3 Compressibility

Compressibility profiles are defined as a relationship between the solid fraction and compression stress (Qiu et al., 2016). Compressibility profiles of SSG, CSS and CP formulations are shown in Figures 6.7-6.9. As magnesium stearate levels for all formulation studied increased, the solid fraction of the tablet produced increased. At specific compression pressure, tablets containing the highest level of magnesium stearate showed a higher solid fraction. This trend was observed will all disintegrant formulation studied. These findings may be related to the ability of magnesium stearate to enhance the flowability of excipients, as previously reported by Morins and Briens (2013). Flowability improvement will therefore increase the solids within powders and consequently increase the solid fraction at specific pressure studied (Morin & Briens, 2013).

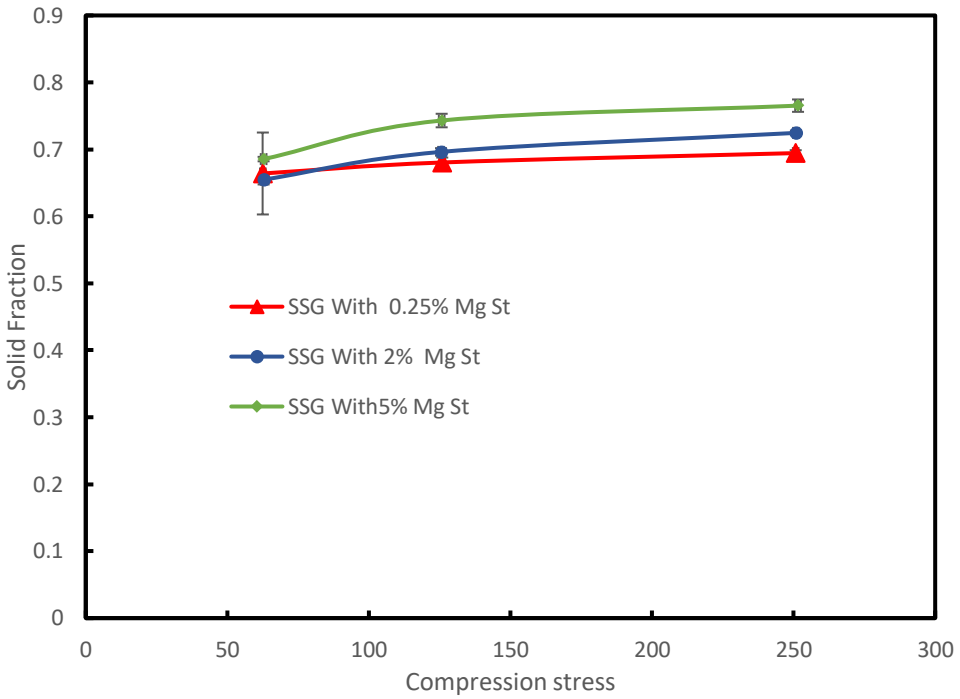

Figure 6.7 Compressibility profiles for SSG formulations

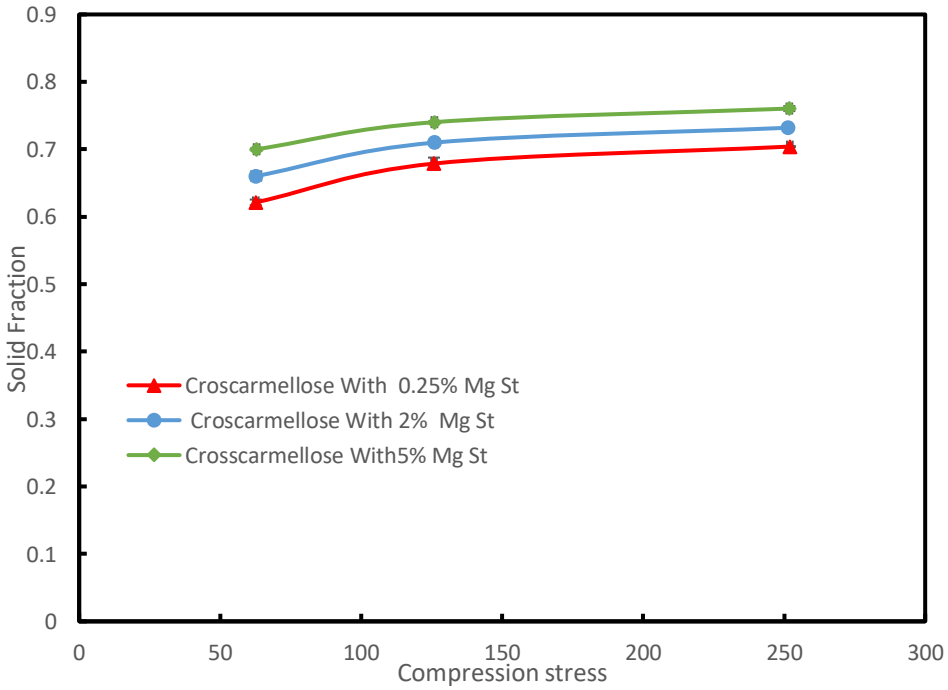

Figure 6.8 Compressibility profiles for CSS formulations

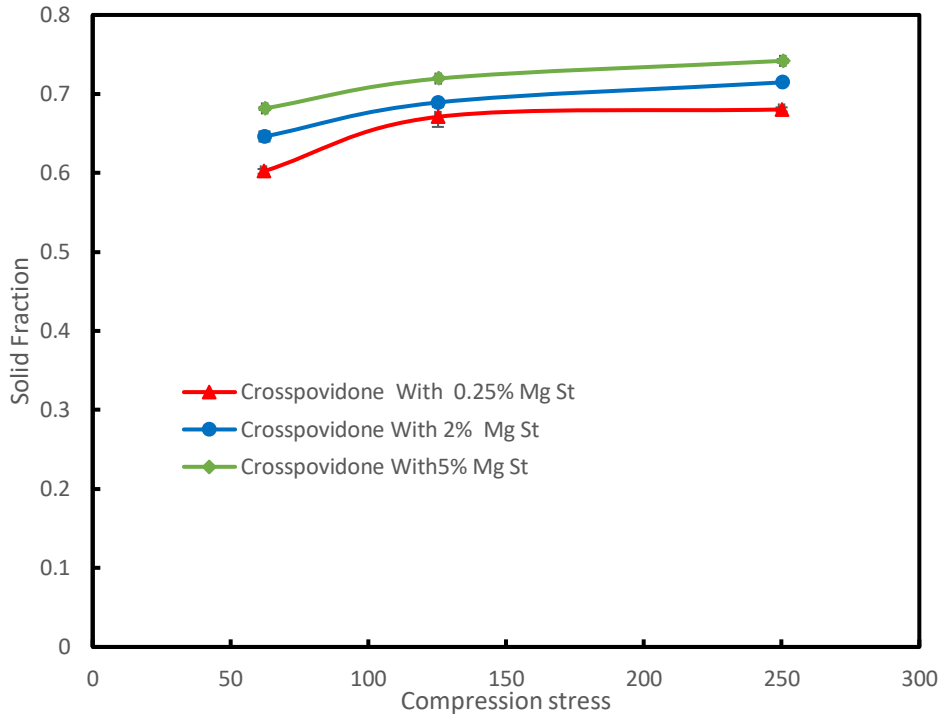

Figure 6.9 Compressibility profiles for CP formulations

6.4.3 Characterisation of the disintegrated particles

Table 6.3 shows an example of the SDI images captured at the initial set-up of the experiment and 5 min after the dosage cell had been filled with water. As can be observed from the images, the tablets entirely disintegrated by the 5 min time point. This trend was observed with all tablets studied. Disintegrated particles were then characterised as described in section 6.4.3.1

Table 6.3 SDI images of tablets before disintegration and 5 min after the cell is completely filled with water

Tablets	Before contact with water	5 min after contact with water
SSG containing tablet	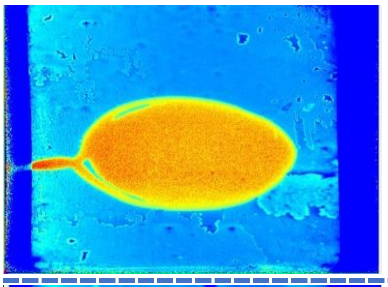	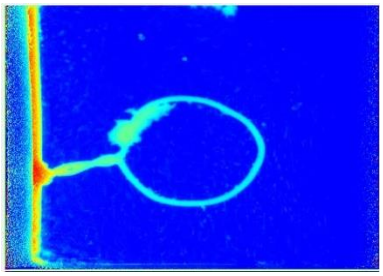
Crosscarmellose containing tablet	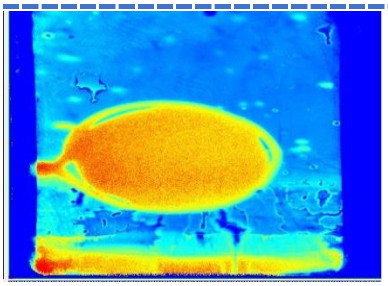	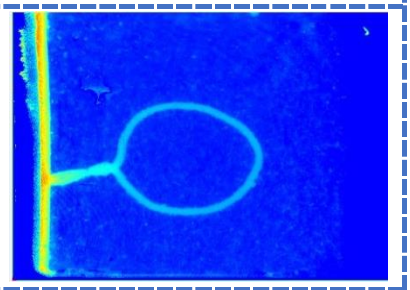
Crosspovidone containing tablet	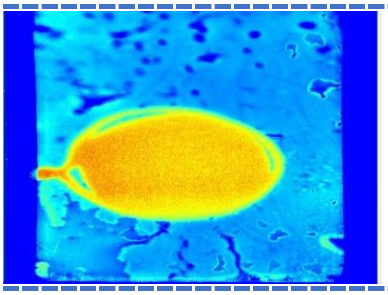	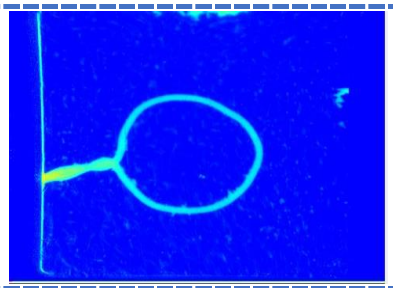

6.4.3.1 Scanning electron microscopy

SEM images of DCP, disintegrated particles of SSG formulations, CSS formulations, and CP formulations are presented in Figures 6.10-6.12 respectively. For SSG, it can be observed that there are distinctive differences in the particle size properties of disintegrated particles obtained with increasing particle size as both magnesium stearate concentration and compression pressure increase. A similar observation was seen with CP particles. However, CSS particles seem to produce a relatively similar

particle size distribution with no major changes in particle size of disintegrant particle as both compression force and magnesium stearate levels increase.

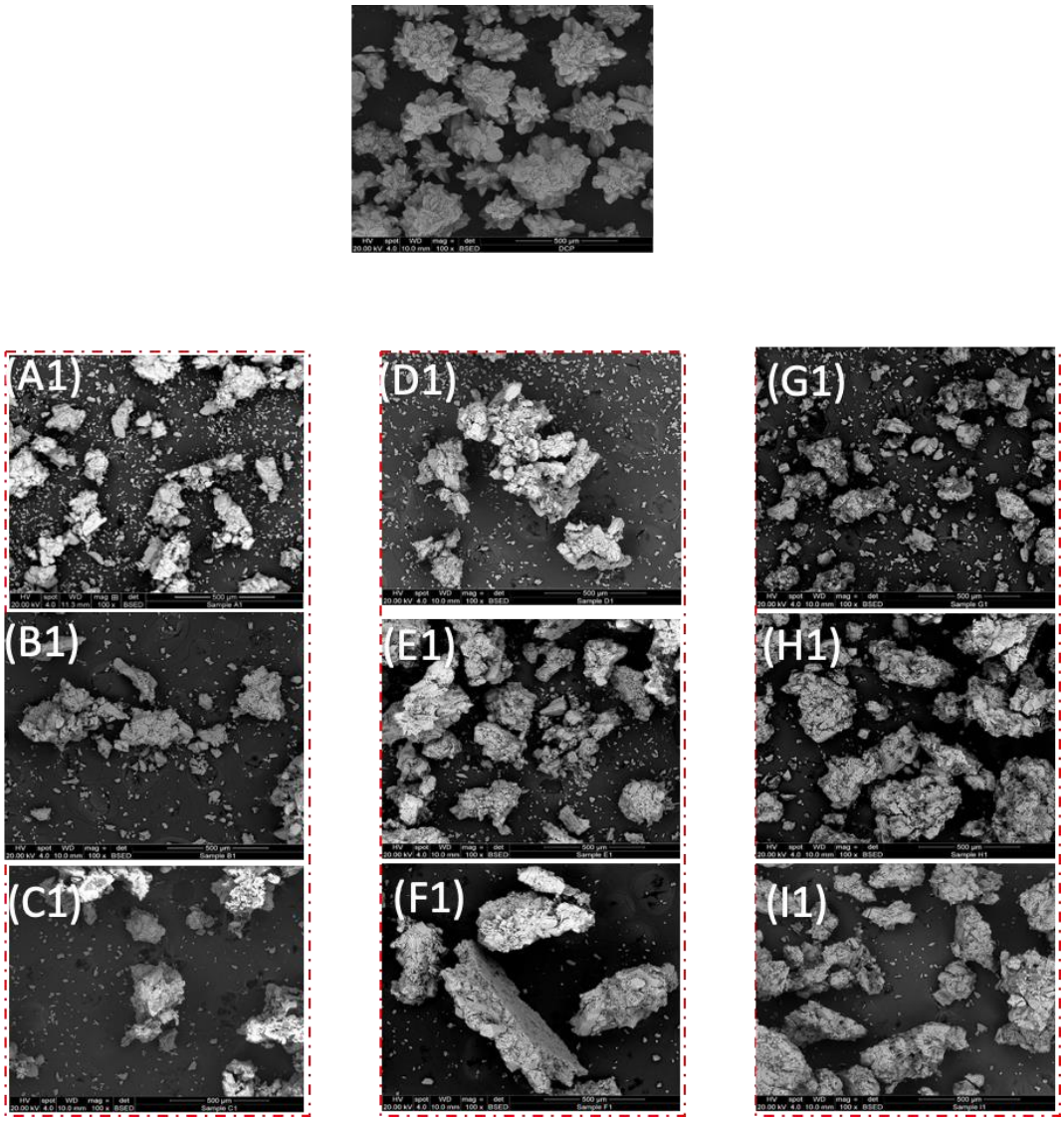

Figure 6.10 SEM pictures of DCP disintegrated particles containing SSG formulation; A1: SSG formulation containing 0.25% Mg St compressed at 5 kN, B1: SSG formulation containing 0.25% Mg St compressed at 10kN, C1: SSG formulation containing 0.25% Mg St compressed at 15KN, D1: SSG formulation containing 2% Mg St compressed at 5 kN, E1: SSG formulation containing 2% Mg St compressed at 10 kN, F1: SSG formulation containing 2% Mg St compressed at 15 kN, G1: SSG formulation containing 5% Mg St compressed at 5 kN, H1: SSG formulation containing 5% Mg St compressed at 10 kN, I1: SSG formulation containing 5% Mg St compressed at 15 kN. Note: Mg St is magnesium sterate

.

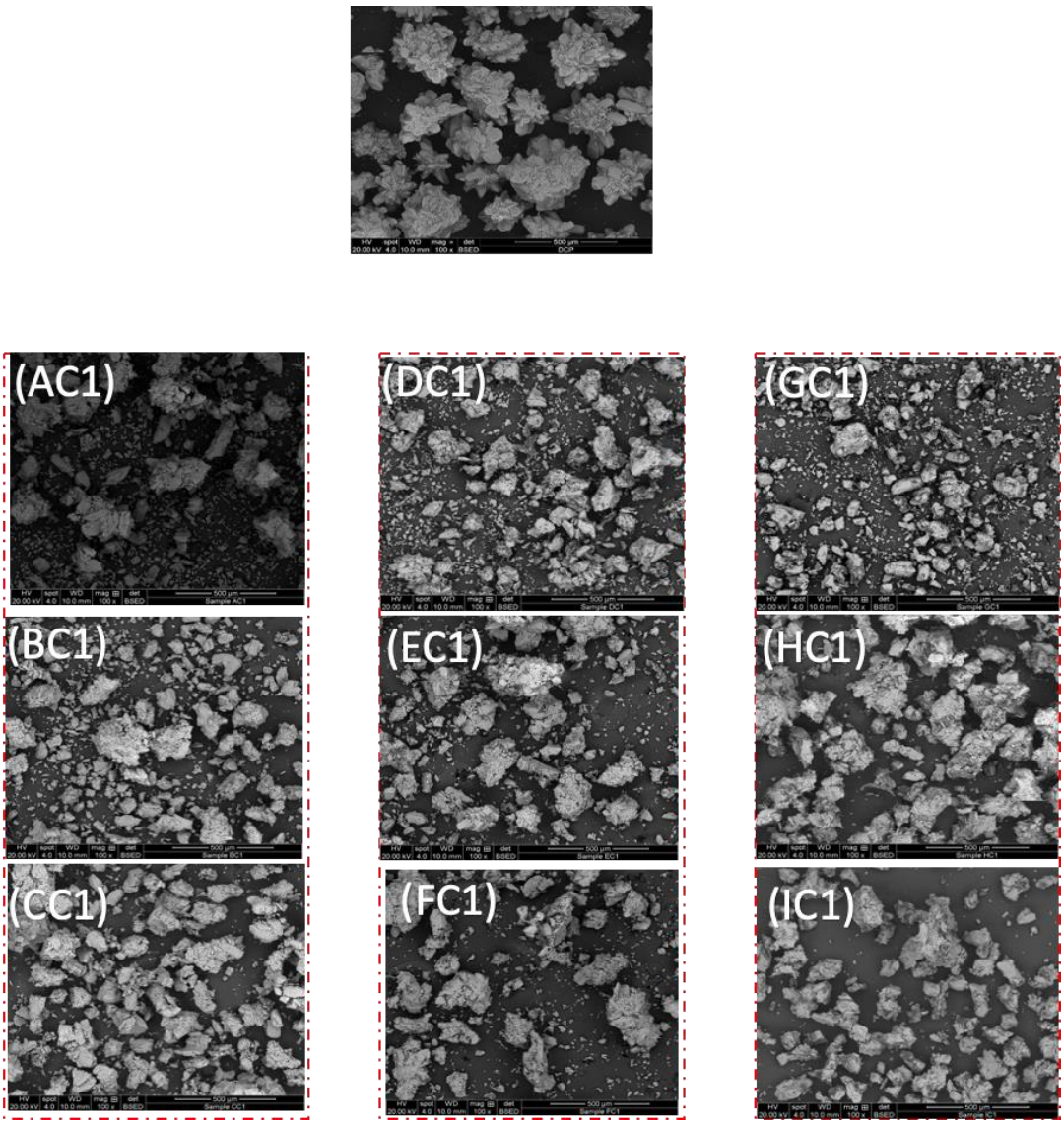

Figure 6.11 SEM pictures of DCP disintegrated particles containing CSS formulation; AC1: CSS formulation containing 0.25% Mg St compressed at 5 kN, BC1: CSS formulation containing 0.25% Mg St compressed at 10 kN, CC1: CSS formulation containing 0.25% Mg St compressed at 15 kN, DC1: CSS formulation containing 2% Mg St compressed at 5 kN, EC1: CSS formulation containing 2% Mg St compressed at 10 kN, FC1: CSS formulation containing 2% Mg St compressed at 15 kN, GC1: CSS formulation containing 5% Mg St compressed at 5 kN, HC1: CSS formulation containing 5% Mg St compressed at 10 kN, IC1: CSS formulation containing 5% Mg St compressed at 15 kN. Note: Mg St is magnesium sterate.

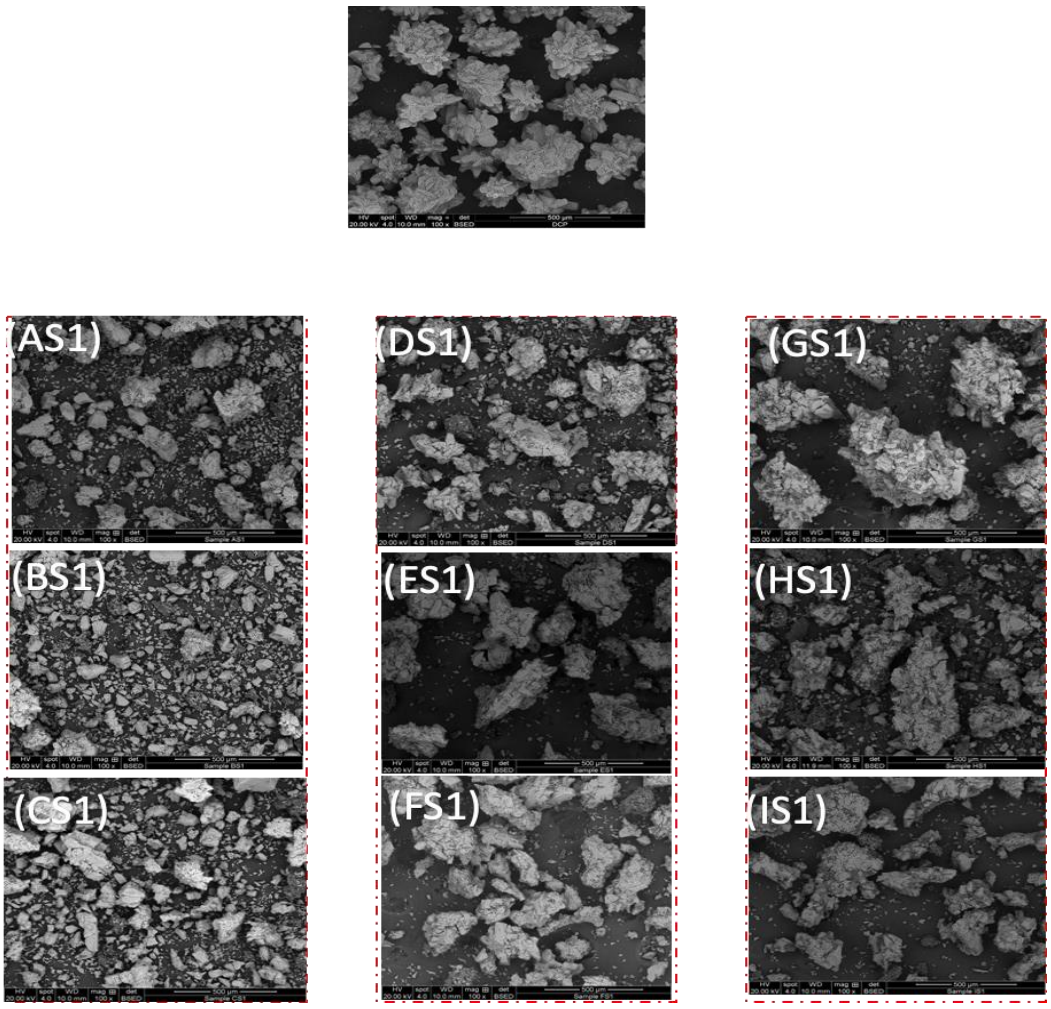

Figure 6.12 SEM pictures of DCP disintegrated particles containing CP formulation; AS1: CP formulation containing 0.25% Mg St compressed at 5 kN, BS1: CP formulation containing 0.25% Mg St compressed at 10 kN, CS1: CP formulation containing 0.25% Mg St compressed at 15 kN, DS1: CP formulation containing 2% Mg St compressed at 5 kN, ES1: CP formulation containing 2% Mg St compressed at 10 kN, FS1: CP formulation containing 2% Mg St compressed at 15 kN, GS1: CP formulation containing 5% Mg St compressed at 5 kN, HS1: CP formulation containing 5% Mg St compressed at 10 kN, IS1: CP formulation containing 5% Mg St compressed at 15 kN. Note: Mg St is magnesium sterate.

6.4.3.2 Particle size analysis

Table 6.4 shows the results of the particle size analysis of disintegrated particles obtained from the SSG containing tablets. It can be observed from this data that the particle size of disintegrated particles increased as the magnesium stearate level increased using the same compression pressure. For example, D[v,0.50] of disintegrated particles obtained from tablet compressed at 5 kN increases from 95.33 µm to 136.54 µm and 198.92 µm when the concentration of magnesium stearate increased from 0.25% to 2% and 5%, respectively. A similar trend was observed with tablets compressed at 10 kN and 15 kN. The effect of compression force on the particle size of disintegrated particles showed a similar trend to this observed with increasing magnesium stearate level. For example, disintegrated particles obtained from tablets containing 0.25% magnesium stearate compressed at 5 kN had a D[v,0.50] of 95.33 µm. While those obtained from tablets made at the same level of magnesium stearate but using 10 kN and 15 kN were 117.74 µm and 131.22 µm, respectively. This can be attributed to the fragmentation behaviour of DCP powders and the formation of solid bridges within the tablet. Increasing the applied pressure resulted in an increase in the fragmentation at the first step (Markl & Zeitler, 2017; Narayan & Hancock, 2005). However, these small particles formed solid bridges as compression increased, which upon water contact resulted in an increase in particle size of the disintegrated particles as pressure increased at the same magnesium stearate concentration. In addition, the addition of magnesium stearate can affect surface roughness as described in section 6.4.4 where increasing magnesium stearate can cause a smoother surface at low compression forces.

Table 6.4 Particle size descriptors of disintegrated particles of tablets containing SSG

Comp Force	Mg st level	D [4, 3] (µm)	D [v,0.10] (µm)	D [v,0.50] (µm)	D [v,0.90] (µm)
5	0.25%	104.25	19.62	95.33	196.82
		5.23	2.73	4.95	7.28
	2.00%	151.74	42.92	136.54	279.87
		4.15	3.27	2.74	4.39
	5.00%	233.24	62.17	198.92	456.49
		13.49	8.56	10.70	5.13
10	0.25%	128.79	22.62	117.74	240.60
		5.71	8.81	12.48	3.38
	2.00%	163.64	34.20	142.88	316.60
		4.99	7.98	11.72	9.39
	5.00%	256.57	55.90	198.58	546.21
		8.76	7.75	4.80	7.92
15	0.25%	151.13	31.90	131.22	291.71
		10.12	11.33	5.70	10.30
	2.00%	204.53	52.44	168.65	409.95
		6.26	8.65	12.45	10.12
	5.00%	260.26	57.90	198.58	569.47
		5.08	2.18	3.93	2.70

Table 6.5 shows the particle size analysis of disintegrated particles for formulations containing CSS as a disintegrant. Results show that at the 5 kN compression force, increasing the Mg St level resulted in an increase in the particle size of disintegrated particles. For example, the D [v,0.50] of disintegrated particles of tablets compressed at 5 kN obtained using 0.25%, 2% and 5% were 63.87 µm, 84.29 µm and 105.34 µm respectively. No increase in D [v,0.50] was observed from tablets compressed at 10 kN when Mg St increased from 0.25% to 2%. However, raising the Mg St level to 5% resulted in nearly doubling the particle size of the disintegrated particles. For those particles that disintegrated at 15 kN, increasing Mg St level from 0.25% to 2% resulted in a slight increase in D [v,0.50] followed by a decrease in D [v,0.50] when Mg St increased to 5% (Table 6.5).

Table 6.5 Particle size descriptors of disintegrated particles of tablets containing CSS

Comp F	Mg st level	D [4, 3] (µm)	D [v,0.10] (µm)	D [v,0.50] (µm)	D [v,0.90] (µm)
5	0.25%	78.65	10.57	63.87	162.86
		7.09	0.66	4.32	6.70
	2.00%	106.11	14.26	84.29	228.90
		8.35	1.24	6.78	10.20
	5.00%	126.34	15.92	105.34	268.05
		5.50	4.26	7.49	4.93
10	0.25%	72.60	10.02	63.25	148.76
		7.17	1.25	6.40	4.14
	2.00%	76.54	10.14	62.80	161.69
		3.82	0.76	3.36	7.23
	5.00%	140.45	24.08	109.33	301.91
		10.35	2.93	9.55	5.30
15	0.25%	113.73	14.54	94.00	242.67
		11.51	2.22	11.53	10.57
	2.00%	158.79	26.15	128.63	335.32
		9.51	1.96	7.02	10.12
	5.00%	139.57	23.60	102.63	308.75
		10.25	1.99	6.24	12.30

Overall, it can be said that there was no clear correlation between compression force, Mg st level and the particle size of disintegrated particles when tablets were made from CSS tablets. This may be attributed to the capillary theory (wicking), which may overcome the effect of compression force and magnesium stearate concentration during disintegration. CSS has been reported in literature to work by two mechanism, mainly swelling and wicking (Gissinger & Stamm, 1980 ; Bi et al., 1999; Desai et al., 2014;). Wicking properties, however, could be responsible for producing similar disintegrated particles in terms of size.

Table 6.6 shows particle size descriptors of disintegrated particles obtained from tablets that contain CP as disintegrant. As it can be seen from the table, an apparent trend was observed between compression force, Mg St level and the particle size of

disintegrated tablets was expressed as D[v,0.50]. Increasing the Mg St level for tablets compressed at the same compression force increased the D[v,0.50] values. For instance, D[v,0.50] increased from 90.99 µm to 127.62 µm and 205.62 µm when the level of Mg St increased from 0.25% to 2% and 5% respectively. A similar trend was observed for the tablets compressed using the same level but different compression force. For example, the D[v,0.50] of disintegrated particles obtained using 0.25% of magnesium stearate compressed at 10 kN and 15 kN were 95.89 µm and 119.40 µm. These similar findings to the ones observed with SSG suggest that both disintegrants work in the same way previously described above.

Table 6.6 Particle size descriptors of disintegrated particles of tablets containing CP

Comp f (KN)	Mg st level	D [4, 3] (µm)	D [v,0.10] (µm)	D [v,0.50] (µm)	D [v,0.90] (µm)
5	0.25%	107.95	16.13	90.99	225.69
		3.39	1.06	3.97	4.60
5	2.00%	143.37	22.09	127.62	287.99
		7.09	1.87	7.38	11.55
5	5.00%	219.34	38.43	205.62	415.62
		10.00	5.07	9.46	9.79
10	0.25%	111.56	17.47	95.89	229.05
		9.87	2.61	10.66	9.76
10	2.00%	166.27	29.11	153.25	319.63
		10.03	4.10	12.92	12.75
10	5.00%	248.50	45.16	233.13	470.30
		12.40	6.27	11.27	10.25
15	0.25%	133.23	25.13	119.40	259.20
		7.56	6.60	9.45	10.12
15	2.00%	181.64	38.09	166.71	343.86
		12.32	8.15	7.55	6.66
15	5.00%	306.22	60.62	279.42	582.04
		10.02	10.55	5.55	5.76

6.4.4 Surface roughness analysis of tablets

Tablet surface analysis was conducted on the SSG containing tablets before previous to performing the disintegration experiments. Figure 6.13 shows the surface topography of these tablets, whilst Figure 6.14 shows the correlation between Sq values obtained at different compression forces and the surface roughness value (Sq). As shown from the two figures, increasing the level of Mg St resulted in a steep decrease in the surface roughness (a decrease in Sq value) for tablets compressed at 5 kN and 10 kN. However, for those tablets compressed at 15 KN, no decrease was observed as Mg St concentration increased. A similar trend was observed with tablets containing CSS (Figure 6.15 and 6.16). An increase in Mg St concentration showed a decrease in surface roughness value expressed by a decrease in Sq value for tablets

compressed at 5 and 10 kN. However, no significant increase in surface roughness value was observed at those compressed at high compression force. CP containing tablets compressed at 5 kN (Figure 6.17 and 6.18) showed a similar trend to both CSS and SSG containing tablets, with a decrease in Sq values as Mg St increased. However, a less significant decrease in Sq value was observed in CP tablets compressed at 10 and 15 kN. It is worth mentioning that in all tablets studied, increasing the compression pressure resulted in a decrease in Sq value at the same level of Mg St concentration (Figures 6.14, 6.16, and 6.18).

Previous studies show that tablet surface roughness correlates with material properties with brittle materials producing a smooth surface due to the fragmentation within the tablet (Narayan & Hancock, 2003). This correlates with the findings in this study where increasing the compression pressure resulted in a smoother surface due to fragmentation. However, in this study, it was proved that the amount of magnesium stearate added to the formulation played a significant role in affecting the surface profiles of tablets, mostly when tablets compressed at low compression forces. This also could have an implication on how disintegration occurred and could explain some aspect of disintegration behaviour observed in section 6.4.3.2.

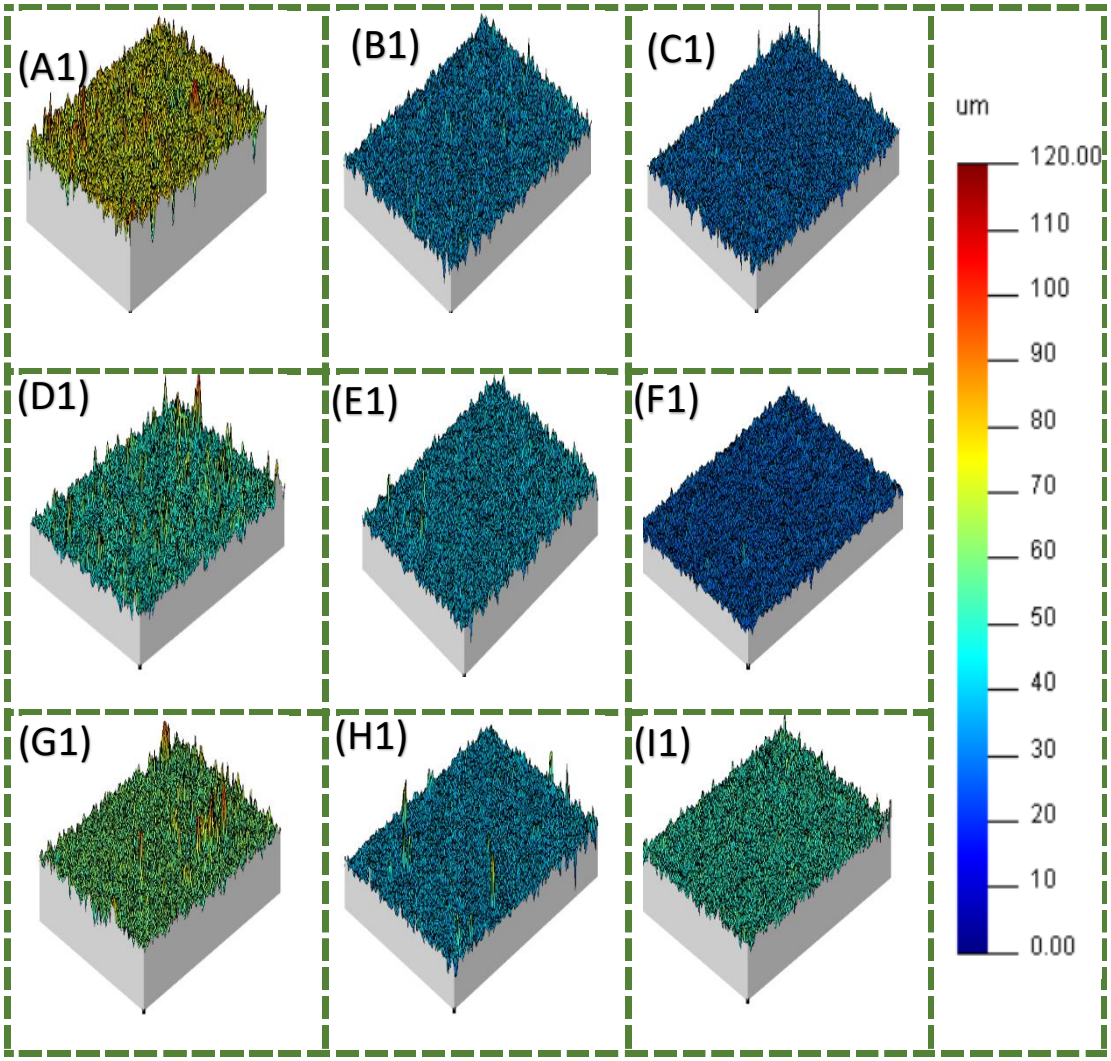

Figure 6.13 Tablet surface analysis diagrams of tablets containing SSG; A1: SSG tablets containing 0.25% Mg St compressed at 5 kN, B1: SSG tablets containing 0.25% Mg St compressed at 10 kN, C1: SSG tablets containing 0.25% Mg St compressed at 15 kN, D1: SSG tablets containing 2% Mg St compressed at 5 kN, E1: SSG tablets containing 2% Mg St compressed at 10 kN, F1: SSG tablets containing 2% Mg St compressed at 15 kN, G1: SSG tablets containing 5% Mg St compressed at 5 kN, H1: SSG tablets containing 5% Mg St compressed at 10 kN, I1: SSG tablets containing 5% Mg St compressed at 15 kN

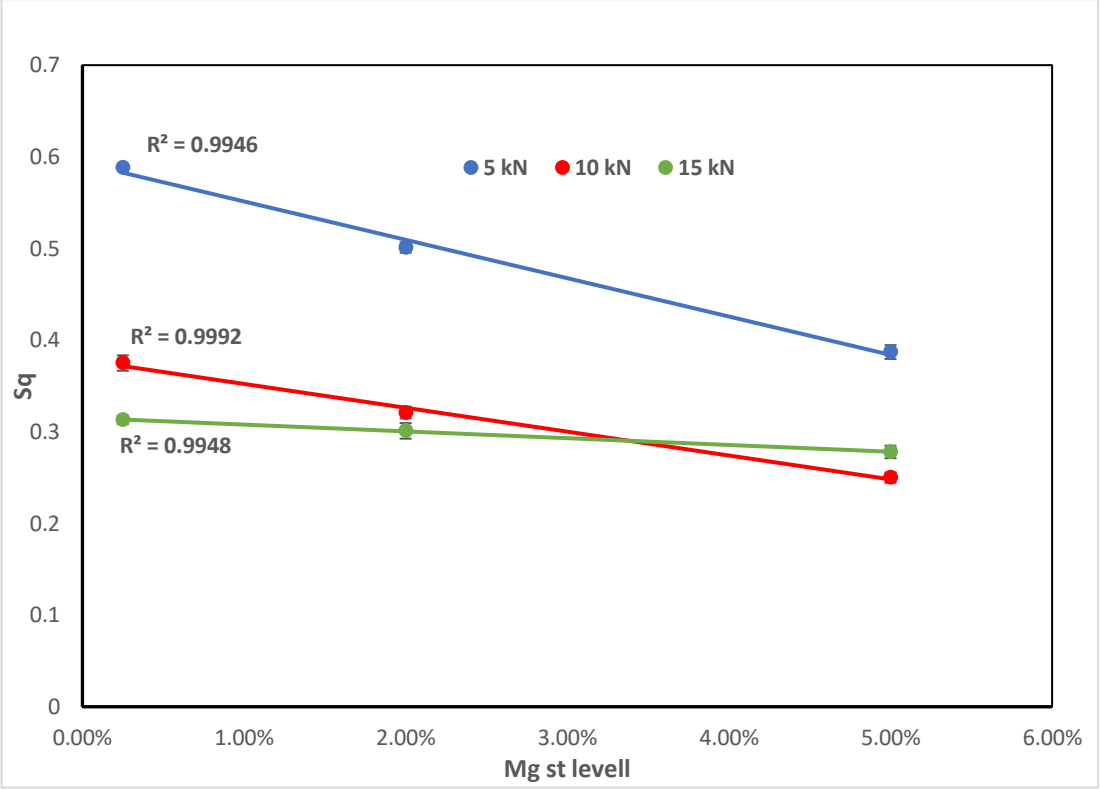

Figure 6.14 Correlation between Sq values for SSG containing tablets and Mg St concentration for different tablets obtained at different compression pressure

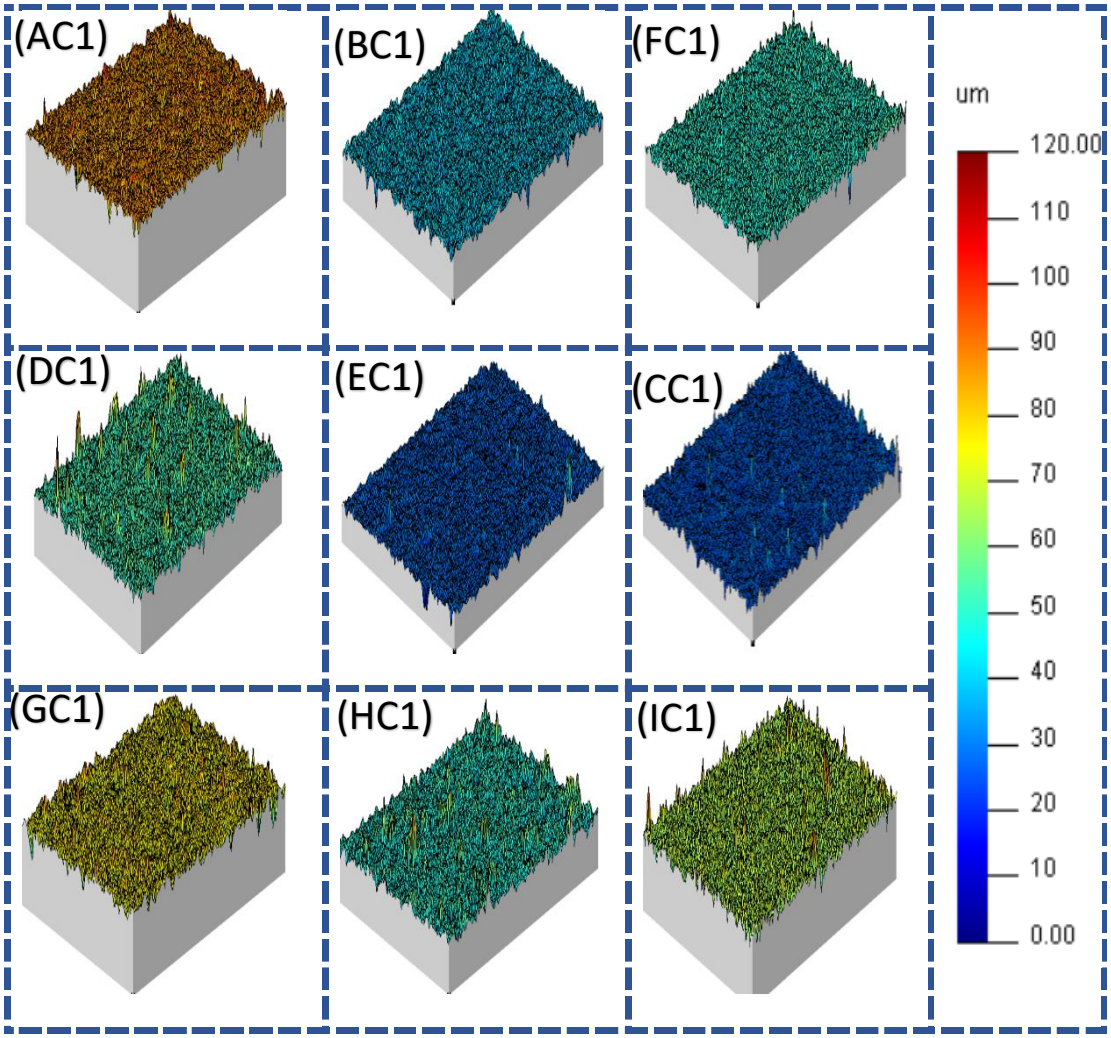

Figure 6.15 Tablet surface analysis diagrams of tablets containing CSS; AC1: CSS tablets containing 0.25% Mg St compressed at 5 kN, BC1: CSS tablets containing 0.25% Mg St compressed at 10 kN, CC1: CSS tablets containing 0.25% Mg St compressed at 15 kN, DC1: CSS tablets containing 2% Mg St compressed at 5 kN, EC1: CSS tablets containing 2% Mg St compressed at 10 kN, FC1: CSS tablets containing 2% Mg St compressed at 15 kN, GC1: CSS tablets containing 5% Mg St compressed at 5 kN, HC1: CSS tablets containing 5% Mg St compressed at 10 kN, IC1: CSS tablets containing 5% Mg St compressed at 15 kN

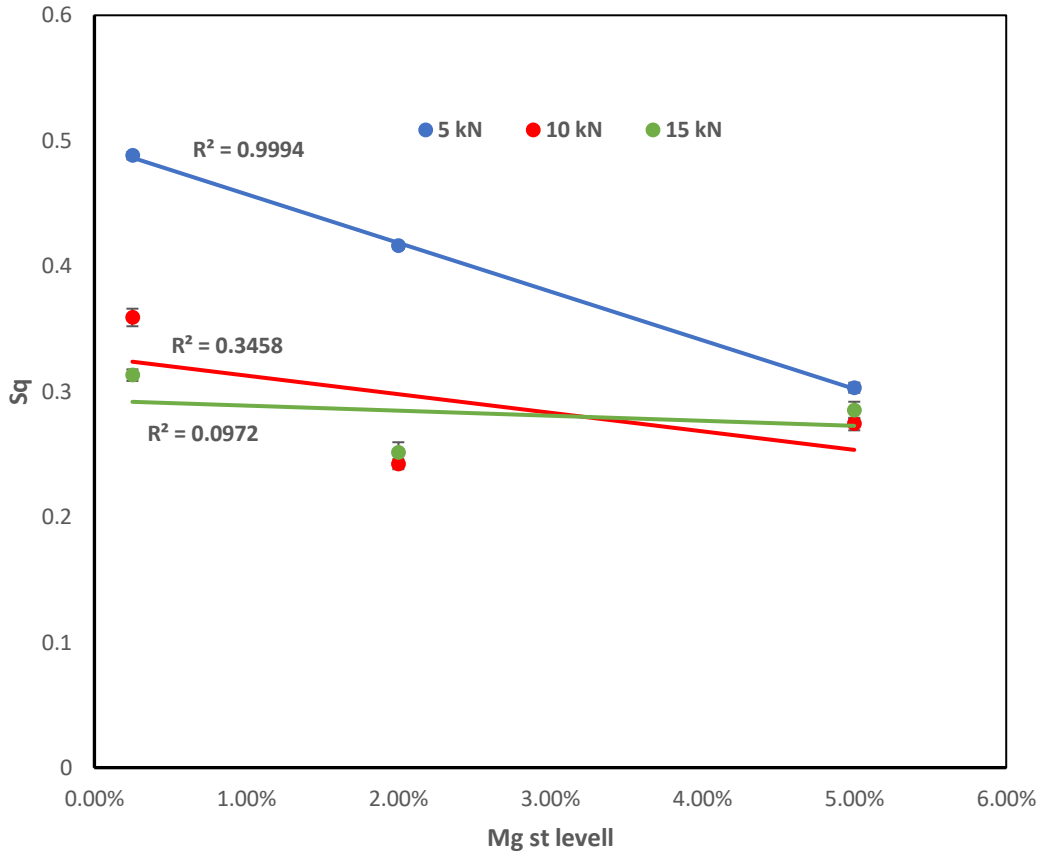

Figure 6.16 Correlation between Sq values for CSS containing tablets and Mg St concentration for different tablets obtained at different compression pressure

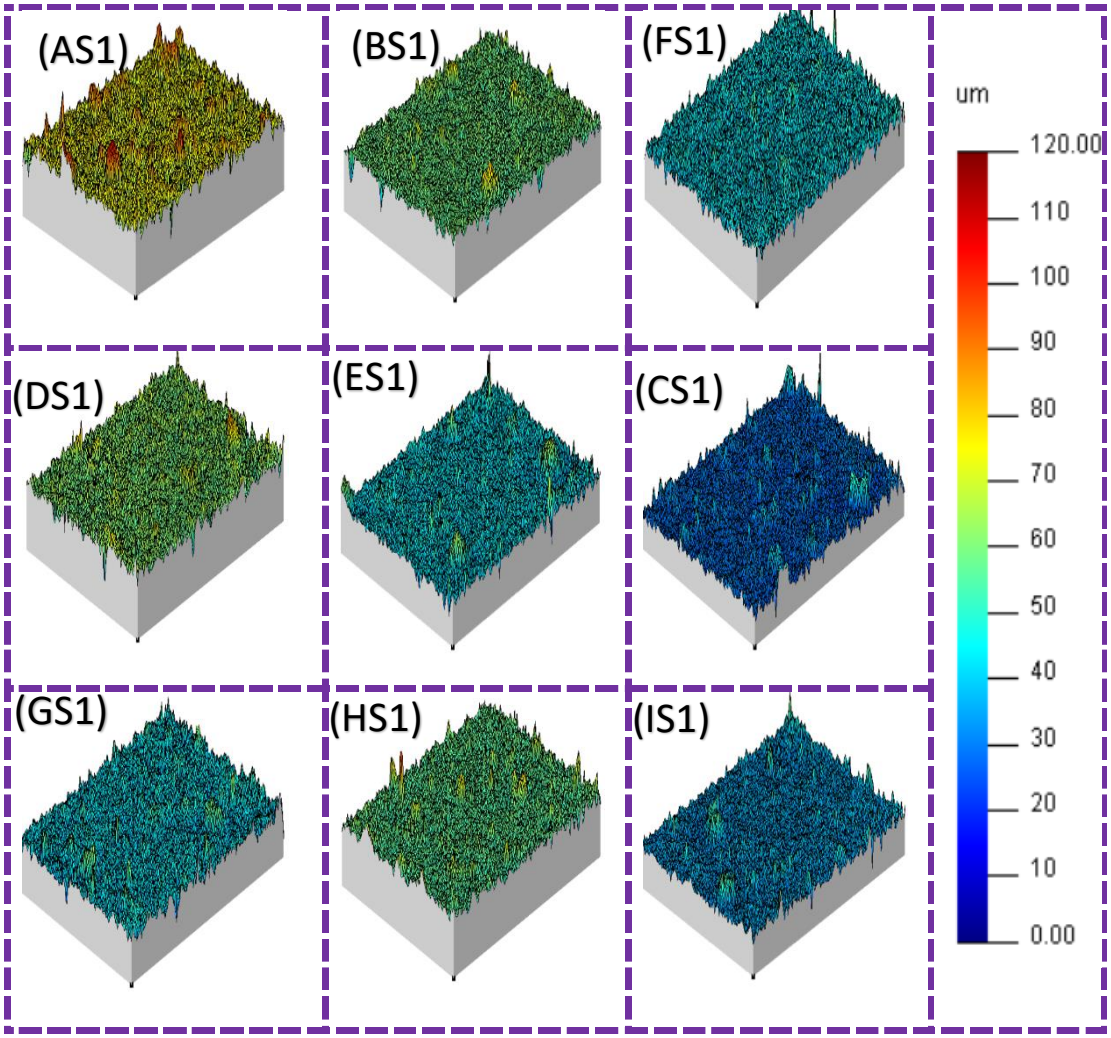

Figure 6.17 Tablet surface analysis diagrams of tablets containing CP; AS1: CP tablets containing 0.25% Mg St compressed at 5 kN, BS1: CP tablets containing 0.25% Mg St compressed at 10 kN, CS1: CP tablets containing 0.25% Mg St compressed at 15 kN, DS1: CP tablets containing 2% Mg St compressed at 5 kN, ES1: CP tablets containing 2% Mg St compressed at 10 kN, FS1: CP tablets containing 2% Mg St compressed at 15 kN, GS1: CP tablets containing 5% Mg St compressed at 5 kN, HS1: CP tablets containing 5% Mg St compressed at 10 kN, IS1: CP tablets containing 5% Mg St compressed at 15 kN

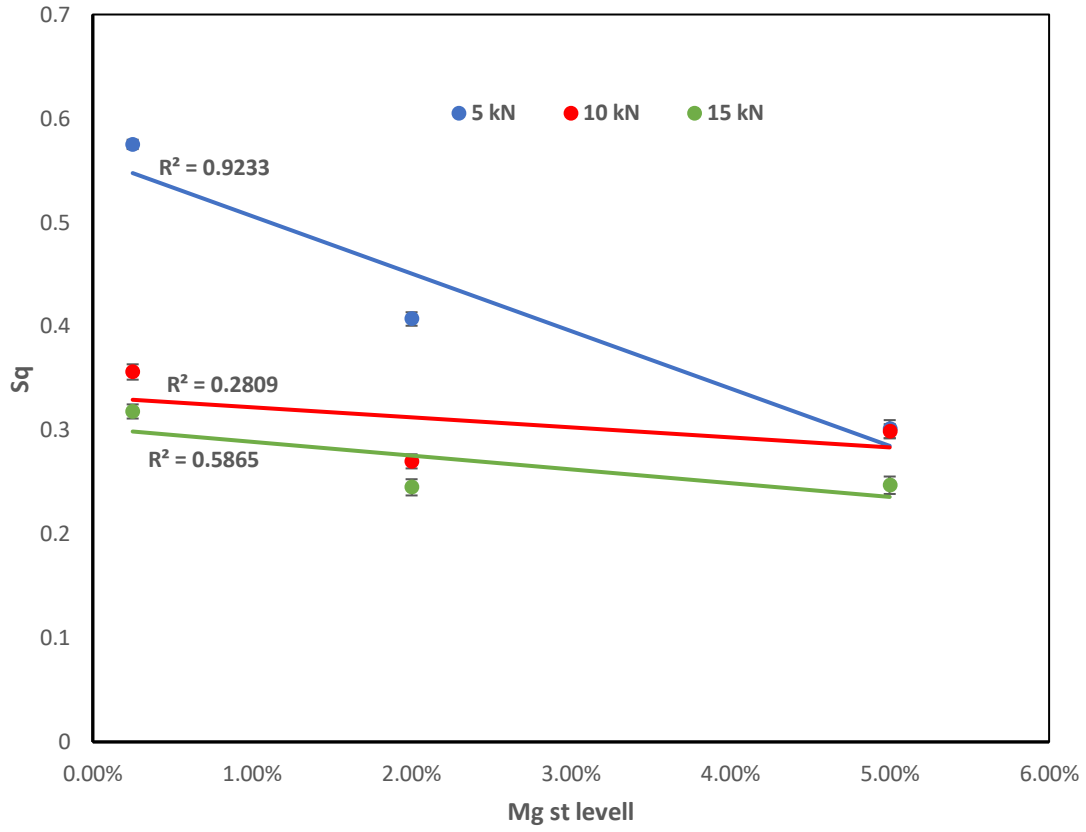

Figure 6.18 Correlation between Sq values for povidone containing tablets and Mg St concentration for different tablets obtained at different compression pressure

6.6 Conclusions

In this chapter, the SDI2 was coupled with an inline particle size analyser to investigate the disintegration phenomena of DCP tablets in more detail. DCP was chosen because of its insoluble nature and it not swelling upon disintegration. The relationship between the level of lubricant, compression force and the surface topography of the resulted tablets was also investigated. Results showed that depending on the disintegrant type used, magnesium stearate concentration, and the applied pressure, the particle size of resulted disintegrated particles may differ. It was found that for both SSG and CP containing tablets, increasing magnesium stearate and compression pressure increased the particle size of disintegrated particles. This can be attributed to; surface roughness, disintegration mechanism, the amount of pressure applied and the deformation mechanism to make tablets. In terms of mechanical properties, this study revealed no significant changes in the plastic work, elastic work and the deformability of tablets studied. This contributes to the fact that the results from the disintegration study can be attributed mainly to the three factors mentioned above

Chapter 7 - The use of a novel modelling techniques to predict powder flow of pharmaceutical materials based on particle size and shape descriptors

Note to reader: Aspects of this chapter has been published under the title “A predictive integrated framework based on the radial basis function for the modelling of the flow of pharmaceutical powders” in the International Journal of Pharmaceutics. https://doi.org/10.1016/j.ijpharm.2019.118542

7.1 Introduction

In this chapter, particulate properties of pharmaceutical powders will be utilised to predict their performance in terms of flow using novel modelling techniques. Figure 7.1 gives a graphical summary about this chapter where data generated from size and shape analysis of 33 pharmaceutical powders and the corresponding blends were used were used as input parameters to predict the flow performance of pharmaceutical powders. The data used in this chapter were generated in chapter 4 and further used in this chapter to build the flow model.

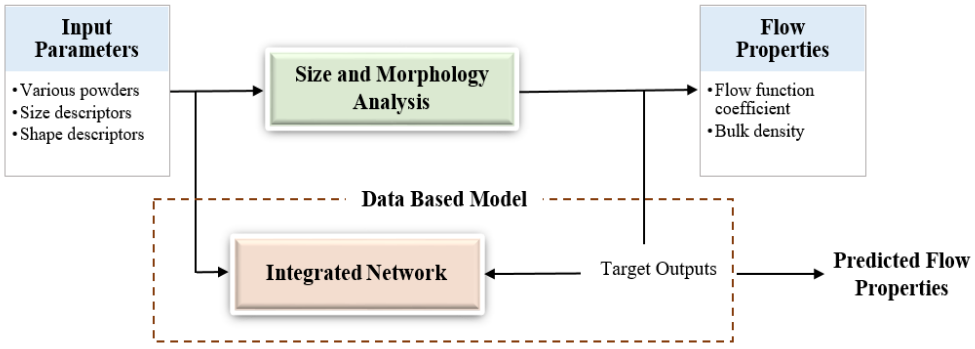

Figure 7.1 Graphical abstract of modelling technique used

Modelling and predicting the powder flow properties of a material are essential in many pharmaceutical, chemical and agricultural applications. As modelling techniques are one of the main aspects of this thesis, it was prudent to discuss the modelling paradigms in more details as in section 1.1.4.

7.2 Aims and objectives

In this chapter, the ultimate aim was to develop a fast, cost effective and more accurate predictive model to represent the powder flow properties of various pharmaceutical powders and blends from single component data. This model can guide formulators to select excipients and their blend concentration that optimises the powder flowability. Two modelling paradigms based on artificial intelligence (AI) namely, a radial basis function (RBF) and an integrated network were employed to model the flowability represented by the flow function coefficient (FFC) and the bulk density (RHOB). Both approaches were utilized to map the input parameters (i.e., particle size, shape descriptors and material type) to the flow properties. The input parameters of the blends were determined from the particle size, shape and material type properties of the single components.

7.3 Materials and methods

The materials studied in this chapter are listed in chapter 4 section 4.3.1. Powder blends at various ratios (3:1, 1:1, 1:3) were also prepared and used according to the method in section 4.3.1. The same batch coding used in section 4.3.1 was used in this chapter. Particle size and morphology analysis was conducted as described in section 4.3.2.1. A Ring shear tester (RST-XS, Dietmar Schulze, Wolfenbuttel, Germany) was utilized to characterise the flow of the powders as described in section 4.3.2.4.

The flowability models were trained and validated on 86 samples including single components and binary mixtures. RBF was implemented first as it is introduced in

section 1.1.4.2.2 and then integrated neural network was investigated as it is previously described in section 1.1.4.2.3.

7.4 Results and discussions

7.4.1 Micrometric and flow properties

The micrometric properties and flow data of the three powder materials (lactose, MCC and DCP) used in this research study are discussed extensively and presented in section 4.4. Correlation coefficient of the particle size and shape descriptors can be found in Table 71. For instance, the relationship between the D_{50} and the FFC of these excipients is stronger than the relationship between the D_{50} and the RHOB. In addition, the relationship between the D_{90} and the FFC is a strong direct relationship (i.e. the correlation coefficient is positive), whereas the relationship between the D_{90} and the RHOB is a weak inverse one (i.e. the correlation coefficient is negative). The analysis of variance showed that the various materials have significant effects on the flow properties, where the p-values were less than 0.05.

Table 7.1 The correlation coefficients between size/shape descriptors and the flow properties

Particle characteristics		Flow properties	
		FFC	RHOB (kg/m^3)
Size descriptors	D_{10}	0.65	-0.01
	D_{50}	0.73	-0.05
	D_{90}	0.59	-0.17
	$D_{4,3}$	0.67	-0.11
Shape descriptors	S_{10}	0.61	0.06
	S_{50}	0.54	0.03

It was also interesting to note that of the true densities determined, the DCP samples had the highest values ranging from 2.38 – 2.92 kg/m^3 whereas the MCC and lactose grades had values ranging from 1.40 – 1.97 kg/m^3 and 1.54 – 1.68 kg/m^3 respectively. More discussion on true densities values can be found in section 4.4.9.

7.4.2 Radial basis function network

An RBF model was employed to model and predict the flowability of the various pharmaceutical powders investigated. The experimental data were randomly classified into two sets: training set (60), which allows the RBF model to learn the input/output relationships, and testing set (26), by which the generalization capabilities of the developed RBF model are tested. In addition to the various powders and the different powder blends used, particle size represented by its descriptors (i.e. D_{10}, D_{50}, D_{90} and $D_{4,3}$) and particle shape represented by its sphericity descriptors (i.e. S_{10} and S_{50}) were considered as input variables, whereas the powder flow represented by the FFC and RHOB was considered as an output. The number of basis functions selected was the one that corresponded to the minimum RMSE values for both training and testing sets. For the FFC, Figure 7.2 shows the RBF performance for both the training and the testing data sets using 6 basis functions, with a RMSE (training, testing) = [2.90, 5.16].

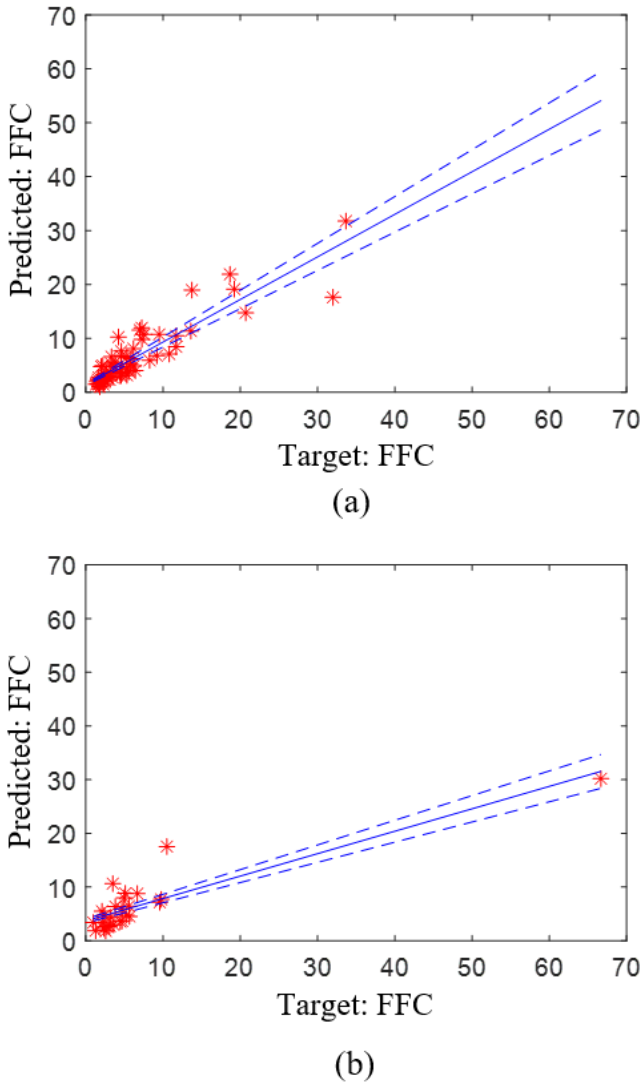

Figure 7.2 The RBF network for the FFC (RBF-FFC1 in Table 7.3): (a) Training, (b) Testing (with 10% bands)

The testing RMSE value is approximately twice the training RMSE value, which, at first glance, could be attributed to an over-training problem. However, it was noted that one of the FFC values in the testing set was larger than 60, whereas, in the training set, most of the values are less than 30, thus, an error residual of 5 is actually less than 10 % of the target value. The coefficient of determination (R^2) values for the training and testing sets are 0.80 and 0.79, respectively. The close R^2 values are evidence that the over-training problem was not the case in this work. In a similar manner, an RBF

model was developed for the RHOB. The performance measures presented by the R^2 (training, testing) and RMSE (training, testing) values are [0.78, 0.77] and [112, 151], respectively, as summarized in Table 7.3. The results obtained indicate that the RBF network cannot represent and accurately predict the flow properties. This can be attributed to the limited number of data points (i.e., powder samples) and to the so-called "curse of dimensionality", which refers to the phenomenon that occurs when one deals with spaces of high dimensionality comprising of many input variables.

Table 7.2 Input and output parameters, coefficient of determination (R2) and root mean squared error for the RBF and integrated networks (INs). x_"full" is defined in Eq. 1.4.

	Input	Output	Number of RBFs	R^2	RMSE
RBF-FFC1	$x = x_{Full}$	FFC	I = 6	[0.80, 0.79]	[2.90, 5.16]
RBF-RHOB1	$x = x_{Full}$	RHOB	I = 6	[0.78, 0.77]	[112, 151]
RBF-FFC2	$x = [D_{50}\ \ D_{4,3}\ \ S_{50}]$	FFC	I = 7	[0.84, 0.85]	[2.12, 4.72]
RBF-RHOB2	$x = [D_{50}\ \ D_{4,3}\ \ S_{50}]$	RHOB	I = 9	[0.82, 0.83]	[109, 142]
IN-FFC	$x = x_{Full}$	FFC	M = 10, K^*= [3, 9]	[0.92, 0.93]	[1.41, 1.92]
IN-RHOB	$x = x_{Full}$	RHOB	M = 10, K^*= [3, 14]	[0.91, 0.90]	[75, 93]

* The number of the basis functions of the RBF models defined in the first stage of the integrated network is in the range provided.

The predictive performance of the RBF model can, thus, be improved by reducing the dimensionality of the process (i.e. reducing the number of input variables). Therefore, an RBF model was developed using the materials and their mixtures, D_{50}, $D_{4,3}$ and S_{50}.

The model performance values for the FFC and the RHOB are R^2 (training, testing) = [0.84, 0.85] and R^2 (training, testing) = [0.82, 0.83], respectively. The RMSE values for the FFC and the RHOB are [2.12, 4.72] and [109, 142], respectively, as listed in Table 7.3. These performance measures indicate that the RBF model developed using less inputs is superior to that of the RBF network developed using all the inputs, with an overall improvement of 7 %. Although, such a model satisfactorily modelled the flow of the investigated powders, reducing the number of inputs may affect the generalization capabilities of the model. All the size descriptors should be included in the model, in order to take into account a multimodal or wide size distribution. Therefore, an integrated network is presented to capture the relationships between all the size and shape descriptors and the flow properties.

7.4.3 Integrated network

In order to implement the integrated network, ten RBF networks, with different number of basis functions and different connecting coefficient values, and a single RBF one in the first and second phases, respectively, were developed (Table 7.3). For each model in the first phase, the data was randomly classified into two sets: training set (60) and testing set (26). For each flow property, the network parameters are listed in Table 7.3. It is worth emphasising at this stage that the number of data points (i.e., powder samples) in training and testing data sets were the same for all RBF networks but their distributions in the space under investigation were different. For this reason, these models can play a complementary role in representing the possible patterns by considering the different areas in the space under investigation.

The integrated network performance measures for the FFC were R^2 (training, testing) = [0.92, 0.93] and RMSE (training, testing) = [1.41, 1.92], as shown in Figure 7.3, while the performance measures for the RHOB were R^2 (training, testing) = [0.91, 0.90] and RMSE (training, testing) = [75, 93], as shown in Figure 7.4. The output predictions in Figures 7.3 and 7.4 elucidate a satisfactory performance, where it was noticeable that most of the predicted values fitted properly within the 90 % confidence interval. In addition, the prediction performance of the integrated network was superior to that of the single RBF network presented, with overall improvements of approximately 16 % and 19 % in R^2 for the FFC and RHOB, respectively. These results prove the ability of the integrated network in handling the difficulties of modelling the powders flowability and in dealing with the limited number of data points, this being due to the dense function represented by the superposition and composition functions presented in Eq. 1.4.

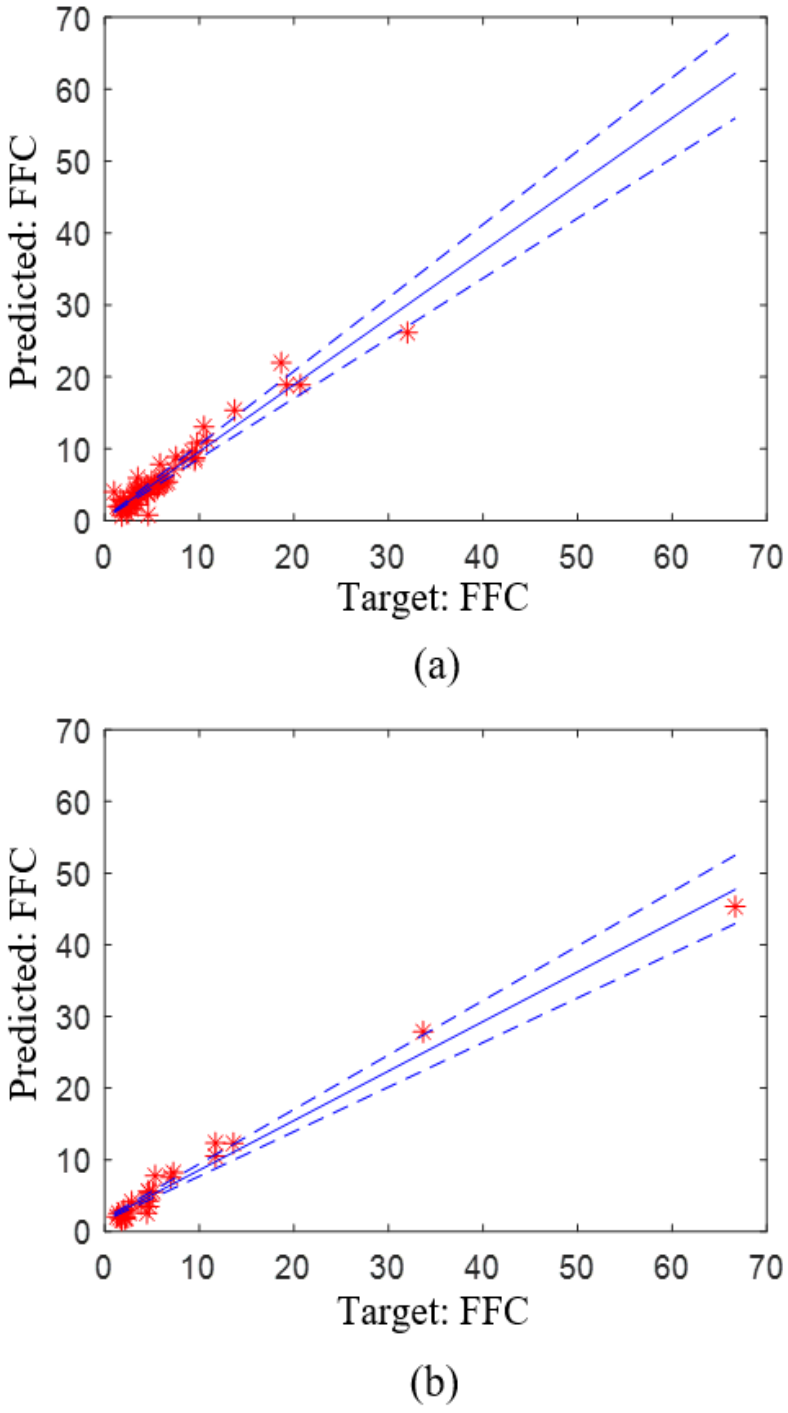

Figure 7.3 The integrated network based on 10 RBF networks for the FFC (IN-FFC in Table 3): (a) Training, (b) Testing (with 10% bands)

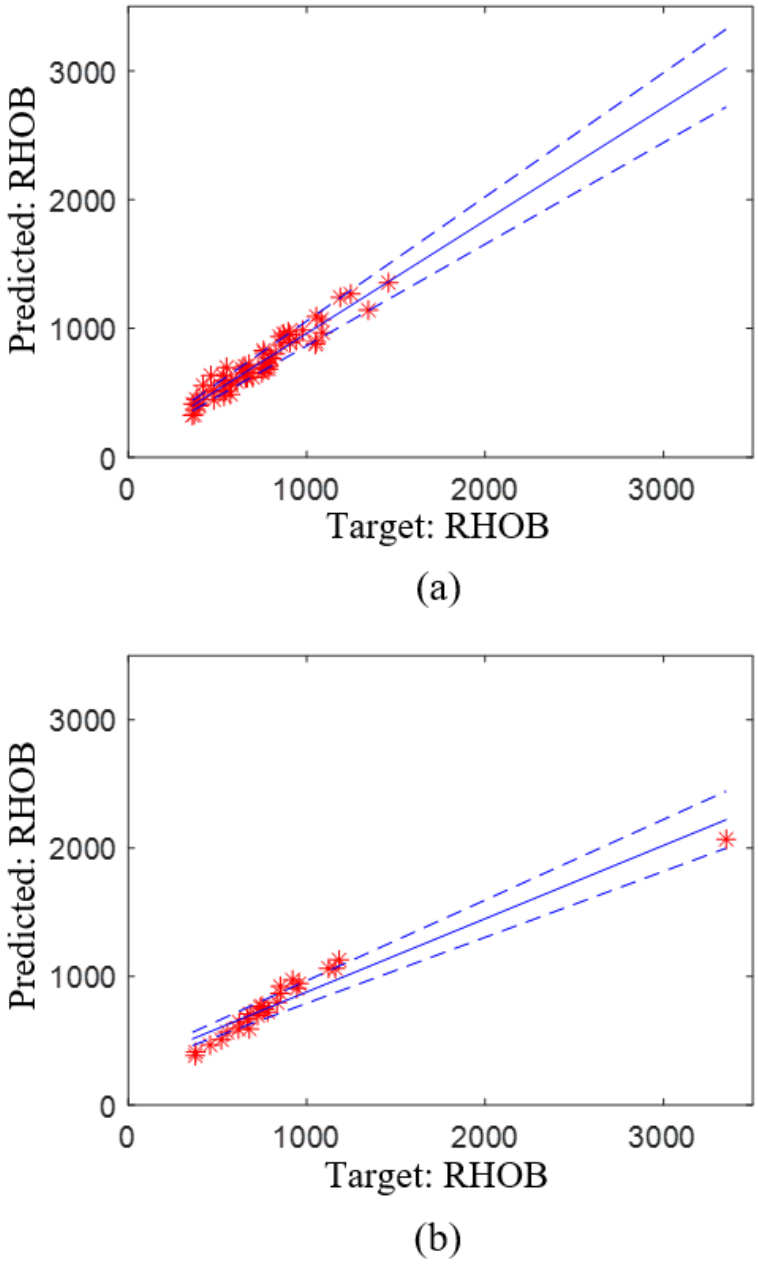

Figure 7.4 The integrated network based on 10 RBF networks for the RHOB (IN-RHOB in Table 7.3): (a) Training, (b) Testing (with 10% bands)

7.5 Conclusions

Modelling and predicting the flow properties of powder materials are essential in many industries, in particular the pharmaceutical industry, this being due to the fact that powder flow behaviour can affect the manufacturing efficiency and determine the final product quality. In this research work, data-driven models were developed to predict the flow properties of various commonly used pharmaceutical powders and their blends. Firstly, a radial basis function (RBF) network was utilized to map the size (i.e. D_{10}, D_{50}, D_{90} and $D_{4,3}$) and shape (i.e. S_{10} and S_{50}) descriptors to the flow properties represented by the flow function coefficient (FFC) and the bulk density (RHOB). The simple RBF network, however, was not able to capture the highly nonlinear input/output relationships and the high dimensionality of the flowability. An integrated network was thus implemented to model the flow properties. In such a structure, the output was predicted by training and modelling the acquired data in two consecutive stages. The integrated network was successfully able to (i) capture the relationships between the particle size and shape and the flow properties, (ii) deal with the high dimensionality of the space under investigation, and (iii) predict the flow properties accurately. Furthermore, the integrated network thus outperformed the single RBF network in terms of the predictive performance and the generalization capabilities. Such a model has the ability to guide formulators in selecting excipients and their blend concentrations that can improve the flowability of a powder blend. Employing such a model can therefore reduce time and material waste. There is however a need to improve the interpretability of the input/output relationships, which can be achieved by incorporating fuzzy logic systems in the modelling structure.

Chapter 8 - Concluding remarks and future work

This thesis provides an in-depth review of the use of the material science tetrahedron concept in pharmaceutical formulation development using novel experimental and modelling techniques. This thesis highlights how formulation properties affect the performance of pharmaceutical formulations using pharmaceutical a range of novel characterisation techniques These techniques included X-ray tomography, dynamic image analysis, dynamic contact angle measurement, SDI imaging and an on-line particle size analyser. It was interesting to note that the dynamic contact angle using biorelevant dissolution testing was able to correlate with dissolution performance. The video images provided by the SDI2 instrument allowed the visualisation of the disintegration process for croscarmellose (CSS), crospovidone(CP) and sodium starch glycolate (SSG) in an insoluble excipient. The wicking process experienced by croscarmellose correlated well with the particle size of disintegrating tablets.

This thesis also highlights the importance of controlling particle properties such as particle size and shape in the performance of pharmaceutical powders. It also provides insights into how these properties can be used to predict the performance of pharmaceutical powders. Predicting the performance of pharmaceutical powders is of great importance, especially in the early stages of pharmaceutical development, where a limited amount of sample is available. This enables development scientists to choose the right powders in terms of shape and size in the early stages of the development process and, therefore, save time and cost. This investigation was conducted by investing time in establishing the correlation between particle properties to two fundamental performance properties of pharmaceutical powders. The first one was the flow which is one of the critical performance properties that affects the pharmaceutical product attributes such as content uniformity and weight uniformity. The second was

mechanical properties which affect the tablet hardness, disintegration, dissolution and packaging. The investigation found that depending on the shape of the particles used during tablet manufacturing, the mechanical properties of tablets will change. Spherical grades tend to have a more porous tablet, while non-spherical grades showed denser and stronger tablets due to mechanical interlocking examined by X-ray tomography. This thesis also examined how interactions with a lubricant such as magnesium stearate can affect the performance of both the flow and mechanical properties of pharmaceutical powders. These results from this study showed that magnesium stearate level would have a direct consequence on solid fraction levels and, therefore, the compactibility and compressibility profiles. The use of focus variation also showed a decrease in the Sq values to be associated with an increase in the magnesium stearate concentration. This was an observation that suggested that smoother surfaces were observed when increasing magnesium stearate concentration. An understanding of these interactions, especially during the tabletting process, allows for care and considerations to be taken to guide pharmaceutical scientists to troubleshoot any formulation issues.

There are many future directions that this research could take. One of the directions would be recrystallisation of APIs with different material properties and exploring how these APIs with different particle properties will perform in terms of flow and mechanical properties. The ability to produce APIs with a very controlled shape would be of great importance. That will enable the understanding of particle properties especially shape effect on the performance, on flow and mechanical properties. This will result in improving modelling activities and therefore building a more accurate

flow model. These models will, in turn, inform both materials and formulation scientists in their decision in choosing materials with the right particle properties for further development. Another direction that this research could investigate is particle shape characterisation using particles produced with a defined size and shape, such as those made using the 3D printing technology. This could help greatly with modelling.

A final part of this development could be designing a more quantitative disintegration tester that could reflect how formulation and particle properties could affect the disintegration behaviour and enable the understanding of the disintegration mechanism in more detail. The surface dissolution imaging technique may well be a way in furthering the understanding of the disintegration mechanism in more detail.

In conclusion, this thesis provides the reader with an appreciation and understanding of how particle and formulation properties can affect pharmaceutical powder performance. It also utilises a range of novel techniques that can open doors to a novel field of study that can benefit research and development and can be used in the early stage of development, manufacture, scale-up and quality control within the pharmaceutical industry.

Chapter 9 - References

1. Abdelbary, G., Eouani, C., Prinderre, P., Joachim, J., Reynier, J., & Piccerelle, P. (2005). Determination of the in vitro disintegration profile of rapidly disintegrating tablets and correlation with oral disintegration. *International Journal of Pharmaceutics*, *292*(1–2), 29–41. https://doi.org/10.1016/j.ijpharm.2004.08.019

2. Aburub, A., Mishra, D., & Buckner, I. (2007). Use of compaction energetics for understanding particle deformation mechanism. *Pharmaceutical Development and Technology*, *12*(4), 405–414. https://doi.org/10.1080/10837450701366952

3. Adebisi, A. O., Kaialy, W., Hussain, T., Al-Hamidi, H., Nokhodchi, A., Conway, B. R., & Asare-Addo, K. (2016). Solid-state, triboelectrostatic and dissolution characteristics of spray-dried piroxicam-glucosamine solid dispersions. *Colloids and Surfaces B: Biointerfaces*, *146*, 841–851. https://doi.org/10.1016/J.COLSURFB.2016.07.032

4. Adeleye, O. A., Femi-Oyewo, M. N., & Odeniyi, M. A. (2015). Effect of compression pressure on mechanical and release properties of tramadol matrix tablets. *Current Issues in Pharmacy and Medical Sciences*, *28*(2), 120–125. https://doi.org/10.1515/cipms-2015-0057

5. Adolfsson, Å., Olsson, H., & Nyström, C. (1997). Effect of particle size and compaction load on interparticulate bonding structure for some pharmaceutical materials studied by compaction and strength characterisation in butanol. *European Journal of Pharmaceutics and Biopharmaceutics*, *44*(3), 243–251. https://doi.org/10.1016/S0939-6411(97)00136-7

6. Al-Chalabi, S. A. M., Jones, A. R., & Luckham, P. F. (1990). A simple method for improving the dispersability of micron-sized solid spheres. *Journal of Aerosol Science*, *21*(6), 821–826. https://doi.org/10.1016/0021-8502(90)90047-2

7. Al-Hamidi, H., Asare-Addo, K., Desai, S., Kitson, M., & Nokhodchi, A. (2015). The dissolution and solid-state behaviours of coground ibuprofen–glucosamine HCl. *Drug Development and Industrial Pharmacy*, *41*(10), 1682–1692. https://doi.org/10.3109/03639045.2014.991401

8. Al-Hamidi, H., Edwards, A. A., Douroumis, D., Asare-Addo, K., Nayebi, A. M., Reyhani-Rad, S., … Nokhodchi, A. (2013). Effect of glucosamine HCl on dissolution and solid state behaviours of piroxicam upon milling. *Colloids and Surfaces B: Biointerfaces*, *103*, 189–199. https://doi.org/10.1016/J.COLSURFB.2012.10.023

9. Al-Hamidi, H., Edwards, A. A., Mohammad, M. A., & Nokhodchi, A. (2010a).

Glucosamine HCl as a new carrier for improved dissolution behaviour: Effect of grinding. *Colloids and Surfaces B: Biointerfaces*, *81*(1), 96–109. https://doi.org/10.1016/J.COLSURFB.2010.06.028

10. Al-Hamidi, H., Edwards, A. A., Mohammad, M. A., & Nokhodchi, A. (2010b). To enhance dissolution rate of poorly water-soluble drugs: Glucosamine hydrochloride as a potential carrier in solid dispersion formulations. *Colloids and Surfaces B: Biointerfaces*, *76*(1), 170–178. https://doi.org/10.1016/J.COLSURFB.2009.10.030

11. AlAlaween, W. H., Khorsheed, B., Mahfouf, M., Gabbott, I., Reynolds, G. K., & Salman, A. D. (2018). Transparent predictive modelling of the twin screw granulation process using a compensated interval type-2 fuzzy system. *European Journal of Pharmaceutics and Biopharmaceutics*, *124*, 138–146. https://doi.org/10.1016/J.EJPB.2017.12.015

12. AlAlaween, W. H., Mahfouf, M., & Salman, A. D. (2017). Integrating the physics with data analytics for the hybrid modeling of the granulation process. *AIChE Journal*, *63*(11), 4761–4773. https://doi.org/10.1002/aic.15831

13. Alghunaim, A., Kirdponpattara, S., & Newby, B. Z. (2016). Techniques for determining contact angle and wettability of powders. *Powder Technology*, *287*, 201–215. https://doi.org/https://doi.org/10.1016/j.powtec.2015.10.002

14. Asare-Addo, K., Alshafiee, M., Walton, K., Ward, A., Totea, A.-M., Taheri, S., … Conway, B. R. (2019). Effect of preparation method on the surface properties and UV imaging of indomethacin solid dispersions. *European Journal of Pharmaceutics and Biopharmaceutics*, *137*. https://doi.org/10.1016/j.ejpb.2019.03.002

15. Asare-Addo, Kofi, Šupuk, E., Al-Hamidi, H., Owusu-Ware, S., Nokhodchi, A., & Conway, B. R. (2015). Triboelectrification and dissolution property enhancements of solid dispersions. *International Journal of Pharmaceutics*, *485*(1–2), 306–316. https://doi.org/10.1016/J.IJPHARM.2015.03.013

16. Augsburger, L. L., & Hoag, S. W. (2016). *Pharmaceutical dosage forms-tablets*. CRC press.

17. Aulton, M. E., & Taylor, K. (2013). *Aulton's pharmaceutics : the design and manufacture of medicines*. Churchill Livingstone/Elsevier.

18. Baxter, J., Abou-Chakra, H., Tüzün, U., & Mills Lamptey, B. (2000). A dem simulation and experimental strategy for solving fine powder flow problems. *Chemical Engineering Research and Design*, *78*(7), 1019–1025. https://doi.org/10.1205/026387600528139

19. Beck, R., & Andreassen, J.-P. (2012). The influence of crystallization conditions on the onset of dendritic growth of calcium carbonate. *Crystal Research and Technology*, *47*(4), 404–408. https://doi.org/10.1002/crat.201100599

20. Beer, P., Wilson, D., Huang, Z., & De Matas, M. (2014). Transfer from high-shear batch to continuous twin screw wet granulation: A case study in understanding the relationship between process parameters and product quality attributes. *Journal of Pharmaceutical Sciences*, *103*(10), 3075–3082. https://doi.org/10.1002/jps.24078

21. Bennett, F. S., Carter, P. A., Rowley, G., & Dandiker, Y. (1999). Modification of electrostatic charge on inhaled carrier lactose particles by addition of fine particles. *Drug Development and Industrial Pharmacy*, *25*(1), 99–103. https://doi.org/10.1081/DDC-100102148

22. Berry, J., Kline, L. C., Sherwood, J. K., Chaudhry, S., Obenauer-Kutner, L., Hart, J. L., & Sequeira, J. (2004). Influence of the size of micronized active pharmaceutical ingredient on the aerodynamic particle size and stability of a metered dose inhaler. *Drug Development and Industrial Pharmacy*, *30*(7), 705–714. https://doi.org/10.1081/DDC-120039213

23. Betageri, G. V., & Makarla, K. R. (1995). Enhancement of dissolution of glyburide by solid dispersion and lyophilization techniques. *International Journal of Pharmaceutics*, *126*(1–2), 155–160. https://doi.org/10.1016/0378-5173(95)04114-1

24. Bi, Y. X., Sunada, H., Yonezawa, Y., & Danjo, K. (1999). Evaluation of rapidly disintegrating tablets prepared by a direct compression method. *Drug Development and Industrial Pharmacy*, *25*(5), 571–581. https://doi.org/10.1081/DDC-100102211

25. Bishop, C. M., & M., C. (1995). *Neural networks for pattern recognition*. Clarendon Press. Retrieved from https://dl.acm.org/citation.cfm?id=525960

26. Blanchard, J., Coleman, J., Hayling, C. D. A., Ghaderi, R., Haeberlin, B., Hart, J., … Wolff, R. (2004, December 1). Foreign particles testing in orally inhaled and nasal drug products. *Pharmaceutical Research*. Springer. https://doi.org/10.1007/s11095-004-7665-7

27. Boiret, M., Gorretta, N., Ginot, Y. M., & Roger, J. M. (2016). An iterative approach for compound detection in an unknown pharmaceutical drug product: Application on Raman microscopy. *Journal of Pharmaceutical and Biomedical Analysis*, *120*, 342–351. https://doi.org/10.1016/j.jpba.2015.12.038

28. Boldyrev, V. V., Shakhtshneider, T. P., Burleva, L. P., & Severtsev, V. A. (1994). Preparation of the disperse systems of sulfathiazole-polyvinylpyhrolidone by mechanical activation. *Drug Development and Industrial Pharmacy*, *20*(6), 1103–1114. https://doi.org/10.3109/03639049409038355

29. Bonakdar, T., & Ghadiri, M. (2018). Analysis of pin milling of pharmaceutical materials. *International Journal of Pharmaceutics*, *552*(1–2), 394–400. https://doi.org/10.1016/j.ijpharm.2018.09.068

30. Bourcier, D., Féraud, J. P., Colson, D., Mandrick, K., Ode, D., Brackx, E., & Puel, F. (2016). Influence of particle size and shape properties on cake resistance and compressibility during pressure filtration. *Chemical Engineering Science*, *144*, 176–187. https://doi.org/10.1016/j.ces.2016.01.023

31. Cabiscol, R., Shi, H., Wünsch, I., Magnanimo, V., Finke, J. H., Luding, S., & Kwade, A. (2020). Effect of particle size on powder compaction and tablet strength using limestone. *Advanced Powder Technology*. https://doi.org/10.1016/j.apt.2019.12.033

32. Calcium hydrogen phosphate | CaHPO4 - PubChem. (n.d.). Retrieved March 9, 2021, from https://pubchem.ncbi.nlm.nih.gov/compound/Calcium-hydrogen-phosphate#section=Other-Experimental-Properties

33. Cao, X., Leyva, N., Anderson, S. R., & Hancock, B. C. (2008). Use of prediction methods to estimate true density of active pharmaceutical ingredients. *International Journal of Pharmaceutics*, *355*(1–2), 231–237. https://doi.org/10.1016/j.ijpharm.2007.12.012

34. Caraballo, I., Millan, M., & Rabasco, A. M. (1996). Relationship between drug percolation threshold and particle size in matrix tablets. *Pharmaceutical Research*, *13*(3), 387–390. https://doi.org/10.1023/A:1016088424993

35. Catellani, P. L., Predella, P., Bellotti, A., & Colombo, P. (1989). Tablet water uptake and disintegration force measurements. *International Journal of Pharmaceutics*, *51*(1), 63–66. https://doi.org/10.1016/0378-5173(89)90075-6

36. Chattoraj, S., & Sun, C. C. (2018). Crystal and Particle Engineering Strategies for Improving Powder Compression and Flow Properties to Enable Continuous Tablet Manufacturing by Direct Compression. *Journal of Pharmaceutical Sciences*, *107*(4), 968–974. https://doi.org/10.1016/J.XPHS.2017.11.023

37. Chew, J. W., Chow, P. S., & Tan, R. B. H. (2007). Automated in-line technique using FBRM to achieve consistent product quality in cooling crystallization. *Crystal Growth and Design*, *7*(8), 1416–1422.

https://doi.org/10.1021/cg060822t

38. Chowhan, Z. T., & Linn, E. E. (1979). Mixing of pharmaceutical solids. I. Effect of particle size on mixing in cylindrical shear and V-shaped tumbling mixers. *Powder Technology*, *24*(2), 237–244. https://doi.org/10.1016/0032-5910(79)87041-2

39. Chu, K. R., Lee, E., Jeong, S. H., & Park, E. S. (2012). Effect of particle size on the dissolution behaviors of poorly water-soluble drugs. *Archives of Pharmacal Research*, *35*(7), 1187–1195. https://doi.org/10.1007/s12272-012-0709-3

40. Cirri, M., Maestrelli, F., Furlanetto, S., & Mura, P. (2004). Solid-state characterization of glyburide-cyclodextrin co-ground products. *Journal of Thermal Analysis and Calorimetry*, *77*(2), 413–422. https://doi.org/10.1023/B:JTAN.0000038982.40315.8f

41. Colburn, M., Johnson, S. C., Stewart, M. D., Damle, S., Bailey, T. C., Choi, B., … Willson, C. G. (1999). Step and flash imprint lithography: a new approach to high-resolution patterning. In Y. Vladimirsky (Ed.), *Emerging Lithographic Technologies III* (Vol. 3676, p. 379). SPIE. https://doi.org/10.1117/12.351155

42. Colombo, P., Caramella, C., Conte, U., Manna, A. La, Guyot-Hermann, A. M., & Ringard, J. (1981). Disintegrating force and tablet properties. *Drug Development and Industrial Pharmacy*, *7*(2), 135–153. https://doi.org/10.3109/03639048109057707

43. Council, N. R. (2000). *Materials science and engineering: Forging stronger links to users* (Vol. 492). National Academies Press.

44. Craig, D. Q. M., & Reading, M. (2006). *Thermal analysis of pharmaceuticals*. CRC press.

45. Curley, L., Hinton, J., Marjoribanks, C., Mirjalili, A., Kennedy, J., & Svirskis, D. (2017). Magnetic Resonance Imaging to Visualize Disintegration of Oral Formulations. *Journal of Pharmaceutical Sciences*, *106*(3), 745–750. https://doi.org/10.1016/j.xphs.2016.11.009

46. Dabbagh, M. A., Ford, J. L., Rubinstein, M. H., & Hogan, J. E. (1996). Effects of polymer particle size, compaction pressure and hydrophilic polymers on drug release from matrices containing ethylcellulose. *International Journal of Pharmaceutics*, *140*(1), 85–95. https://doi.org/10.1016/0378-5173(96)04599-1

47. DANJO, K., KINOSHITA, K., KITAGAWA, K., IIDA, K., SUNADA, H., & OTSUKA, A. (1989). Effect of particle shape on the compaction and flow properties of powders. *CHEMICAL & PHARMACEUTICAL BULLETIN*, *37*(11), 3070–3073. https://doi.org/10.1248/cpb.37.3070

48. Dansereau, R., & Peck, G. E. (1987). The effect of the variability in the physical and chemical properties of magnesium stearate on the properties of compressed tablets. *Drug Development and Industrial Pharmacy*, *13*(6), 975–999. https://doi.org/10.3109/03639048709068365

49. De Boer, A. H., Bolhuis, G. K., & Lerk, C. F. (1978). Bonding characteristics by scanning electron microscopy of powders mixed with magnesium stearate. *Powder Technology*, *20*(1), 75–82. https://doi.org/10.1016/0032-5910(78)80011-4

50. De, S., & Robinson, D. H. (2004). Particle size and temperature effect on the physical stability of PLGA nanospheres and microspheres containing bodipy. *AAPS PharmSciTech*, *5*(4), 18–24. https://doi.org/10.1208/pt050453

51. de Vegt, O., Vromans, H., den Toonder, J., & van der Voort Maarschalk, K. (2009). Influence of flaws and crystal properties on particle fracture in a jet mill. *Powder Technology*, *191*(1–2), 72–77. https://doi.org/10.1016/j.powtec.2008.09.014

52. Desai, P. M., Er, P. X. H., Liew, C. V., & Heng, P. W. S. (2014). Functionality of disintegrants and their mixtures in enabling fast disintegration of tablets by a quality by design approach. *AAPS PharmSciTech*, *15*(5), 1093–1104. https://doi.org/10.1208/s12249-014-0137-4

53. Djuris, J., Nikolakakis, I., Ibric, S., Djuric, Z., & Kachrimanis, K. (2013). Preparation of carbamazepine–Soluplus® solid dispersions by hot-melt extrusion, and prediction of drug–polymer miscibility by thermodynamic model fitting. *European Journal of Pharmaceutics and Biopharmaceutics*, *84*(1), 228–237. https://doi.org/10.1016/J.EJPB.2012.12.018

54. Donauer, N., & Löbenberg, R. (2007). A mini review of scientific and pharmacopeial requirements for the disintegration test. *International Journal of Pharmaceutics*, *345*(1–2), 2–8.

55. Doshi, N., Zahr, A. S., Bhaskar, S., Lahann, J., & Mitragotri, S. (2009). Red blood cell-mimicking synthetic biomaterial particles. *Proceedings of the National Academy of Sciences of the United States of America*, *106*(51), 21495–21499. https://doi.org/10.1073/pnas.0907127106

56. Duda, R. O., Hart, P. E. (Peter E., & Stork, D. G. (2001). *Pattern classification*.

Wiley. Retrieved from https://www.wiley.com/en-gb/Pattern+Classification%2C+2nd+Edition-p-9780471056690

57. Durbin, S. D., & Feher, G. (1990). Studies of crystal growth mechanisms of proteins by electron microscopy. *Journal of Molecular Biology*, *212*(4), 763–774. https://doi.org/10.1016/0022-2836(90)90235-E

58. Egusa, K., Okazaki, F., Schiewe, J., Werthmann, U., & Wolkenhauer, M. (2017). Identification of Polymorphic Forms of Active Pharmaceutical Ingredient in Low-Concentration Dry Powder Formulations by Synchrotron X-Ray Powder Diffraction. *Drugs in R and D*, *17*(3), 413–418. https://doi.org/10.1007/s40268-017-0196-6

59. Eshel, G., Levy, G. J., Mingelgrin, U., & Singer, M. J. (2004). Critical Evaluation of the Use of Laser Diffraction for Particle-Size Distribution Analysis. *Soil Science Society of America Journal*, *68*(3), 736–743. https://doi.org/10.2136/sssaj2004.7360

60. Fahr, A., & Liu, X. (2007). Drug delivery strategies for poorly water-soluble drugs. *Expert Opinion on Drug Delivery*, *4*(4), 403–416. https://doi.org/10.1517/17425247.4.4.403

61. FDA. (2004). *PAT — A Framework for Innovative Pharmaceutical Development, Manufacturing, and Quality Assurance | FDA*. Retrieved from https://www.fda.gov/regulatory-information/search-fda-guidance-documents/pat-framework-innovative-pharmaceutical-development-manufacturing-and-quality-assurance

62. Felton, L. A., & McGinity, J. W. (1999). Influence of pigment concentration and particle size on adhesion of an acrylic resin copolymer to tablet compacts. *Drug Development and Industrial Pharmacy*, *25*(5), 597–604. https://doi.org/10.1081/DDC-100102214

63. Ferreira, A. P., & Tobyn, M. (2015, August 1). Multivariate analysis in the pharmaceutical industry: Enabling process understanding and improvement in the PAT and QbD era. *Pharmaceutical Development and Technology*. Taylor and Francis Ltd. https://doi.org/10.3109/10837450.2014.898656

64. Finholt, P. (1974). Influence of formulation on dissolution rate. *Dissolution Technology*.

65. Fonner, D. E., Banker, G. S., & Swarbrick, J. (1966). Micromeritics of Granular Pharmaceutical Solids I. *Journal of Pharmaceutical Sciences*, *55*(2), 181–186. https://doi.org/10.1002/jps.2600550211

66. Fraige, F. Y., Langston, P. A., & Chen, G. Z. (2008). Distinct element modelling of cubic particle packing and flow. *Powder Technology*, *186*(3), 224–240. https://doi.org/10.1016/J.POWTEC.2007.12.009

67. Fu, X., Huck, D., Makein, L., Armstrong, B., Willen, U., & Freeman, T. (2012). Effect of particle shape and size on flow properties of lactose powders. *Particuology*, *10*(2), 203–208. https://doi.org/10.1016/J.PARTIC.2011.11.003

68. Gaisford, S., & Saunders, M. (2013). *Essentials of pharmaceutical preformulation*. Wiley-Blackwell. Retrieved from https://www.wiley.com/en-gb/Essentials+of+Pharmaceutical+Preformulation-p-9780470976364

69. Gamble, J. F., Dennis, A. B., Hutchins, P., Jones, J. W., Musembi, P., & Tobyn, M. (2017). Determination of process variables affecting drug particle attrition withinmulti-component blends during powder feed transmission. *Pharmaceutical Development and Technology*, *22*(7), 904–909. https://doi.org/10.1080/10837450.2016.1200616

70. Gamble, J. F., Tobyn, M., & Hamey, R. (2015, September 5). Application of image-based particle size and shape characterization systems in the development of small molecule pharmaceuticals. *Journal of Pharmaceutical Sciences*. John Wiley and Sons Inc. https://doi.org/10.1002/jps.24382

71. Garekani, H. A., Ford, J. L., Rubinstein, M. H., & Rajabi-Siahboomi, A. R. (2001). Effect of compression force, compression speed, and particle size on the compression properties of paracetamol. *Drug Development and Industrial Pharmacy*, *27*(9), 935–942. https://doi.org/10.1081/DDC-100107674

72. Garg, V., Mallick, S. S., Garcia-Trinanes, P., & Berry, R. J. (2018). An investigation into the flowability of fine powders used in pharmaceutical industries. *Powder Technology*, *336*, 375–382. https://doi.org/10.1016/J.POWTEC.2018.06.014

73. Gedeon, C., Kapur, B., Aleksa, K., & Koren, G. (2008). A simple and rapid HPLC method for the detection of glyburide in plasma original research communication (analytical). *Clinical Biochemistry*, *41*(3), 167–173. https://doi.org/10.1016/J.CLINBIOCHEM.2007.07.025

74. Geng, Y., Dalhaimer, P., Cai, S., Tsai, R., Tewari, M., Minko, T., & Discher, D. E. (2007). Shape effects of filaments versus spherical particles in flow and drug delivery. *Nature Nanotechnology*, *2*(4), 249–255. https://doi.org/10.1038/nnano.2007.70

75. Gissinger, D., & Stamm, A. (1980). A comparative evaluation of the properties of some tablet disintegrants. *Drug Development and Industrial Pharmacy*,

6(5), 511–536. https://doi.org/10.3109/03639048009068720

76. Glangchai, L. C., Caldorera-Moore, M., Shi, L., & Roy, K. (2008). Nanoimprint lithography based fabrication of shape-specific, enzymatically-triggered smart nanoparticles. *Journal of Controlled Release*, *125*(3), 263–272. https://doi.org/10.1016/j.jconrel.2007.10.021

77. Goh, H. P., Heng, P. W. S., & Liew, C. V. (2018). Comparative evaluation of powder flow parameters with reference to particle size and shape. *International Journal of Pharmaceutics*, *547*(1–2), 133–141. https://doi.org/10.1016/j.ijpharm.2018.05.059

78. Gong, X., Chang, S. Y., Osei-Yeboah, F., Paul, S., Perumalla, S. R., Shi, L., … Sun, C. C. (2015). Dependence of tablet brittleness on tensile strength and porosity. *International Journal of Pharmaceutics*, *493*(1–2), 208–213. https://doi.org/10.1016/j.ijpharm.2015.07.050

79. González-Rodríguez, M. L., Pérez-Martínez, J. I., Merino, S., Fini, A., & Rabasco, A. M. (2001). Channeling agent and drug release from a central core matrix tablet. *Drug Development and Industrial Pharmacy*, *27*(5), 439–446. https://doi.org/10.1081/DDC-100104319

80. Gratton, S. E. A., Pohlhaus, P. D., Lee, J., Guo, J., Cho, M. J., & DeSimone, J. M. (2007). Nanofabricated particles for engineered drug therapies: A preliminary biodistribution study of PRINT™ nanoparticles. *Journal of Controlled Release*, *121*(1–2), 10–18. https://doi.org/10.1016/j.jconrel.2007.05.027

81. Gratton, S. E. A., Ropp, P. A., Pohlhaus, P. D., Luft, J. C., Madden, V. J., Napier, M. E., & DeSimone, J. M. (2008). The effect of particle design on cellular internalization pathways. *Proceedings of the National Academy of Sciences of the United States of America*, *105*(33), 11613–11618. https://doi.org/10.1073/pnas.0801763105

82. Guillory, J. K. (2003). Handbook of Pharmaceutical Salts: Properties, Selection, and Use Edited by P. Heinrich Stahl and Camile G. Wermuth. VHCA, Verlag Helvetica Chimica Acta, Zürich, Switzerland, and Wiley-VCH, Weinheim, Germany. 2002. vix + 374 pp. 17.5 × 24.5 cm. ISBN 3-906390-26-8. $130.00. https://doi.org/10.1021/JM030019N

83. Guo, M., Fu, Q., Wu, C., Guo, Z., Li, M., Sun, J., … Yang, L. (2015). Rod shaped nanocrystals exhibit superior in vitro dissolution and in vivo bioavailability over spherical like nanocrystals: A case study of lovastatin. *Colloids and Surfaces B: Biointerfaces*, *128*, 410–418. https://doi.org/10.1016/j.colsurfb.2015.02.039

84. H. WOLD. (1966). Estimation of principal components and related models by iterative least squares. Retrieved January 12, 2021, from https://www.scienceopen.com/document?vid=d2270c89-22fd-4226-8080-5bc4aed0ee1a

85. Hamad, M. L., Bowman, K., Smith, N., Sheng, X., & Morris, K. R. (2010). Multi-scale pharmaceutical process understanding: From particle to powder to dosage form. *Chemical Engineering Science*, *65*(21), 5625–5638. https://doi.org/10.1016/j.ces.2010.01.037

86. Han, X., Ghoroi, C., To, D., Chen, Y., & Davé, R. (2011). Simultaneous micronization and surface modification for improvement of flow and dissolution of drug particles. *International Journal of Pharmaceutics*, *415*(1–2), 185–195. https://doi.org/10.1016/j.ijpharm.2011.05.070

87. Hancock, B. C., Colvin, J. T., Mullarney, M. P., & Zinchuk, A. V. (2003). *The Relative Densities of Pharmaceutical Powders, Blends, Dry Granulations, and Immediate-Release Tablets*. Retrieved from www.pharmtech.com

88. Hancock, B. C., & Mullarney, M. P. (2005). X-ray microtomography of solid dosage forms. *Pharm Technol*, *29*(44), 92–100.

89. Hassanpour, A., Hare, C., & Pasha, M. (2019). *Powder Flow*. The Royal Society of Chemistry. https://doi.org/10.1039/9781788016100

90. Haware, R. V., Shivagari, R., Johnson, P. R., Staton, S., Stagner, W. C., & Gupta, M. R. (2014). Application of multivariate methods to evaluate the functionality of bovine- and vegetable-derived magnesium stearate. *Journal of Pharmaceutical Sciences*, *103*(5), 1466–1477. https://doi.org/10.1002/jps.23920

91. He, X., Secreast, P. J., & Amidon, G. E. (2007). Mechanistic Study of the Effect of Roller Compaction and Lubricant on Tablet Mechanical Strength. *Journal of Pharmaceutical Sciences*, *96*(5), 1342–1355. https://doi.org/10.1002/jps.20938

92. He, Y., Li, Y. Y., Evans, T. J., Yu, A. B., & Yang, R. Y. (2019). Effects of particle characteristics and consolidation pressure on the compaction of non-spherical particles. *Minerals Engineering*, *137*, 241–249. https://doi.org/10.1016/j.mineng.2019.04.007

93. He, Yan, Ho, C., Yang, D., Chen, J., & Orton, E. (2017). Measurement and Accurate Interpretation of the Solubility of Pharmaceutical Salts. *Journal of Pharmaceutical Sciences*, *106*(5), 1190–1196. https://doi.org/10.1016/J.XPHS.2017.01.023

94. Heng, P. W. S., Chan, L. W., Easterbrook, M. G., & Li, X. (2001). Investigation of the influence of mean HPMC particle size and number of polymer particles on the release of aspirin from swellable hydrophilic matrix tablets. *Journal of Controlled Release*, *76*(1–2), 39–49. https://doi.org/10.1016/S0168-3659(01)00410-2

95. Herting, M. G., & Kleinebudde, P. (2007). Roll compaction/dry granulation: Effect of raw material particle size on granule and tablet properties. *International Journal of Pharmaceutics*, *338*(1–2), 110–118. https://doi.org/10.1016/j.ijpharm.2007.01.035

96. Herting, M. G., Klose, K., & Kleinebudde, P. (2007). Comparison of Different Dry Binders for Roll Compaction/Dry Granulation. *Pharmaceutical Development and Technology*, *12*(5), 525–532. https://doi.org/10.1080/10837450701557303

97. Hiestand, E. N. (1997). Mechanical properties of compacts and particles that control-tableting success. *Journal of Pharmaceutical Sciences*, *86*(9), 985–990. https://doi.org/10.1021/js9701061

98. Hintz, R. J., & Johnson, K. C. (1989). The effect of particle size distribution on dissolution rate and oral absorption. *International Journal of Pharmaceutics*, *51*(1), 9–17. https://doi.org/10.1016/0378-5173(89)90069-0

99. Ho, C. C., Keller, A., Odell, J. A., & Ottewill, R. H. (1993). Preparation of monodisperse ellipsoidal polystyrene particles. *Colloid & Polymer Science*, *271*(5), 469–479. https://doi.org/10.1007/BF00657391

100. Ho, R., Naderi, M., Heng, J. Y. Y., Williams, D. R., Thielmann, F., Bouza, P., … Burnett, D. J. (2012). Effect of milling on particle shape and surface energy heterogeneity of needle-Shaped crystals. *Pharmaceutical Research*, *29*(10), 2806–2816. https://doi.org/10.1007/s11095-012-0842-1

101. Hooper, D., Clarke, F. C., Docherty, R., Mitchell, J. ., & Snowden, M. J. (2017). Effects of crystal habit on the sticking propensity of ibuprofen—A case study. *International Journal of Pharmaceutics*, *531*(1), 266–275. https://doi.org/10.1016/J.IJPHARM.2017.08.091

102. Hou, H., & Sun, C. C. (2008). Quantifying Effects of Particulate Properties on Powder Flow Properties Using a Ring Shear Tester. *Journal of Pharmaceutical Sciences*, *97*(9), 4030–4039. https://doi.org/10.1002/jps.21288

103. Huang, J., Goolcharran, C., & Ghosh, K. (2011). A Quality by Design approach to investigate tablet dissolution shift upon accelerated stability by multivariate methods. *European Journal of Pharmaceutics and*

Biopharmaceutics, *78*(1), 141–150. https://doi.org/10.1016/j.ejpb.2010.12.012

104. Huang, J., Kaul, G., Cai, C., Chatlapalli, R., Hernandez-Abad, P., Ghosh, K., & Nagi, A. (2009). Quality by design case study: An integrated multivariate approach to drug product and process development. *International Journal of Pharmaceutics*, *382*(1–2), 23–32. https://doi.org/10.1016/j.ijpharm.2009.07.031

105. Huang, Z., Scicolone, J. V., Gurumuthy, L., & Davé, R. N. (2015). Flow and bulk density enhancements of pharmaceutical powders using a conical screen mill: A continuous dry coating device. *Chemical Engineering Science*, *125*, 209–224. https://doi.org/10.1016/j.ces.2014.05.038

106. Ibrahim, T. H., Burk, T. R., Etzler, F. M., & Neuman, R. D. (2000). Direct adhesion measurements of pharmaceutical particles to gelatin capsule surfaces. *Journal of Adhesion Science and Technology*, *14*(10), 1225–1242. https://doi.org/10.1163/156856100742177

107. International Organization for standarisation. (2012). *Geometrical product specifications (GPS) — Surface texture: Areal — Part 2: Terms, definitions and surface texture parameters*. ISO.

108. Islam, N., Stewart, P., Larson, I., & Hartley, P. (2004). Effect of carrier size on the dispersion of salmeterol xinafoate from interactive mixtures. *Journal of Pharmaceutical Sciences*, *93*(4), 1030–1038. https://doi.org/10.1002/jps.10583

109. Ivanisevic, I., McClurg, R. B., & Schields, P. J. (2010). Uses of X-Ray Powder Diffraction In the Pharmaceutical Industry. In *Pharmaceutical Sciences Encyclopedia* (pp. 1–42). Hoboken, NJ, USA: John Wiley & Sons, Inc. https://doi.org/10.1002/9780470571224.pse414

110. Jallo, L. J., Ghoroi, C., Gurumurthy, L., Patel, U., & Davé, R. N. (2012). Improvement of flow and bulk density of pharmaceutical powders using surface modification. *International Journal of Pharmaceutics*, *423*(2), 213–225. https://doi.org/10.1016/j.ijpharm.2011.12.012

111. Jinno, J. I., Kamada, N., Miyake, M., Yamada, K., Mukai, T., Odomi, M., … Kimura, T. (2006). Effect of particle size reduction on dissolution and oral absorption of a poorly water-soluble drug, cilostazol, in beagle dogs. *Journal of Controlled Release*, *111*(1–2), 56–64. https://doi.org/10.1016/j.jconrel.2005.11.013

112. Kachrimanis, K., Karamyan, V., & Malamataris, S. (2003). Artificial neural

networks (ANNs) and modeling of powder flow. *International Journal of Pharmaceutics*, *250*(1), 13–23. https://doi.org/10.1016/S0378-5173(02)00528-8

113. Kaerger, J. S., Edge, S., & Price, R. (2004). Influence of particle size and shape on flowability and compactibility of binary mixtures of paracetamol and microcrystalline cellulose. *European Journal of Pharmaceutical Sciences*, *22*(2–3), 173–179. https://doi.org/10.1016/j.ejps.2004.03.005

114. Kaerger, J. S., & Price, R. (2004). Processing of Spherical Crystalline Particles via a Novel Solution Atomization and Crystallization by Sonication (SAXS) Technique. *Pharmaceutical Research*, *21*(2), 372–381. https://doi.org/10.1023/B:PHAM.0000016252.97296.f1

115. Kaialy, W., Bello, H., Asare-Addo, K., & Nokhodchi, A. (2016). Effect of solvent on retarding the release of diltiazem HCl from Polyox-based liquisolid tablets. *Journal of Pharmacy and Pharmacology*, *68*(11), 1396–1402. https://doi.org/10.1111/jphp.12643

116. Kapłonek, W., Nadolny, K., & Królczyk, G. M. (2016). The use of focus-variation microscopy for the assessment of active surfaces of a new generation of coated abrasive tools. *Measurement Science Review*, *16*(2), 42–53.

117. Kašpar, O., Tokárová, V., Oka, S., Sowrirajan, K., Ramachandran, R., & Štěpánek, F. (2013). Combined UV/vis and micro-tomography investigation of acetaminophen dissolution from granules. *International Journal of Pharmaceutics*, *458*(2), 272–281. https://doi.org/10.1016/j.ijpharm.2013.10.032

118. Katikaneni, P. R., Upadrashta, S. M., Neau, S. H., & Mitra, A. K. (1995). Ethylcellulose matrix controlled release tablets of a water-soluble drug. *International Journal of Pharmaceutics*, *123*(1), 119–125. https://doi.org/10.1016/0378-5173(95)00060-V

119. Khan, K. A. (1975). The concept of dissolution efficiency. *Journal of Pharmacy and Pharmacology*, *27*(1), 48–49.

120. Khorsheed, B., Gabbott, I., Reynolds, G. K., Taylor, S. C., Roberts, R. J., & Salman, A. D. (2019). Twin-screw granulation: Understanding the mechanical properties from powder to tablets. *Powder Technology*, *341*, 104–115. https://doi.org/10.1016/j.powtec.2018.05.013

121. Kim, H. J., Lee, S. H., Lee, J. H., & Jang, S. P. (2015). Effect of particle shape on suspension stability and thermal conductivities of water-based bohemite alumina nanofluids. *Energy*, *90*, 1290–1297.

https://doi.org/10.1016/j.energy.2015.06.084

122. Kimura, S. I., Uchida, S., Kanada, K., & Namiki, N. (2015). Effect of granule properties on rough mouth feel and palatability of orally disintegrating tablets. *International Journal of Pharmaceutics*, *484*(1–2), 156–162. https://doi.org/10.1016/j.ijpharm.2015.02.023

123. Klang, V., Valenta, C., & Matsko, N. B. (2013, January 1). Electron microscopy of pharmaceutical systems. *Micron*. Pergamon. https://doi.org/10.1016/j.micron.2012.07.008

124. Kougoulos, E., Chadwick, C. E., & Ticehurst, M. D. (2011). Impact of agitated drying on the powder properties of an active pharmaceutical ingredient. *Powder Technology*, *210*(3), 308–314. https://doi.org/10.1016/j.powtec.2011.03.041

125. Kowalski, B. R. (1975). Chemometrics: Views and Propositions. *Journal of Chemical Information and Computer Sciences*, *15*(4), 201–203. https://doi.org/10.1021/ci60004a002

126. Kushner, J., Langdon, B. A., Hiller, J. I., & Carlson, G. T. (2011). Examining the impact of excipient material property variation on drug product quality attributes: A quality-by-design study for a roller compacted, immediate release tablet. *Journal of Pharmaceutical Sciences*, *100*(6), 2222–2239. https://doi.org/10.1002/jps.22455

127. Kushner, J., & Moore, F. (2010). Scale-up model describing the impact of lubrication on tablet tensile strength. *International Journal of Pharmaceutics*, *399*(1–2), 19–30. https://doi.org/10.1016/J.IJPHARM.2010.07.033

128. Kwieciński, S., Weychert, M., Jasiński, A., Kulinowski, P., Wawer, I., & Sieradzki, E. (2002). Tablet disintegration monitored by magnetic resonance imaging. *Applied Magnetic Resonance*, *22*(1), 23–29. https://doi.org/10.1007/BF03170520

129. Laity, P. R., Asare-Addo, K., Sweeney, F., Šupuk, E., & Conway, B. R. (2015). Using small-angle X-ray scattering to investigate the compaction behaviour of a granulated clay. *Applied Clay Science*, *108*, 149–164. https://doi.org/10.1016/J.CLAY.2015.02.013

130. Laity, P. R., & Cameron, R. E. (2008). A small-angle X-ray scattering study of powder compaction. *Powder Technology*, *188*(2), 119–127. https://doi.org/10.1016/j.powtec.2008.04.006

131. Leane, M., Pitt, K., Reynolds, G. K., Dawson, N., Ziegler, I., Szepes, A., …

Dall Agnol, R. (2018, November 26). Manufacturing classification system in the real world: factors influencing manufacturing process choices for filed commercial oral solid dosage formulations, case studies from industry and considerations for continuous processing. *Pharmaceutical Development and Technology*. Taylor and Francis Ltd. https://doi.org/10.1080/10837450.2018.1534863

132. Lefebvre, G., Galet, L., & Chamayou, A. (2011). Dry coating of talc particles: effect of material and process modifications on their wettability and dispersibility. *AIChE Journal*, *57*(1), 79–86.

133. Lekhal, A., Girard, K. P., Brown, M. A., Kiang, S., Glasser, B. J., & Khinast, J. G. (2003). Impact of agitated drying on crystal morphology: KCl-water system. *Powder Technology*, *132*(2–3), 119–130. https://doi.org/10.1016/S0032-5910(03)00056-1

134. Lekhal, A., Girard, K. P., Brown, M. A., Kiang, S., Khinast, J. G., & Glasser, B. J. (2004). The effect of agitated drying on the morphology of L-threonine (needle-like) crystals. *International Journal of Pharmaceutics*, *270*(1–2), 263–277. https://doi.org/10.1016/j.ijpharm.2003.10.022

135. Leleux, J., & Williams, R. O. (2014). Recent advancements in mechanical reduction methods: Particulate systems. *Drug Development and Industrial Pharmacy*. Informa Healthcare. https://doi.org/10.3109/03639045.2013.828217

136. Leon Shargel, A. B. C. Y. (2012). *Applied Biopharmaceutics & Pharmacokinetics, 7e | AccessPharmacy | McGraw-Hill Medical*. Retrieved from https://accesspharmacy.mhmedical.com/book.aspx?bookID=1592

137. Leturia, M., Benali, M., Lagarde, S., Ronga, I., & Saleh, K. (2014). Characterization of flow properties of cohesive powders: A comparative study of traditional and new testing methods. *Powder Technology*, *253*, 406–423. https://doi.org/10.1016/j.powtec.2013.11.045

138. Leuenberger, H. (1982). The compressibility and compactibility of powder systems. *International Journal of Pharmaceutics*, *12*(1), 41–55. https://doi.org/10.1016/0378-5173(82)90132-6

139. Leung, L. Y., Mao, C., Srivastava, I., Du, P., & Yang, C. Y. (2017). Flow Function of Pharmaceutical Powders Is Predominantly Governed by Cohesion, Not by Friction Coefficients. *Journal of Pharmaceutical Sciences*, *106*(7), 1865–1873. https://doi.org/10.1016/j.xphs.2017.04.012

140. Liew, C. V., Chan, L. W., Ching, A. L., & Heng, P. W. S. (2006). Evaluation

of sodium alginate as drug release modifier in matrix tablets. *International Journal of Pharmaceutics*, *309*(1–2), 25–37. https://doi.org/10.1016/j.ijpharm.2005.10.040

141. Liu, L. X., Marziano, I., Bentham, A. C., Litster, J. D., E.T.White, & Howes, T. (2008). Effect of particle properties on the flowability of ibuprofen powders. *International Journal of Pharmaceutics*, *362*(1–2), 109–117. https://doi.org/10.1016/j.ijpharm.2008.06.023

142. Liu, R., Yin, X., Li, H., Shao, Q., York, P., He, Y., … Zhang, J. (2013). Visualization and quantitative profiling of mixing and segregation of granules using synchrotron radiation X-ray microtomography and three dimensional reconstruction. *International Journal of Pharmaceutics*, *445*(1–2), 125–133. https://doi.org/10.1016/j.ijpharm.2013.02.010

143. Liu, Y., Tan, J., Thomas, A., Ou-Yang, D., & Muzykantov, V. R. (2012, February 2). The shape of things to come: Importance of design in nanotechnology for drug delivery. *Therapeutic Delivery*. Future Science Ltd London, UK . https://doi.org/10.4155/tde.11.156

144. Liversidge, G. G., & Cundy, K. C. (1995). Particle size reduction for improvement of oral bioavailability of hydrophobic drugs: I. Absolute oral bioavailability of nanocrystalline danazol in beagle dogs. *International Journal of Pharmaceutics*, *125*(1), 91–97. https://doi.org/10.1016/0378-5173(95)00122-Y

145. Löbenberg, R., Krämer, J., Shah, V. P., Amidon, G. L., & Dressman, J. B. (2000). Dissolution Testing as a Prognostic Tool for Oral Drug Absorption: Dissolution Behavior of Glibenclamide. *Pharmaceutical Research*, *17*(4), 439–444. https://doi.org/10.1023/A:1007529020774

146. Lourenço, V., Lochmann, D., Reich, G., Menezes, J. C., Herdling, T., & Schewitz, J. (2012). A quality by design study applied to an industrial pharmaceutical fluid bed granulation. *European Journal of Pharmaceutics and Biopharmaceutics*, *81*(2), 438–447. https://doi.org/10.1016/j.ejpb.2012.03.003

147. Luding, S. (2005). Shear flow modeling of cohesive and frictional fine powder. *Powder Technology*, *158*(1–3), 45–50. https://doi.org/10.1016/J.POWTEC.2005.04.018

148. Lumay, G., Traina, K., Boschini, F., Delaval, V., Rescaglio, A., Cloots, R., & Vandewalle, N. (2016). Effect of relative air humidity on the flowability of lactose powders. *Journal of Drug Delivery Science and Technology*, *35*, 207–212. https://doi.org/10.1016/J.JDDST.2016.04.007

149. Machin, M., Liesum, L., & Peinado, A. (2011). Implementation of modeling approaches in the QbD framework: examples from the Novartis experience. *Europ. Pharmaceut. Rev*, *16*(6).

150. MacKaplow, M. B., Rosen, L. A., & Michaels, J. N. (2000). Effect of primary particle size on granule growth and endpoint determination in high-shear wet granulation. *Powder Technology*, *108*(1), 32–45. https://doi.org/10.1016/S0032-5910(99)00203-X

151. Markl, D, Yassin, S., Wang, P., & Zeitler, J. A. (2016). Characterisation of microstructural changes during the hydration of pharmaceutical tablets using terahertz pulsed imaging. In *2016 41st International Conference on Infrared, Millimeter, and Terahertz waves (IRMMW-THz)* (pp. 1–2). https://doi.org/10.1109/IRMMW-THz.2016.7758451

152. Markl, Daniel, Wang, P., Ridgway, C., Karttunen, A. P., Chakraborty, M., Bawuah, P., … Zeitler, J. A. (2017). Characterization of the Pore Structure of Functionalized Calcium Carbonate Tablets by Terahertz Time-Domain Spectroscopy and X-Ray Computed Microtomography. *Journal of Pharmaceutical Sciences*, *106*(6), 1586–1595. https://doi.org/10.1016/j.xphs.2017.02.028

153. Markl, Daniel, & Zeitler, J. A. (2017, May 1). A Review of Disintegration Mechanisms and Measurement Techniques. *Pharmaceutical Research*. Springer New York LLC. https://doi.org/10.1007/s11095-017-2129-z

154. Martin, R. J. (2002). Therapeutic significance of distal airway inflammation in asthma. *Journal of Allergy and Clinical Immunology*, *109*(2 SUPPL.), S447–S460. https://doi.org/10.1067/mai.2002.121409

155. Martino, P. Di, Censi, R., Malaj, L., Martelli, S., Joiris, E., & Barthélémy, C. (2007). Influence of metronidazole particle properties on granules prepared in a high-shear mixer-granulator. *Drug Development and Industrial Pharmacy*, *33*(2), 121–131. https://doi.org/10.1080/03639040601085417

156. Megarry, A. J., Swainson, S. M. E., Roberts, R. J., & Reynolds, G. K. (2019). A big data approach to pharmaceutical flow properties. *International Journal of Pharmaceutics*, *555*, 337–345. https://doi.org/10.1016/j.ijpharm.2018.11.059

157. Mercier, S. M., Diepenbroek, B., Dalm, M. C. F., Wijffels, R. H., & Streefland, M. (2013). Multivariate data analysis as a PAT tool for early bioprocess development data. *Journal of Biotechnology*, *167*(3), 262–270. https://doi.org/10.1016/j.jbiotec.2013.07.006

158. Merkus, H. G. (2009). Particle Size, Size Distributions and Shape. In *Particle Size Measurements* (pp. 13–42). Springer Netherlands. https://doi.org/10.1007/978-1-4020-9016-5_2

159. Mesnier, X., Althaus, T. O., Forny, L., Niederreiter, G., Palzer, S., Hounslow, M. J., & Salman, A. D. (2013). A novel method to quantify tablet disintegration. *Powder Technology*, *238*, 27–34. https://doi.org/10.1016/j.powtec.2012.06.038

160. Mitchell, K., Ford, J. L., Armstrong, D. J., Elliott, P. N. C., Hogan, J. E., & Rostron, C. (1993). The influence of the particle size of hydroxypropylmethylcellulose K15M on its hydration and performance in matrix tablets. *International Journal of Pharmaceutics*, *100*(1–3), 175–179. https://doi.org/10.1016/0378-5173(93)90088-W

161. Mizumoto, T., Tamura, T., Kawai, H., Kajiyama, A., & Itai, S. (2008). Formulation Design of Taste-Masked Particles, Including Famotidine, for an Oral Fast-Disintegrating Dosage Form. *CHEMICAL & PHARMACEUTICAL BULLETIN*, *56*(4), 530–535. https://doi.org/10.1248/cpb.56.530

162. Modi, S. R., Dantuluri, A. K. R., Puri, V., Pawar, Y. B., Nandekar, P., Sangamwar, A. T., … Bansal, A. K. (2013). Impact of crystal habit on biopharmaceutical performance of celecoxib. *Crystal Growth and Design*, *13*(7), 2824–2832. https://doi.org/10.1021/cg400140a

163. Moore, M. D., Cogdill, R. P., & Wildfong, P. L. D. (2009). Evaluation of chemometric algorithms in quantitative X-ray powder diffraction (XRPD) of intact multi-component consolidated samples. *Journal of Pharmaceutical and Biomedical Analysis*, *49*(3), 619–626. https://doi.org/10.1016/j.jpba.2008.12.007

164. Morin, G., & Briens, L. (2013). The effect of lubricants on powder flowability for pharmaceutical application. *AAPS PharmSciTech*, *14*(3), 1158–1168. https://doi.org/10.1208/s12249-013-0007-5

165. Morrison, H. G., Sun, C. C., & Neervannan, S. (2009). Characterization of thermal behavior of deep eutectic solvents and their potential as drug solubilization vehicles. *International Journal of Pharmaceutics*, *378*(1–2), 136–139. https://doi.org/10.1016/j.ijpharm.2009.05.039

166. Mosharraf, M., & Nyström, C. (1995). The effect of particle size and shape on the surface specific dissolution rate of microsized practically insoluble drugs. *International Journal of Pharmaceutics*, *122*(1–2), 35–47. https://doi.org/10.1016/0378-5173(95)00033-F

167. Mu, X., Tobyn, M. J., & Staniforth, J. N. (2003). Development and evaluation of bio-dissolution systems capable of detecting the food effect on a polysaccharide-based matrix system. *Journal of Controlled Release*, *93*(3), 309–318. https://doi.org/10.1016/J.JCONREL.2003.08.013

168. Muro, S., Garnacho, C., Champion, J. A., Leferovich, J., Gajewski, C., Schuchman, E. H., … Muzykantov, V. R. (2008). Control of endothelial targeting and intracellular delivery of therapeutic enzymes by modulating the size and shape of ICAM-1-targeted carriers. *Molecular Therapy*, *16*(8), 1450–1458. https://doi.org/10.1038/mt.2008.127

169. Nagy, Z. K., Balogh, A., Vajna, B., Farkas, A., Patyi, G., Kramarics, Á., & Marosi, G. (2012). Comparison of Electrospun and Extruded Soluplus®-Based Solid Dosage Forms of Improved Dissolution. *Journal of Pharmaceutical Sciences*, *101*(1), 322–332. https://doi.org/10.1002/JPS.22731

170. NAKAMURA, H., YANAGIHARA, Y., SEKIGUCHI, H., OHTANI, M., KARIYA, S., UCHINO, K., … IGA, T. (2004). Effect of Particle Size on Mixing Degree in Dispensation. *YAKUGAKU ZASSHI*, *124*(3), 135–139. https://doi.org/10.1248/yakushi.124.135

171. Narayan, P., & Hancock, B. C. (2003). The relationship between the particle properties, mechanical behavior, and surface roughness of some pharmaceutical excipient compacts. *Materials Science and Engineering A*, *355*(1–2), 24–36. https://doi.org/10.1016/S0921-5093(03)00059-5

172. Narayan, P., & Hancock, B. C. (2005). The influence of particle size on the surface roughness of pharmaceutical excipient compacts. *Materials Science and Engineering A*, *407*(1–2), 226–233. https://doi.org/10.1016/j.msea.2005.06.060

173. Navaneethan, C. V., Missaghi, S., & Fassihi, R. (2005). Application of powder rheometer to determine powder flow properties and lubrication efficiency of pharmaceutical particulate systems. *AAPS PharmSciTech*, *6*(3), E398–E404. https://doi.org/10.1208/pt060349

174. Nep, E. I., Mahdi, M. H., Adebisi, A. O., Dawson, C., Walton, K., Bills, P. J., … Asare-Addo, K. (2017). The influence of hydroalcoholic media on the performance of Grewia polysaccharide in sustained release tablets. *International Journal of Pharmaceutics*, *532*(1), 352–364. https://doi.org/10.1016/J.IJPHARM.2017.09.022

175. Newman, A., Nagapudi, K., & Wenslow, R. (2015). Amorphous solid dispersions: a robust platform to address bioavailability challenges. *Therapeutic Delivery*, *6*(2), 247–261. https://doi.org/10.4155/tde.14.101

176. Nokhodchi, A., Al-Hamidi, H., Adebisi, A. O., Asare-Addo, K., & Maniruzzaman, M. (2017). The use of various organic solvents to tailor the properties of ibuprofen–glucosamine HCl solid dispersions. *Chemical Engineering Research and Design*, *117*, 509–519. https://doi.org/10.1016/J.CHERD.2016.11.004

177. Otsuka, M., Yamane, I., & Matsuda, Y. (2004). Effects of lubricant mixing on compression properties of various kinds of direct compression excipients and physical properties of the tablets. *Advanced Powder Technology*, *15*(4), 477–493. https://doi.org/10.1163/1568552041270563

178. Patterson, J. E., James, M. B., Forster, A. H., Lancaster, R. W., Butler, J. M., & Rades, T. (2005). The Influence of Thermal and Mechanical Preparative Techniques on the Amorphous State of Four Poorly Soluble Compounds. *Journal of Pharmaceutical Sciences*, *94*(9), 1998–2012. https://doi.org/10.1002/jps.20424

179. Patterson, J. E., James, M. B., Forster, A. H., Lancaster, R. W., Butler, J. M., & Rades, T. (2007). Preparation of glass solutions of three poorly water soluble drugs by spray drying, melt extrusion and ball milling. *International Journal of Pharmaceutics*, *336*(1), 22–34. https://doi.org/10.1016/j.ijpharm.2006.11.030

180. Paudel, A., Worku, Z. A., Meeus, J., Guns, S., & Van den Mooter, G. (2013). Manufacturing of solid dispersions of poorly water soluble drugs by spray drying: Formulation and process considerations. *International Journal of Pharmaceutics*, *453*(1), 253–284. https://doi.org/10.1016/J.IJPHARM.2012.07.015

181. Paul, S., & Sun, C. C. (2017). Lubrication with magnesium stearate increases tablet brittleness. *Powder Technology*, *309*, 126–132. https://doi.org/10.1016/j.powtec.2016.12.012

182. Perfetti, G., Casteele, E. Van De, Rieger, B., Wildeboer, W. J., & Meesters, G. M. H. (2010). X-ray micro tomography and image analysis as complementary methods for morphological characterization and coating thickness measurement of coated particles. In *Advanced Powder Technology* (Vol. 21, pp. 663–675). Elsevier. https://doi.org/10.1016/j.apt.2010.08.002

183. Pfannmöller, M., Flügge, H., Benner, G., Wacker, I., Sommer, C., Hanselmann, M., … Schröder, R. R. (2011). Visualizing a homogeneous blend in bulk heterojunction polymer solar cells by analytical electron microscopy. *Nano Letters*, *11*(8), 3099–3107. https://doi.org/10.1021/nl201078t

184. Pitt, K., & Sinka, C. (2007). Tabletting. In *Handbook of powder technology*

(Vol. 11, pp. 735–778). Elsevier.

185. Podczeck, F., & Miah, Y. (1996). The influence of particle size and shape on the angle of internal friction and the flow factor of unlubricated and lubricated powders. *International Journal of Pharmaceutics*, *144*(2), 187–194. https://doi.org/10.1016/S0378-5173(96)04755-2

186. Ponnammal, P., Kanaujia, P., Yani, Y., Ng, W., Tan, R., Ponnammal, P., … Tan, R. B. H. (2018). Orally Disintegrating Tablets Containing Melt Extruded Amorphous Solid Dispersion of Tacrolimus for Dissolution Enhancement. *Pharmaceutics*, *10*(1), 35. https://doi.org/10.3390/pharmaceutics10010035

187. Qin, S. J., & McAvoy, T. J. (1992). Nonlinear PLS modeling using neural networks. *Computers and Chemical Engineering*, *16*(4), 379–391. https://doi.org/10.1016/0098-1354(92)80055-E

188. Qiu, Y., Chen, Y., Zhang, G. G. Z., Yu, L., & Mantri, R. V. (2016). *Developing solid oral dosage forms: pharmaceutical theory and practice*. Academic press.

189. Quodbach, J., Moussavi, A., Tammer, R., Frahm, J., & Kleinebudde, P. (2014). Tablet disintegration studied by high-resolution real-time magnetic resonance imaging. *Journal of Pharmaceutical Sciences*, *103*(1), 249–255. https://doi.org/10.1002/jps.23789

190. Rabinow, B. E. (2004). Nanosuspensions in drug delivery. *Nature Reviews Drug Discovery*, *3*(9), 785–796. https://doi.org/10.1038/nrd1494

191. Rabinski, G., & Thomas, D. (2004). Dynamic digital image analysis: Emerging technology for particle characterization. *Water Science and Technology*, *50*(12), 19–26. https://doi.org/10.2166/wst.2004.0691

192. Rajkumar, A. D., Reynolds, G. K., Wilson, D., Wren, S., Hounslow, M. J., & Salman, A. D. (2016). Investigating the effect of processing parameters on pharmaceutical tablet disintegration using a real-time particle imaging approach. *European Journal of Pharmaceutics and Biopharmaceutics*, *106*, 88–96. https://doi.org/10.1016/j.ejpb.2016.06.005

193. Ramirez, M., David, S. E., Schwalbe, C. H., Asare-Addo, K., Conway, B. R., & Timmins, P. (2017). Crystal Packing Arrangement, Chain Conformation, and Physicochemical Properties of Gemfibrozil Amine Salts. *Crystal Growth & Design*, *17*(7), 3743–3750. https://doi.org/10.1021/acs.cgd.7b00352

194. Rao, K. P., Chawla, G., Kaushal, A. M., & Bansal, A. K. (2005). Impact of solid-state properties on lubrication efficacy of magnesium stearate. *Pharmaceutical Development and Technology*, *10*(3), 423–437.

https://doi.org/10.1081/PDT-54462

195. Rasenack, N., & Müller, B. W. (2002). Crystal habit and tableting behavior. *International Journal of Pharmaceutics*, *244*(1–2), 45–57. https://doi.org/10.1016/S0378-5173(02)00296-X

196. Rhodes, M. J. (Martin J. . (2008). *Introduction to particle technology*. Wiley. Retrieved from https://www.wiley.com/en-us/Introduction+to+Particle+Technology%2C+2nd+Edition-p-9780470014288

197. Roberts, K. J., Hammond, R. B., Ramachandran, V., & Docherty, R. (2016). Synthonic engineering:from molecular and crystallographic structure to the rational design of pharmaceutical solid dosage forms. In *Computational Pharmaceutical Solid State Chemistry, First Edition.* John Wiley & Sons, Inc.

198. Rohrs, B. R., Amidon, G. E., Meury, R. H., Secreast, P. J., King, H. M., & Skoug, C. J. (2006, May 1). Particle size limits to meet USP content uniformity criteria for tablets and capsules. *Journal of Pharmaceutical Sciences*. John Wiley and Sons Inc. https://doi.org/10.1002/jps.20587

199. Sadeghi, F., Garekani, H. A., & Goli, F. (2004). Tableting of eudragit RS and propranolol hydrochloride solid dispersion: Effect of particle size, compaction force, and plasticizer addition on drug release. *Drug Development and Industrial Pharmacy*, *30*(7), 759–766. https://doi.org/10.1081/DDC-120039652

200. Sager, M., Grimm, M., Jedamzik, P., Merdivan, S., Kromrey, M. L., Hasan, M., … Weitschies, W. (2019). Combined Application of MRI and the Salivary Tracer Technique to Determine the in Vivo Disintegration Time of Immediate Release Formulation Administered to Healthy, Fasted Subjects. *Molecular Pharmaceutics*, *16*(4), 1782–1786. https://doi.org/10.1021/acs.molpharmaceut.8b01320

201. Saleem, I. Y., & Smyth, H. D. C. (2010). Micronization of a soft material: Air-jet and micro-ball milling. *AAPS PharmSciTech*, *11*(4), 1642–1649. https://doi.org/10.1208/s12249-010-9542-5

202. Sandler, N., & Wilson, D. (2010). Prediction of granule packing and flow behavior based on particle size and shape analysis. *Journal of Pharmaceutical Sciences*, *99*(2), 958–968. https://doi.org/10.1002/jps.21884

203. Savjani, K. T., Gajjar, A. K., & Savjani, J. K. (2012). Drug Solubility: Importance and Enhancement Techniques. *ISRN Pharmaceutics*, *2012*(100 mL), 1–10. https://doi.org/10.5402/2012/195727

204. Schmitt, W., & Willmann, S. (2004, December 1). Physiology-based pharmacokinetic modeling: Ready to be used. *Drug Discovery Today: Technologies*. Elsevier Ltd. https://doi.org/10.1016/j.ddtec.2004.09.006

205. Serajuddin, A. T. M. (1999). Solid dispersion of poorly water-soluble drugs: Early promises, subsequent problems, and recent breakthroughs. *Journal of Pharmaceutical Sciences*, *88*(10), 1058–1066. https://doi.org/10.1021/js980403l

206. Shah, R. B., Tawakkul, M. A., & Khan, M. A. (2008). Comparative evaluation of flow for pharmaceutical powders and granules. *AAPS PharmSciTech*, *9*(1), 250–258. https://doi.org/10.1208/s12249-008-9046-8

207. Shah, S. P., & Misra, A. (2004). Liposomal amikacin dry powder inhaler: Effect of fines on in vitro performance. *AAPS PharmSciTech*, *5*(4), 107–113. https://doi.org/10.1208/pt050465

208. Shah, U., & Augsburger, L. (2002). Multiple sources of sodium starch glycolate, NF: evaluation of functional equivalence and development of standard performance tests. *Pharmaceutical Development and Technology*, *7*(3), 345–359. https://doi.org/10.1081/pdt-120005731

209. Shah, U. V., Olusanmi, D., Narang, A. S., Hussain, M. A., Gamble, J. F., Tobyn, M. J., & Heng, J. Y. Y. (2014). Effect of crystal habits on the surface energy and cohesion of crystalline powders. *International Journal of Pharmaceutics*, *472*(1–2), 140–147. https://doi.org/10.1016/j.ijpharm.2014.06.014

210. Sheskey, P. J., Cook, W. G., & Cable, C. G. (2017). *Handbook of pharmaceutical excipients* (8th Revise). Pharmaceutical Press. Retrieved from https://www.pharmpress.com/product/9780857112712/excipients

211. Shi, Z., Zaborenko, N., & Reed, D. E. (2013). Latent variables-based process modeling of a continuous hydrogenation reaction in API synthesis of small molecules. *Journal of Pharmaceutical Innovation*, *8*(1), 1–10. https://doi.org/10.1007/s12247-012-9141-y

212. SHIRAISHI, T., SANO, A., KONDO, S., YUASA, H., & KANAYA, Y. (1995). Studies on the Granulation Process of Granules for Tableting with a High Speed Mixer. II. Influence of Particle Size of Active Substance on Granulation. *CHEMICAL & PHARMACEUTICAL BULLETIN*, *43*(4), 654–659. https://doi.org/10.1248/cpb.43.654

213. Shyam Karki Tomislav Friščić László Fábián Peter R. Laity Graeme M. Day William Jones. (2009). Improving Mechanical Properties of Crystalline Solids

by Cocrystal Formation: New Compressible Forms of Paracetamol. *Advanced Materials*, *21*(38â□“39), 3905–3909. https://doi.org/10.1002/adma.200900533

214. Sirius. (2017). *Product Information – Sirius SDi2*.

215. Solanki, N. G., Tahsin, M., Shah, A. V., & Serajuddin, A. T. M. (2018). Formulation of 3D Printed Tablet for Rapid Drug Release by Fused Deposition Modeling: Screening Polymers for Drug Release, Drug-Polymer Miscibility and Printability. *Journal of Pharmaceutical Sciences*, *107*(1), 390–401. https://doi.org/10.1016/J.XPHS.2017.10.021

216. Spillmann, A., Sonnenfeld, A., & Rudolf von Rohr, P. (2008). Effect of Surface Free Energy on the Flowability of Lactose Powder Treated by PECVD. *Plasma Processes and Polymers*, *5*(8), 753–758. https://doi.org/10.1002/ppap.200800069

217. Storey, R. A., & Ymén, I. (2011). *Solid state characterization of pharmaceuticals*. John Wiley & Sons.

218. Sun, C. C. (2009). Materials science tetrahedron—A useful tool for pharmaceutical research and development. *Journal of Pharmaceutical Sciences*, *98*(5), 1671–1687.

219. Sun, C. C. (2011). Decoding powder tabletability: Roles of particle adhesion and plasticity. *Journal of Adhesion Science and Technology*, *25*(4–5), 483–499. https://doi.org/10.1163/016942410X525678

220. Sun, C. C., & Grant, D. J. W. (2004). Improved tableting properties of p-hydroxybenzoic acid by water of crystallization: A molecular insight. *Pharmaceutical Research*, *21*(2), 382–386.

221. Sun, C., & Grant, D. J. W. (2001). Influence of crystal structure on the tableting properties of sulfamerazine polymorphs. *Pharmaceutical Research*, *18*(3), 274–280. https://doi.org/10.1023/A:1011038526805

222. Sun, Changquan, & Grant, D. J. W. (2001a). Effects of initial particle size on the tableting properties of L-lysine monohydrochloride dihydrate powder. *International Journal of Pharmaceutics*, *215*(1–2), 221–228. https://doi.org/10.1016/S0378-5173(00)00701-8

223. Sun, Changquan, & Grant, D. J. W. (2001b). Influence of Crystal Structure on the Tableting Properties of Sulfamerazine Polymorphs. *Pharmaceutical Research*, *18*(3), 274–280. https://doi.org/10.1023/A:1011038526805

224. Šupuk, E., Ghori, M. U., Asare-Addo, K., Laity, P. R., Panchmatia, P. M., & Conway, B. R. (2013). The influence of salt formation on electrostatic and compression properties of flurbiprofen salts. *International Journal of Pharmaceutics*, *458*(1), 118–127. https://doi.org/10.1016/J.IJPHARM.2013.10.004

225. Swaminathan, V., & Kildsig, D. O. (2002). Polydisperse powder mixtures: Effect of particle size and shape on mixture stability. *Drug Development and Industrial Pharmacy*, *28*(1), 41–48. https://doi.org/10.1081/DDC-120001484

226. Sympatec. (2018). Particle Shape descriptors. Retrieved June 4, 2018, from https://www.sympatec.com/en/particle-measurement/glossary/particle-shape/

227. Tao, L., Zhao, X. M., Gao, J. M., & Hu, W. (2010). Lithographically defined uniform worm-shaped polymeric nanoparticles. *Nanotechnology*, *21*(9), 095301. https://doi.org/10.1088/0957-4484/21/9/095301

228. Tay, T., Das, S., & Stewart, P. (2010). Magnesium stearate increases salbutamol sulphate dispersion: What is the mechanism? *International Journal of Pharmaceutics*, *383*(1–2), 62–69. https://doi.org/10.1016/j.ijpharm.2009.09.006

229. Teng, S., Wang, P., Zhu, L., Young, M. W., & Gogos, C. G. (2009). Experimental and numerical analysis of a lab-scale fluid energy mill. *Powder Technology*, *195*(1), 31–39. https://doi.org/10.1016/j.powtec.2009.05.013

230. Thakkar, R., Thakkar, R., Pillai, A., Ashour, E. A., & Repka, M. A. (2020). Systematic screening of pharmaceutical polymers for hot melt extrusion processing: a comprehensive review. *International Journal of Pharmaceutics*, *576*, 118989. https://doi.org/https://doi.org/10.1016/j.ijpharm.2019.118989

231. Torrance, S. E., Sun, Z., & Sevick-Muraca, E. M. (2004). Impact of excipient particle size on measurement of active pharmaceutical ingredient absorbance in mixtures using frequency domain photon migration. *Journal of Pharmaceutical Sciences*, *93*(7), 1879–1889. https://doi.org/10.1002/jps.20103

232. Tritt-Goc, J., & Kowalczuk, J. (2002). In situ, real time observation of the disintegration of paracetamol tablets in aqueous solution by magnetic resonance imaging. *European Journal of Pharmaceutical Sciences*, *15*(4), 341–346. https://doi.org/10.1016/S0928-0987(02)00016-7

233. Upadhyay, P., Khomane, K. S., Kumar, L., & Bansal, A. K. (2013). Relationship between crystal structure and mechanical properties of ranitidine hydrochloride polymorphs. *CrystEngComm*, *15*(19), 3959–3964.

https://doi.org/10.1039/c3ce40201k

234. Usmani, O. S., Biddiscombe, M. F., & Barnes, P. J. (2005). Regional lung deposition and bronchodilator response as a function of β2-agonist particle size. *American Journal of Respiratory and Critical Care Medicine*, *172*(12), 1497–1504. https://doi.org/10.1164/rccm.200410-1414OC

235. USP convention. (2020a). *General Chapters: <699> DENSITY OF SOLIDS*. Retrieved from http://www.pharmacopeia.cn/v29240/usp29nf24s0_c699.html

236. USP convention. (2020b). USP–NF | USP-NF. Retrieved May 4, 2020, from https://www.uspnf.com/

237. Van den Mooter, G. (2012). The use of amorphous solid dispersions: A formulation strategy to overcome poor solubility and dissolution rate. *Drug Discovery Today: Technologies*, *9*(2), e79–e85. https://doi.org/10.1016/J.DDTEC.2011.10.002

238. Van der Jeught, S., & Dirckx, J. J. J. (2015). Real-time structured light profilometry: A review. *Optics and Lasers in Engineering*, *87*, 18–31. https://doi.org/10.1016/j.optlaseng.2016.01.011

239. Velasco, M. V., Ford, J. L., Rowe, P., & Rajabi-Siahboomi, A. R. (1999). Influence of drug:hydroxypropylmethylcellulose ratio, drug and polymer particle size and compression force on the release of diclofenac sodium from HPMC tablets. *Journal of Controlled Release*, *57*(1), 75–85. https://doi.org/10.1016/S0168-3659(98)00110-2

240. Venables, H. J., & Wells, J. I. (2001). Powder mixing. *Drug Development and Industrial Pharmacy*. Taylor & Francis. https://doi.org/10.1081/DDC-100107316

241. Verhoeven, E., Vervaet, C., & Remon, J. P. (2006). Xanthan gum to tailor drug release of sustained-release ethylcellulose mini-matrices prepared via hot-melt extrusion: in vitro and in vivo evaluation. *European Journal of Pharmaceutics and Biopharmaceutics*, *63*(3), 320–330. https://doi.org/10.1016/j.ejpb.2005.12.004

242. Viana, M., Jouannin, P., Pontier, C., & Chulia, D. (2002). About pycnometric density measurements. *Talanta*, *57*(3), 583–593. https://doi.org/10.1016/S0039-9140(02)00058-9

243. Visser, J. (1989). Van der Waals and other cohesive forces affecting powder fluidization. *Powder Technology*, *58*(1), 1–10. https://doi.org/10.1016/0032-5910(89)80001-4

244. Vogt, M., Kunath, K., & Dressman, J. B. (2008). Dissolution improvement of four poorly water soluble drugs by cogrinding with commonly used excipients. *European Journal of Pharmaceutics and Biopharmaceutics*, *68*(2), 330–337. https://doi.org/10.1016/j.ejpb.2007.05.009

245. Wang, J., Wen, H., & Desai, D. (2010). Lubrication in tablet formulations. *European Journal of Pharmaceutics and Biopharmaceutics*, *75*(1), 1–15. https://doi.org/10.1016/J.EJPB.2010.01.007

246. Wang, Y., Koynov, S., Glasser, B. J., & Muzzio, F. J. (2016). A method to analyze shear cell data of powders measured under different initial consolidation stresses. *Powder Technology*, *294*, 105–112. https://doi.org/10.1016/j.powtec.2016.02.027

247. Ward, A., Walton, K., Box, K., Østergaard, J., Gillie, L. J., Conway, B. R., & Asare-Addo, K. (2017). Variable-focus microscopy and UV surface dissolution imaging as complementary techniques in intrinsic dissolution rate determination. *International Journal of Pharmaceutics*, *530*(1–2), 139–144. https://doi.org/10.1016/J.IJPHARM.2017.07.053

248. Wei, H., Dalton, C., Di Maso, M., Kanfer, I., & Löbenberg, R. (2008a). Physicochemical characterization of five glyburide powders: A BCS based approach to predict oral absorption. *European Journal of Pharmaceutics and Biopharmaceutics*, *69*(3), 1046–1056. https://doi.org/10.1016/J.EJPB.2008.01.026

249. Wei, H., Dalton, C., Di Maso, M., Kanfer, I., & Löbenberg, R. (2008b). Physicochemical characterization of five glyburide powders: A BCS based approach to predict oral absorption. *European Journal of Pharmaceutics and Biopharmaceutics*, *69*(3), 1046–1056. https://doi.org/10.1016/J.EJPB.2008.01.026

250. Wei, H., & Obenberg, R. (2006). Biorelevant dissolution media as a predictive tool for glyburide a class II drug. https://doi.org/10.1016/j.ejps.2006.05.004

251. Wilson, D., Wren, S., & Reynolds, G. (2012). Linking dissolution to disintegration in immediate release tablets using image analysis and a population balance modelling approach. *Pharmaceutical Research*, *29*(1), 198–208. https://doi.org/10.1007/s11095-011-0535-1

252. Witt, W., Köhler, U., & List, J. (2004). Direct Imaging of very fast Particles Opens the Application of Powerful (Dry) Dispersion for Size and Shape Characterisation. Partec.

253. Wu, J., Chen, J., & Yang, Y. (2008). A modified kinematic model for particle

flow in moving beds. *Powder Technology*, *181*(1), 74–82. https://doi.org/10.1016/J.POWTEC.2007.06.014

254. Xu, J., Wong, D. H. C., Byrne, J. D., Chen, K., Bowerman, C., & DeSimone, J. M. (2013). Future of the Particle Replication in Nonwetting Templates (PRINT) Technology. *Angewandte Chemie International Edition*, *52*(26), 6580–6589. https://doi.org/10.1002/anie.201209145

255. Yacoub, F., Lautens, J., Lucisano, L., & Banh, W. (2011, June 10). Application of quality by design principles to legacy drug products. *Journal of Pharmaceutical Innovation*. Springer. https://doi.org/10.1007/s12247-011-9101-y

256. Yang, J., Sliva, A., Banerjee, A., Dave, R. N., & Pfeffer, R. (2005). Dry particle coating for improving the flowability of cohesive powders. *Powder Technology*, *158*(1–3), 21–33. https://doi.org/10.1016/J.POWTEC.2005.04.032

257. Yang, Q., Yuan, F., Ma, Y., Shi, K., Yang, G., & Zhu, J. (2020). Electrostatic powder coated osmotic pump tablets: Influence factors of coating powder adhesion and film formation. *Powder Technology*, *360*, 444–451. https://doi.org/10.1016/j.powtec.2019.10.084

258. YAO, T., YAMADA, M., YAMAHARA, H., & YOSHIDA, M. (1998). Tableting of Coated Particles. II. Influence of Particle Size of Pharmaceutical Additives on Protection of Coating Membrane from Mechanical Damage during Compression Process. *CHEMICAL & PHARMACEUTICAL BULLETIN*, *46*(5), 826–830. https://doi.org/10.1248/cpb.46.826

259. York, P. (1975a). Application of powder failure testing equipment in assessing effect of glidants on flowability of cohesive pharmaceutical powders. *Journal of Pharmaceutical Sciences*, *64*(7), 1216–1221. https://doi.org/10.1002/jps.2600640721

260. York, P. (1975b). q. *Journal of Pharmaceutical Sciences*, *64*(7), 1216–1221. https://doi.org/10.1002/jps.2600640721

261. Yost, E., Chalus, P., Zhang, S., Peter, S., & Narang, A. S. (2019). Quantitative X-ray microcomputed tomography assessment of internal tablet defects. *Journal of Pharmaceutical Sciences*, *108*(5), 1818–1830.

262. Yu, W., & Hancock, B. C. (2008). Evaluation of dynamic image analysis for characterizing pharmaceutical excipient particles. *International Journal of Pharmaceutics*, *361*(1–2), 150–157. https://doi.org/10.1016/j.ijpharm.2008.05.025

263. Yu, W., Muteki, K., Zhang, L., & Kim, G. (2011). Prediction of Bulk Powder Flow Performance Using Comprehensive Particle Size and Particle Shape Distributions. *Journal of Pharmaceutical Sciences*, *100*(1), 284–293. https://doi.org/10.1002/jps.22254

264. Zeng, X. M., Martin, G. P., & Marriott, C. (2000). *Particulate Interactions in Dry Powder Formulation for Inhalation*. CRC Press.

265. Zhang, D., Flory, J. H., Panmai, S., Batra, U., & Kaufman, M. J. (2002). Wettability of pharmaceutical solids: its measurement and influence on wet granulation. *Colloids and Surfaces A: Physicochemical and Engineering Aspects*, *206*(1), 547–554. https://doi.org/https://doi.org/10.1016/S0927-7757(02)00091-2

266. Zhang, F., Aaltonen, J., Tian, F., Saville, D. J., & Rades, T. (2009). Influence of particle size and preparation methods on the physical and chemical stability of amorphous simvastatin. *European Journal of Pharmaceutics and Biopharmaceutics*, *71*(1), 64–70. https://doi.org/10.1016/j.ejpb.2008.07.010

267. Zhao, N., & Augsburger, L. L. (2006). The influence of product brand-to-brand variability on superdisintegrant performance: A case study with croscarmellose sodium. *Pharmaceutical Development and Technology*, *11*(2), 179–185. https://doi.org/10.1080/10837450600561281

268. Zhou, Q. (Tony), Denman, J. A., Gengenbach, T., Das, S., Qu, L., Zhang, H., … Morton, D. A. V. (2011). Characterization of the surface properties of a model pharmaceutical fine powder modified with a pharmaceutical lubricant to improve flow via a mechanical dry coating approach. *Journal of Pharmaceutical Sciences*, *100*(8), 3421–3430. https://doi.org/10.1002/jps.22547

Appendix

Table A 1 Particle size descriptors of MCC grades

GRADE	D [0.1, V] (µM)	D [0.5, V] (µM)	D [0.9, V] (µM)	D [4,3] (µM)	D [0.16, V] (µM)	D [0.84, V] (µM)	D [0.99, V] (µM)	SMD (µM)
MCC PH100	177.16	217.91	272.19	222.16	183.27	263.98	331.24	215.80
RSD %	0.42	0.11	0.21	0.41	0.37	0.18	3.45	3.29
MCC PH101	32.51	68.09	126.21	75.32	39.15	113.94	170.28	74.32
RSD %	0.41	1.13	1.32	1.47	0.44	1.76	3.75	2.20
MCC PH102	39.98	89.96	213.06	111.07	93.99	185.48	332.47	73.30
RSD %	0.31	1.05	2.29	1.62	79.81	2.90	2.05	0.76
MCC PH105	13.52	34.15	235.41	104.74	16.18	95.51	217.48	104.71
RSD %	0.42	0.84	1.22	1.79	0.64	1.39	2.31	1.64
MCC PH200	241.02	313.56	384.33	311.00	256.65	358.66	429.68	273.25
RSD %	5.06	4.17	27.38	9.07	5.89	10.55	57.46	39.22
MCC PH302	37.32	104.49	241.62	122.38	72.14	211.36	334.54	74.23
RSD %	0.80	2.01	1.84	2.10	45.46	1.29	4.01	1.50
MCC PROSOLV 50	31.77	68.51	116.92	72.26	39.58	101.92	166.34	55.14
RSD %	0.20	0.18	0.69	0.40	0.17	0.34	1.02	0.49
MCC PROSOLV 90	40.04	97.64	201.77	111.16	50.51	172.72	320.58	74.61
RSD %	0.07	0.96	3.57	1.70	0.16	3.87	4.71	0.51

Table A 2Particle shape descriptors of MCC grades

GRADE/PARTICLE SHAPE DESCRIPTORS	ASPECT RATIO						SPHERICITY					
	S10,3	S50,3	S90,3	s16,3	s84,3	s99,3	S10,3	S50,3	S90,3	s16,3	s84,3	s99,3
MCC PH100	0.605	0.784	0.896	0.648	0.877	0.944	0.831	0.883	0.905	0.850	0.900	0.918
RSD%	0.003	0.002	0.001	0.001	0.001	0.001	0.001	0.000	0.000	0.002	0.000	0.000
MCC PH101	0.388	0.599	0.792	0.432	0.756	0.887	0.556	0.727	0.847	0.592	0.827	0.904
RSD%	0.001	0.001	0.001	0.001	0.001	0.002	0.005	0.005	0.002	0.005	0.003	0.001
MCC PH102	0.356	0.577	0.783	0.400	0.744	0.883	0.541	0.696	0.825	0.573	0.802	0.892
RSD%	0.000	0.002	0.001	0.000	0.002	0.002	0.000	0.001	0.001	0.001	0.001	0.001
MCC PH105	0.441	0.610	0.785	0.463	0.752	0.857	0.205	0.664	0.858	0.355	0.848	0.946
RSD%	0.006	0.010	0.001	0.014	0.005	0.029	0.002	0.002	0.042	0.002	0.006	0.001
MCC PH200	0.705	0.865	0.936	0.767	0.928	0.965	0.864	0.892	0.906	0.871	0.902	0.916
RSD%	0.003	0.001	0.001	0.001	0.001	0.002	0.002	0.001	0.001	0.002	0.002	0.001
MCC PH302	0.440	0.644	0.816	0.483	0.784	0.888	0.621	0.761	0.849	0.640	0.834	0.899
RSD%	0.001	0.001	0.002	0.002	0.002	0.016	0.034	0.002	0.001	0.003	0.001	0.001
MCC Prosolv 50	0.383	0.592	0.793	0.425	0.755	0.885	0.571	0.720	0.845	0.602	0.822	0.914
RSD%	0.002	0.002	0.002	0.002	0.002	0.002	0.005	0.003	0.001	0.004	0.001	0.000
MCC Prosolv 90	0.409	0.624	0.808	0.453	0.775	0.893	0.605	0.742	0.846	0.637	0.826	0.906
RSD%	0.001	0.001	0.001	0.001	0.001	0.001	0.001	0.001	0.001	0.001	0.001	0.000

Table A 3 Particle size descriptors of lactose grades

Grade/Particle Size Descriptor	D [0.1, V] (µM)	D [0.5, V] (µM)	D [0.9, V] (µM)	D [4,3] (µM)	D [0.16, V] (µM)	D [0.84, V] (µM)	D [0.99, V] (µM)	SMD (µM)
Flowlac 90	67.02	145.56	231.67	148.51	82.11	210.28	325.84	137.07
RSD%	6.66	10.52	13.96	9.75	8.99	7.60	7.11	22.65
Flowlac 100	58.33	139.92	240.00	145.50	73.38	213.15	339.79	104.49
RSD%	3.30	6.14	7.61	5.25	4.59	5.00	3.67	4.29
Granulac 70	42.02	131.02	238.36	137.27	57.63	209.74	349.88	81.54
RSD%	0.37	0.35	1.33	0.64	0.49	0.86	8.57	0.44
Granulac 200	17.60	50.32	113.87	58.90	22.84	97.76	167.19	35.00
RSD%	0.07	0.17	0.49	0.21	0.06	0.27	0.65	0.08
Inhalac 250	27.23	64.56	101.20	65.36	34.16	95.33	130.98	47.96
RSD%	0.12	0.22	0.22	0.22	0.14	0.21	0.34	0.17
Inhalac 400	8.44	22.38	42.46	24.60	10.19	37.34	65.00	16.62
RSD%	0.30	0.21	1.07	0.51	0.36	0.87	3.82	0.31
Tablettose 80	40.77	138.18	433.12	191.53	53.31	334.80	756.42	87.33
RSD%	0.36	4.21	29.98	8.92	0.68	21.11	7.22	1.54

Table A 4 Particle shape descriptors of lactose grades

GRADE/PARTICLE SHAPE DESCRIPTORS	ASPECT RATIO						SPHERICITY					
	S10,3	S50,3	S90,3	s16,3	s84,3	s99,3	S10,3	S50,3	S90,3	s16,3	s84,3	s99,3
Flowlac 90	0.684	0.881	0.942	0.737	0.933	0.966	0.806	0.914	0.939	0.836	0.935	0.950
RSD%	0.006	0.001	0.001	0.008	0.001	0.001	0.004	0.001	0.001	0.004	0.000	0.000
Flowlac 100	0.675	0.871	0.939	0.724	0.929	0.963	0.812	0.907	0.937	0.839	0.932	0.950
RSD%	0.002	0.001	0.001	0.003	0.001	0.001	0.003	0.001	0.001	0.003	0.001	0.001
Ganulac 70	0.559	0.717	0.850	0.596	0.826	0.914	0.695	0.837	0.895	0.739	0.885	0.925
RSD%	0.001	0.001	0.001	0.001	0.001	0.001	0.002	0.002	0.001	0.002	0.001	0.001
Granulac 200	0.515	0.689	0.832	0.554	0.804	0.904	0.593	0.806	0.897	0.646	0.885	0.940
RSD%	0.002	0.002	0.002	0.001	0.002	0.001	0.021	0.009	0.001	0.020	0.002	0.001
inhalac 250	0.533	0.702	0.840	0.570	0.813	0.909	0.597	0.810	0.899	0.649	0.887	0.936
RSD%	0.001	0.001	0.000	0.001	0.001	0.000	0.004	0.001	0.000	0.003	0.001	0.000
Inhalac 400	0.449	0.670	0.810	0.507	0.779	0.895	0.515	0.785	0.902	0.568	0.893	0.955
RSD%	0.001	0.008	0.006	0.011	0.007	0.002	0.028	0.031	0.007	0.031	0.004	0.006
Tablettose 80	0.599	0.747	0.861	0.634	0.839	0.917	0.708	0.817	0.887	0.741	0.873	0.929
RSD%	0.003	0.001	0.002	0.002	0.002	0.001	0.001	0.002	0.001	0.003	0.002	0.001

Table A 5 Particle size descriptors of DCP grades

GRADE/PARTICLE SIZE DESCRIPTOR	D [0.1, V] (µM)	D [0.5, V] (µM)	D [0.9, V] (µM)	D [4,3] (µM)	D [0.16, V] (µM)	D [0.84, V] (µM)	D [0.99, V] (µM)	SMD (µM)
A12	8.43	24.94	45.01	26.87	10.69	39.98	89.48	20.87
RSD%	0.19	0.63	1.31	1.06	0.32	1.44	16.06	6.00
A60	38.08	68.06	98.27	76.12	45.83	91.13	299.78	59.81
RSD%	1.23	0.18	0.65	5.58	0.31	0.60	12.57	0.45
A150	53.40	155.56	269.03	160.27	72.61	258.47	360.55	94.06
RSD%	2.85	4.87	2.36	3.92	4.16	22.57	2.03	3.78
D14	8.19	22.41	43.66	25.36	10.07	38.23	104.26	16.57
RSD%	0.17	1.00	3.00	2.93	0.27	3.02	75.59	0.63
D160	96.57	170.69	264.43	160.37	112.02	241.93	354.10	130.27
RSD%	3.59	3.81	2.97	29.26	2.82	4.12	3.01	3.19

Table A 6 Particle size descriptors of DCP grades

GRADE/PARTICLE SHAPE DESCRIPTORS	AR						SPHERICITY					
	S10,3	S50,3	S90,3	s16,3	s84,3	s99,3	S10,3	S50,3	S90,3	s16,3	s84,3	s99,3
A12	0.467	0.701	0.840	0.534	0.814	0.906	0.485	0.772	0.899	0.537	0.892	0.981
RSD%	0.006	0.001	0.002	0.005	0.002	0.001	0.014	0.003	0.000	0.013	0.001	0.024
A60	0.643	0.791	0.886	0.684	0.869	0.932	0.712	0.870	0.922	0.758	0.914	0.946
RSD%	0.005	0.001	0.000	0.002	0.001	0.000	0.001	0.001	0.001	0.002	0.001	0.001
A150	0.595	0.754	0.869	0.633	0.848	0.924	0.596	0.761	0.855	0.640	0.837	0.911
RSD%	0.002	0.003	0.002	0.001	0.002	0.001	0.017	0.009	0.005	0.015	0.006	0.003
D14	0.449	0.680	0.820	0.513	0.787	0.897	0.505	0.778	0.898	0.560	0.892	0.955
RSD%	0.000	0.005	0.006	0.002	0.004	0.002	0.039	0.027	0.002	0.037	0.003	0.004
D160	0.608	0.756	0.867	0.644	0.847	0.920	0.681	0.783	0.850	0.711	0.836	0.896
RSD%	0.006	0.002	0.001	0.005	0.000	0.001	0.013	0.004	0.001	0.011	0.002	0.001

Table A 7 Flow data of MCC grades (RHOB is the bulk density calculated in kg/m3, PHIE is the effective angle of friction, PHIILIN is the effective angle of internal friction, PHISF is the angle of surface friction, FFC is the flow function coefficient

Grade	RHOB (KG/M^3)	PHIE (°)	PHILIN (°)	PHISF (°)	FFC
MCC PH100	940.33	32.97	31.60	30.63	18.67
RSD%	24.99	0.81	0.79	0.55	2.25
MCC PH101	419.33	44.47	38.03	40.90	3.83
RSD%	10.12	0.67	0.72	0.53	0.06
MCC PH102	370.33	44.43	39.70	41.13	4.97
RSD%	1.53	0.38	0.36	0.31	0.06
MCC PH105	360.00	51.13	37.00	42.90	2.00
RSD%	3.61	0.40	0.79	0.26	0.10
MCC PH200	921.00	30.70	29.93	28.07	33.67
RSD%	3.61	0.30	0.15	0.31	5.51
MCC PH302	480.00	41.13	36.97	38.20	5.87
RSD%	3.61	0.25	0.38	0.17	0.15
MCC Prosolv 50	394.67	43.67	39.27	41.03	5.34
RSD%	4.04	0.23	0.21	0.40	0.20
MCC Prosolv 90	1597.33	40.90	37.63	38.20	7.27
RSD%	2.89	0.96	0.95	0.92	0.64

Table A 8 Flow data of lactose grades (RHOB is the bulk density calculated in kg/m3, PHIE is the effective angle of friction, PHIILIN is the effective angle of internal friction, PHISF is the angle of surface friction, FFC is the flow function coefficient

Grade	RHOB (KG/M3)	PHIE (°)	PHILIN (°)	PHISF (°)	FFC
Flowlac 90	667.67	32.20	30.43	29.60	13.73
RSD %	8.14	0.17	0.21	0.10	1.10
Flowlac 100	678.67	32.63	31.33	29.90	19.23
RSD %	2.89	0.65	0.76	0.40	2.62
Ganulac 70	851.00	38.73	35.20	35.20	7.00
RSD %	8.72	0.42	0.40	0.36	0.10
Granulac 200	770.00	44.57	36.60	38.97	3.27
RSD %	6.56	0.31	0.46	0.29	0.06
Inhalac 250	795.00	41.07	35.10	37.13	4.23
RSD %	4.36	0.42	0.36	0.51	0.06
Inhalac 400	522.33	83.67	35.00	47.10	0.99
RSD %	7.51	1.99	1.00	0.20	0.04
Tablettose 80	697.67	38.70	36.43	34.63	10.50
RSD %	4.04	0.56	0.57	0.38	0.36

Table A 9 Flow data of DCP grades (RHOB is the bulk density calculated in kg/m3, PHIE is the effective angle of friction, PHIILIN is the effective angle of internal friction, PHISF is the angle of surface friction, FFC is the flow function coefficient)

Grade	RHOB (KG/M^3)	PHIE (°)	PHILIN (°)	PHISF (°)	FFC
A12	1247.00	47.57	36.03	39.80	2.40
RSD %	1.00	1.12	0.68	0.70	0.10
A60	1458.67	34.83	33.67	31.83	20.70
RSD %	8.08	0.80	0.81	0.85	2.01
A150	786.00	37.40	36.87	34.40	32.00
RSD %	6.00	0.26	0.23	0.78	2.00
D14	782.00	48.23	34.70	40.20	2.10
RSD %	11.53	0.91	0.30	0.82	0.10
D160	896.67	42.37	42.13	35.27	66.67
RSD %	6.66	1.10	1.01	6.70	6.03